UNIVERSIDADE ESTADUAL PAULISTA
"JÚLIO DE MESQUITA FILHO"
Câmpus de Rio Claro

INSTITUTO DE GEOCIÊNCIAS E CIÊNCIAS EXATAS
CÂMPUS DE RIO CLARO

Programa de Pós-Graduação em Geociências e Meio Ambiente

EVOLUÇÃO SEDIMENTAR E PALEOAMBIENTAL DA FORMAÇÃO SETE LAGOAS (GRUPO BAMBUÍ, NORTE DE MINAS GERAIS) NO CONTEXTO DAS BACIAS SEDIMENTARES DO PERÍODO EDIACARANO TERMINAL

JULIANA OKUBO

Orientador: Prof. Dr. Lucas Veríssimo Warren

UNIVERSIDADE ESTADUAL PAULISTA

Instituto de Geociências e Ciências Exatas

Campus de Rio Claro

EVOLUÇÃO SEDIMENTAR E PALEOAMBIENTAL DA FORMAÇÃO SETE LAGOAS (GRUPO BAMBUÍ, NORTE DE MINAS GERAIS) NO CONTEXTO DAS BACIAS SEDIMENTARES DO PERÍODO EDIACARANO TERMINAL

JULIANA OKUBO

Orientador: Prof. Dr. Lucas Veríssimo Warren

Tese de Doutorado apresentada ao Programa de Pós-Graduação em Geociências e Meio Ambiente, como parte dos requisitos para obtenção do título de Doutor em em Geociências e Meio Ambiente.

Rio Claro - SP
2019

O41e

Okubo, Juliana

Evolução sedimentar e paleoambiental da Formação Sete Lagoas (Grupo Bambuí, norte de Minas Gerais) no contexto das bacias sedimentares do Período Ediacarano terminal / Juliana Okubo. -- Rio Claro, 2019

190 p. : il., tabs., fotos

Tese (doutorado) - Universidade Estadual Paulista (Unesp), Instituto de Geociências e Ciências Exatas, Rio Claro

Orientador: Prof. Dr. Lucas Veríssimo Warren

1. Fm. Sete Lagoas. 2. Grupo Bambuí. 3. capa carbonática. 4. sedimentologia. 5. estratigrafia. I. Título.

Sistema de geração automática de fichas catalográficas da Unesp. Biblioteca do Instituto de Geociências e Ciências Exatas, Rio Claro. Dados fornecidos pelo autor(a).

Essa ficha não pode ser modificada.

ERRATA

OKUBO, J. **Evolução sedimentar e paleoambiental da Formação Sete Lagoas (Grupo Bambuí, norte de Minas Gerais) no contexto das bacias sedimentares do Período Ediacarano terminal.** 2019, 190p. Tese (Doutorado) – Instituto de Geociências e Ciências Exatas, Universidade Estadual Paulista, campus Rio Claro, Rio Claro, 2019.

Folha	Linha	Onde se lê	Leia-se
Agradecimentos	1	À Universidade Estadual Paulista (UNESP) e Fundação de Amparo à Pesquisa do Estado de São Paulo (FAPESP processos 2015/07391-0 e BEPE 2017/19023-1) pelo apoio logístico e financeiro.	À Universidade Estadual Paulista (UNESP) – Campus Rio Claro, pelo apoio institucional. Ao apoio da Fundação de Amparo à Pesquisa do Estado de São Paulo (FAPESP processos 2015/07391-0 e BEPE 2017/19023-1), pela concessão de bolsa de doutorado. Além disso, o presente trabalho foi realizado com o apoio da Coordenação de Aperfeiçoamento de Pessoal de Nível Superior – Brasil (CAPES) – Código de Financiamento 001.

EVOLUÇÃO SEDIMENTAR E PALEOAMBIENTAL DA FORMAÇÃO SETE LAGOAS (GRUPO BAMBUÍ, NORTE DE MINAS GERAIS) NO CONTEXTO DAS BACIAS SEDIMENTARES DO PERÍODO EDIACARANO TERMINAL

JULIANA OKUBO

Tese de Doutorado apresentada ao Instituto de Geociências e Ciências Exatas do Campus de Rio Claro, da Universidade Estadual Paulista "Júlio de Mesquita Filho", como parte dos requisitos para obtenção do título de Doutor em Geociências e Meio Ambiente.

Comissão Examinadora

Prof. Dr. Lucas Veríssimo Warren – orientador (IGCE/UNESP)
Prof. Dra. Lucía Gomez-Peral (UNLP – Argentina)
Prof. Dr. Alexandre Uhlein (IGC/UFMG)
Prof. Dr. Claudio Riccomini (IEE/USP)
Prof. Dr. Ricardo Ivan Ferreira da Trindade (IAG/USP)

Conceito: Aprovado

Rio Claro/SP, 19 de setembro de 2019

AGRADECIMENTOS

À Universidade Estadual Paulista (UNESP) – Campus Rio Claro, pelo apoio institucional.

Ao apoio da Fundação de Amparo à Pesquisa do Estado de São Paulo (FAPESP processos 2015/07391-0 e BEPE 2017/19023-1), pela concessão de bolsa de doutorado. Além disso, o presente trabalho foi realizado com o apoio da Coordenação de Aperfeiçoamento de Pessoal de Nível Superior – Brasil (CAPES) – Código de Financiamento 001.

Ao meu orientador e amigo Prof. Dr. Lucas V. Warren por ter me apresentado o mundo Ediacarano e incentivado a ir ao campo na Namíbia, o qual me permitiu visualizar os melhores caminhos a serem traçados durante estea pesquisa.

Ao Prof. Dr. Shuhai Xiao, por me receber em meu doutorado sanduíche e compartilhar seu vasto conhecimento sobre paleontologia e geoquímica do Ediacarano. Agradeço também ao Dr. Drew Muscente, pelas discussões iniciais sobre isótopos de enxofre que inspiraram esse trabalho.

Agradeço também aos Profs. Drs. Benjamin Gill e Robert J. Bodnar, também da Virginia Tech, pelos aprendizados sobre os isótopos de enxofre e inclusões fluidas, respectivamente, bem como pelo uso das instalações de seus laboratórios.

Aos Profs. Drs. Alexandre Uhlein, Ricardo I. F. Trindade, Lucía Gomez-Peral e Claudio Riccomini, pelas valiosas contribuições durante a defesa. Agradeço também ao Prof. Dr. Mario L. Assine, pelas enriquecedoras discussões a respeito da estratigrafia e das paleocorrentes e ao amigo e Prof. Dr. Gabriel Uhlein, pelas discussões sobre o Grupo Bambuí.

Aos Profs. Drs. Leonardo Fadel Cury e Anelise Bahniuk e toda equipe do laboratório LAMIR (UFPR) pelas análises isotópicas de carbono e oxigênio.

Ao pessoal da Pós-Graduação da UNESP, Lucas Inglez, Regiane, Fer Menin, Rodox, Marcela, Juninho, Antonio, Silvia e também o pessoal do LESTE (Michele, Patricia, Filipe, Milena e Fernanda Quaglio) pela amizade, momentos compartilhados e pelas ótimas discussões filosóficas e geológicas.

Ao pessoal da Virginia Tech (Dr. Qing Tang, Morrison Nolan, Dana Korneisel, Maxwell Schwid e Fanfan Kong), pela amizade, momentos compartilhados e discussões enriquecedoras durante nossas reuniões semanais durante a minha estadia em Blacksburg.

Ao amigo Hamilton Sales dos Reis por toda a assistência durante os trabalhos de campo.

À MF, Adriano, Victor e Desi, em especial, Joca e Lulu. por me apoiarem e estarem sempre comigo. Aos novos amigos Brit, Khanh, Matt, Renatha, Léo, Wallace e Najla que tornaram minha vida muito mais leve e prazerosa durante o período que passei em Blacksburg.

Encerro agradecendo a todos que, de alguma forma, contribuíram direta ou indiretamente para a conclusão deste trabalho.

RESUMO

Drásticas mudanças climáticas, tectônicas, geoquímicas e bioevolutivas ocorreram ao final da Era Neoproterozoica e seu registro pode ser encontrado em diversas sucessões sedimentares ao redor do mundo. Uma dessas sucessões é a Formação Sete Lagoas, unidade carbonática basal do Grupo Bambuí, aflorante tanto na porção central e sul do Cráton do São Francisco. Considerando a extensa área de afloramento e grande continuidade estratigráfica desta unidade na região de Januária (norte de MG), este trabalho teve como objetivo definir a evolução sedimentar e paleoambiental da Formação Sete Lagoas a partir de uma abordagem sedimentológica, estratigráfica e geoquímica integrada, buscando compreender, por exemplo, variações nas condições *redox*, modificações no ciclo do carbono, temperatura da água e produtividade orgânica primária. Na área estudada, cinco associações de fácies foram definidas, da base para o topo: capa dolomítica (AF1), associação de carbonatos de perimaré (AF2), rampa carbonática influenciada por sismos (AF3), cordão oolítico litorâneo (AF4) e planície de maré dominada por microbialitos (AF5). Devido sua singularidade e importância no registro, duas sucessões distintas foram estudadas detalhadamente: os precipitados de fundo oceânico pertencente à capa dolomítica e a brecha intraformacional (*flat-pebble breccia*) nas porções basal e intermediária da unidade, respectivamente. Os precipitados de fundo oceânico são representados por leques carbonáticos (pseudomorfos de aragonita), barita e cimentos apatíticos autigênicos, estes últimos ineditamente descritos em contexto de capa carbonática. Devido à importância dos leques de barita na definição de idade (Marinoana) para os carbonatos de capa estudados, deu-se especial atenção ao estudo da origem (diagenética, hidrotermal ou metanogênica) deste mineral. A precipitação da capa carbonática com os leques de fundo oceânico (AF1) foi sucedida pela deposição de fácies de água rasa (AF2), compondo um ambiente no qual proliferaram os metazoários *Cloudina* e *Corumbella* associados à trombólitos e esteiras microbianas. Estes depósitos de perimaré foram sucedidos por brechas intraformacionais, interpretadas como *flat-pebble breccia*, formada por eventos de sismicidade que atingiram e modificaram substancialmente a arquitetura da plataforma carbonática (AF3). Dados de direção dos clastos alongados de AF3 e de paleocorrentes da AF4 indicam que a linha de costa original estava posicionada na direção NE-SW, com abertura oceânica para SE. Extensos depósitos de cordões oolíticos e estromatólitos dômicos (AF4) sucedidos por planícies de maré de clima árido com microbialitos (AF5) representam a última etapa de deposição da sucessão da Formação Sete Lagoas, precedendo o afogamento da plataforma carbonática representado pela deposição de pelitos da Formação Serra de Santa Helena. As associações de fácies interpretadas foram organizadas em três sequências deposicionais distintas, com expressivo espessamento de seção na direção E-NE, possivelmente relacionado a um aumento na taxa de subsidência nesta porção da bacia. Ao longo da sucessão carbonática, os valores isotópicos de C_{carb} e O_{carb} mostram uma excursão negativa na base passando para valores progressivamente mais positivos em direção ao topo. Os valores isotópicos de $^{34}S_{CAS}$ mostram co-variância com os valores de $^{13}C_{carb}$, indicando que a pirita e o carbono orgânico foram oxidados e soterrados a uma mesma taxa. As concentrações de sulfato contido no carbonato (CAS – sigla em inglês) medidas mostram um pico de oxigenação na porção basal da unidade seguida por condições anóxicas, semelhante às estimativas anteriores do reservatório de sulfato em outras unidades do final do Ediacarano.

Palavras-chave: Neoproterozoico, Grupo Bambuí, Formação Sete Lagoas, estratigrafia, sedimentologia, geoquímica

ABSTRACT

Major climatic, tectonic, biogeochemical and evolutionary changes occurred during Late Neoproterozoic are recorded in several sedimentary successions around the world. One of these successions is the Sete Lagoas Formation, the basal unit of the Bambuí Group, present both in the southern and central part of São Francisco Craton. Because of excellent exposure and and great stratigraphic continuity of this unit, this study focused on the the sedimentary and paleoenvironmental evolution of the Sete Lagoas Formation near Januária area– MG in the central São Francisco Craton, based on a sedimentological, stratigraphic and geochemical approaches. Five facies associations were defined in the studied area: cap dolostone (FA1), peritidal carbonates (FA2), seismic-influenced carbonate ramp (FA3), oolitic belt (FA4) and tidal flat dominated by microbialites (FA5). Due to their importance in the rock record, two distinct intervals were studied in detail: the seafloor precipitates and the flat-pebble breccia from the lower and middle part of the unit, respecively. The seafloor precipitates are represented by carbonate fans (aragonite pseudomorphs), barite and authigenic apatitic cements. The latter was described here for the first time in a cap carbonate context, and this mineralogical association is interpreted as the result of iron reduction of sediments in conjunction with high alkalinity of the seawater. Since barite fans have been used to infer the Marinoan age of this cap carbonate, it is important to test whether its origin relates to early diagenetic or hydrothermal processes. The FA1 was succeeded by the deposition of peritidal carbonates (FA2), marked by the presence of thrombolites and laminated microbialites, which provided environmental conditions for the proliferation of the *Cloudina* and *Corumbella* metazoans. These shallow-water deposits are overlaid by intraformational breccias, interpreted as flat-pebble breccia, formed by seismic events (FA3). Clast measurements of the paleocurrent data from FA4 indicate a NE-SW coastline with ocean opening for SE. Extensive ooid shoals (FA4) succeeded by tidal flats dominated by microbialites (FA5), represent the last deposition cycle of the Sete Lagoas Formation, preceding the drowning of the carbonate platform represented by pelitic rocks from the Serra de Santa Helena Formation. The Sete Lagoas carbonate platform deposits are arranged into three depositional sequences with thickening towards E-NE, possibly related to an increase of subsidence rate in this part of the basin. Throughout the entire carbonate succession, C and O isotopic values show a large negative excursion in the base, increasing to positive values upward. The $^{34}S_{CAS}$ isotopic values covary with $^{13}C_{carb}$, indicating that pyrite and organic carbon were oxidized and buried at the same rate. Measured carbonate-associated sulfate (CAS) concentrations show an oxygenation peak in the lower part of the unit, followed by anoxic conditions, similar to previous estimates of sulfate reservoir in other late Ediacaran carbonate units.

Keywords: Neoproterozoic, Bambui Group, Sete Lagoas Formation, stratigraphy, sedimentology, geochemistry

SUMÁRIO

1. INTRODUÇÃO 13

1.1. Objetivos 14
1.2. Localização e acessos 15

2 MATERIAIS E MÉTODOS UTILIZADOS 16
3 ASPECTOS GEOQUÍMICOS, PALEONTOLÓGICOS, PALEOCLIMÁTICOS E GEOTECTÔNICOS DO PERÍODO EDIACARANO 23

3.1 Glaciações globais neoproterozoicas 23
3.2 Capas carbonáticas 24
3.3 Assinaturas isotópicas e condições de oxigenação nos oceanos durante o Ediacarano 27
3.4 Inovações paleobiológicas, paleoecológicas e evolutivas no Ediacarano 29

4 CONTEXTO GEOLÓGICO REGIONAL 30

4.1 Formação Sete Lagoas 34

4.1.1 Idade dos depósitos carbonáticos 38

5. "SEDIMENTARY EVOLUTION AND INTEGRATED HIGH-RESOLUTION GEOCHEMISTRY (C, O AND S) OF THE SETE LAGOAS FORMATION, BAMBUÍ GROUP (NORTHERN MINAS GERAIS STATE, BRAZIL)", A SER SUBMETIDO PARA O PERIÓDICO *PRECAMBRIAN RESEARCH* 40

5.1 Introduction 42
5.2 Geological Setting 43
5.3 Material and Methods 48
5.4 Results 50

5.4.1 Facies and facies association of the Sete Lagoas Formation 50
5.4.2 Sequence stratigraphy framework 57
5.4.3 Stable isotope geochemistry and evaluation of diagenetic alteration 62

5.5 Discussions 64

5.5.1 Interpreting the sulfur and carbon signatures 64
5.5.2 Paleoenvironmental implications for the Sete Lagoas Formation: the marine sulfate reservoir 65

5.6 Conclusions 68

6. "PHOSPHOGENESIS, ARAGONITE FAN FORMATION, AND SEAFLOOR ENVIRONMENTS FOLLOWING THE MARINOAN GLACIATION", PUBLICADO NA REVISTA PRECAMBRIAN RESEARCH (2018, 311: 24-36) 74

6.1 Introduction 75
6.2 Geological Setting 76
6.3 Material and Methods 78
6.4 Results 78
6.5 Discussions 78
6.6 Conclusions 85

7. "HYDROTHERMAL INFLUENCE ON BARITE PRECIPITATES IN THE BASAL EDIACARAN SETE LAGOAS CAP CARBONATE, SÃO FRANCISCO CRATON, CENTRAL BRAZIL", ARTIGO SUBMETIDO A UM VOLUME ESPECIAL DA REVISTA PRECAMBRIAN RESEARCH 88

7.1 INTRODUCTION 90
7.2 GEOLOGICAL SETTING 92
7.3 METHODS 94
7.4 RESULTS 96

7.4.1 Petrography, microCT, and sulfur isotope data 96
7.4.2 Raman spectroscopy and fluid inclusions 98

7.5 DISCUSSIONS 103
7.6 CONCLUSIONS 107

8. **"THE ENIGMATIC FLAT-PEBBLE BRECCIA OF THE SETE LAGOAS FORMATION (BAMBUÍ GROUP, BRAZIL): EVIDENCES OF SEISMIC-INDUCED DEFORMATION IN AN EDIACARAN CARBONATE PLATFORM", SUBMETIDO PARA O PERIÓDICO JOURNAL OF SOUTH AMERICAN EARTH SCIENCES 113**

8.1 INTRODUCTION **115**
8.2 GEOLOGICAL SETTING **116**
8.3 MATERIAL AND METHODS **118**
8.4 RESULTS **118**

8.4.1 Facies associations of the Sete Lagoas Formation 118
8.4.1.1 Peritidal facies association 119
8.4.1.2 Flat-pebble breccias facies association 119
8.4.1.3 Subtidal facies association 121

8.4.2 *SEDIMENTARY CHARACTERISTICS OF THE SETE LAGOAS FLAT-PEBBLE BRECCIA DEPOSITS* *122*
8.5 DISCUSSIONS **129**

8.5.1 The flat-pebble breccia problem: distinct triggers, processes and products 129
8.5.2 Flat pebble carbonate breccia as evidence of synsedimentary tectonic activity 131

8.6 CONCLUSIONS **134**

9. CONCLUSÕES 140
10. REFERÊNCIAS BIBLIOGRÁFICAS 143

LISTA DE FIGURAS

Figura 1.1: A) Localização da área de estudo, destacando as principais vias de acesso. B) Localização das seções estudadas na área de Januária e Montalvânia-MG. 16
Figura 3.1: Síntese dos principais eventos tectônicos, bioevolutivos e paleoclimáticos ocorridos no final do Neoproterozoico e início do Cambriano, extraído de Spence et al. (2016). As linhas vermelhas correspondem às anomalias negativas de isótopos de carbono. Baseado em Nogueira (2003) e Warren (2011), com compilações de Canfield et al. (2008), Lenton et al. (2014), Spence et al. (2016). 25
Figura 3.2: Mapa da localização do Cráton do São Franscisco e das faixas móveis Brasília e Araçuaí. Fonte: Alkmim and Martins-Neto (2001). 30
Figura 3.3: Mapa geológico simplificado do cráton São Francisco. Compilado do banco de dados da CPRM (Geobank). 31
Figura 3.4: Coluna estratigráfica do Grupo Bambuí (baseado em Dardenne, 1978). Espessuras compiladas por Lima (2005) e os ciclos de sedimentação segundo Dardenne (1978), Martins (1999) e Martins-Neto e Alkmim (2001). 33
Figura 3.5: A) Mapa esquemático da bacia Bambuí mostrando a distribuição de altos e baixos do embasamento. (Fonte: Alkmim & Martins-Neto, 2001). O retângulo representa a localização da área estudada. 36

Figure 5.1: A) Simplified geological map of the São Francisco Craton, showing the glaciogenic units and the Bambuí Group. B) Outcrop area of the Sete Lagoas Formation at Januária area and location of the studied sections 45
Figure 5.2: Lithostratigraphy of the Bambuí Group 46
Figure 5.3: Facies associations of the Sete Lagoas Formation at Januária region 52
Figure 5.4: Facies associations of the Sete Lagoas Formation at Januária region. 54
Figure 5.5: Paleocurrents of the oolitic belt facies association of the Sete Lagoas Formation in the study area and rose diagrams of azimuthal orientation of elongate clasts in flat-pebble breccia near Barreiro section 57
Figure 5.6: Sequence stratigraphic framework of the Sete Lagoas Formation 59
Figure 5.7: Paleocurrent data, stratigraphic surfaces, columnar sections and respective $\delta^{13}C_{carb}$ (‰, VPDB) and $\delta^{14}S_{CAS}$ (‰, VPDB) profiles of the Sete Lagoas Formation 61
Figure 5.8: Composite stratigraphic column, geochemical data (C_{carb}, O_{carb} and S_{CAS} isotopes), CAS concentration, carbonate content and Sr/Ca and Mn/Sr ratios for the Sete Lagoas Formation at Januária area 62
Figure 5.9: Isotope and elemental cross-plots for the Sete Lagoas Formation 64
Figure 5.10: Sensitivity of the marine sulfate reservoir size to deposition rate, calculated using Kah et al. (2004) approach. 67

Figure 6.1: Location of the São Francisco Craton and the Bambuí Group in the Januária region. B) Geologic map of the Sete Lagoas Formation and stratigraphic section. 77
Figure 6.2: Measured stratigraphic sections of the lower Sete Lagoas Formation. 79
Figure 6.3: Photographs and photomicrographs of barite- and aragonite-bearing layers of the lower Sete Lagoas Formation. 80
Figure 6.4: BSE-SEM images of aragonite fan crystals and encrusting apatitic cements 81
Figure 6.5: BSE-SEM images and EDS spectra of the aragonite and barite fans. 82
Figure 6.6: BSE-SEM images and WDS elemental maps of the contact between the barite fans and the underlying microbialite. 83
Figure 6.7: BSE-SEM image and WDS elemental maps of barite associated with iron oxide pseudomorph of pyrite in microbialites. 83
Figure 6.8: BSE-SEM image and WDS elemental maps of aragonite fans, showing barite inclusions with carbonate fan crystals. 84

Figure 6.9: Sedimentary model for aragonite crystal fan formation and phosphogenesis in the Sete Lagoas Formation....84

Figure 7.1: Simplified geological map, generalized schematic stratigraphic columns of the carbonate units of the São Francisco Craton and composite section of the Sete Lagoas Formation at Januária area 93
Figure 7.2: Mesoscopic and microscopic features of the barite layer....97
Figure 7.3: X-ray CT three-dimensional reconstruction of a Sete Lagoas sample that contains a layer of void-filling barite crystals and a layer of the host rock....98
Figure 7.4: Carbonaceous material (CM) Raman spectra and CM Raman temperatures....100
Figure 7.5: Fluid inclusions in barite crystals, showing secondary trails and some primary fluid inclusions. 100
Figure 7.6: Methane-bearing fluid inclusions....102
Figure 7.7: Representative Raman spectrum of fluid inclusions in barite crystals of the Sete Lagoas Formation and calibration Raman spectra showing Raman O-H stretching bands for water with known salinities 102
Figure 7.8: Sulfur isotope data of sulfides and sulfates from Sete Lagoas Formation and other supposedly correlative units (Salitre Formation and Vazante Group) of the São Francisco Craton 105

Figure 8.1: Location of the São Francisco Craton and the Bambuí Group in the Minas Gerais State, central Brazil, geological map of Ediacaran Sete Lagoas Formation in the vicinity of the town of Januária-MG and location of the columnar sections, and lithostratigraphic column of the Bambuí Group in the study area 117
Figure 8.2: Representative sedimentary facies of the Sete Lagoas Formation in the studied area. 120
Figure 8.3: Different types of breccia deposits present in the Sete Lagoas Formation succession in the studied area 122
Figure 8.4: Correlation of stratigraphic columnar sections showing the flat-pebble breccia of the Sete Lagoas Formation in the Januária region....123
Figure 8.5: Outcrop photograph of flat-pebble breccia beds at Barreiro section and representative sketch of A showing the arrange of the clasts....124
Figure 8.6: Sedimentary features of the flat-pebble breccia and their relationship with underlying and overlying layers....125
Figure 8.7: Representative sketch of flat-pebble breccia beds at the Barreiro section 125
Figure 8.8: Size measurements of clasts in the lower breccia interval at the Barreiro section....126
Figure 8.9: Thin section microphotographs and compositional EDS maps of the flat-pebble breccia at the Barreiro section. 127

Figure 8.10: Deformation features of the flat-pebble beds....128

Figure 8.11: Paleocurrents of the subtidal facies association positioned stratigraphically above the flat-pebble breccia interval and rose diagrams of azimuthal orientation of elongate clasts in flat-pebble breccia near Barreiro section....129
Figure 8.12: Magnetometric map of Januária region....134
Figure 8.13: Schematic model for the seismic origin of flat-pebble breccia from Sete Lagoas Formation in the Januária region. 134

LISTA DE APÊNDICES

Apêndice A: Dados isotópicos e geoquímicos referentes às amostras estudadas 155
Apêndice B: Co-autoria em artigos científicos relacionados ao tópico da tese: Inglez et al. (2019) **"**Discs and discord: The paleontological record of Ediacaran discoidal structures in the South American continent". *Journal of South America Earth Sciences*, 89: 319-336. 158
Apêndice C: Co-autoria em artigos científicos relacionados ao tópico da tese: Uhlein et al. (2019). "Ediacaran paleoenvironmental changes recorded in the mixed carbonatesiliciclastic Bambuí Basin, Brazil", *Palaeogeography, Palaeoclimatology, Palaeoecology*, 517: 39-51. 177

Apresentação

A presente tese está estruturada em dez capítulos. O Capítulo 1 apresenta a problemática tratada nesta tese. Nos capítulos seguintes, são apresentados os métodos e técnicas analíticas utilizados nesta pesquisa (Cap. 2), uma contextualização dos principais eventos geotectônicos e bioevolutivos ocorridos ao final do Ediacarano (Cap. 3) e os aspectos geológicos regionais da área de estudo (Cap. 4).

Os resultados estão apresentados na forma de quatro artigos científicos (Cap. 5 a 8). O Capítulo 5 corresponde ao manuscrito em preparação intitulado "*Sedimentary evolution and integrated high-resolution geochemistry (C, O and S) of the Sete Lagoas Formation, Bambuí Group (northern Minas Gerais State, Brazil)*", que será submetido à revista *Precambrian Research*. Este trabalho busca apresentar um quadro estratigráfico, paleoambiental e quimioestratigráfico completo para a Formação Sete Lagoas na região de Januária-MG. O Capítulo 6 corresponde ao artigo publicado no periódico *Precambrian Research,* intitulado "*Phosphogenesis, aragonite fan formation and seafloor environments following the Marinoan glaciation*". Este trabalho aborda a relação dos leques de aragonita e de barita com o processo de fosfatização no contexto de capa carbonática que ocorre na base da Formação Sete Lagoas. O Capítulo 7, intitulado "*Hydrothermal influence on barite precipitates in the basal Ediacaran Sete Lagoas cap carbonate, São Francisco Craton, central Brazil*", corresponde ao manuscrito em preparação, que será submetido à um volume especial da revista *Precambrian Research*. Neste trabalho, discute-se a origem e a história termal da barita presente na capa carbonática, discutindo sua relação com eventos hidrotermais vigentes no cráton São Francisco durante o final do Período Ediacarano. O último artigo (Capítulo 8) apresenta o manuscrito em revisão no periódico *Journal of South American Earth Sciences*, cujo título é "*The enigmatic flat-pebble breccias of the Sete Lagoas Formation (Bambuí Group, Brazil): evidences of seismic-induced deformation in an Ediacaran carbonate platform*". Este artigo trata da análise sedimentológica e estratigráfica das brechas carbonáticas (*flat pebble breccia*) incomuns que ocorrem na porção intermediária da Formação Sete Lagoas, destacando a sismicidade como o principal mecanismo de formação destes depósitos particulares.

O Capítulo 9 apresenta as conclusões obtidas ao longo da pesquisa e por fim as respectivas referências bibliográficas utilizadas no presente trabalho (Cap. 10). Ao final deste volume, estão apresentados uma tabela (Apêndice A) integrando todos os dados geoquímicos (isótopos de C_{carb}, O_{carb} e S_{CAS}, elementos maiores, menores e traço), bem como dois artigos científicos em que a autora da presente tese de doutoramento participou como co-autora (Apêndices B e C).

1. Introdução

Várias unidades ediacaranas têm sido estudadas em todo o mundo sob diversos aspectos geológicos ao longo das últimas décadas. O reaparecimento de formações ferríferas após um hiato de 1 Ga no registro geológico representa uma importante mudança sedimentológica e geoquímica ocorrida ao final do Neoproterozoico (Hoffman e Schrag, 2002). Estas formações ferríferas estão intimamente relacionadas a diamictitos glaciais criogenianos depositados em latitudes equatoriais (Cox et al., 2016, 2013), indicando que estas glaciações foram as mais severas da história da Terra (Evans, 2000; Trindade e Macouin, 2007; Williams, 1975). As assinaturas geoquímicas e isotópicas preservadas nas rochas são anômalas em relação ao restante do registro geológico, especialmente durante o Ediacarano, revelando profundas mudanças na composição química dos oceanos e do ciclo biogeoquímico do carbono (Kaufman et al., 1997, 1991; Knoll et al., 1986). Associado a este contexto de importantes mudanças paleoclimáticas e em um oceano quimicamente diferente do atual, surgem os primeiros organismos macroscópicos complexos entre 575 e 565 Ma, seguidos pelas inovações biológicas como mobilidade (>555 Ma), calcificação (550 Ma) e predação (<549 Ma) (Narbonne, 2005).

Apesar do crescente volume de dados obtidos em sucessões ediacaranas ao redor do globo, diversas questões ainda são motivo de intenso debate na literatura (Spence et al., 2016; Xiao et al., 2016), incluindo o sincronismo dos supostos eventos glaciais globais, sua distribuição latitudinal, o significado de diversas estruturas sedimentares anômalas e o significado das importantes excursões isotópicas de C, O e S, observadas nas capas carbonáticas (Hoffman e Schrag, 2002).

Na América do Sul, uma das unidades neoproterozoicas mais estudadas é a Formação Sete Lagoas, base do Grupo Bambuí, devido à sua extensa exposição sobre o Cráton do São Francisco (CSF). Alguns autores dividem o cráton em três compartimentos (Alkmim et al., 1996, 1993; Alkmim e Martins-Neto, 2001; Coelho et al., 2008): (i) compartimento oeste, que corresponde à porção externa da Faixa Brasília; (ii) porção central, cujas unidades neoproterozoicas do Grupo Bambuí encontram-se praticamente indeformadas, e (iii) compartimento leste, que corresponde à porção externa da Faixa Araçuaí.

As áreas de afloramento da Formação Sete Lagoas sem deformação tectônica ocorrem principalmente nas regiões de Januária, Arcos e Sete Lagoas nas bordas leste e sul do cráton, respectivamente. Tais áreas apresentam excelentes exposições para estudos sedimentológicos e estratigráficos, ainda que surpreendentemente pese a ausência de trabalhos de detalhe na porção norte do CSF. Devido à descoberta do fóssil-guia *Cloudina* na região de Januária (Warren et al., 2014) e ao fato das outras regiões (Arcos e Sete Lagoas) terem sido amplamente estudadas ao longo das últimas décadas por vários autores (Cruz e Nobre-Lopes, 1992; Hidalgo, 2007; Kuchenbecker, 2011; Nobre-Lopes, 1995; Paula-Santos, 2012; Vieira, 2007), o presente trabalho procurou concentrar seus estudos na região de Januária (municípios de Januária, Itacarambi e Montalvânia, MG), buscando um melhor entendimento da sucessão sedimentar da Formação Sete Lagoas nesta porção da Bacia Bambuí.

A Formação Sete Lagoas apresenta características sedimentológicas distintas nas suas ocorrências nas porções sul (região de Sete Lagoas, área-tipo da unidade) e central do CSF (região de Januária, área de estudo). Fácies de águas profundas, como os ritmitos de calcilutito cinza e pelitos (Vieira et al., 2007a), não são, à título de exemplo, encontradas na região de Januária. Por outro lado, as brechas intraformacionais (*flat-pebble breccias*) que ocorrem extensivamente na região de estudo parecem não ocorrer em outras porções do Grupo Bambuí. Porém, similaridades também ocorrem, como a presença de estruturas sedimentares anômalas na base da Formação Sete Lagoas, tais como pseudomorfos de aragonita e megamarcas onduladas, similares àquelas reconhecidas globalmente para as capas carbonáticas neoproterozoicas (Vieira et al., 2007a, 2015). Além disso, as brechas hidrotermais ricas em Pb e Zn, descritas no topo da unidade em Januária por Nobre-Lopes (2002), apresentam características semelhantes e se correlacionam com outras unidades proterozoicas da bacia, como a Formação Salitre na Bacia Irecê e parte do Grupo Vazante (ver Misi et al., 2005, 2014).

Considerando o panorama acima exposto, este trabalho almejou o estudo integrado (estratigráfico, sedimentológico e geoquímico) da sucessão sedimentar da Formação Sete Lagoas na porção central do Cráton do São Francisco (região de Januária-MG), buscando traçar sua evolução sedimentar e paleoambiental e, portanto, preencher importante lacuna no conhecimento geológico do Neoproterozoico brasileiro.

1.1. Objetivos

A presente tese de doutoramento teve como objetivo principal a realização de estudo sedimentológico, estratigráfico e geoquímico de detalhe da Formação Sete Lagoas (Grupo Bambuí) dentro do contexto evolutivo das sucessões neoproterozoicas desenvolvidas nas paleomargens do Cráton São Francisco. Como objetivos específicos, buscou-se:

- Descrever as associações de fácies e definir os sistemas deposicionais vigentes durante a sedimentação da Formação Sete Lagoas. Adicionalmente, detalhou-se os processos formadores de brechas incomuns presentes na porção intermediária da succession estudada;

- Definir padrões arquiteturais e de empilhamento das sucessões, bem como caracterizar superfícies estratigráficas a fim de compor o quadro estratigráfico adequado para a Formação Sete Lagoas na região de Januária, MG;
- Caracterizar em detalhe os precipitados de fundo oceânico presentes na capa carbonática da porção inferior da unidade;
- Identificar variações nos padrões isotópicos de carbono e oxigênio visando auxiliar a correlação da unidade com outras porções da bacia;
- Estabelecer uma inédita curva isotópica de enxofre para a unidade, cujo significado está intimamente relacionado com a composição da água do mar e a oxigenação dos oceanos no Período Ediacarano.

1.2. Localização e acessos

A área de estudo está localizada na porção norte do estado de Minas Gerais (Figura 1.1A), na margem esquerda do Vale do São Francisco, nos arredores do município de Januária (595 km a norte da capital do estado, Belo Horizonte). Nesta região, afloram rochas do Grupo Bambuí, compreendendo uma cobertura cratônica extensa em contato erosivo com rochas arqueanas e paleoproterozoicas do embasamento do Cráton São Francisco. Localmente, a unidade apresenta espessura total da ordem de 700-1000 m (Misi et al., 2007) e compreende calcários e dolomitos da Formação Sete Lagoas na base que gradam em direção ao topo para folhelhos e siltitos da Formação Serra de Santa Helena, seguidos por margas, siltitos, calcários e arenitos das formações Lagoa do Jacaré, Serra da Saudade e Três Marias.

As seções estudadas podem ser acessadas, a partir de Belo Horizonte, pelas rodovias BR 040 e BR-135 até a cidade de Montes Claros, totalizando 425 km de percurso. Rodovias estaduais e federais irradiam dessa cidade e servem de ligação com outros municípios da área investigada. Destacam-se a BR-135 para Januária, Manga e Montalvânia. Destaca-se também a presença na área de estudo do Parque Parque Nacional Cavernas do Peruaçu (municípios de Januária, Itacarambi e São João das Missões), no qual ocorrem inúmeras cavernas que expõem de maneira espetacular as rochas da sucessão basal e intermediária da Formação Sete Lagoas.

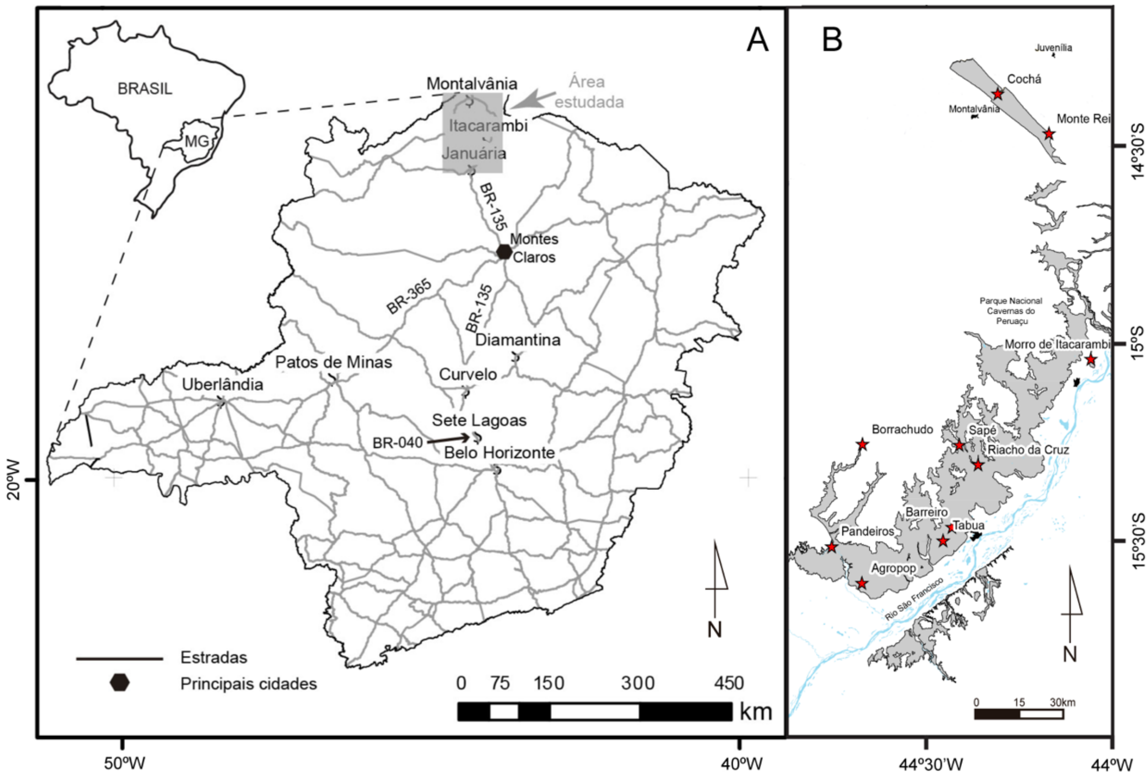

Figura 1.1: A) Localização da área de estudo, destacando as principais vias de acesso. B) Localização das seções estudadas na área de Januária e Montalvânia-MG.

2 Materiais e métodos utilizados

2.1 Trabalhos de campo

Foram realizadas três campanhas de campo, totalizando 21 dias de campo, nos arredores dos municípios de Januária-MG, Itacarambi-MG e Montalvânia-MG (Fig. 1.1A). Como material de suporte de campo, foram utilizadas cartas plani-altimétricas em escala 1:100.000 da porção setentrional do estado de Minas Gerais (Januária, SD-23-Z-C-II, Região Leste do Brasil, Serviço Geográfico do Exército) e imagens SRTM georreferenciados e tratadas no software ARCGIS 10, além dos mapas geológicos da CODEMIG (Projeto Fronteiras de Minas - 2015, escala 1:100.000, Folha Januária, Catolé, Montalvânia).

Antes da aquisição das seções colunares foi priorizado o reconhecimento regional dos afloramentos, com o intuito de elencar as melhores seções existentes na área de estudo. As exposições mais completas verticalmente foram mensuradas e descritas em detalhe (escala 1:50), resultando em dez seções estratigráficas de alta resolução (ver localização na Figura 1.1B). Durante o procedimento de levantamento das seções colunares, buscou-se reconhecer as características faciológicas mais marcantes, como geometria dos depósitos, identificação de estruturas sedimentares e diferenças entre microbialitos, extensão lateral e vertical das camadas, e presença de espécimes fósseis e icnofósseis. A etapa de campo também teve por objetivo a coleta de amostras de acordo com variações litológicas, faciológicas e conteúdo fossilífero. As amostras coletadas foram sistematicamente classificadas e selecionadas para a confecção de seções delgadas, captação de imagens por meio de microscópio Zeiss® e preparação de material para análises de isótopos estáveis de C, O e S.

2.2 Análise de fácies sedimentares

Walker (1992, 2006) define o termo fácies sedimentar como um conjunto de rochas geneticamente relacionadas que corresponde ao registro geológico de um processo sedimentar particular. Esta unidade pode ser distinguida das demais por suas características litológicas, granulação, grau de seleção e de arredondamento dos grãos, estruturas sedimentares, geometria dos estratos, fósseis e coloração. Este conjunto de feições envolve os processos sedimentares particulares observados na natureza ou reproduzidos experimentalmente em laboratório. Tais processos sedimentares podem ser os mesmos em diversos ambientes deposicionais, o que torna necessário agrupar as fácies geneticamente relacionadas e com significado ambiental (associação de fácies).

Os sistemas deposicionais são representações tridimensionais das associações de fácies aos quais estão incorporados os efeitos produzidos por controles externos, tais como as variações relativas do nível de base provocadas por mudanças climáticas, causas tectônicas e variações orbitais (Catuneanu, 2006). Um modelo de fácies adequado deve, portanto, ser verossímil ao sistema deposicional que representa e servir de modelo preditivo ou de comparação com exemplos atuais e do registro geológico (Walker, 2006, 1992).

No presente trabalho, as fácies sedimentares foram inicialmente descritas macroscopicamente em campo, priorizando-se a identificação da geometria do depósito, estruturas sedimentares, organização interna, mineralogia e textura dos grãos. Nesta etapa, as fácies foram individualmente fotografadas, amostradas para análises em laboratório e identificadas nas diferentes seções estratigráficas adquiridas. Depois disso, a descrição macroscópica foi refinada a partir da análise de lâminas petrográficas (microfácies).

2.3 Análise petrográfica

As amostras foram serradas e polidas no Laboratório de Laminação, Departamento de Petrologia e Metalogenia (DPM), Instituto de Geociências e Ciências Exatas (IGCE), UNESP

Rio Claro. Foram realizadas as seguintes etapas: (i) corte em serra diamantada; (ii) desbaste com rebolo de carbeto de tungstênio e suspensão de carbeto de tungstênio (grana 600); (iii) pré-polimento com rebolo de aço fundido e suspensão de carbeto de tungstênio (grana 800), e (iv) polimento em politriz com tecido para polimento e pasta diamantada (1μ).

As amostras foram submetidas à laminação e, posteriormente, à análise dos diferentes litotipos e microfácies carbonáticas sob microscópio petrográfico Zeiss. A descrição petrográfica das seções delgadas de rochas carbonáticas foi feita com base na classificação de Dunham (1962) e Embry e Klovan (1971). A análise e documentação das lâminas delgadas foi realizada em um microscópio petrográfico Zeiss Axiscope, acoplado à câmera digital Canon EOS 5D Mark II, no Laboratório de Fotomicroscopia do DPM, IGCE/UNESP.

2.4 Análises em Microscópio Eletrônico de Varredura (MEV) e Microssonda Eletrônica (EPMA)

Foram selecionadas amostras, das quais foram confeccionadas lâminas polidas. A análise em MEV e EPMA teve por objetivo investigar a morfologia e mineralogia em escala de microdetalhe, assim como a relação temporal entre os minerais formados. As análises em Microscópio Eletrônico de Varredura (MEV) e Microssonda Eletrônica (EPMA) foram realizadas no Laboratório de Microscopia Eletrônica de Varredura e Laboratório de Microssonda Eletrônica, do Departamento de Petrologia e Metalogenia (DPM), UNESP Rio Claro, respectivamente.

As imagens de MEV foram geradas em um microscópio eletrônico de varredura modelo JEOL JSM 6010 LA, utilizando voltagem de 15 keV e distância de trabalho de 10mm. Os mapas composicionais gerados pela Microssonda Eletrônica (EPMA) foram obtidos a partir do equipamento JEOL JXA 8230, equipado com 5 espectrômetros WDS e um sistema pancromático de catodoluminescência (XM-26730PCL). As amostras analisadas na EPMA foram metalizadas com carbono, e os mapas elementares foram adquiridos a uma voltagem de 15 keV e corrente de 20 nA visando identificar os elementos maiores: Fe (Kα), Ca (Kα), Mg (Kα), Ba (Lα), S (Kα), Si (Kα) e Al (Kα).

2.5 Análise de paleocorrentes

A análise de paleocorrentes é uma ferramenta muito utilizada na análise de bacias sedimentares com grande potencial para a reconstituição da história deposicional. O reconhecimento de padrões medidos em estruturas sedimentares primárias é importante para a reconstituição paleogeográfica de bacias, visto que auxilia na definição de áreas de deposição preferencial e padrão de dispersão sedimentar (Potter e Pettijohn, 1977).

A análise dos padrões de dispersão possibilita delimitar espacialmente as províncias fisiográficas de um dado contexto deposicional e o sentido de influxo sedimentar, auxiliando na definição de paleolinhas de costa e no sentido de migração de dunas subaquosas.

Os dados de paleocorrentes coletados em campo foram tratados no software Rockworks®. As medidas obtidas em diferentes níveis estratigráficos estão indicadas nas colunas estratigráficas de detalhe, sendo que o padrão de dispersão dos grupos de dados é apresentado na forma de rosetas.

2.6 Análise estratigráfica

A análise estratigráfica se pautou principalmente na integração dos dados oriundos da análise de fácies sedimentares, paleocorrentes e padrões de variação dos isótopos de C e S ao longo das seções estratigráficas.

A análise integrada de associações de fácies e dos ciclos sedimentares possibilitou a caracterização dos sistemas deposicionais e padrões de empilhamento diferenciados, o que auxiliou na definição da arquitetura da sucessão. Os ciclos sedimentares são definidos como camadas, ou conjunto de camadas, geneticamente relacionadas que compõem arranjos de arquitetura progradacional, agradacional ou retrogradacional, depositados sob mesmas condições de nível de base. Para sucessões carbonáticas, os ciclos de alta frequência podem ser utilizados como análogos às parassequências em sucessões terrígenas no intuito de se comporem os tratos de sistemas (Mitchum e Van Wagoner, 1991) . A identificação do arranjo vertical e lateral destes ciclos permitiu definir pacotes depositados em diferentes ciclos de nível de base (Kerans e Tinker, 1997) e, assim, compor um arcabouço estratigráfico adequado.

A partir daí, foi priorizada a identificação de superfícies estratigráficas que possibilitassem a melhor compreensão dos padrões arquiteturais e correlação das associações de fácies entre as diferentes sucessões estudadas. Estas superfícies compreendem discordâncias regionais representativas da queda brusca do nível do mar, superfícies-chave (transgressão e máxima inundação) e variações gerais no padrão de empilhamento de ciclos de alta e média frequências. A identificação tentativa das superfícies foi realizada a partir de diversos parâmetros, tais como oscilação de espessuras das camadas, variação vertical na quantidade e espessura dos termos pelíticos, variação no modelo de associação e sucessão de fácies, alterações nas tendências de paleocorrentes, presença de depósitos de exposição subaérea e variações nos valores isotópicos de C.

Por fim, utilizou-se o método de estratigrafia de sequências, que permite interpretar espessas sucessões sedimentares do ponto de vista genético, geométrico e evolutivo, bem como efetuar correlações de diferentes sucessões em nível de bacia (Posamentier et al., 1988; Vail et al., 1991, 1977; Van Wagoner et al., 1988).

2.7 Análise de Fluorescência de Raio-X (FRX) e Difração de Raio-X

Com o intuito de se avaliar se o sinal isotópico aferido é primário (original da deposição), foram analisadas 35 amostras, abrangendo toda a sucessão da Formação Sete Lagoas. As análises de elementos maiores, menores e traço foram realizadas pelo método de Espectrometria de Fluorescência de Raios-X (FRX), utilizando-se o espectrômetro de raios-X Philips PW2400 do Laboratório de Geoquímica do Departamento de Petrologia e Metalogenia do IGCE/UNESP.

Para isso, foram utilizadas razões geoquímicas como parâmetros de identificação destas alterações, visto que a presença de fluidos durante a diagênese, dolomitização ou metamorfismo de rochas carbonáticas leva a um aumento nas razões Mn/Sr, Fe/Sr, Rb/Sr e $^{87}Sr/^{86}Sr$, bem como um descréscimo nos valores de $\delta^{13}C$ e $\delta^{18}O$ destes litotipos (Banner e Hanson, 1990). Valores de $\delta^{13}C_{carb}$ menos alterados são mais prováveis de ocorrer em amostras com Mn/Sr <10, Fe/Sr < 50 e $\delta^{18}O_{carb}$ mais negativos que -10‰ (Frimmel e Folmi, 2002). Além disso, a correlação positiva (covariação) entre os valores de $\delta^{13}C$ e $\delta^{18}O$ de uma mesma sucessão pode indicar alteração pós-deposicional da assinatura isotópica original (Derry, 2010).

2.8 Análise isotópica de C_{carb} e O_{carb}

Todos as amostras coletadas foram posicionadas estratigraficamente em seções colunares levantadas em escala de detalhe (1:50). O procedimento laboratorial para as amostras previamente selecionadas em campo envolveu primeiramente a escolha de pontos com textura original da rocha preservada por meio da análise petrográfica. Desta maneira, evitou-se as fraturas, estilolitos, vênulas e porções diagenética ou pedogeneticamente alteradas, além de exemplares ricos em terrígenos. Após esta etapa procedeu-se com a análise por catodoluminescência em amostras potencialmente diagenéticas, usando equipamento JEOL JXA 8230, equipado com 5 espectrômetros WDS e um sistema pancromático de catodoluminescência (XM-26730PCL). Segundo Hemming et al. (1989), Kaufman et al. (1993)

e Kaufman e Knoll (1995), porções não luminescentes são consideradas pouco alteradas, sendo que áreas mais claras são relacionadas à calcita neoformada em veios, estilolitos e poros, associados à presença de Mn oriundo de águas meteóricas. Após a etapa inicial de seleção de áreas adequadas à amostragem, sucedeu-se a extração com broca milimétrica de vídia de pequenas porções pulverizadas, que foram acondicionadas em recipientes herméticos individuais do tipo *Eppendorff*.

Todos os valores de isótopos estáveis de C e O estão apresentado no Apêndice I. Segundo o procedimento usual para a análise isotópica de elementos leves, conduziu-se inicialmente a extração do gás CO_2 de amostras pulverizadas a partir da reação com ácido fosfórico 100% à temperatura constante de 25ºC durante 24 ou 72 horas, dependendo da razão entre material calcítico e dolomítico. Após a extração do gás, este foi purificado criogenicamente a partir do uso de armadilha química de nitrogênio líquido e álcool, a fim de se retirar a água gerada durante a reação do carbonato e o ácido. A amostra de gás foi analisada em um espectrômetro de massa de razão isotópica com cromatografia gasosa, acoplado com o sistema *Gas Bench II*, por extração *online* (*Gas Chromatography – Isotope Ratio Mass Spectrometer*, GC-IRMS), Thermo Scientifique modelo Delta V Advantage, do Laboratório de Análise de Minerais e Rochas (LAMIR), da Universidade Federal do Paraná - UFPR. A normalização dos resultados isotópicos obtidos foi realizada mediante a técnica de dois pontos, usando padrões internacionais (NBS18 e NBS19). Os resultados, apresentados na notação per mil, apresentam referência ao padrão VPDB (Viena - "*Pee Dee Belemnite*").

No intuito de avaliar o grau de alteração diagenética e intempérica dos carbonatos coletados, o que poderia alterar os valores iniciais de $\delta^{13}C$ e $\delta^{18}O$, os dados foram analisados do ponto de vista de seus elementos maores e traço e através da relação entre os valores de $\delta^{13}C$ e $\delta^{18}O$, sendo que este último tende a decrescer na presença de águas meteóricas ou fluidos hidrotermais (Kaufman e Knoll, 1995).

2.9 Análise isotópica de S_{CAS} (Carbonate Associated Sulfate)

O sulfato associado ao carbonato (*Carbonate Associated Sulfate* - CAS) corresponde a pequenas quantidades deste elemento incorporadas na estrutura cristalina do carbonato de cálcio durante a precipitação, sendo amplamente utilizada para identificar a composição isotópica de enxofre da água do mar especialmente durante o final do Pré-Cambriano (Burdett et al., 1989; Gellatly e Lyons, 2005). Os desdobramentos da análise deste *proxy* se estendem para a aferição da variação de oxigênio atmosférico, diversificação dos eucariontes, bem como possíveis implicações tectônicas na quantidade deste isótopo na água do mar (McFadden et al. 2008).

A composição isotópica do enxofre da extração com sulfato associado ao carbonato (CAS) comumente é conduzida usando o protocolo estabelecido por Gill et al. (2011). Inicialmente, serão escolhidas amostras com a textura original da rocha preservada, evitando fraturas, estilólitos, vênulas e porções diageneticamente, ou pedogeneticamente, alteradas. Aproximadamente 100g de amostra é pulverizada e tratada com uma solução de 10% NaCl por 24h a fim de remover o sulfato ligado não-estruturalmente e o enxofre orgânico que pode contaminar o CAS. Esta etapa tem por objetivo remover sulfatos solúveis que podem estar, por ventura, presentes nas rochas. Dois enxágues com água deionizada são então realizados antes da amostra ser dissolvida utilizando-se 4N HCl (acidificação). Após a etapa de acidificação, a amostra resultante é centrifugada e filtrada à vácuo (45μm) para remover a porção insolúvel. Aproximadamente 100 ml de uma solução saturada em $BaCl_2$ são adicionados à solução que contém a amostra dissolvida para forçar a precipitação do sulfato na forma de barita. Estes precipitados de barita foram centrifugados, lavados, secados e pesados.

As amostras de $BaSO_4$ em pó foram então homogeneizadas e carregadas em cápsulas de prata com excesso de V_2O_5 e finalmente analisadas quanto às suas razões isotópicas $^{34}S/^{32}S$. As análises foram realizadas na *Virginia Polytechnic Institute and State University (Virginia Tech)*, como parte do doutorado sanduíche da autora sob supervisão internacional do Prof. Dr. Shuhai Xiao da referida instituição. Para os procedimentos de aferição das razões isotópicas de $^{34}S/^{32}S$, foi utilizado um espectrômetro de massa de razão isotópica (IRMS) equipado com um analisador elementar vario ISOTOPE Cube EA para combustão e análise de amostras online. Os resultados, apresentados na notação “per mil”, serão referentes ao padrão V-CDT (*Vienna Canyon Diablo Troilite*) e estão apresentados no Apêndice A.

3 Aspectos geoquímicos, paleontológicos, paleoclimáticos e geotectônicos do Período Ediacarano

O Período Ediacarano é caracterizado pelas mais pronunciadas mudanças climáticas, tectônicas, biogeoquímicas e evolutivas da história do planeta (Figura 3.1), destacando-se como principais eventos: (i) múltiplas glaciações globais que se estenderam até latitudes equatoriais (Fairchild e Kennedy, 2007; Hoffman et al., 1998; Hoffman e Schrag, 2002; Kaufman et al., 1997; Kirschvink, 1992; Ridgwell et al., 2003; Spence et al., 2016); (ii) precipitação carbonática sincrônica imediatamente após as glaciações globais contendo fácies sedimentares anômalas (Allen e Hoffman, 2005; Corsetti et al., 2004; Hoffman et al., 2011; James et al., 2001; Kennedy, 1996; Lamb et al., 2012); (iii) grandes variações isotópicas no clclo do carbono (Halverson et al., 2010, 2005; Kaufman e Knoll, 1995; Rothman et al., 2003); (iv) aumento nos níveis de oxigênio do sistema atmosfera-oceano (Macdonald et al., 2013; McFadden et al., 2008; Poulton et al., 2014); (v) surgimento da primeira fauna de metazoários (Canfield et al., 2007a; Corsetti et al., 2006; McFadden et al., 2008); e (vi) término do ciclo de rifteamento de Rodínia e formação de Gondwana (Hoffman, 1999).

3.1 Glaciações globais neoproterozoicas

Diversas evidências geológicas apontam que durante o Neoproterozoico ocorreram ao menos três grandes glaciações de amplitude global, compreendidas pela teoria conhecida como “*Snowball Earth”* (Kirschvink, 1992; Hoffman et al., 1998). Diamictitos glaciais supostamente depositados próximo a linha do Equador (Evans e Raub, 2011; Trindade e Macouin, 2007) ocorrem ao redor do mundo e são associados a três episódios glaciais conhecidos como Sturtiano, Marinoano e *Gaskiers* (Figura 3.1, Halverson et al., 2005). A interpretação destes depósitos glaciais como equatoriais é suportada por uma combinação de evidências sedimentológicas (diamictitos com presença de seixos estridados e múltiplas fontes de clastos) e paleomagnéticas (latitudes baixas a moderadas obtidas em pólos paleomagnéticos em que a magnetização é primária), conferindo a estes depósitos uma posição paleogeográfica relativamente confiável (Evans, 2000).

Depósitos glaciogênicos Sturtianos são reconhecidos em 14 diferentes paleocontinentes, porém há uma grande incerteza quanto à duração dos episódios glaciais quando comparado aos depósitos Marinoanos mais jovens (Hoffman e Li, 2009). Tais depósitos são representados pela Formação Sturt na Austrália (Le Heron et al., 2011), pela Formação Chuos na Namíbia (Kennedy et al., 1998), pelo Membro Scott Mountain da Formação Pocatello, oeste dos EUA

(Fanning e Link, 2004), entre outros. Já, os depósitos glaciogênicos Marinoanos ocorrem em pelo menos 15 paleocontinentes (Hoffman e Li, 2009), sendo o início e o fim desta glaciação datados em 654.5+3.8 Ma e 635.2+0.4 Ma, respectivamente. Estes depósitos correspondem aos diamictitos da Formação Ghaub na Namíbia (Hoffmann et al., 2004), da Formação Elatina na Austrália (Williams et al., 2008), da Formação Nantuo no sul da China (Zhang et al., 2008), da Formação Fiq em Omã (Allen et al., 2004), entre outros. Por fim, a última glaciação regional é denominada de *Gaskiers* e é reconhecida em pelo menos 8 paleocontinentes (Hoffman e Li, 2009), porém somente a ocorrência em Newfoundland no Canadá foi datada diretamente, obtendo-se uma idade em torno de 580 Ma. Devido esta particularidade, sua idade, duração e extensão permanecem ainda como objeto de intenso debate (Myrow e Kaufman, 2012; Pu et al., 2016; Spence et al., 2016).

Alguns destes depósitos glaciais apresentam clastos facetados e estriados e contêm estruturas de deformação possivelmente causadas por fluxo glacial (Deynoux, 1985; Hoffman e Schrag, 2002; McMechan, 2000), algumas destas unidades supostamente glaciomarinhas provavelmente representam depósitos de diamictitos formados por fluxo de massa relacionados a falhas produzidas durante os estágio finais da ruptura de Rodínia (Eyles e Januszczak, 2004; van Loon, 2008). Tal hipótese alternativa é denominada de *Zipper Rift*.

A partir de dados estratigráficos de diferentes ocorrências globais, notou-se que a maioria destes depósitos glaciais são sobrepostos por sedimentos carbonáticos e, secundariamente, pelíticos. Essa sedimentação carbonática pós-glacial é denominada de capa carbonática.

3.2 Capas carbonáticas

Capas carbonáticas são unidades contínuas de dolomitos puros (e localmente calcários), com espessuras da ordem de dezenas de metros (Corsetti e Lorentz, 2006; Hoffman et al., 2007a; Hoffman e Schrag, 2002; James et al., 2001), que sobrepõem em contato abrupto os depósitos glaciais e de fluxo de massa subaquosos relacionados à glaciações globais Neoproterozoicas. As estruturas interpretadas como representantes dos primeiros registros sedimentares dos eventos de deglaciação (capas Sturtinianas, Hoffman et al., 1998; Fairchild e Kennedy, 2007) geralmente constituem depósitos finamente laminados (localmente rítmicos), escuros, e ocasionalmente ricos em matéria orgânica e ferro.

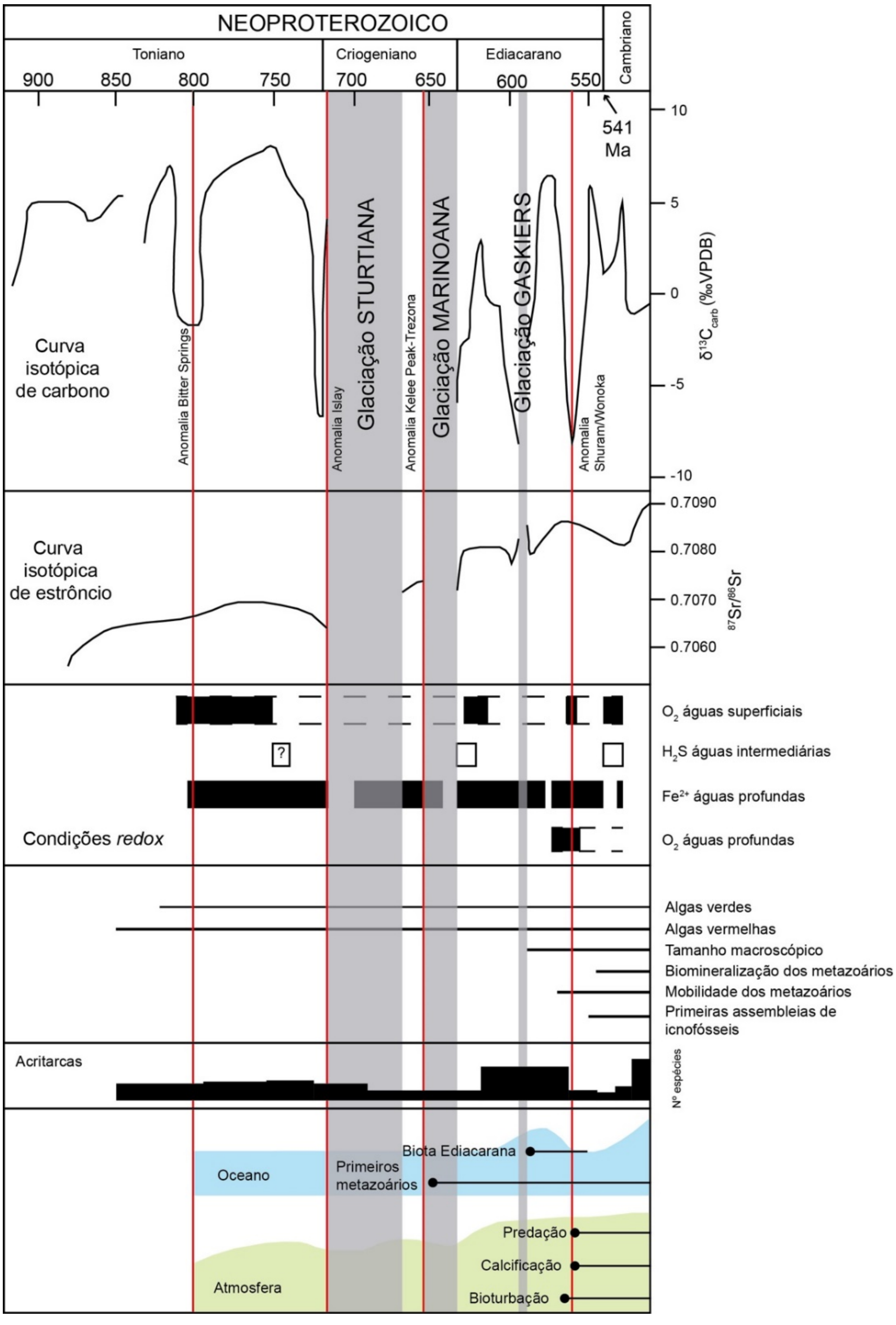

Figura 3.1: Síntese dos principais eventos tectônicos, bioevolutivos e paleoclimáticos ocorridos no final do Neoproterozoico e início do Cambriano, extraído de Spence et al. (2016). As linhas vermelhas correspondem às anomalias negativas de isótopos de carbono. Baseado em Nogueira (2003) e Warren (2011), com compilações de Canfield et al. (2008), Lenton et al. (2014), Spence et al. (2016).

Estas unidades, por vezes, contém estruturas do tipo *roll-up*, e geralmente apresentam valores de $\delta^{13}C > 0$ (Corsetti e Lorentz, 2006; Kennedy et al., 1998). As capas carbonáticas que sobrepõem diamictitos marinoanos por sua vez, são tipicamente menores que 10 m de espessura e incluem camadas constituídas por macropelóides, estromatólitos, cristais de barita e estruturas em tubo ou *tubestones* (Hoffman e Schrag, 2002; James et al., 2001; Jiang et al., 2006; Kennedy, 1996). Estas feições são comumente recobertas por carbonatos ricos em leques de cristais de aragonita e/ou por sedimento siliciclástico fino depositados em condições de água profunda.

Atualmente, três modelos não-excludentes têm sido utilizados para explicar a origem das capas carbonáticas a partir de condições geoquímicas anomalas. O primeiro assume que os altos níveis de $p$$CO_2$ atmosférica foram responsáveis pela deglaciação (modelo *Snowball Earth*), levando ao intenso intemperismo químico dos continentes e consequente aumento da alcalinidade da água do mar. A alta concentração de nutrientes e minerais dissolvidos teria então promovido a rápida precipitação de capas carbonáticas sobre depósitos interpretados como glaciais (Higgins e Schrag, 2003; Hoffman et al., 1998; Hoffman e Schrag, 2002). O segundo modelo assume que a glaciação causou uma estratificação física e criou forte gradiente isotópico de carbono da superfície até águas profundas. Neste contexto, a ressurgência ou inundação associada à transgressão pós-glacial pode ter trazido águas profundas mais alcalinas para plataformas continentais e bacias interiores (modelo de ressurgência ou *overturn*), resultando na precipitação de uma capa carbonática (Grotzinger e Knoll, 1995; Kaufman et al., 1997; Ridgwell et al., 2003). Finalmente, o terceiro modelo propõe que o frio extremo promoveu a supersaturação inorgânica do carbono no oceano (modelo de metanogênese), e a oxidação do metano poderia explicar a deposição de capas carbonáticas associadas a baixos valores isotópicos (Jiang et al., 2003; Kennedy et al., 2001).

Crostas, leques de cristais e cimentos fibrosos calcíticos, bem como pseudomorfos de aragonita, ocorrem de forma anômala nas capas carbonáticas (Grotzinger e Knoll, 1995; Pruss et al., 2008; Sumner and Grotzinger, 2004). Leques de pseudomorfos de aragonita são consideradas as fácies sedimentares mais comuns das capas e ocorrem em várias unidades ediacaranas ao redor do mundo (Corsetti et al., 2004; Hoffman et al., 1998; Hoffman e Schrag, 2002; James et al., 2001; Kennedy, 1996; Lorentz et al., 2004; Nogueira et al., 2003; Peryt et al., 1990; Pruss et al., 2008; Vieira et al., 2015). As condições ambientais que propiciaram a formação destes leques são ainda pouco compreendidas, porém é consenso que tenham se formado em águas com pH neutro a alcalino, em ambientes com baixa taxa de sedimentação e baixo aporte de material detrítico (Sumner e Grotzinger, 2004). Neste contexto, a ocorrência de leques de barita é mais restrita, ocorrendo principalmente no noroeste da África, sul da China, Austrália central, norte da Mongólia, noroeste do Canadá e agora Brasil (Crockford et al., 2017; Hoffman e Halverson, 2011; Jiang et al., 2006; Kennedy, 1996; Shields et al., 2007).

Depósitos fosfáticos que ocorrem no início do Ediacarano têm sido relacionados à atividade de comunidades microbianas em condições anóxicas (Nelson et al., 2010; Papineau, 2010), mas sua relação estratigráfica com as capas carbonáticas não é bem entendida (Hoffman et al., 2011). A formação destes fosforitos pode estar relacionada à eventos de ressurgência, à decomposição microbial de matéria orgânica dentro dos sedimentos ou mesmo o retrabalhamento de camadas fosfáticas primárias (Glenn et al., 1994). É importante ressaltar que este tipo de depósito preserva um registro excepcional de vida multicelular ediacarana, principalmente constituída por microfósseis de organismos protistas (Xiao et al., 1998, 2014b; Xiao e Knoll, 1999; Zhou et al., 2002; Uchio et al., 2008; Muscente et al., 2015).

Desta forma, os minerais eodiagenéticos e autigênicos que se formam em contexto de capa carbonática constituem evidência direta (ou indireta) da composição dos elementos dissolvidos na água dos oceanos e seu estudo pode, portanto, fornecer importante informação a respeito da composição e evolução da água do mar ao final da Era Neoproterozoica.

3.3 Assinaturas isotópicas e condições de oxigenação nos oceanos durante o Ediacarano

O aumento progressivo na razão $^{87}Sr/^{86}Sr$ nos sedimentos marinhos durante o final do Neoproterozoico e início do Cambriano indica um aumento no intemperismo químico e no aporte de nutrientes que chega aos oceanos, aumentando as taxas de soterramento de carbono orgânico e favorecendo a produtividade primária e fosfogênese (Och e Shields-Zhou, 2012; Papineau, 2010).

Excursões positivas de $\delta^{13}C$ estão comumente relacionadas ao aumento do grau de soterramento da matéria orgânica devido a altas taxas de sedimentação e/ou alta produtividade primária principalmente por organismos fitoplanctônicos. Por outro lado, variações isotópicas negativas, comuns às capas carbonáticas, estão relacionadas a mudanças paleoceanográficas significativas, interpretadas como: (i) resultado de mistura rápida por ressurgência após eventos de glaciação de águas profundas depletadas em $\delta^{13}C$ com águas rasas; (ii) diminuição da produtividade biológica (abundância de $\delta^{12}C$) relacionada à cobertura dos oceanos por lencóis de gelo, no modelo *Snowball Earth*; (iii) desestabilização de gás hidrato no *permafrost* terrestre e transgressão seguindo rápido aquecimento pós-glacial (Kennedy et al., 2001).

Vários autores compilaram curvas compostas de $\delta^{13}C$ para o Ediacarano (Halverson et al., 2010, 2005; Macdonald et al., 2013), mostrando uma ampla excursão negativa de $\delta^{13}C$ (Figura 3.1), correlacionável em várias sucessões carbonáticas ediacaranas ao redor do mundo

(Shuram em Omã, EN3 no topo da Formação Doushantuo no sul da China, Zhuya na Sibéria, Wonoka no sul da Austrália, Gametrail no noroeste do Canadá e Kanies/Mara no sul da Namíbia, Xiao et al., 2016).

Durante o final do Período Neoproterozoico, um significativo aumento nas concentrações de oxigênio na atmosfera e nos oceanos, conhecido como "*Neoproterozoic Oxygenation Event*" (NOE) pode ter estimulado a evolução dos animais multicelulares macroscópicos e a subsequente radiação dos organismos biomineralizados (Fike et al., 2006; Och e Shields-Zhou, 2012).

Com base em análises de especiação de ferro e isótopos de enxofre de sedimentos ediacaranos de água profunda em Newfoundland (Canadá), Canfield et al. (2007) propuseram que as águas profundas eram ferruginosas e anóxicas antes e durante a glaciação Gaskiers (~580Ma), porém daí em diante começam a ser oxigenadas.

Análises isotópicas de carbono (C_{carb} e C_{org}) e enxofre ($S_{sulfato}$ e S_{pirita}) do Supergrupo Huqf de idade ediacarana em Omã (Fike et al., 2006) e a Formação Doushantuo no sul da China (McFadden et al., 2008) revelaram a possibilidade de vários pulsos de oxigenação depois da glaciação Marinoana. Da mesma forma, Sahoo et al. (2016) propuseram uma série de eventos de oxigenação (OOE – sigla em inglês) nos oceanos neoproterozoicos amplamente anóxicos, com base em análises de especiação de ferro, isótopos de enxofre e enriquecimentos de elementos sensíveis à variação *redox* (U, Mo, Re, V, Cr).

Os isótopos de carbono e enxofre de diferentes seções ao longo da bacia Doushantuo indicam que o oceano no começo do Ediacarano no sul da China deve ter sido fortemente estratificado (Huang et al., 2013) com um grande reservatório de carbono inorgânico dissolvido (DIC – sigla em inglês) (Jiang et al., 2007) e um gradiente de concentração de sulfato da plataforma para a bacia profunda (Li et al., 2010; Shen et al., 2008).

Outros indicadores, como os isótopos de cromo e razões de cério, têm sido utilizados como indicadores de oxigenação. Fracionamentos positivos em isótopos de Cr ($\delta^{53}Cr > +4.9$ ‰) em formações ferríferas do Canadá indicam evidência independente para a progressiva oxigenação em águas rasas nos oceanos durante o final do Ediacarano (Frei et al., 2009). Similarmente, anomalias negativas de Ce obtidas para as formações Dengying e Yanjiahe no sul da China tembém sugerem oxigenação das águas superficiais durante a transição Ediacarano-Cambriano (Ling et al., 2013).

Por outro lado, reconstruções geoquímicas em estratos ediacaranos obtidas por Johnston et al. (2013) no noroeste do Canadá revelam condições dominantemente anóxicas para o oceano ediacarano, contrastando com a oxigenação formulada para este período. Além disso, valores negativos de $\delta^{238}U$ apresentados para os carbonatos do Grupo Nama (Namíbia) por Tostevin et al. (2019) e para a Formação Dengying (sul da China) por Zhang et al. (2018) também sugerem uma extensa anoxia em torno de ~550Ma.

Portanto, com base em diferentes indicadores geoquímicos e isotópicos, as condições *redox* da água do mar parecem ter flutuado ou serem heterogêneas de bacia para bacia durante a transição Ediacarano-Cambriano (Shen et al., 2008; Tostevin et al., 2017; Wei et al., 2019).

3.4 Inovações paleobiológicas, paleoecológicas e evolutivas no Ediacarano

O Ediacarano figura entre o período geológico do planeta em que se processaram as mais profundas inovações do ponto de vista evolutivo e biológico, principalmente marcadas pelo surgimento dos metazoários (Xiao e Laflamme, 2009; Wood, 2011). Três grandes assembleias de macrofósseis ediacaranos têm sido reconhecidas em todo o mundo, *Avalon*, *White Sea* e *Nama* e representam três diferentes estágios evolutivos da denominada Biota de Ediacara. A assembleia *Avalon* (575-560Ma) é caracterizada pela presença de rangeomorfos e formas cosmopolitas, como *Charniodiscus* (Clapham et al., 2003; Clapham e Narbonne, 2002), que viviam em ambiente de água profunda e afóticas após a glaciação Gaskiers (Narbonne e Gehling, 2003). A assembleia *White Sea* (560-550Ma) contém a maior diversidade taxonômica e os primeiros traços não-ambíguos feitos por animais (Jensen et al., 2006) e é notadamente reconhecida nas montanhas Flinders na Austrália e na localidade do Mar Branco na Federação Russa.

A assembleia *Nama* (550-541Ma) inclui vários rangeomorfos e ernietomorfos (Grazhdankin e Seilacher, 2005, 2002; Narbonne et al., 1997), além dos representantes biomineralizados mais antigos. Metazoários esqueletais do final do Ediacarano são representados por tubos (Grant, 1990), microfósseis possivelmente silicosos (Gehling e Rigby, 1996; Kontorovich et al., 2008) e animais com carapaças calcárias (Grant, 1992; Grotzinger et al., 2000; Wood et al., 2002). Organismos calcificados incluem *Cloudina* (Germs, 1972), *Namacalathus* (Grotzinger et al., 2000), *Namapoikia* (Wood et al., 2002) e alguns outros táxons problemáticos (Zhuravlev et al., 2011) de afinidade incerta, mas provavelmente representantes de *Eumetazoa*, *Cnidaria* ou *Bilateria* (Bengtson and Morris, 1992; Kruse et al., 1995). Todos são organismos bentônicos sésseis que viveram em ambientes carbonáticos marinhos rasos equatoriais e têm sido descritos globalmente em localidades como Sibéria, China, Omã, Brasil, Espanha, Paraguai e Namíbia (Grant, 1990; Grotzinger et al., 2000; Morris et al., 1990; Warren et al., 2011; Wood et al., 2002; Yuan et al., 2005; Zhuravlev et al., 2011).

Outra inovação paleobiológica marcante foi o aparecimento de organismos bioturbadores durante a transição Ediacarano-Cambriano, que transformou o fundo oceânico, permitindo a oxigenação do substrato na chamada Revolução Agronômica (Buatois e Mángano, 2018; Jensen, 2006; Figura 3.1).

4 Contexto geológico regional

O Grupo Bambuí é o registro sedimentar de uma extensa plataforma epicontinental siliciclástico-carbonática desenvolvida sobre o Cráton São Francisco ao final da Era Neoproterozoica (Alkmim et al., 1993; Martins-Neto, 2009; Alkmim e Martins-Neto, 2012). Localiza-se na porção centro-leste do Brasil e compreende uma extensa cobertura plana em contato erosivo com as rochas do embasamento Paleoproterozoico e Arqueano do Cráton São Francisco e encontra-se delimitado pelas Faixas Araçuaí e Brasília nas porções leste e oeste, respectivamente (Figura 2.2). Próximo à estes limites, a sucessão sedimentar apresenta algum metamorfismo e intensa deformação, caracterizada pela presença de dobras localmente com flanco invertido e falhas inversas (Alkmim et al., 2006, 1996; Coelho et al., 2008; Marshak e Alkmim, 1989).

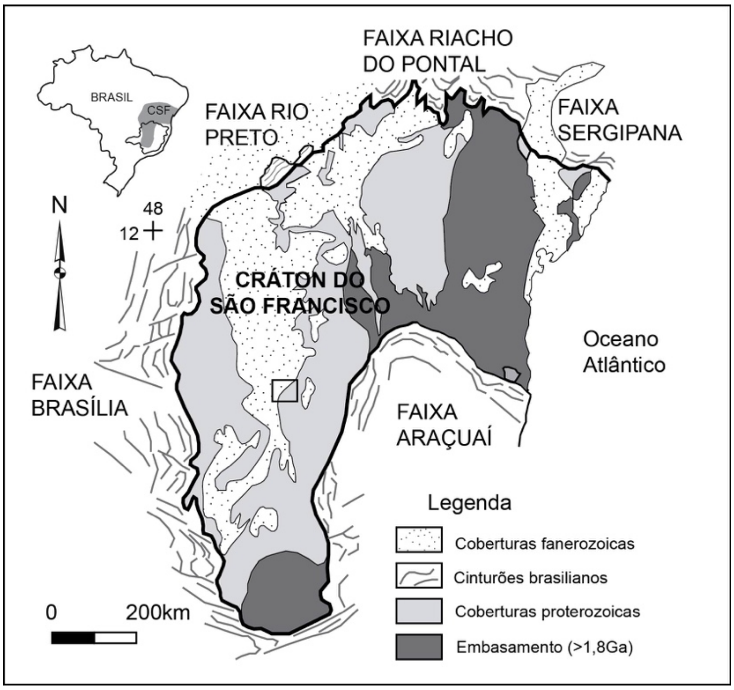

Figura 2.2: Mapa da localização do Cráton do São Franscisco e das faixas móveis Brasília e Araçuaí. Fonte: Alkmim and Martins-Neto (2001).

Historicamente, o Grupo Bambuí tem sido interpretado como depositado supostamente em uma bacia tipo *foreland*, associada ao desenvolvimento orogênico da Faixa Brasília (Alkmim e Martins-Neto, 2001; Castro e Dardenne, 2000; Chang et al., 1988; Dardenne, 2000; Guimarães, 1997). Segundo Martins-Neto e Alkmim (2001), um contexto de bacia de *foreland* é suportado: (i) pela geometria da bacia de acordo com os perfis sísmicos regionais (Romeiro-Silva e Zalán, 2005), nos quais os depósitos do Gr. Bambuí constituem uma cunha com espessuras significativas a oeste (Faixa Brasília) e pouco expressivas a leste (Faixa Araçuaí); (ii) pelo imbricamento tectônico entre fatias da Faixa Brasília e depósitos Bambuí sintectônicos de derivação local (Castro, 1997; Valeriano, 1992); (iii) pela distribuição regional de sistemas deposicionais e dispersão de sedimentos (Castro e Dardenne, 2000; Castro, 1997; Chiavegatto, 1992); e (iv) por estudos de proveniência que indicam fontes mistas (plutônicas, vulcânicas e metamórficas), derivadas da erosão de um orógeno em evolução (Castro e Dardenne, 2000; Dardenne, 2000; Uhlein et al., 2017).

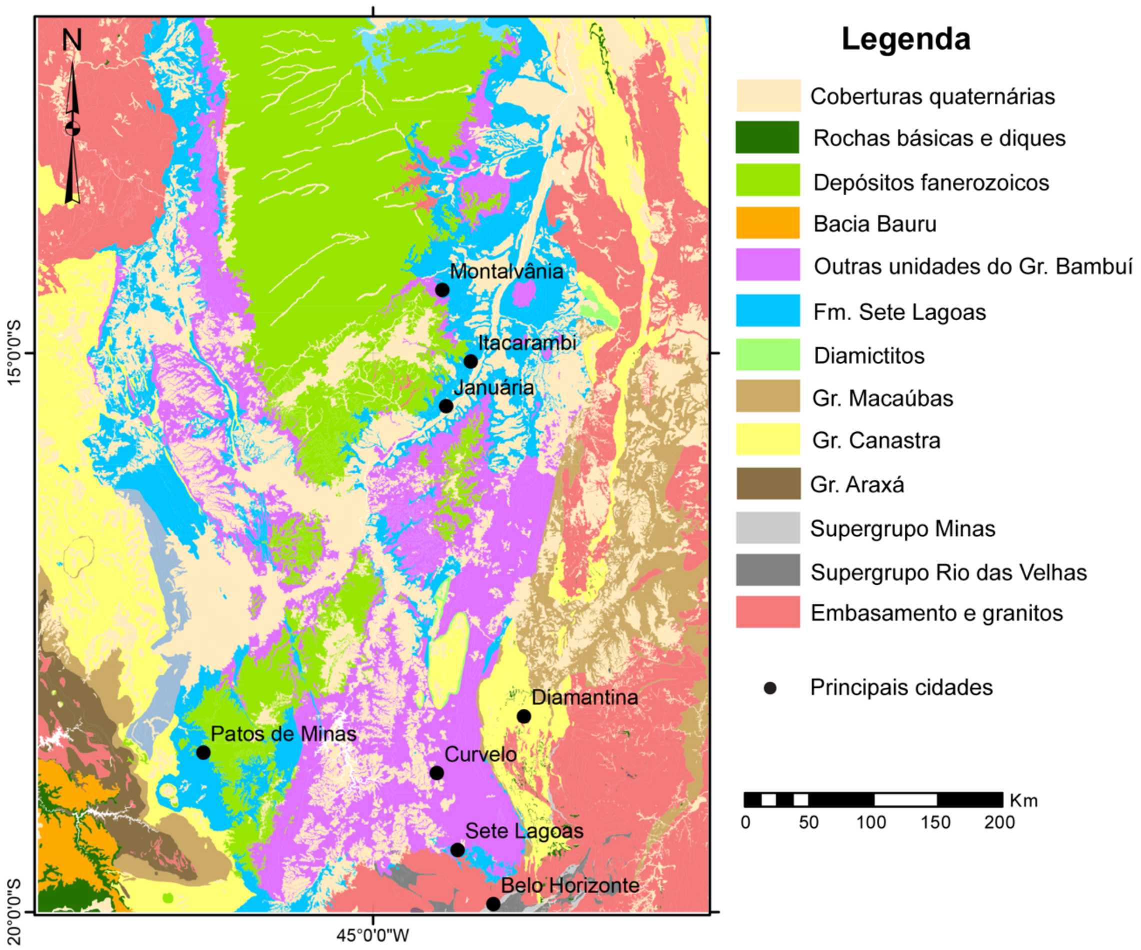

Figura 3.3: Mapa geológico simplificado do cráton São Francisco. Compilado do banco de dados da CPRM (Geobank).

Romeiro-Silva e Zalán (2005) e Martins e Lemos (2007) interpretam que o Grupo Bambuí apresenta características de bacia intracratônica em sua base, transicionando para uma bacia *foreland* apenas nas unidades superiores. Um dos argumentos aventados por estes autores é a correlação das sucessões estratigráficas ao longo de várias centenas de quilômetros (Sial et al., 2016). Contudo, segundo Romeiro-Silva e Zalán (2005), não há espessamento significativo desta unidade neoproterozoica de leste para oeste, nem variações faciológicas nítidas (sísmicas ou reconhecidas em campo) que permitam considerar o Grupo Bambuí uma sequência de antepaís, depositada concomitantemente com a deformação do Ciclo Orogênico Brasiliano e sob sua influência. Fatores impeditivos à hipótese de deposição em bacia do tipo *foreland* ainda incluem evidências paleontológicas e geocronológicas (Warren et al., 2014; Paula-Santos et al., 2015) que indicam que as rochas da base do Grupo Bambuí teriam sido depositadas ao final do Ediacarano e, portanto, muito após o pico de atividade tectônica das faixas móveis Brasilia e Araçuaí. Deste modo, evidências recentes indicam que, a priori, não existe relação de causa e efeito entre a atividade orogênica das faixas móveis marginais e ciclos de subsidência e deposição da Bacia Bambuí durante o Neoproterozoico.

Litoestratigrafia

A subdivisão estratigráfica clássica, e mais usual, do Grupo Bambuí foi proposta por Dardenne (1978). Litoestratigraficamente, o Grupo Bambuí tem aproximadamente 700 metros de espessura, alcançando localmente 1000 m (Misi et al., 2007), e compreende carbonatos e dolomitos da Formação Sete Lagoas (a qual será detalhada na seção 4.1) na base que grada em direção ao topo para folhelhos e siltitos da Formação Serra de Santa Helena. Esta unidade é coberta por margas, siltitos, carbonatos e arenitos das formações Lagoa do Jacaré, Serra da Saudade e Três Marias (Figura 3.4). Algumas modificações foram feitas nos últimos anos neste esquema, atribuíndo algumas unidades que representam variações laterais das unidades inicialmente descritas e que não ocorrem em toda a extensão do Cráton São Francisco (e.g., Lagoa Formosa e Gorutuba, Uhlein et al., 2011b; Kuchenbecker et al., 2016).

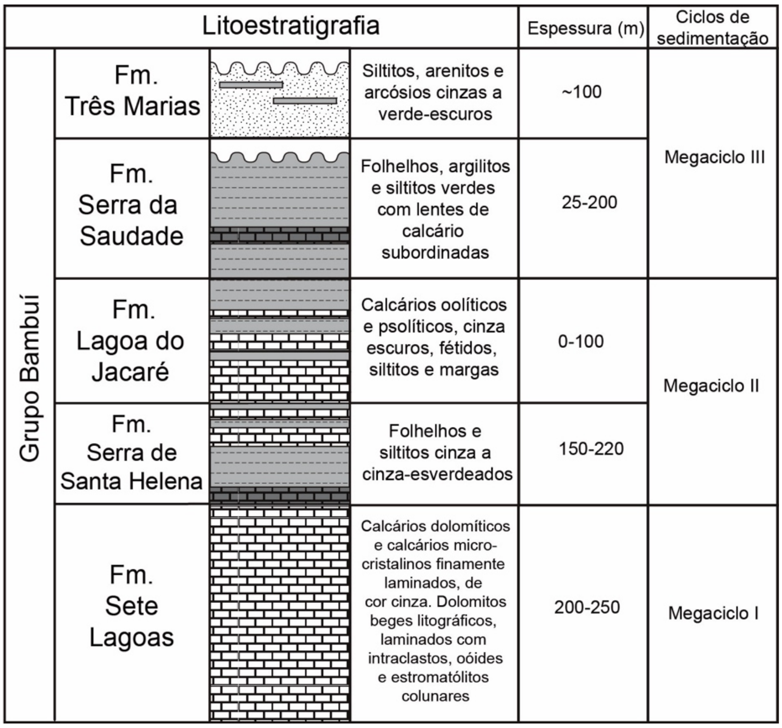

Figura 3.4: Coluna estratigráfica do Grupo Bambuí (baseado em Dardenne, 1978). Espessuras compiladas por Lima (2005) e os ciclos de sedimentação segundo Dardenne (1978), Martins (1999) e Martins-Neto e Alkmim (2001).

As unidades do Grupo Bambuí assentam-se diretamente em contato erosivo sobre rochas granito-gnáissicas do embasamento arqueano/paleoproterozoico, rochas glaciogênicas ou rochas metassedimentares. As unidades glaciogênicas presentes no Cráton São Francisco correspondem à Formação Jequitaí, Formação Carrancas e Grupo Macaúbas. A Formação Jequitaí é constituída por diamictitos intercalados por arenitos e pelitos de origem glacial e ocorre principalmente na região da Serra do Cabral e Serra da Água Fria (MG) e nas imediações da Faixa Brasília (Alvarenga et al., 2012; Uhlein et al., 2011a, 2004). Composta por conglomerados, siltitos, ritmitos e raros dolomitos, a Formação Carrancas foi inicialmente definida por Costa e Branco (1961) como um Membro dentro da Formação Sete Lagoas, devido ao seu caráter descontínuo. Posteriormente, revista por outros autores ao longo dos últimos anos, foi elevada à hierarquia de Formação Carrancas e posicionada na base do Grupo Bambuí meridional (Uhlein et al., 2011b).

Algumas unidades, como as formações Samburá (conglomerado e arenito) e Lagoa Formosa (conglomerado, siltito, calcário e jaspilito) ocorrem apenas na porção oeste da bacia (Uhlein et al., 2011c), enquanto que os calcários da Formação Jaíba afloram exclusivamente na porção leste da bacia (Chiavegatto et al., 2003) e representam provavelmente uma plataforma carbonática localizada (Uhlein et al., 2019).

A Formação Serra de Santa Helena é composta por siltitos e argilitos com arenitos e lentes carbonáticas subordinadas. Fluxos gravitacionais sub-aquosos de baixa densidade relacionados à atuação de correntes de turbidez e retrabalhamento por ondas de tempestade são os principais mecanismos deposicionais associados à esta unidade (Lima, 2005). A Formação Lagoa do Jacaré compreende *grainstones* oolíticos a pisolíticos cinza-escuros a pretos, localmente com estratificação cruzada tipo *hummocky* e intercalado com folhelhos e margas.

A Formação Serra da Saudade é dominada por folhelhos e siltitos, estes últimos podem ocorrer como laminados esverdeados ricos em glauconita e com teor de K_2O de cerca de 15% ou localmente fosfáticos (7-20% P_2O_5). Localmente, os diamictitos, siltitos, arenitos, jaspilitos e carbonatos da Formação Lagoa Formosa, aflorantes em grande parte do limite meridional sudoeste do Cráton São Francisco, representam uma variação lateral da Formação Serra da Saudade (Uhlein et al., 2011c) e representa leques clásticos provenientes das frentes de empurrão da Faixa Brasília (Castro e Dardenne, 2000; Seer et al., 1987; Uhlein et al., 2011c, 2017).

A Formação Três Marias é composta por arenitos finos, quase sempre feldspáticos ou líticos, com laminações e estratificações cruzadas, estratificação *hummocky*, bem como dobras convolutas, marcas onduladas e gretas de contração (Chiavegatto, 1992). A deposição da Formação Três Marias ocorreu em ambiente deltaico e fluvial a leste e em ambiente plataformal, com ação de ondas de tempestade, a oeste (Chiavegatto, 1992; Lima, 2005), e representa o assoreamento final da Bacia Bambuí. Lateralmente à esta unidade, foi definida recentemente a Formação Gorutuba, que apresenta em sua parte basal uma brecha composta por clastos de calcário imersos em matriz arcoseana. Arenitos arcoseanos com estratificações cruzadas acanaladas tornam-se predominantes em direção ao topo, bem como eventuais lentes de conglomerado e pelito. Tal unidade possivelmente registra um período de soerguimento, exposição e erosão da extensa plataforma marinha representada pelo Grupo Bambuí (Kuchenbecker et al., 2016a).

4.1 Formação Sete Lagoas

A Formação Sete Lagoas é a unidade basal do Grupo Bambuí e é basicamente constituída por carbonatos e pelitos subordinados (Dardenne, 1978; Vieira et al., 2007a). Tal unidade repousa em discordância sobre o embasamento granito-gnáissico e, localmente sobre os diamictitos das formações Carrancas e Jequitaí (Dardenne, 1978). Dois importantes altos do embasamento ocorrem no compartimento central do Cráton do São Francisco (Figura 3.5): o

Alto de Sete Lagoas (a sul), no qual a área-tipo da unidade foi descrita, e o Alto de Januária (a norte), que engloba a área estudada.

Schöll (1976) subdividiu a Formação Sete Lagoas em dois membros, da base para o topo: (i) Membro Pedro Leopoldo, com espessura de 40 a 100 m, sendo constituído por margas e calcários impuros e calcários dolomíticos impuros que gradam para siltitos e filitos em direção à borda da bacia; e (ii) Membro Lagoa Santa, com espessura de 100 a 150 m, sendo constituído por calcários puros, com matéria orgânica e laminação rítmica. Esta descrição, embora muito utilizada em trabalhos de mapeamento, dificulta a interpretação mais detalhada dos aspectos sedimentológicos e estratigráficos que possibilitem uma ampla correlação da unidade.

Em sua área-tipo ou seção-tipo (proximidades da cidade homônima a sul do Estado de Minas Gerais), Vieira et al. (2007a, b) estimaram a espessura da Formação Sete Lagoas em 200 m, organizadas em duas sequências deposicionais em uma rampa carbonática homoclinal com conexão oceânica supostamente para oeste. A sequência basal inicia-se com os precipitados de fundo oceânico (pseudomorfos de aragonita), cujos valores de $\delta^{13}C$ negativos chegam a -4,5‰. Tais fácies são interpretadas como capa carbonática na acepção clássica de Hoffman e Schrag (2002). No topo desta sequência basal, ocorrem depósitos carbonáticos sustentados por grãos com laminação planar, por vezes *hummocky*, que gradam lateralmente para calcários com laminação planar, que podem apresentar estruturas heterolíticas e *climbing ripples*. Estas fácies são interpretadas como depositadas, respectivamente, em rampa dominada por tempestade e rampa dominada por maré, apresentando valores de $\delta^{13}C$ próximos à 0‰. A segunda sequência inicia-se com ritmitos de calcário com pelitos que gradam em direção ao topo para calcários negros com laminação planar ou truncada de baixo ângulo, depositados em rampa profunda. O início desta segunda sequência é caracterizado por um pronunciado salto isotópico na curva de $\delta^{13}C$ de valores levemente positivos para valores da ordem de +8‰. No topo desta sequência, calcários negros com laminação truncada e presença de estromatólitos depositados em rampa dominada por ondas, gradam lateralmente para calcários negros com laminação convoluta, indicando inclinação pronunciada do substrato. Os valores de $\delta^{13}C$ neste intervalo são amplamente positivos e podem chegar até 14‰ (Vieira et al., 2007b). Alguns autores como (Martins e Lemos, 2007; Romeiro-Silva e Zalán, 2005; Vieira et al., 2007a) sugerem uma discordância na porção média da Formação Sete Lagoas, dividindo-as nas duas sequências supracitadas.

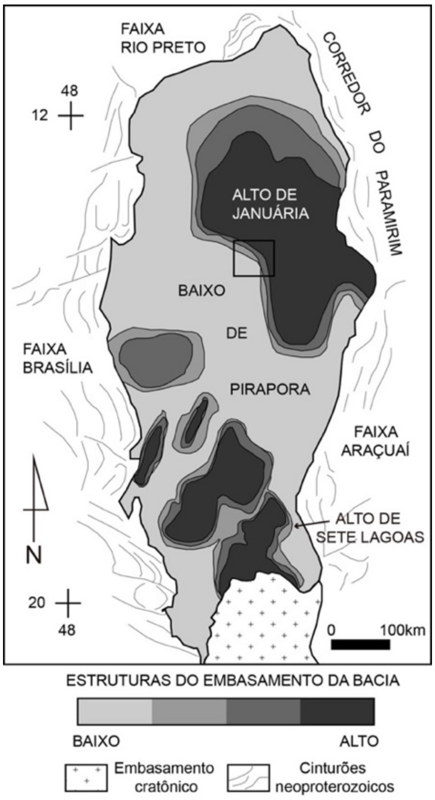

Figura 3.5: A) Mapa esquemático da bacia Bambuí mostrando a distribuição de altos e baixos do embasamento. (Fonte: Alkmim & Martins-Neto, 2001). O retângulo representa a localização da área estudada.

Abreu Lima (1997) e Nobre-Lopes (2002) estudaram os carbonatos da Formação Sete Lagoas na região norte de Minas Gerais. Nobre-Lopes (2002) abordou as relações existentes entre as mineralizações de Zn/Pb e as rochas encaixantes da Formação Sete Lagoas na região de Januária, focando principalmente na evolução diagenética dos carbonatos desta unidade e subdividindo a unidade em sete litofacies (ou membros informais), a saber:

(i) Dolomito basal: esta fácies é representada por dolomito rosa, laminado (Abreu-Lima, 1997), intercalado com níveis mais calcíticos, alcançando uma espessura de até 5 m;

(ii)) Calcários argilosos: calcários argilosos, roxos, microcristalinos, freqüentemente dolomíticos, finamente laminados, sendo o limite das camadas delimitado por filmes argilosos verdes. A espessura desta litofácies foi estimada em 20 metros;

(iii) Calcários escuros: São calcários finamente cristalinos, bem estratificados, com bancos variando de 5 a 40 cm. São comuns interestratificações argilosas rosadas, assim como horizontes e nódulos de chert preto. Gretas de contração, marcas onduladas e estratificações tipo *hummocky* foram observadas nestes calcários. Esta litofácies apresenta grande continuidade ao longo das serras de Januária e Itacarambi e sua espessura foi estimada em cerca de 80 metros;

(iv) Calcirruditos: caracterizada por apresentar brechas intraformacionais com fragmentos de forma lamelar (0,5 a 15 cm), matriz cinza (calcítica) e rósea (magnesiana). Segundo Nobre-Lopes (2002), os intervalos de brecha podem formar ciclos gradacionais centimétricos a decimétricos e apresentar intraclastos maiores na base e menores no topo, passando, para camadas com laminação plano-paralela. Esta litofácies alcança até 15 metros de espessura;

(v) Calcarenito dolomítico: é constituída por calcarenitos dolomíticos rosados ou cinza-claros, oolíticos, apresentando por vezes, intercalações de níveis intraclásticos. Os calcarenitos quando róseos, são dolomíticos e exibem textura sacaróide, enquanto que as porções de cor cinza são calcíticas e finamente cristalinas. Estes calcarenitos são bem laminados e apresentam frequentes estratificações cruzadas de baixo ângulo. Pode alcançar até 30 metros de espessura;

(vi) Dolomito rosado: dolomito rosado, localmente cinza, sacaróide, vacuolar e localmente silicoso, com estratificações cruzadas geralmente muito afetadas pela dolomitização e brechação. No topo deste nível, ocorre a maioria das mineralizações de Pb-Zn exploradas na região. Nobre-Lopes (2002) dividiu estes dolomitos em três subunidades informais: dolomito, dolomito estromatolítico e dolomito oolítico e intraclástico, alcançando uma espessura estimada de 50 metros;

(vii) Dolomito bege: unidade constituída por dolomitos cinza claros a beges, laminados, organizados em camadas de 0,40 a 1,5m. Localmente podem apresentar estruturas microbianas e estromatólitos associados. A espessura média desta unidade é superior a 30 metros.

Na região de Januária, o contato da Formação Sete Lagoas com a Formação Serra de Santa Helena é concordante e transicional, sendo representado pelo aumento gradual do conteúdo de pelitos nos carbonatos de topo da unidade, passando para margas cinza-esverdeadas da base da Formação Serra de Santa Helena.

Quanto à arquitetura geral da sucessão da Formação Sete Lagoas, Abreu-Lima (1997) e Dardenne (1972) sugerem que esta represente, pelo menos, um ciclo regressivo terminando nos dolomitos rosa sacaroidais da litofácies 6 de Nobre-Lopes (2002). Para esta autora, a Fm. Sete Lagoas é composta por sucessões do tipo *shallowing-upward*, em que cada topo de ciclo é interpretado como depositado em águas cada vez mais rasas.

De um modo geral, as formações que constituem o Grupo Bambuí compõem dois ciclos de sedimentação carbonática e pelítica-psamítica, representativas de três ciclos de sedimentação regressiva num contexto de ambiente marinho raso (Alkmim e Martins-Neto, 2001; Dardenne, 1978; Martins, 1999; Figura 5). Na porção leste, o primeiro megaciclo inicia-se com uma sucessão de calcilutitos dolomíticos e ritmitos carbonáticos jazem ora sobre o embasamento granítico-gnáissico ora sobre os diamictitos Carrancas, caracterizando a base do primeiro megaciclo neste domínio. O topo do primeiro megaciclo é representado por calcarenitos e calcissiltitos cinza escuros de água rasa portadores de estromatólitos.

De acordo com os autores supracitados, o segundo megaciclo inicia-se com folhelhos da Formação Serra de Santa Helena, que mostram uma tendência de aumento progressivo do retrabalhamento por ondas de tempestade, da proporção siltítica e da intercalação de lentes e camadas silto-arenosas em direção ao topo. Calcarenitos oolíticos e oncolíticos de águas rasas intensamente retrabalhados por ondas da Formação Lagoa do Jacaré completam o segundo megaciclo. Sucessões em *shallowing upward* de ordem hierárquica inferior ocorrem bem desenvolvidas na transição de águas profundas para águas rasas (zona de transição entre as formações Serra de Santa Helena e Lagoa do Jacaré).

O terceiro megaciclo inicia-se com os pelitos da Formação Serra da Saudade, terminando com os depósitos da Formação Três Marias. Ao contrário dos megaciclos anteriores, o sistema de topo deste megaciclo (Formação Três Marias) não contém calcários, sendo caracterizado por arcóseos, arenitos e conglomerados de origem marinha rasa a fluvial (Chiavegatto, 1992).

4.1.1 Idade dos depósitos carbonáticos

A idade de deposição do Grupo Bambuí tem sido tópico de ampla discussão e constitui uma questão importante para a correta correlação das sucessões neoproterozoicas do SW de Gondwana, tais como os grupos Corumbá (Brasil), Itapucumi (Paraguai), Arroyo del Soldado (Uruguai), Sierras Bayas (Argentina) e Nama (Namíbia). A determinação de idades precisas dos depósitos ediacaranos na Formação Sete Lagoas é dificultada pela aparente ausência de níveis de tufos vulcânicos, que poderiam fornecer idades de deposição confiáveis para os depósitos glaciais e capas carbonáticas associadas. Trabalhos recentes concordam em considerar as rochas da base da Formação Sete Lagoas como depositadas em contexto de capa carbonática pós-glacial, apesar de discordarem quanto à idade dos depósitos glaciais cobertos por elas, se Sturtiana (Babinski et al., 2012, 2007; Vieira et al., 2007b) ou Marinoana (Caxito et al., 2012; Okubo et al., 2018).

Rodrigues (2008) e Pimentel et al. (2011) dataram zircões detríticos coletados na transição entre as formações Sete Lagoas e Serra de Santa Helena em 610 Ma, indicando uma possível discordância, com um hiato de aproximadamente 120 Ma separando os carbonatos de capa marinoanos do restante da Formação Sete Lagoas. Zircões de cerca de 540-510 Ma também têm sido encontrados nas formações Sete Lagoas e Serra de Santa Helena (Paula-Santos et al., 2015; Pimentel et al., 2011), o que reforça a idade Ediacarana terminal para, ao menos parte da sucessão. Na borda oeste do cráton do São Francisco, idades K-Ar das rochas das *nappes* da Faixa Brasília que cavalgam as unidades inferiores do Grupo Bambuí, sugerem uma idade mínima de deposição para as mesmas em torno de 567 Ma (Valeriano et al., 2000). Já na borda leste, a sucessão inteira do Grupo Bambuí é afetada pela deformação vergente para oeste da Faixa Araçuaí, cujo pico metamórfico foi atingido em torno de 575 Ma (Silva et al., 2011).

O trabalho de Sanchez (2014)**,** reuniu e discutiu as principais ocorrências paleontológicas encontradas na Formação Sete Lagoas (Sommer, 1971, 1982, 1981; Simonetti e Fairchild, 1989; Hidalgo, 2007; Warren et al., 2014). No entanto, a reinterpretação e o correto posicionamento estratigráfico destes fósseis interpretados originalmente como pertencentes genericamente ao Grupo Bambuí, levou ao entendimento de que alguns destes de fato ocorriam em unidades por vezes mais antigas do que a Formação Sete Lagoas (grupos Macaúbas e Paranoá), ou penecontemporâneas, mas com outro contexto deposicional (Grupo Una). Independentemente deste fato, a presença de microbialitos, como *Conophyton*, esteiras microbiais silicificadas e raros microfitólitos e algas fossilizadas na Formação Sete Lagoas não contribuem com uma determinação precisa da idade (Fairchild e Subacius, 1986; Marchese, 1974; Nobre-Lopes e Coimbra, 2000). Microfósseis, como cianobactérias filamentosas e cocoidais encontradas em camadas de sílex, também não apresentam qualquer significado bioestratigráfico (Fairchild et al., 1996). Uma exceção, ainda que inconclusiva, é uma espécie tentativamente identificada como acritarca planctônico com ornamentações e espinhos da Formação Sete Lagoas, que sugere idade presumivelmente Ediacarana para a base do Grupo Bambuí (Cruz e Nobre-Lopes, 1992; Hidalgo, 2007).

A recente descoberta do fóssil-guia *Cloudina* da Fm. Sete Lagoas representa um dado bioestratigráfico robusto e assegura uma idade entre 550-542 Ma ao menos para a porção média da Formação Sete Lagoas (Warren et al., 2014). Recentemente, Linnemann et al. (2019) propuseram que a biozona da Cloudina se estenderia até 538 Ma. Neste sentido, a ocorrência de *Cloudina* e a datação de zircões detríticos com idades mais jovens que 560Ma (Paula-Santos et al., 2015), constituem as evidências mais fortes de idade Ediacarana Terminal para a base do Grupo Bambuí.

5. "Sedimentary evolution and integrated high-resolution geochemistry (C, O and S) of the Sete Lagoas Formation, Bambuí Group (northern Minas Gerais State, Brazil)" a ser submetido para o periódico *Precambrian Research*

Okubo, J.[a], Warren, L.W.[a], Xiao, S.[b], Marroquín, S.[b], Bahniuk, A.[c], Uhlein, G.J.[d], Assine, M.L.[a]

[a] Department of Applied Geology, Institute of Geosciences and Exact Sciences, São Paulo State University (Unesp), Rio Claro-SP, Brazil
[b] Department of Geosciences, Virginia Tech, Blacksburg, Virginia 24061, USA
[c] Universidade Federal do Paraná, UFPR, LAMIR, Rua Francisco. H. dos Santos, 100, Curitiba, PR, Brazil
[d] Centro de Pesquisas Manoel Teixeira da Costa, Instituto de Geociências, Universidade Federal de Minas Gerais, Campus Pampulha, Av. Antônio Carlos 6627, 31270-901 Belo Horizonte, MG, Brazil

Nas últimas décadas, a Formação Sete Lagoas, tem sido extensivamente estudada do ponto de vista de seus aspectos quimioestratigráficos, paleomagnéticos, tectônicos e geocronológicos. No entanto, informações detalhadas acerca da estratigrafia e sedimentologia desta unidade (incluindo dados paleontológicos) ainda são bastante escassos, especialmente na porção norte da Bacia Bambuí.

Devido à excelente exposição das rochas na região de Januária (norte do Estado de Minas Gerais), ampla continuidade em área e grande variedade de fácies sedimentares carbonáticas, a Formação Sete Lagoas constitui nesta localidade uma unidade ideal para a aquisição de dados de cunho estratigráfico, sedimentológico e geoquímico. Deste modo, procedeu-se um estudo voltado a compreensão dos padrões sedimentares e paleoambientais que condicionaram a deposição da Formação Sete Lagoas nesta porção da Bacia Bambuí. Este estudo foi embasado por descrições de facies sedimentares, (posteriormente relacionadas em associações de facies), reconhecimento de padrões arquiteturais e superfícies de correlação estratigráfica, paleocorrentes e dados isotópicos de C, O e S. Neste sentido, são apresentados dados inéditos de isótopos de enxofre que possibilitaram determinar as condições *redox*, estratificação da água e influência tectônica no ambiente marinho interior em que se depositou a Formação Sete Lagoas.

O resultado desta abordagem integrativa foi um modelo deposicional inédito coerente com toda a sucessão da Formação Sete Lagoas na área de estudo, bem como inferências importantes quanto aos parâmetros paleoambientais então atuantes durante o Ediacarano na porção SW do proto-supercontinente Gondwana.

Abstract

Large excursions in $\delta^{13}C$ and $\delta^{34}S$ are found in sedimentary succesions from the Ediacaran Period that may provide detailed mechanistic information about oxidation of Earth's surface, variations in the carbon cycle and climatic conditions. However, poor stratigraphic resolution and diagenetic concerns have thus far limited the interpretation of these records. Here we present an integrated sedimentological, stratigraphic and new $\delta^{13}C$ and $\delta^{34}S$ isotopic data of the Sete Lagoas Formation (SLF), Bambuí Group at Januária region (northern of Minas Gerais State, Brazil), central part of the São Francisco Craton. Eighteen sedimentary facies were described and grouped into five facies associations, from base to top: cap dolostone, peritidal carbonates, seismic-influenced carbonate ramp, oolitic belt and microbialitic tidal flat. Clast measurements of the flat-pebble breccia and paleocurrent data allow us to interpret a NE paleoshoreline. The entire sedimentary succession consists of two depositional sequences deposited in a large rimmed carbonate ramp open to the ocean southeastward. The basal sequence (S1) comprises a cap dolostone deposition related to a rapid transgression (TST1), where seafloor precipitates, like carbonate fans and void-filling barite, represent the maximum flooding surface (MFS). The presence of seafloor precipitates both in and out the regional basement high and the increase in thickness towards E-NE indicate the basin depocenter and thus, an area characterized by more pronounced subsidence rate. In this context, the peritidal facies represent a highstand system tract (HST1) that culminate with the deposition of the very shallow flat-pebble breccia facies. A second transgressive system tract (TST 2) begins with the deposition of ooid shoals and domal stromatolites, representing a relatively deepening in water depth (MFS 2). The third transgressive system tract (TST 3) is bounded at the base by a karstic surface (SB3), which constitutes a regional unconformity, followed by tidal deposits that grades to the fine siliciclastic succession of the Serra de Santa Helena Formation. Sulfur and carbon isotopic excursions are coupled, but concentration of carbonate-associated sulfate (CAS) shows an inverse pattern. Using different depositional rates and age uncertainties, we estimated the minimum and maximum sulfate reservoir size of the lower SLF, suggesting an oxygenation peak just above the cap dolostone, followed by a widespread low sulfate, which is consistent to previous estimates for the Ediacaran sulfate reservoir.

5.1 Introduction

Integrated sedimentological, stratigraphic, paleontological and geochemical studies of terminal Ediacaran carbonate successions records have been widely employed to understand environmental changes coincident with the origination and evolution of complex animals (Cui et al., 2016; Hall et al., 2013; Smith et al., 2016), the redox conditions of the oceans (Hurtgen et al., 2006; Johston et al., 2013) and the origin and significance of isotopic anomalies (Cui et al., 2017; Loyd et al., 2013; Macdonald et al., 2013; Zhu et al., 2013).

In the past few decades, the Bambuí Group, particularly the Sete Lagoas Formation, has been extensively studied, concerning mainly chemostratigraphic (Alvarenga et al., 2004; Guacaneme et al., 2017; Kuchenbecker et al., 2016; Paula-Santos et al., 2017; Santos et al., 2004; Uhlein et al., 2019), paleomagnetic (D'Agrella-Filho et al., 2000; Raposo et al., 2006), tectonic (Reis et al., 2017; Reis and Suss, 2016; Uhlein et al., 2017) and geochronological aspects (Paula-Santos et al., 2015). Paleontological data are still scarce in the Sete Lagoas Formation, relying mostly in the Ediacaran index fossil *Cloudina* (Warren et al., 2014, Perrella Jr. et al., 2017) and some sparse microfossil data (Simonetti and Fairchild, 2000). Recently, redox proxies, such as chromium isotopes, rare-earth elements and redox-sensitive elements, have been used to infer seawater conditions following the Marinoan glaciation (Caxito et al., 2018; Paula-Santos et al., 2018; Hippertt et al., 2019), trying to define the onset of more complex life and ecologies in this basin. However, the analysis of the available literature reveals that the vast majority of geochemical data is focused on the analysis, in greater or lesser detail, of carbon and oxygen isotope data from southern and/or northern part of the Bambuí basin area (see Fig. 1, Alvarenga et al., 2014; Guacaneme et al., 2017; Paula-Santos et al., 2017; Perrella et al., 2017; Uhlein et al., 2019; Caetano-Filho et al., 2019). Thus, despite the importance of this approach for the definition of putative variations in primary productivity, burial of organic matter and restriction of the basin, some important insights on the biological and physical processes operating in the post-Marinoan oceans are still lacking. In this way, recent work has demonstrated the growing importance of the use of paired carbon and sulfur isotope proxies in order to determine redox conditions, ocean stratification and tectonic influence on the sulfur content in the Ediacaran oceans (Cui et al., 2016; McFadden et al., 2008). The marine biogeochemical sulfur and carbon cycles are interconnected via their respective redox-sensitive reservoirs and fluxes. Both elements have a single, large oxidized oceanic reservoir (dissolved sulfate and inorganic carbon) and the burial of their reduced species (pyrite and organic carbon) represents the two main net sources of oxygen to the surface environment. Even though the concentration and isotope composition of sulfate may vary within and among marine basins (Kah et al., 2004), the seawater sulfate sulfur isotope ($\delta^{34}S_{CAS}$, as recorded by carbonate-associated sulfate) and carbon isotope ($\delta^{13}C_{carb}$, as recorded in carbonate) records allow redox changes in the surface environment to be traced through geological time.

Due to its excellent exposure, stratigraphic continuity and high carbonate-content, the Sete Lagoas Formation at Januária area (northern Minas Gerais State, central east Brazil) is ideally suited for reconstructing the chemistry of the post-Marinoan ocean. Some studies, mainly focused on facies (Perrella Jr et al., 2017), sequence stratigraphy (Caetano-Filho et al., 2019), geochemical proxies (Hippert et al., 2019; Uhlein et al., 2019) have been carried out, but none of them contains a complete and integrated analyze of the Sete Lagoas Formation succession in this part of the Bambuí Basin. Thus, this work aims to fill an important gap in the study of this terminal Ediacaran unit, including, i) a detailed sedimentary facies description, ii) sequence stratigraphy framework, iii) contribute complementary $\delta^{13}C$ and $\delta^{18}O$ data, and iv) new detailed results on the $\delta^{34}S$ composition and concentrations of carbonate-associated sulfate (CAS) of the entire succession of Sete Lagoas Formation. The analysis of these proxies allows the depositional and stratigraphic contextualization and spatio-temporal positioning of these variables, making it possible to increase the biostratigraphic resolution of the terminal Ediacaran in the SW Gondwana and allowing to assess if there is a causal relationship between environmental variations and important evolutionary events.

5.2 Geological Setting

The Bambuí basin covers the São Francisco Craton (SFC) in central-eastern part of Brazil, exposing a large diversity of Neoproterozoic mixed terrigenous-carbonate deposits (Fig. 5.1). Originally, the Bambuí Group was interpreted as entirely deposited in a foreland basin developed in response to the uplift of the southern Brasília orogenic belt along the western margin of the SFC (Alkmim and Martins-Neto, 2012; Reis et al., 2017; Reis and Suss, 2016). This interpretation was accepted for decades mainly due: i) the thickness variation of this unit in their western and eastern parts (4 km thick adjacent to the Brasília fold belt and only few hundred meters thick close to the Araçuaí fold belt, Martins-Neto, 2009; Reis et al., 2017); ii) tectonic imbrication between Brasília fold belt slices and Bambuí deposits, such as Samburá and Lagoa Formosa formations (Uhlein et al., 2017), and iii) provenance data indicating mixed (magmatic arc, plutonic and metamorphic) sources and derivation from erosion of the hinterland during thrusting (Uhlein et al., 2017). An alternative interpretation suggests deposition on an epeiric ramp for the Sete Lagoas Formation (Drummond et al., 2015; Hippertt et al., 2019, transitioning to a foreland system towards the upper units of Bambuí Group (Martins and Lemos, 2007). However, recent geochronologic and paleontological data (Warren et al. 2014; Paula-Santos et al. 2015) indicate an Ediacaran age for the base of the Bambuí Group which is substantially younger than the peak activity age of the Brasilia and Araçuaí mobile belts. This strongly suggests an independent evolution of the surrounding orogens and Bambuí Basin, which possibly evolves much more like an intracontinental (epeiric) basin than a foreland system.

The classic stratigraphy of the Bambuí Group, defined by Dardenne (1978), comprises six formal units, from base to top (Fig. 5.2): i) Jequitaí Formation (glacially-related diamictite, conglomerate, sandstone and shale); ii) Sete Lagoas Formation (limestone and dolostone); iii) Serra de Santa Helena Formation (siltstone and marl); iv) Lagoa do Jacaré Formation (dark limestone and shale); v) Serra da Saudade Formation (green siltstone, shale and sandstone; and vi) Três Marias Formation (arkose, conglomerate and shale).

5.2.1 Stratigraphy and depositional aspects of the Sete Lagoas Formation

The Sete Lagoas Formation is essentially a carbonate unit that overlies glaciogenic diamictites or resting unconformably on Archean-Paleoproterozoic basement; its thickness vary from 130 to 180 m (Caetano-Filho et al., 2019; Drummond et al., 2015; Kuchenbecker et al., 2016; Vieira et al., 2007)(Caetano-Filho et al., 2019; Drummond et al., 2015; Kuchenbecker et al., 2016b; Vieira et al., 2007b).

The basal part of the Sete Lagoas Formation is constituted by a cap dolostone characterized by seafloor precipitated typical from the aftermath of Marinoan glaciation. This unit is recognized in both southern, central and northern parts of SFC (Vieira et al., 2007; Alvarenga et al., 2014; Perrella et al., 2017). Aragonite fans were identified in western area, such as Serra de São Domingos locality (Alvarenga et al., 2014), and eastern margins of the SFC, as well as in the southern boundary, such as Arcos and Sete Lagoas areas (Vieira et al., 2007; Kuchenbecker et al., 2016). Void-filling barite and apatite cement were also reported in the central part of Bambuí Basin (Okubo et al., 2018).

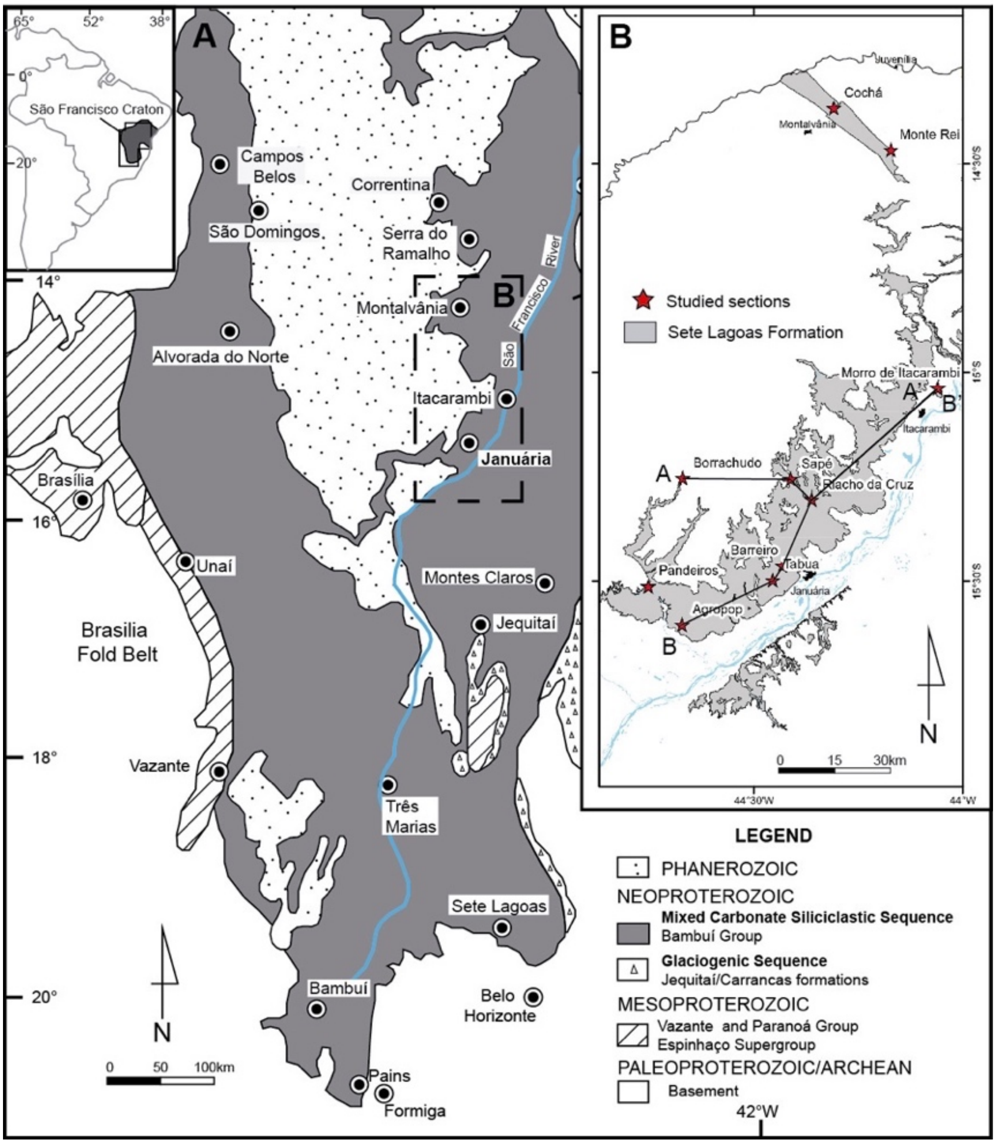

Figure 5.1: A) Simplified geological map of the São Francisco Craton, showing the glaciogenic units and the Bambuí Group. The dashed rectangle represents the studied area. B) Outcrop area of the Sete Lagoas Formation at Januária area and location of the ten studied sections (red stars). Sections A-A’ and B-B’ are represented in the Figs. 6 and 7, respectively.

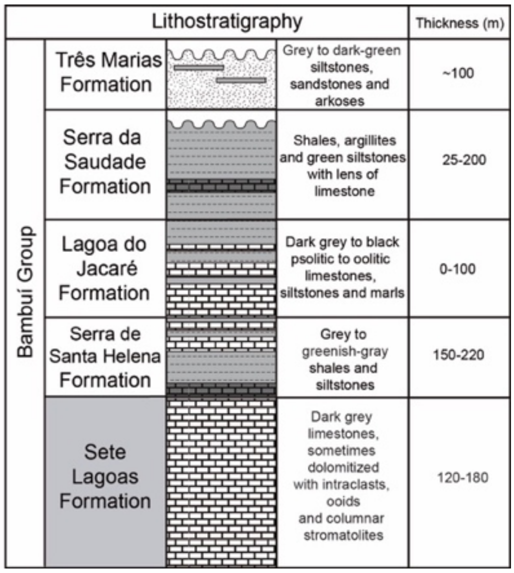

Figure 5.2: Lithostratigraphy of the Bambuí Group, with the main lithotypes of each unit and estimated thickness. The gray box represents the Sete Lagoas Formation.

Following the basal cap carbonate interval, a typical shallow platform sedimentation took place and is essentially characterized by peritidal carbonate facies. This succession is recognized in different parts of the Bambuí Basin, such as the Correntina, Campos Belos and Bezerra areas (Alvarenga et al., 2014; Caxito et al., 2012; Drummond et al., 2015) and Januária area (Perrella Jr. et al., 2017) on the northern and central part of the Bambuí Basin, respectively. In central-northern part of the Bambuí Basin, the peritidal facies association is composed of microbialite facies, as well as grainstones with plane-parallel and undulating laminations, wavy and linsen cross-laminations, cross-bedded grainstones and marl locally, presenting mud cracks, tepees and possible salt pseudomorphs interpreted as deposited in inner to middle ramp settings (Caxito et al., 2012). Pristine *in situ* francolite was locally reported in intertidal flat settings (Drummond et al., 2015). Towards the southern part of SFC, rhytmites and shales with hummocky cross-stratification cover the $CaCO_3$ oversaturated deep platform (Vieira et al., 2007). In Arcos area, aragonite fans-bearing grainstones are overlain by 12 m-thick succession of green marl, mudstone and shales, suggesting deposition in distal environment (Kuchenbecker et al., 2016; Reis and Suss, 2016). Intraformational breccias are recognized at Januária area (Perrella Jr. et al., 2017), but apparently it is not present on the northern part of Bambuí Basin.

5.2.2 Sete Lagoas Formation age constraints and geochemistry

Paula-Santos et al. (2017) defined three distinct chemostratigraphic intervals for the Sete Lagoas Formation: i) the basal CI-1 is composed of cap dolostone succession, with carbon isotope values ranging from -3 to -5 ‰; ii) the intermediate interval characterized by negative values increasing upward until the CI-2, where carbonates show $\delta^{13}C$ values varying in a narrow range around 0 ‰; and iii) the uppermost CI-3 interval, comprising dark laminated and massive carbonate, showing a major positive shift carbon isotope record from 4 to 16‰. In the upper part of the unit, the extreme $\delta^{13}C_{carb}$ positive excursion have been considered a regional chemostratigraphic marker in the basin probably related to variations in the organic production, high concentration of dissolved CO_2 in the ocean waters, high rates of organic burial, methanogenesis and/or reservoir effect due basin restrictions (Iyer et al., 1995; Martins and Lemos, 2007; Sansjofre et al., 2011; Paula-Santos et al., 2017, 2015; Santos et al., 2004; Vieira et al., 2007; Uhlein et al., 2019).

$^{87}Sr/^{86}Sr$ data show constant values around 0.7075, rarely reaching up to 0.7083 (Alvarenga et al., 2014; Caxito et al., 2012, 2018; Paula-Santos et al., 2017). $^{87}Sr/^{86}Sr$ values of 0.7074-0.7076 are characteristic of both lower and upper Sete Lagoas Formation in different localities (references in Caxito et al., 2012). The lack of secular variation in $^{87}Sr/^{86}Sr$ suggests that the Bambuí Group was deposited over a relatively short time interval (Misi et al., 2007). Paula-Santos et al. (2015) proposed high Sr influx due to chemical weathering of ancient carbonates from the surrounding orogenic belts to explain the low $^{87}Sr/^{86}Sr$ ratios in Sr-rich carbonates from the upper Sete Lagoas Formation. Paula-Santos et al. (2017) and Uhlein et al. (2019) also suggested that the upper part of the unit would be entirely deposited in a restrict basin probably isolated from the ocean.

Some redox proxies, such as rare earth elements (REE) and Cr isotopes, have also been used to determine the conditions during the deposition of the Sete Lagoas carbonates. Cap dolostone samples from both southern and northern occurrences of the Sete Lagoas Formation in the SFC are enriched in REE and Y and flat type shale normalized distributions, which has been interpreted as a large input of freshwater in shallow marine environment following deglaciation (Caxito et al, 2018; Paula-Santos et al., 2018). Additionally, Hippertt et al. (2019) suggested that lower Sete Lagoas Formation was marked by oscillating oxygenation pulses evidenced by iron speciation data, pointing towards oxygenated bottom waters. Fully oxygenated conditions were interpreted just above the middle Sete Lagoas Formation based on seawater-like REE+Y, positive $\delta^{53}Cr$ and high U/Th (Caxito et al., 2018).

Babinski et al. (2007) obtained a Pb-Pb whole isochron array of 740 + 20 Ma on carbonates containing aragonite fan pseudomorphs in the southern part of the São Francisco Craton, suggesting a middle-Cryogenian (post-Sturtian) age for the Sete Lagoas cap carbonate.

However, previous studies from Babinski et al. (1999) and D'Agrella-Filho et al. (2000) suggested that a large-scale fluid percolation event reset the Pb isotope compositions of the entire Bambuí basin and caused widespread remagnetization throughout the SFC. Trindade et al. (2004) support this hypothesis and suggested that this regional-scale fluid migration occurred close to ~520Ma, whereas Gonçalves et al. (2019) pointed out that the massive fluid flow event occurred between 515 Ma and 495 Ma. Consequently, interpretation of Pb isotope data and Pb-Pb ages for the Sete Lagoas Formation carbonates is not straightforward and has to be analyzed with parsimony. The precise age of the basal cap carbonate of the Sete Lagoas Formation remains unsolved, but the presence of pink cap dolostone with negative $\delta^{13}C$ and $\delta^{18}O$ values and overlying carbonate with aragonite and barite fans points to a post-Marinoan age for its deposition (Caxito et al. 2012, Okubo et al. 2018). This age is reinforced by the negative triple oxygen isotope anomalies found in thin barite layers on top of the cap dolostone that can be tentatively correlated to other Marinoan-related carbonates around the world (Crockford et al., 2017). On the other hand, the age of deposition of the intermediate portion of the Sete Lagoas Formation succession is well constrained and is interpreted as occurred in the late Ediacaran due to the presence of *Cloudina* index fossil in peritidal carbonates (Warren et al., 2014) and detrital zircons younger than ca. 560 Ma (Paula-Santos et al., 2015).

In sum, assuming a Marinoan age for the cap dolostone, a possible unconformity is suggested separating this basal unit and the upper strata containing Ediacaran detrital zircons and *Cloudina* fragments (Uhlein et al. 2019). This unconformity, probably representing an 85Ma long hiatus, is tentatively characterized by a regional karstification in the top of the basal to intermediate shallowing-upward cycle in the Sete Lagoas Formation (Martins and Lemos, 2007) or significant alterations in the seawater geochemistry without any obvious depositional change (Caxito et al. 2018).

5.3 Material and Methods

Ten columnar sections were measured in detail (1:50 scale) in the Januária region, northern part of the Minas Gerais State, Brazil. Four sections (Barreiro, Agropop, Morro de Itacarambi and Riacho da Cruz, see Fig. 5.1B) named by their proximity to the main farms or localities in the study area were used to build the composite section. Eighteen sedimentary facies were described and grouped into five facies associations: i) cap dolostone (FA1), ii) peritidal (FA2), iii) seismic-influenced carbonate ramp (FA3), iv) oolitic belt (FA4), and v) microbialitic tidal flat (FA5). The facies analysis, definition of depositional systems and the vertical stacking pattern of the Sete Lagoas Formation succession led to the identification of main stratigraphic surfaces (sequence boundary – SB, maximum flooding surface – MFS, transgressive surface – TS), allowing the correct positioning of the depositional system tracts (high stand system tract – HST and transgressive system tract – TST) in a sequence stratigraphic framework (Fig. 5.4). A total of 105 paleocurrents were measured from cross stratified ooid grainstone (FA4) from the middle part of the Sete Lagoas Formation.

Samples were collected at regular intervals (~1m), or according to facies changes and sectioned and polished for macroscopic analysis. Additionally, 22 petrographic thin-sections were examined under normal and polarized light in the Laboratory of Petrography from the Department of Petrology and Metallogeny, São Paulo State University (UNESP), Brazil. Several not weathered samples were selected and analyzed for major and trace elements, carbonate-associated sulfate concentration and carbon, oxygen and sulfur isotopic composition ($\delta^{13}C_{carb}$, $\delta^{18}O_{carb}$, $\delta^{34}S_{CAS}$).

Major and trace elements were determined using a Philips PW2400 X-ray spectrometer at Geochemistry Laboratory of the Petrology and Metallogeny Department of the São Paulo State University (UNESP). For major element analysis, ~0.7g of carbonate powder was melted with 6.5g of $Li_2B_4O_7$. Rb and Sr analysis was undertaken using X-ray fluorescence of 6.0g of carbonate powders mixed with 1.5g of wax binder. This mixture was covered with H_3BO_3 and then pressed.

A total of 66 samples were carried out for carbon, oxygen and sulfur isotopic analyses. For the determination of carbon and oxygen isotopes, homogeneous samples were selected avoiding fractured, weathered, and mineral-filled zones and were pulverized using a microdrilling device. The powder obtained was reacted with 100% H_3PO_4 under a He atmospheric conditions. The carbon and oxygen isotopic compositions of the CO_2 extracted in the process were then measured in a Delta Advantage mass spectrometer in the Federal University of Paraná (UFPR), Brazil. Isotopic results are reported in the conventional per-mil delta notation ($\delta^{13}C_{carb}$ and $\delta^{18}O_{carb}$) with respect to Vienna Pee Dee Belemnite (VPDB).

The sample preparation and sulfur isotopic analysis of carbonate-associated sulfate (CAS) geochemical analyses were performed in the Department of Geosciences at Virginia Tech, USA. Approximately 100 g of sample was powdered and treated with a 10% sodium chloride solution to remove soluble sulfate. These samples were rinsed three times with deionized water between each leach. After each rinse, the sample was allowed to settle, and the overlying water was carefully decanted. The carbonate was then dissolved in 4N HCl (acidification) and the supernatant solution was separated and allowed to react with saturated $BaCl_2$ solution. At this step, the acid-leachable sulfate was precipitated as barite. In order to avoid the oxidation of the ore sulfides, 8 out of 66 samples from the Mississippi-Valley type mineralization breccia interval were acidified in an anaerobic atmosphere. The barite was then filtered from the solution using a 0.45 µm membrane filter and allowed to dry. The filter with barite precipitate was then dried and weighed. The $BaSO_4$ precipitates were then homogenized and loaded into tin capsules with excess V_2O_5 and analyzed for their $^{34}S/^{32}S$ isotope ratio on an Isoprime 100 isotope ratio mass spectrometer (IRMS) coupled with a vario ISOTOPE Cube EA. Sulfur isotope compositions are reported in standard delta notation as per mil (‰) deviations from the Vienna Canyon Diablo Troilite (V-CDT) and calibrated using international standards (IAEA-SO-5, IAEA-SO-6 and NBS-17).

The $\delta^{34}S_{sulfate}$ composition is dictated by the mass and isotopic compositions of S fluxes into and out of the ocean. Mass balance equations for $\delta^{34}S_{sulfate}$ (adopted from Kah et al., 2004) are used to illustrate how the individual residence times of marine dissolved sulfate influence the degree to which perturbations to the coupled geochemical cycles of C and S affect the rate and magnitude of isotopic change. The model, including the rationale behind assigned values of all of the variables and our sensitivity analyses, are further discussed in detail.

5.4 Results

5.4.1 Facies and facies association of the Sete Lagoas Formation

The macroscopic description of the sedimentary facies in the study area, complemented by petrographic description of representative samples, were represented in ten detailed (1:50) columnar sections (see Fig. 5.1B for location of the sections). The different facies described and summarized in the Table 1 were grouped into five facies associations (FA): a) cap dolostone (FA1); b) peritidal carbonates (FA2); c) seismic-influenced carbonate ramp (FA3); d) oolitic belt (FA4) and e) microbialitic tidal flat (FA5).

The cap dolostone facies association (FA1) lies directly above a regional unconformity characterized by an irregular basement paleosurface and is represented by ~2.5 m of dolomitized domal stromatolite (Fig. 5.3A). On top of the cap dolostone, 1–2 cm thick (locally reaching 15 cm) layers of aragonite crystal fans (F2) and void-filling barite cement (F3) occur in laminated grainstone and microbial facies and extend laterally for at least 30 km (Fig. 5.3B). Carbonate fans consist of (sub-) acicular (needle-like) crystal units with hexagonal (~200 µm diameter) cross sections and square terminations, like aragonite crystals. Each crystal unit is composed of numerous small equant calcite crystals. When associated with carbonate fan crystals, barite occurs as radiating bladed crystals isolated in the rock matrix or minor void-filling cements. In addition, microcrystalline barite and pyrite fill void space and encrust apatite cement.

The lack of current or wave-related sedimentary structures and the presence of preserved seafloor precipitates suggest deposition below the storm wave base level (Hoffman et al., 2017, 2011) associated with an enhanced seawater alkalinity (Higgins and Schrag, 2003; Vieira et al., 2015). Also, the co-occurrence of carbonate crystal fans and phosphate cements reflects high seawater dissolved inorganic carbon, phosphorus, and calcium concentrations increased by the continental weathering and ocean upwelling (Bergmann et al., 2013; Okubo et al., 2018).

The peritidal carbonate facies association (FA2) correspond to a ~60-meters-thick succession well exposed in Barreiro, Sapé and Riacho da Cruz sections (Figs. 5.5 and 5.7). This facies association is mainly composed of cross-stratified and laminated grainstones (F8, F10 and F11), heterolithic facies (F5) and mudstones (F4), occasionally associated with swaley cross bedded fine grainstone (F12). Evaporitic breccia (F13), laminated microbialites and continuous thrombolytic biostromes (F6 and F7) occur interbedded with these facies. The thrombolites show great lateral extension and are composed of low domes up to 0.1 to 0.4 m high containing irregular spheroidal cm-scale clotted grains and pustules (Fig. 5.3C). Similar to other Ediacaran carbonate successions, *Cloudina* and rare *Corumbella* fragments occur as loosely packed bioclastic deposits associated with trombolytic facies (Warren et al., 2014). Locally, biostromes up to 0.5 m high are present, showing domal shape and internal wrinkled lamination. The alternation of stromatolites and thrombolites represent lateral variation of facies and could reflect changes in environmental parameters, such as hydrodynamic conditions and/or variations in water depth and luminosity (Feldmann and McKenzie, 1998).

The heterolithic wavy beds (F5, Fig 5.3E) and fine grainstone facies present wave- and current-ripple cross-lamination (Fig. 5.3D) suggesting the action of wave orbitals and tidal currents in shallow water conditions. The presence of contorted and laterally interrupted microbialites with tepee structures also indicate subaerial exposure of microbial mats and mudstones under evaporitic conditions and reinforce the hypothesis of deposition in reduced bathymetry probably in inter to supratidal settings (peritidal). The sparse presence of swaley and hummocky cross-stratified grainstone (Fig. 5.3F) indicates that occasionally storms could affect the carbonate platform, reworking and transporting shallow sediments and possibly skeletal bioclasts (i.e., *Cloudina*) to deeper parts of the basin. The presence of terrigenous facies in both Sapé and Riacho da Cruz sections suggests relative proximity to the continental sources and sporadic input of detrital sediment in the microbial carbonate factory.

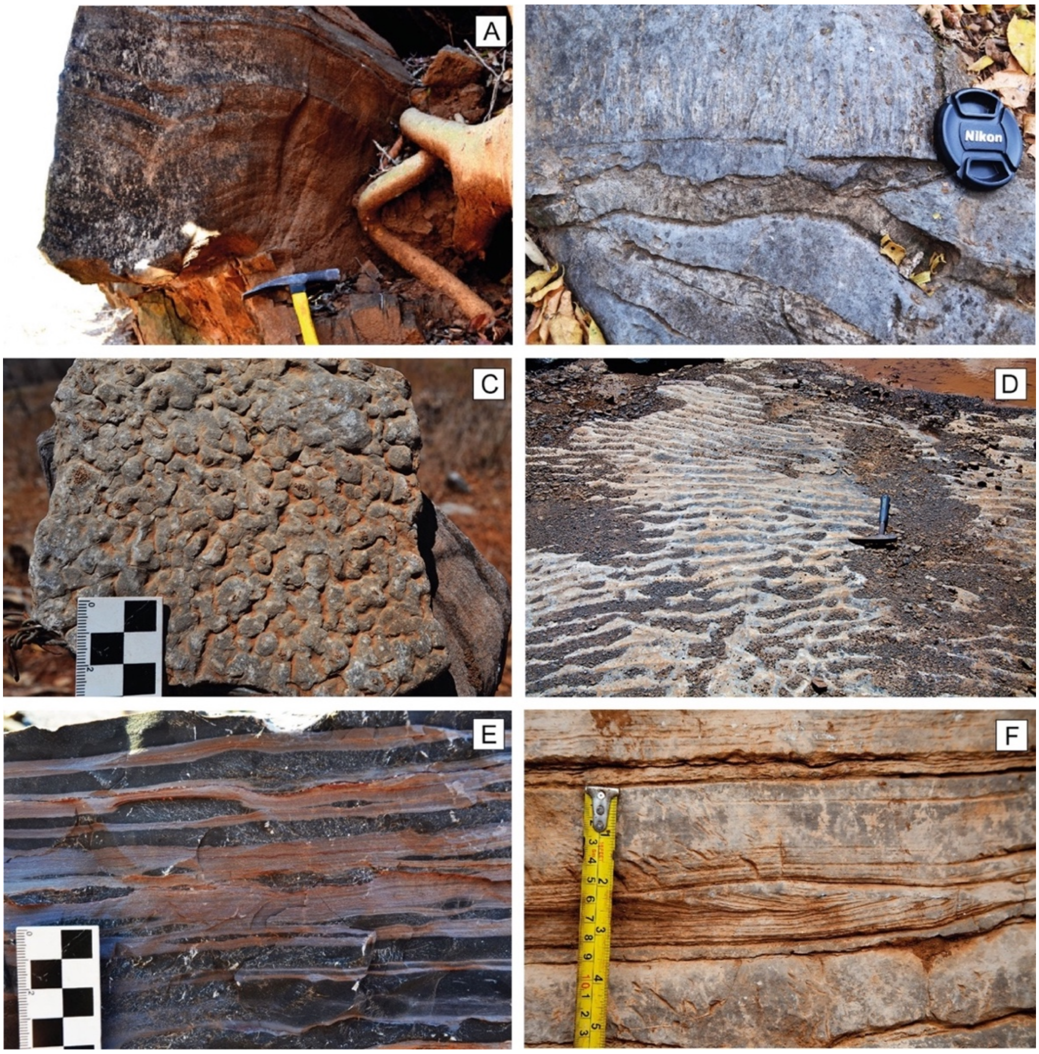

Figure 5.3: Facies associations of the Sete Lagoas Formation at Januária region. A) Contact between the Sete Lagoas cap dolostone and the basement. B) Aragonite fans (on the top) and void-filling barite (dark layer in the center) present in the cap dolostone as seafloor precipitates. C) Thrombolites constituted by irregular nodules from the peritidal facies association (FA2) at Barreiro section. D) Wave ripples in cross-bedded grainstones of peritidal facies association (FA2). E) Interbedded cm-thick layers of mudstone/marls with cross-laminated grainstone, forming wavy heterolithic bedding. F) Small size hummocky cross-stratified grainstone above a thrombolite layer (FA2).

The FA3 is ~20-m-thick and represents a local stratigraphic marker in the studied sections. These deposits consist of alternation of flat-pebble breccia and laminated microbialites. Breccia beds range from 0.4 to 2.2 m in thickness, whereas microbialite beds vary from 0.1 to 2.1 m thick. Individually, each breccia bed shows tabular geometry with sharp and undulated contacts with both underlying and overlying undeformed planar microbialite beds. The flat-pebble breccia is mostly clast-supported, where the clasts are usually platy or oblate with angular edges (Fig. 5.4A) and mainly disposed horizontally within the sedimentary bed. Few clasts are sub-vertical or chaotically disperse and some levels show bidirectional imbrication. There is no evidence of normal gradation and ductile deformation. The latter suggests that the clasts were deposited as rigid objects. The angulosity, shape, size and sorting of the clasts also suggests deposition in very shallow batymetry with reduced clast transport or reworking. The presence of vertical clasts, deformation increasing upward, lateral continuity of breccia beds and the alternation of breccia and undeformed beds in abrupt contact led us to interpret an in-situ fragmentation of early lithified microbialite beds due to the impact of shock waves related to seismic activity concomitant to sedimentation (see Okubo et al. under review for detailed explanation). Usually, gravel shorefaces tend to show crestlines nearly parallel to the paleoshoreline (Hart and Plint, 1995). Thus, size measurements of the largest axes of clast (Fig. 5.5B) allow us to interpreted that the most elongated pebbles in the breccia facies tend to deposit parallel to the shoreline in a NE direction (Fig. 5.5A).

The succession that covers the flat-pebble breccia and peritidal facies from the FA2 and FA3 was deposited in an inner middle ramp environment rimmed by an oolitic belt (FA4). FA4 corresponds a typical oolitic belt facies association and has thickness ranging from10 to 30 m, reaching maximum of 140 m near Montalvânia town.These subtidal deposits consist of meter-scale thick sets of trough cross-bedded ooidgrainstones interbedded with tabular beds with normal gradation (F15),low-angle cross-stratified grainstone (F10) and wave cross-laminated grainstone (F8). The ooids are 300 μm in diameter, spherical, concentric and often intensely recrystallized (Fig. 5.4C). Ooids are commonly formed in environments with agitated water commonly, such as shallow subtidal environments located in platform margins, straits and seaways between (barrier) islands (e.g. Rankey et al., 2006); c) in subtidal hypersaline lagoons (e.g., Jahnert and Collins, 2011) and in subtidal platform interiors where wave and storm action are more important than tides. The prevalence of facies F15 and F10 suggests deposition in shallow bathymetry from the migration of ooid sand bars and dunes, similarly to those reported in coastal oolitic belts present in other Ediacaran carbonate ramps (Warren et al. 2019).

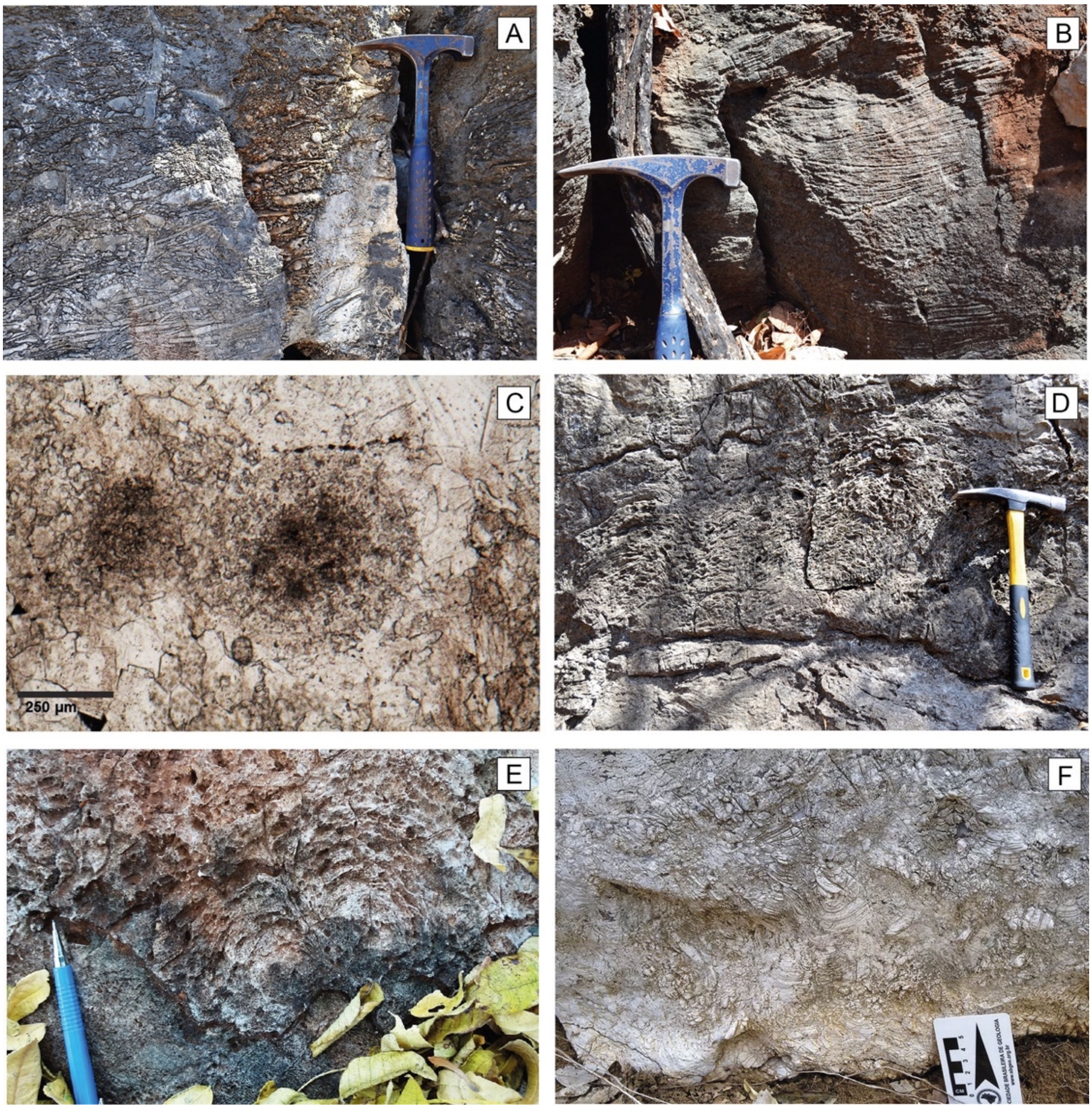

Figure 5.4: Facies associations of the Sete Lagoas Formation at Januária region. A) Clast-supported flat-pebble breccia in the middle part of the Sete Lagoas succession (FA3) in the Barreiro section. Note the presence of vertical clasts and punctual imbrication at the base. B) Trough cross-stratified grainstone from the oolitic belt facies association (FA4) at Agropop section. C) Recrystallized ooids from the trough cross-stratified dolograinstones from the Agropop section. Note that they still preserve the concentric microstructure, but it is not possible to identify the original composition of the nuclei. D) Decimetric layer of domal stromatolite, strongly recrystallized from the oolitic belt facies association (FA4). The limits between the domes are not well-marked, but the wrinkle lamination is clearly present. E) Small coalescent stromatolites from the oolitic belt facies association (FA4) in the Morro de Itacarambi section. F) Brecciated stromatolite representing a karstification surface at the base of the tidal flat association (FA5).

Domal stromatolite (F16), sometimes fractured and silicified, is also interbedded with ooid grainstones. They usually have 0.4 to 1.2 m in height (Fig. 5.4D) and present smooth to wrinkle lamination that grew into pseudo-columnar, sometimes coalescent, structures (Fig. 5.4E). The domal morphology suggests accretion under high energy and shallow water conditions and is coherent with deposition in stabilized substrates located in shallow trough areas between oolitic bars.

Several paleocurrent data (n=105) acquired from low-angle and cross-stratified ooidgrainstone facies and indicate main sedimentary transport towards NW (Fig. 5.5), reinforcing that the paleoshoreline presented NE-SW direction and the offshore setting (ocean waters) was located to SE quadrant. The predominant NW paleocurrent direction indicates the dominance of flood-tidal currents. The broad dispersion to SE may indicate subordinate ebb tidal currents. The E-W direction from Agropop section may represent ebb and flood tidal currents in a channel or reentrance of the shoreline.

Selective dolomitization is present in the FA4 succession, either as a result of early or burial diagenesis and/or a product of hydrothermal activity (Nobre-Lopes, 2002). The percolation of hot fluids through the ooid grainstone facies in this part of the basin is reinforced by a restricted interval of Pb-Zn breccia (F17) possibly formed during the hydrothermal event (Nobre-Lopes, 2002).

The FA5 succession is ~10 m thick and represents intertidal to supratidal deposits mainly composed of laminated to crenulated microbialites sometimes showing disrupted layers and wrinkle lamination. Brecciated stromatolite (F18) is a ~0.3 m thick bed, clast-supported and consists of cm-sized angular fragments, sometimes preserving thin lamination (Fig. 5.4F). The last few meters of the Sete Lagoas Formation are marked by 1-5 cm thick black chert layers interbedded with laminated microbialites. These black chert layers are recrystallized and sometimes peloidal in composition, usually not preserving their original peloidal microstructure. The brecciated stromatolite (F18) indicate fragmentation due to subaerial exposure of microbialite from the underlying facies association and development of a regional karstic surface. The presence of black chert facies in this context may represent a more evaporitic conditions towards the top of the Sete Lagoas Formation. This succession is finally covered by siltstones of the Serra de Santa Helena Formation, characterizing a transgressive surface over a regional erosive unconformity.

Table 5.1: Facies, facies associations and interpretations of the Sete Lagoas Formation at Januária area. FA: facies associations

FA	Facies	Description	Interpretation
FA1 - Cap carbonate	F1 - Domal stromatolite	Dolomitized meter scale domal stromatolite, associated with seafloor precipitates (aragonite pseudomorphs and void-filling barite) preserved on top of the domes	Microbial accretion in reduced bathymetry in seawater with high alkalinity, associated to deglaciation (after the Marinoan glacial event)
	F2 - Aragonite pseudomorphs (carbonate fans)	Carbonate fans (originally aragonite) occur in multiple thin layers (5-10cm), that grew as radiating crystals upward-oriented (seafloor perpendicular). Phosphatic cements occur associated to these facies	Iron reduction associated to high alkalinity in a cap carbonate context
	F3 - Veins and void-filling barite cement	Irregular cm-thick veins and major void-filling cement occur in multiple layers, sometimes interbedded with aragonite fans and concordant with the bedding. Barite crystals, commonly forming rosettes, grew both upwards and downwards in stratigraphic orientation	Barite precipitation during early diagenesis related to the cap carbonate context, later influenced by hydrothermal fluids
	F4 - Carbonate mudstone	Centimeter to decimeter scale tabular beds of carbonate mudstone dominated by micrite	Carbonate mud settling in stagnant and shallow water conditions
FA2 - Peritidal	F5 - Grainstone and mudstone heterolitic beds	Fine grained cross-laminated grainstone intercalated with varying proportions of carbonate mudstones (wavy structures), with some terrigenous contribution	Alternated traction by oscillatory flows related to fair-weather wave orbitals and settling processes
	F6 - Thrombolite	Centimeter thick irregular beds composed of irregular centimeter to decimeter scale low domes, showing rounded to irregular clotted fabric internally	Carbonate precipitation induced by microbial activity in shallow waters occasionally exposed to subaerial conditions and reworking processes.
	F7 - Laminated microbialite	Centimeter to decimeter scale thick tabular beds of finely, irregularly smooth laminated carbonates sometimes presenting V-shaped diseccation cracks	Microbial mat deposits in shallow water subjected to subaerial exposure and reworking
	F8 - Wave cross laminated grainstone	Centimeter to decimeter scale thick tabular to lenticular beds of very fine to fine grained grainstones showing cross-laminations with opposite dip directions	Migration of symmetrical ripples related to sediment transport by fair-weather wave orbitals in shallow waters
	F9 - Black chert (bands/layers and nodules)	Centimetric layers or nodules of black chert, usually associated with wave cross laminated grainstone and thrombolite	Percolation and precipitation of silica-rich waters during eodiagenesis filling vugs and other cavities
	F10 - Low-angle cross-bedded grainstone	Decimeter to meter scale thick tabular beds of fine to medium grainstones showing low angle cross-stratification	Migration of low amplitude bedforms formed under upper flow regime, probably related to swash and back wash flows (foreshore)
	F11 - Laminated grainstone	Tabular beds, decimeter to meter-scale thick, laterally continuous for tens of meters, internally composed of fine to very fine grained grainstone with planar lamination	Vertical accretion of horizontal bedforms formed under upper flow regime, also related to swash and back wash flows as facies F10
	F12 - Swaley cross bedded grainstone (SCS)	Lenticular to tabular, centimeter to decimeter beds of fine grained grainstones with symetrical swaley cross stratification. SCS commonly occur associated with wave cross laminated grainstone.	Migration of ripples produced by combined oscillatory and unidirectional flow, related to storm events in shallow areas (lower shoreface)
	F13 - Evaporitic breccia	Centimeter to decimeter scale tabular beds of clast-supported breccia constituted of centimetric clasts of microbialites. Horizontal stylolites, tepees and salt pseudomorphs are present.	Subaerial exposure of microbialite facies (F6 and F7), associated with crystallization of salts in evaporitic conditions
FA3	F7 - Laminated microbialite	See above	See above
	F14 - Flat pebble breccia	Tabular beds of clast-supported monomitic breccia, constituted mostly of fitted tabular clasts. Rounded clasts are rare. Clast imbrication and tepee structures are locally observed.	In situ fragmentation of early lithified microbialite beds, rearranged by episodic seismic events
FA4 - Oolitic belt	F10 - Low-angle cross-bedded grainstone	See above	See above
	F15 - Cross-bedded grainstones	Lenticular, decimeter beds of cross-stratified ooid grainstone stacked in meter scale thick cosets. Coarse-grained deposits usually present trough cross-stratifications whereas fine to medium grained deposits commonly show tabular cross-stratification. Selective dolomitization is present	Migration of 2D and 3D dunes (bars) by action of longshore currents and/or action of breaking fair-weather wave orbitals (upper shoreface)
	F16 - Domal to pseudo columnar stromatolite	Dolomitized, sometimes silicified, meter scale domal stromatolite, locally pseudocolumnar. Intensely fractured and recrystallized.	Carbonate precipitation induced by microbial activity in shallow waters rarely exposed to subaerial conditions. Variation in bathymetry, accommodation space, hydrodynamics and sediment availability explain changes in the morphology.
	F17 - Hydrothermal breccia	Meter-scale tabular beds of clast-supported breccia constituted of angular clasts and crosscut by quartz veins. Intense silicification and interparticle porosity	Percolation of Pb-Zn hydrothermal fluids in grainstone facies
FA5 - Microbialitic tidal flat	F7 - Laminated microbialite	See above	See above
	F8 - Black chert (bands/layers and nodules)	See above	See above
	F18 - Brecciated stromatolite	Centimeter to decimeter scale beds of clast-supported breccia constituted of angular stromatolite fragments Some of the fragments preserve microbial lamination	Subaerial exposure of stromatolites, associated to karstification process

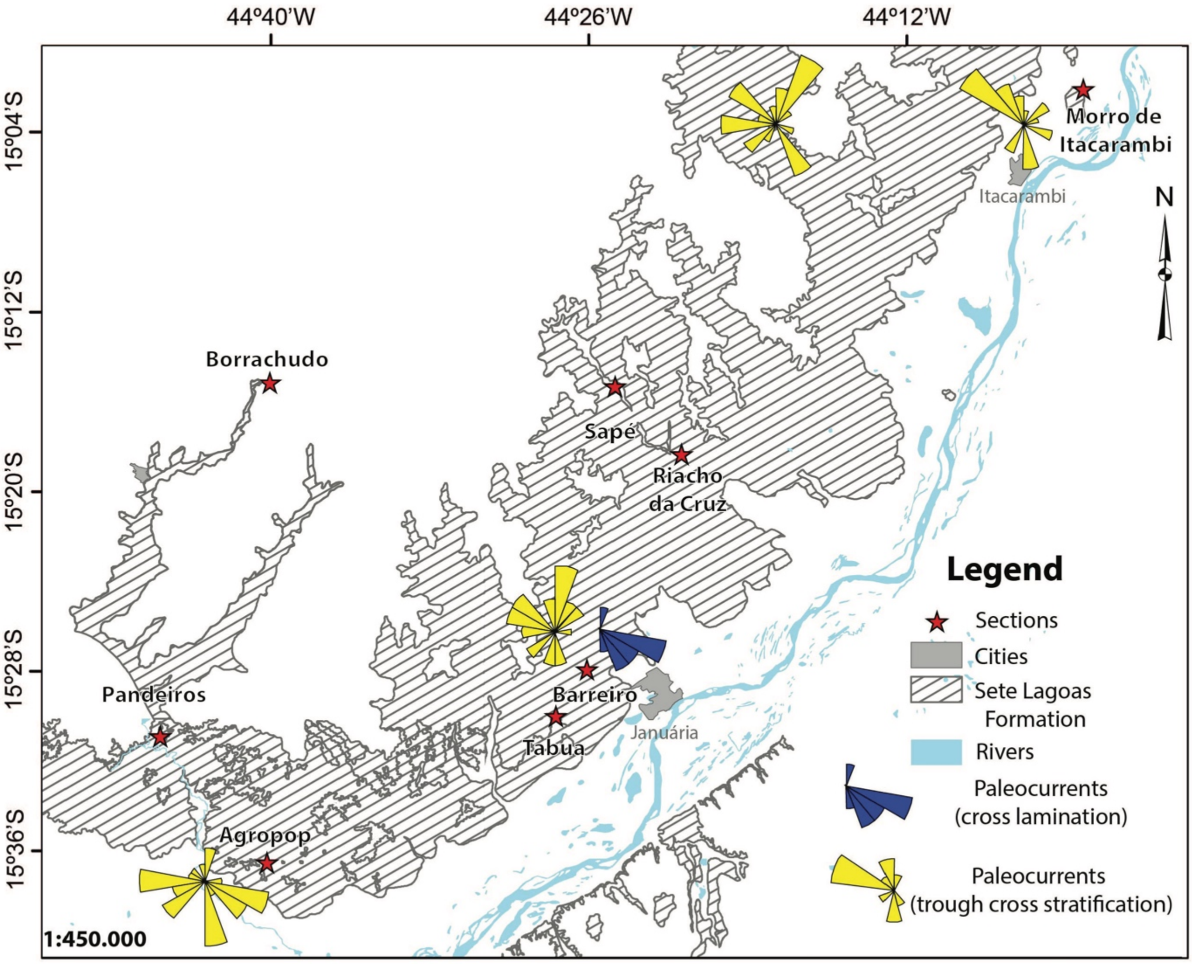

Figure 5.5: A) Paleocurrents from trough-cross stratified grainstones of the oolitic belt facies association (FA4) of the Sete Lagoas Formation in the study area. B) Rose diagrams of azimuthal orientation of 243 elongate clasts in flat-pebble breccia near Barreiro section.

5.4.2 Sequence stratigraphy framework

In the study area, the Sete Lagoas Formation comprises a complete 3rd order sequence (Sequence 1 – S1) bounded at the base by regional erosive unconformity (Figs. 5.6 and 5.7) with the Paleoproterozoic basement and at the top by the shallower facies represented by the seismic influenced carbonate ramp (FA3). A second transgressive system tract (TST2) corresponds to an increase in the accommodation space, allowing the deposition of ooid shoals and domal stromatolites in deeper conditions. This succession is covered by microbialitic tidal deposits separated from the siliciclastic succession of the Serra de Santa Helena Formation by a well-developed karstic surface (SB3).

The sequence boundary 1 (SB1) is characterized by a regional unconformity developed at the Paleoproterozoic basement, forming an irregular erosive paleosurface. Above this unconformity, well-preserved seafloor precipitates overlying domal stromatolites from the FA1 constitute a typical transgressive pattern, representative of the coastal onlap migration due to post-glacial (Marinoan) deglaciation and rise of sea level. The SB1 and TS1 occur amalgamated in a configuration commonly related to intracratonic basins and homoclinal ramps without slope (Lindsay et al., 1993). The deposits from the basal cap dolostone (FA1) were interpreted as representative of the initial stages of the transgressive system tract (TST1), similarly to coeval cap carbonates from Namibia, Canada and China (Hoffman et al., 2017; Hoffman and Schrag, 2002; Saylor et al., 1995). The maximum flooding surface (MFS1, Figs. 5.6 and 5.7) was marked by the appearance of aragonite and barite seafloor precipitates level. These particular structures (e.g. carbonate fans and void-filling barite cements) are discontinuously preserved along the cap carbonate in different parts of the Bambuí Basin in which the Sete Lagoas Formation crops out, such as Arcos (Kuchenbecker et al., 2016), Sete Lagoas (Vieira et al., 2015) and Serra de São Domingos areas (Alvarenga et al., 2014).

In the Borrachudo section (Fig. 5.6), peritidal (FA2), seismic-influenced carbonate ramp (FA3) and oolitic belt (FA4) facies associations are missing, which led us to interpret that these facies associations truncate against an original inclined surface (SB1), representative of the irregular basement paleosurface (Fig. 5.6). The onlapping against the basement and the terrigenous contribution in the lower part of the unit corroborates the interpretation of Januária area acted as a paleo-high during the deposition of Sete Lagoas Formation. The absence of these facies associations (FA2, FA3 and FA4) in the Borrachudo section may be interpreted as a higher subsidence rate towards E-NE part of the basin, which is corroborated by thicker ooid deposits from the (FA4) near Montalvânia town.

Above the MFS 1, the succession is composed of peritidal deposits (FA2) containing Cloudina fragments (Warren et al., 2014) and pristine francolite (Drummond et al., 2015). This succession was interpreted as representative of the initial stages of the high-stand system tract (HST1). In Campos Belos area (Drummond et al., 2015), intertidal to subtidal deposits, represented by phosphate-bearing siltstones and sandstones, could represent a lateral variation of the FA2 with significantly higher siliciclastic input, probably reflecting proximity to the Brasilia orogenic belt. According to Caetano-Filho et al. (2019), the correlative of the FA2 succession is marked by high Sr/Ca ratios, which is consistent the data presented here (Fig. 5.8) and probably represent an increased incorporation of Sr in carbonate minerals due to progressive basin restriction.

Paula-Santos et al. (2015, 2017) and Uhlein et al. (2016, 2017, 2019) have suggested a possible unconformity between cap carbonate from the FA1 and peritidal deposits of the FA2 (respectively, C-1 and C-2 intervals from these authors), aiming to explain a possible age difference between the Marinoan cap dolostone and the succession bearing the index fossil Cloudina. However, no evidence for this unconformity at top the Sete Lagoas cap carbonate was recognized in the field and are here considered conjectural in this part of the basin.

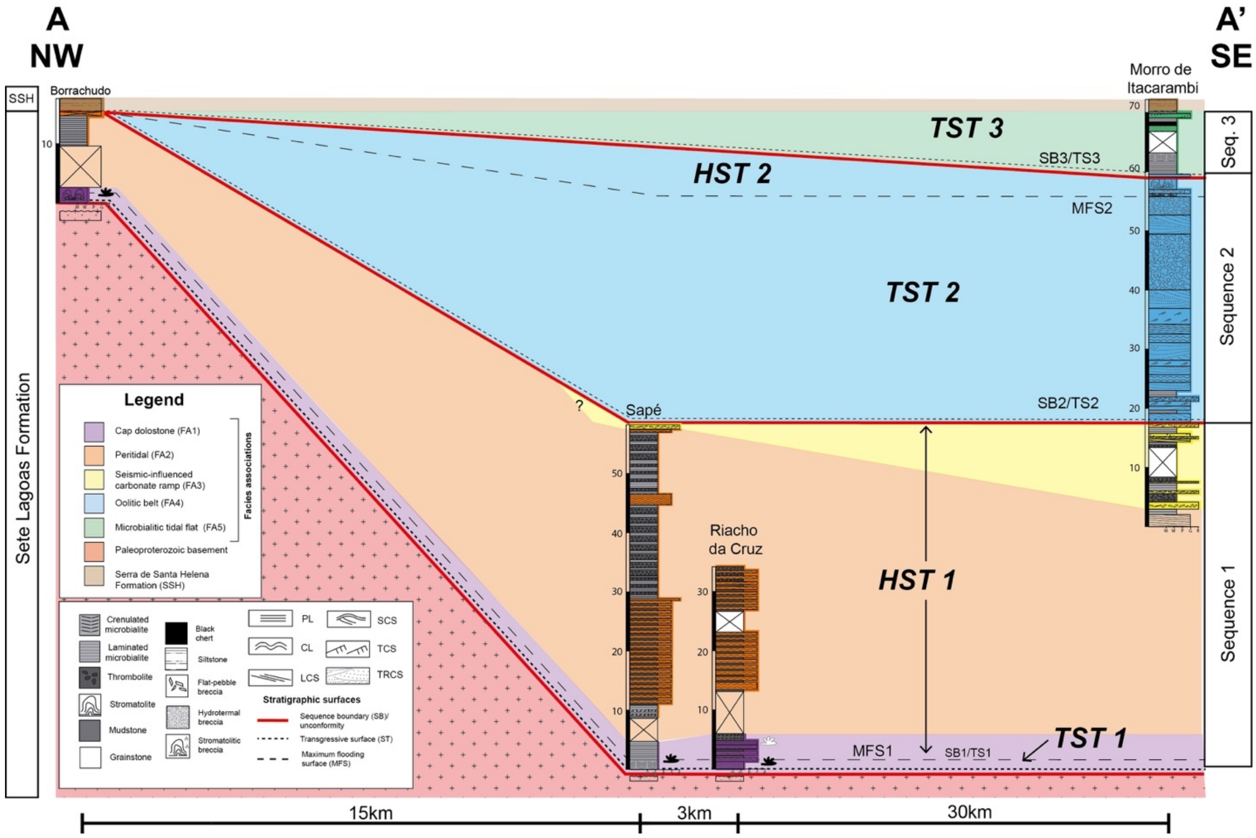

Figure 5.6: Sequence stratigraphic framework of the Sete Lagoas Formation. Note that the Borrachudo section is located on top of the Januária structural high. For the localization of the columnar sections in the study area, please see Fig. 1. PL: parallel lamination; CL: cross lamination; LCS: low-angle cross stratification; SCS: swaley cross stratification; TCS: tabular cross stratification; TRCS: trough cross stratification.

The appearance of brecciated deposits (FA3) overlying the peritidal succession were interpreted as the result of synsedimentary seismicity affecting the carbonate ramp (Okubo et al. under review) during the final stages of the HST1. The intraclastic calcarenite (Kuchenbecker et al., 2016) in Arcos section and intraclastic breccia (Drummond et al., 2015) in Campos Belos area can be potentially correlated with this seismic interval and possibly represent a stratigraphic marker for the basin. Reworked phosphorite grains are also attributed to reworked and transport of peritidal sediments from the FA2 (Drummond et al., 2015).

The sequence S1 is limited at the top by a sequence boundary (SB2, Fig. 5.7), placed on top of the flat-pebble breccia. The sequence S2 begins with the SB2, which is amalgamated with the transgressive surface (TS2) that limits the base of the TST2. Above these stratigraphic surfaces, bars and dunes from the oolitic belt system (FA4) overlie the flat-pebble breccia (FA3) and peritidal (FA2) facies, configuring a retrogradational pattern representative of the initial stages of the TST2. In this environment, ooidgrainstones and stromatolites represent the lateral variations of the inter- to subtidal settings. This ooid succession are usually 20 to 30 meters thick in Arcos and Januária area (Caetano-Filho et al. 2019), but they can reach hundreds of meters at Montalvânia area, suggesting that the basin was progressively deeper in the E-NE direction. The maximum flooding surface was placed at the base of the upper domal stromatolite (F16) interval (Fig. 5.7), which is interpreted to form deeper than the ooidgrainstones. This interval probably reflects the maximum production of the carbonate factory related with the increasing accommodation space, allowing the deposition of few hundred meters of ooidgrainstones and domal stromatolites rather than thrombolites and laminated microbialites (shallower facies).

The brecciated stromatolite (F18) facies marks a subaerial exposure of the stromatolites in the carbonate ramp, which corresponds to the upper sequence boundary (SB3). Microbialites in a tidal flat setting (FA5) alternate between laminated and crenulated during the final moments of Sete Lagoas deposition. This interval is marked by the decreasing in the carbonate production, development of a regional karstic paleosurface (SB3), followed by an increase in the terrigenous input, representative of the beginning of the sedimentation of tidal flat siltstones and marls from the Serra de Santa Helena Formation.

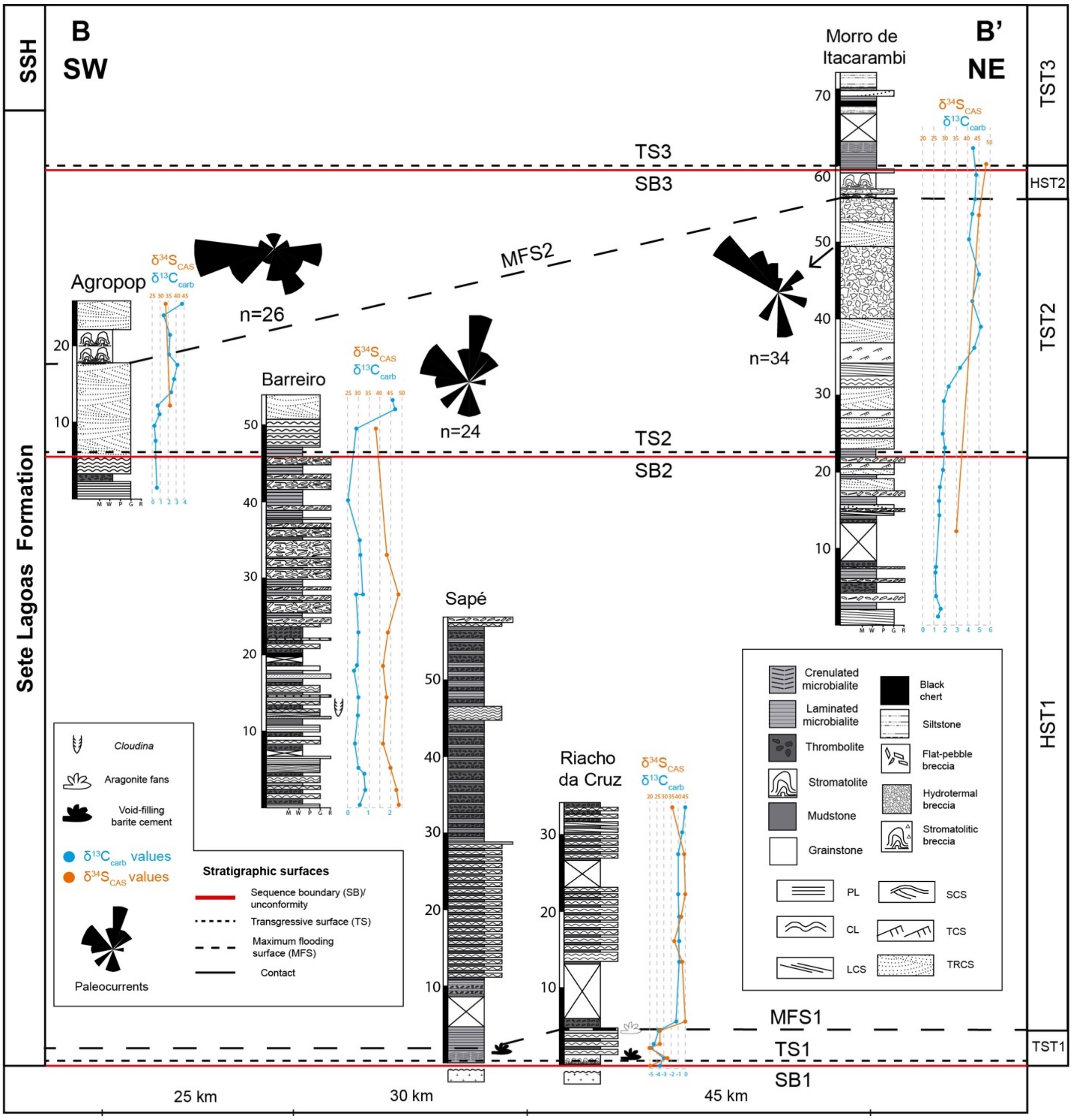

Figure 5.7: Paleocurrent data, stratigraphic surfaces, columnar sections and respective $\delta^{13}C_{carb}$ (‰, VPDB) and $\delta^{14}S_{CAS}$ (‰, VPDB) profiles of the Sete Lagoas Formation. For the localization of the columnar sections in the study area, please see Fig. 1. PL: parallel lamination; CL: cross lamination; LCS: low-angle cross stratification; SCS: swaley cross stratification; TCS: tabular cross stratification; TRCS: trough cross stratification.

5.4.3 Stable isotope geochemistry and evaluation of diagenetic alteration

Carbon isotope values vary between -4.33 ‰ PDB and 4.77 ‰ PDB, and the oxygen isotopes vary between -4.45 ‰PDB and -12.77 ‰ PDB throughout the Sete Lagoas succession (Figs 7 and 8). $\delta^{34}S_{CAS}$ values range from +21.26 ‰ CDT to +53.14 ‰CDT over all sampled facies. CAS concentrations vary between 12.83 and 367.28 ppm (mean = 64.52, n = 66), showing a persistent negative stratigraphic trend (Fig. 5.8).

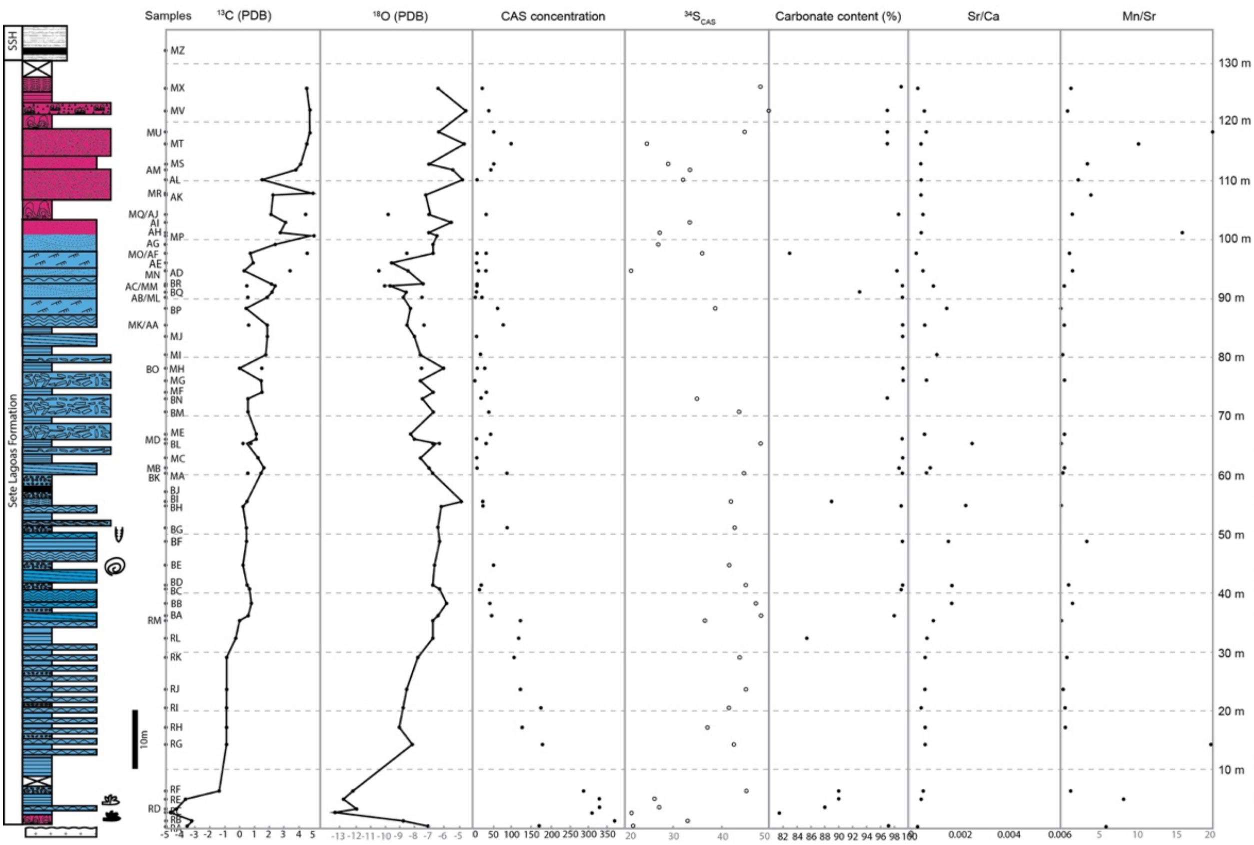

Figure 5.8: Composite stratigraphic column, geochemical data (C_{carb}, O_{carb} and S_{CAS} isotopes), CAS concentration, carbonate content and Sr/Ca and Mn/Sr ratios for the Sete Lagoas Formation at Januária area. Pink color in the section represents dolomite and blue are calcite.

Because both $\delta^{18}O$ and Mn/Sr original values are usually modified during diagenesis, these parameters have been commonly used as diagenetic indicators for the quality of the $\delta^{13}C$ signal (Kaufman and Knoll, 1995). $\delta^{18}O_{carb}$ is a useful indicator of alteration as $\delta^{18}O$, suggesting that there is no significant influence of diagenesis in their isotopic composition (Fig. 5.9A).

$\delta^{34}S$ and CAS concentrations also do not covary, suggesting that they are essentially primary values. In addition, they do not seem to correlate directly with facies or stratigraphic surfaces (Fig. 5.9B). The carbon and sulfur isotopic curves are positively correlated through the entire succession of the Sete Lagoas Formation, but CAS concentration shows an inverse pattern (Fig. 5.8). Most of Mn/Sr ratios are lower than 10 in this study and the absence of covariation between Mn/Sr and CAS concentration is consistent with minimal diagenetic overprinting (Fig. 5.9C). The absence of any correlation between $\delta^{34}S$ and $\delta^{18}O_{carb}$ (Fig. 5.9D) suggests that post-depositional processes did not alter significantly the S isotope composition of CAS.

Importantly, the cap dolostone samples from the base of the base of the Sete Lagoas Formation (FA1) show higher CAS concentration, decreasing towards the top of the unit. Below the 10 m mark, CAS concentrations are higher than 250 ppm and $\delta^{34}S$ values vary from 22.2 to 32.8 ‰ CDT. CAS concentrations from the peritidal facies association (FA2) are highly variable, from 2.16 to 287.5 ppm. Flat-pebble breccia interval (FA3) corresponds to very low CAS concentrations (from 9.58 to 45.81 ppm) and relatively high $\delta^{34}S_{CAS}$ values (43.9 to 48.2 ‰ CDT).

Low CAS concentrations in the oolitic belt facies association (FA4) could also be alternatively related to dolomitization (Fig. 5.8). During diagenesis (e.g., dolomitization), CAS could be released from the crystal lattice of precursor carbonate minerals (e.g. aragonite, high-Mg calcite), and sulfate in pore water could be incorporated in stabilized carbonate minerals (e.g., low-Mg calcite, dolomite), reflecting a relative decrease in CAS concentration (Gill et al., 2008; Shen et al., 2010). However, Gill et al. (2008) studied the impact of meteoric diagenesis on CAS and concluded that $\delta^{34}S_{CAS}$ is relatively unaffected and still preserves primary $\delta^{34}S_{sulfate}$ values.

Between 90 and 120 m height (FA4), the $\delta^{34}S_{CAS}$ profile is depleted and shows great variation (Fig. 5.8). Samples JJ17H, JJ17K and JJ17L show anomalous concentrations of Zn (2323, 139 and 269 ppm, respectively), possibly reflecting a Pb-Zn MVT mineralization interval in the oolitic belt facies association (FA4), as previously observed by Nobre-Lopes (2002). Marenco et al. (2008) and Mazumdar et al. (2008) have demonstrated that pyrite oxidation during the CAS extraction procedure can alter the primary values both [CAS] and $\delta^{34}S_{CAS.}$ Due to this, we acidified samples from this interval potentially enriched in sulfides in an anoxic environment in order to avoid sulfide oxidation and the lack of correlation between Fe concentration and $\delta^{34}S_{CAS}$ and [CAS] (Figs. 5.9E and 5.9F). Our results reinforce that pyrite oxidation was not significant and the pyrite oxidation during CAS extractions is unlikely to have caused significant change in the $\delta^{34}S_{CAS}$ values.

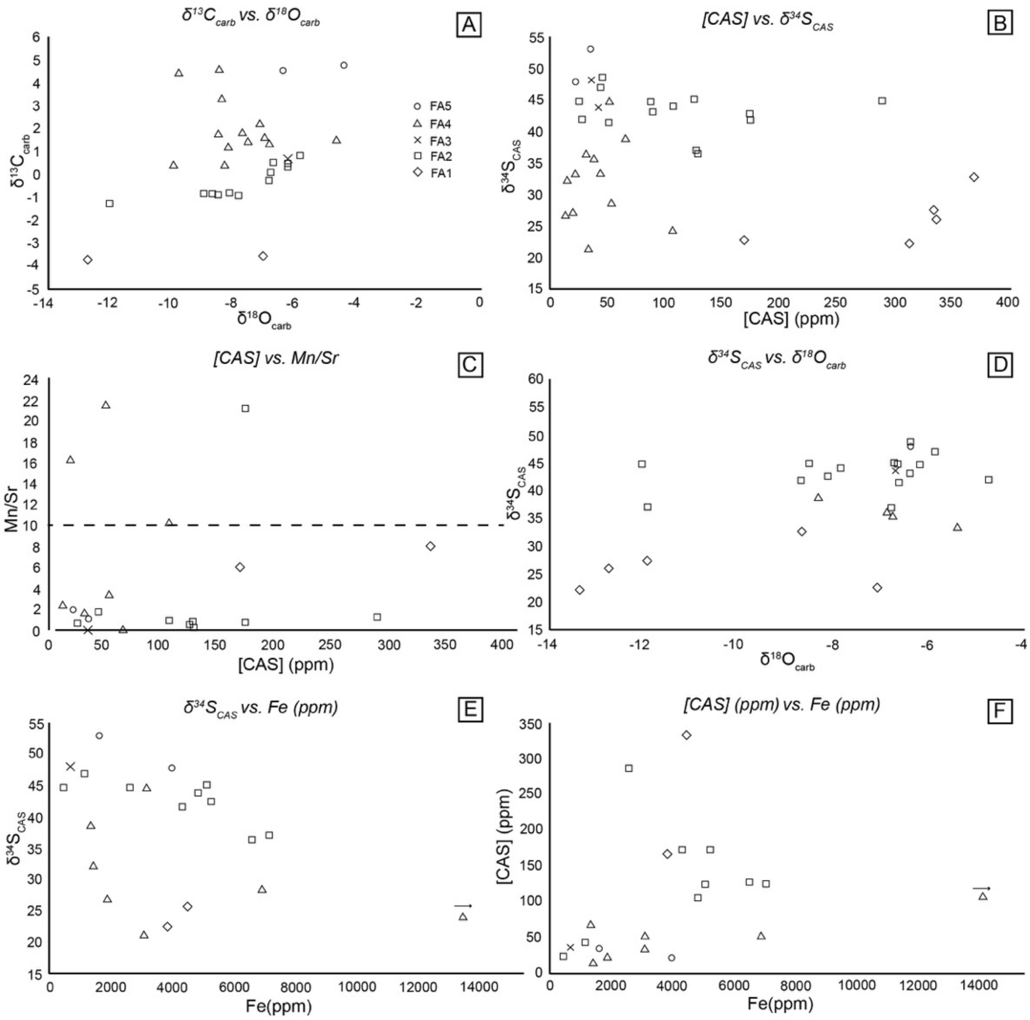

Figure 5.9: Isotope and elemental cross-plots for the Sete Lagoas Formation. A) $\delta^{18}O_{carb}$ vs. $\delta^{13}C_{carb}$; B) [CAS] vs. $\delta^{34}S_{CAS}$; C) [CAS] vs. Mn/Sr; D) $\delta^{34}S_{CAS}$ vs. $\delta^{18}O_{carb}$; E) $\delta^{34}S_{CAS}$ vs. [Fe]; F) [CAS] vs. [Fe].

5.5 Discussions

5.5.1 Interpreting the sulfur and carbon signatures

Carbon and sulfur isotopic curves are coupled, but CAS concentration shows an inverse pattern. An inverse correlation between sulfate concentrations and the $^{34}S_{sulfate}$ might suggest that microbial sulfate reduction was responsible for decreasing sulfate concentrations in pore waters and enriching any residual sulfate with respect to 34S (Hurtgen et al., 2002; Tostevin et al., 2017).

C_{carb} and S_{CAS} isotopes seem to correlate positively, which means that both patterns were driven by the co-burial of reduced C and reduced S (i.e. pyrite and organic carbon) This pattern is commonly observed in the Phanerozoic geologic record (e.g. Gill et al., 2011). In this system, organic matter fuels microbial sulfate reduction, and pyrite is formed when H_2S produced from microbial sulfate reduction reacts with iron minerals and is buried along with the residual organic matter. The carbon and sulfur leaving the ocean through burial are enriched in ^{12}C and ^{32}S via isotope fractionations accompanying photosynthetic and microbial sulfate reduction pathways, respectively, leaving the seawater correspondingly enriched in ^{13}C and ^{34}S. This coupling can result in positive shifts for both species in seawater.

Carbonate-associated sulfate and $\delta^{34}S_{pyrite}$ data from Namibia, South China and Australia suggested that marine sulfate concentrations were particularly low following Neoproterozoic glacial events (Hurtgen et al., 2002; McFadden et al., 2008; Loyd et al., 2012; Tostevin et al., 2017). When sulfate concentrations are lower, rapid temporal changes in $\delta^{34}S_{SW}$ are usually interpreted as a modification of original $\delta^{34}S_{SW}$ of marine sulfate signal by local processes like river fluxes or to show inter-basin heterogeneity. Rates of change in $\delta^{34}S_{SW}$ are commonly used to estimate the size of the marine sulfate reservoir, assuming that faster rates of change represent a smaller marine sulfate reservoir that can be more easily perturbed over short timescales (Algeo et al., 2015; Kah et al., 2004; Loyd et al., 2012).

5.5.2 Paleoenvironmental implications for the Sete Lagoas Formation: modeling the marine sulfate reservoir

Here we used a mass balance-based modeling of the sulfur cycle to identify global environmental parameters that could have contributed to changes in the mass and $\delta^{34}S$ of the marine sulfate reservoir. For this, the composite section (Fig. 5.8) was divided into two intervals: a non-steady state (0 to 40 m height) and a steady-state interval (40 to 130 m height). In the first interval, CAS decreases from 350 ppm to 50 ppm and $\delta^{34}S_{CAS}$ increases from 25‰ to 40‰.

In order to discuss rates of change, it is necessary to establish a depositional timescale, which is often difficult for Precambrian successions. The Sete Lagoas Formation is bounded below by a cap carbonate, with an inferred age of 635Ma (Caxito et al., 2012; Crockford et al., 2017). Given the lack of well-dated horizons in this interval, we estimate a minimum and maximum mass of the sulfate reservoir (M) using accumulation rates in a non-steady state model (Fig. 5.10). The mass of sulfate reservoir was calculated using the following equation and the parameters from Kah et al. (2004):

$$M_o = [F_w\,(\delta_w - \delta_{sulfate}) - F_{py}\,\Delta^{34}S] / (d\delta_{sulfate}/dt) \qquad [1]$$

where $d\delta_{sulfate}/dt$ is the change in the sulfur isotopic composition of oceanic sulfate, $\delta_{sulfate}$ (‰), through time in units of ‰/Myr, F_w is the total flux of sulfur entering the oceans as sulfate ("weathering" flux) in mol/Myr with isotopic composition δ_w in ‰, F_{py} is the flux of sulfur leaving the oceans as pyrite, $\Delta^{34}S$ is the difference between the isotopic composition of coeval sulfide and sulfate, and M_o is the mass of sulfate in the oceans. Estimates for modern fluxes and their isotopic compositions are as follows: $F_w = 1x10^{14}$ g yr $^{-1}$, $\delta_w = +6‰$, $F_{py} = 4x10^{13}$ g yr $^{-1}$, $\Delta^{34}S = 25$ ‰.

For the minimum M, we assume that the 40 m-thick strata between the Marinoan cap carbonate and the *Cloudina* occurrence was deposited in 5 Ma, duration proposed by Hoffman et al. (1998) for a Snowball Earth episode, resulting in a very high depositional rate of 8 m/Myr. For the maximum M, we assume that the same strata would last no more than 80 Ma, which is aproximately the difference between the Marinoan age and the index fossil, resulting in a very low depositional rate of 0.5 m/Myr. Considering these assumptions, we constrain the total marine sulfate reservoir of the Sete Lagoas Formation between 1 x 10^{18} mol and 1.6 x 10^{19} mol (SO_4^{-2} concentrations of 0.83-13.3 mM, respectively), which is consistent with the range of sulfate concentrations calculated for another Brazilian Marinoan cap carbonate from the Mirassol d'Oeste Formation, Araras Group (Sansjofre et al., 2016).

Considering that sedimentation rate was relatively constant during this time interval, it is very unlikely that the sedimentation rate was very low as 0.5 m/Ma (depositional rate considering no unconformities), compared to the conservative depositional rates between 30 or 40 m/Ma for the late Neoproterozoic assumed by Kah et al. (2004) in their model. Thus, besides the possibility of a regional unconformity in this interval, another alternative interpretation could be different sedimentation rates throughout the lower Sete Lagoas Formation due to local variations in the basin subsidence. Future studies should focus on recognizing tie-points with reliable ages, which can be used to generate a more refined model.

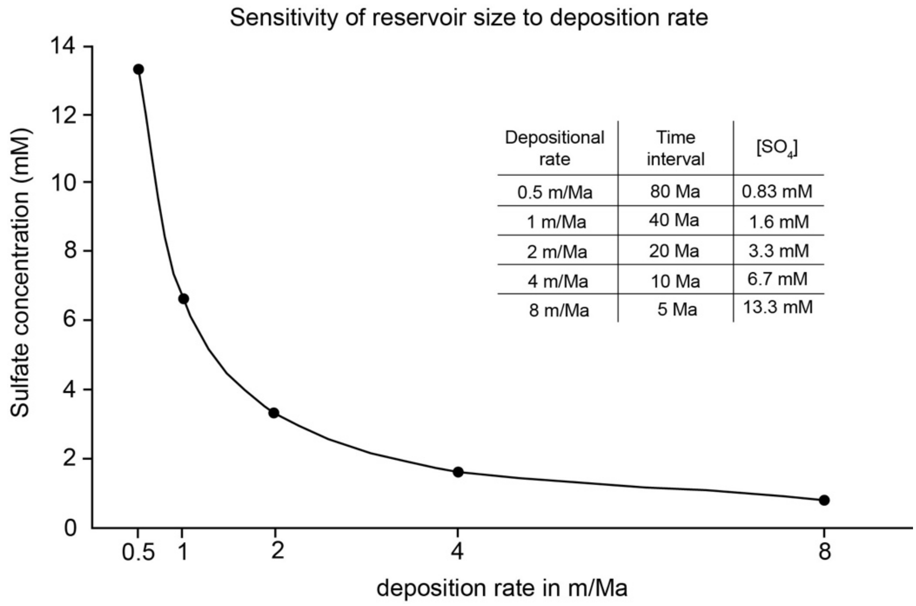

Figure 5.10: Sensitivity of the marine sulfate reservoir size to deposition rate, calculated using Kah et al. (2004) approach The sensitivity of M_o to changes in $d\delta_{sulfate}/dt$ varies as a natural log with respect to deposition rate. M_o is most sensitive at deposition rates < 2 m/Ma (~3.4 mM increase for 1 m/Ma rate increase), moderately sensitive at rates of 2-4 m/Ma (~1.1 mM per 1 m/Ma rate increase), and insensitive at rates > 6 m/Ma (~ 0.2 mM per 1 m/Ma rate increase).

Based on the measured CAS concentration, we interpreted an oxygenation event (367 ppm or 3.82 mM) at the top of cap dolostone, followed by a widespread low sulfate conditions (125 ppm or 1.3 mM) during the first stage of deposition of the lower Sete Lagoas Formation. This increase in oxygen probably favored the sulfate formation, and consequently, barite precipitation.

Finally, in terms of the paleoenvironmental evolution of the Sete Lagoas Formation, a protracted watermass oxygenation, is consistent with our CAS concentration interpretation. It is important to note that this regional event representing a global oxygenation phenomenon registered in several contemporaneous post-Marinoan deposits (Caxito et al. 2018; Hippertt et al. 2019). In the same interval, the lower $\delta^{34}S$ values could be explained by the large input of freshwater, similarly to those interpreted by Paula-Santos et al. (2018), based on REE data in the lower Sete Lagoas Formation. Following this oxygenation event, positive Ce/Ce* values from Paula-Santos et al. (2018) reflect bottom water anoxia for both shallow and deep settings. This anoxia could also explain our low CAS concentrations in the steady-state interval.

5.6 Conclusions

Based on detailed sedimentologic, stratigraphic and new C, O and S isotopic data from the Sete Lagoas succession in the Januária área (northern Minas Gerais State, Brazil), we conclude that:

- Five facies associations were defined for the Sete Lagoas Formation at Januária área: i) cap dolostone, ii) peritidal, iii) seismic-influenced carbonate ramp, iv) oolitic belt, v) microbialitic tidal flat;
- The basal sequence (S1) comprises the cap dolostone deposition related to a rapid transgression (TST1), culminating in a seafloor precipitates layer interpreted as a maximum flooding surface (MFS1). Following this, diferente facies were deposited in peritidal settings until the flat-pebble breccia deposition in a shoreface position and corresponding to a highstand system tract (HST1). A second transgressive system tract (TST2) corresponds to an increase in the accommodation space rate, allowing the deposition of ooid shoals and domal stromatolites in deeper water conditions. This succession is covered by microbialitic tidal deposits separated from the Serra de Santa Helena Formation by a pronounced regional karstic paleosurface (SB3);
- Clast measurements, paleocurrent data and stratigraphic analyses allow us to intepret a NE-SE shoreline direction with offshore setting (ocean waters) located to SE quadrante. The thickening of the oolitic belt succession (FA4) suggests an increase in the subsidence rates towards E-NE;
- Carbon and sulfur isotopic curves are coupled, but CAS concentration shows an inverse pattern. The positive correlation between C_{carb} and S_{CAS} isotopes probably means that both patterns were driven by the co-burial of reduced C and reduced S (i.e., pyrite and organic carbon). This pattern is commonly identified in early Phanerozoic successions.
- Low sulfate concentrations are required to adequate the high rates of isotopic change observed in the Sete Lagoas Formation succession and agrees with previous estimates for the size of the Ediacaran sulfate reservoir. However, our data suggest a significant increase in sulfate concentration in the lower Sete Lagoas Formation, which is consistente with the oxygenation intepreted by recente studies based on Cr isotopes (Caxito et al., 2018), REE data (Paula-Santos et al., 2018) and iron speciation and RSE data (Hippertt et al., 2019) in other localities of SFC.

ACKNOWLEDGEMENTS

This study was funded by Fundação de Amparo à Pesquisa do Estado de São Paulo (FAPESP 2015/07391-0, 2017/19023-1 and 2018/26230-6). S.X. acknowledges funding from the NASA Exobiology and Evolutionary Biology Program (80NSSC18K1086). L. V. Warren is fellow of the CNPq.

5.7 REFERENCES

Alkmim, F.F., Martins-Neto, M.A., 2012. Proterozoic first-order sedimentary sequences of the São Francisco craton, eastern Brazil. Mar. Pet. Geol. 33, 127–139.

Alvarenga, C.J.S., Santos, R. V., Dantas, E.L., 2004. C-O-Sr isotopic stratigraphy of cap carbonates overlying Marinoan-age glacial diamictites in the Paraguay Belt, Brazil. Precambrian Res. 131, 1–21.

Alvarenga, C.J.S., Santos, R. V., Vieira, L.C., Lima, B.A.F., Mancini, L.H., 2014. Meso-Neoproterozoic isotope stratigraphy on carbonates platforms in the brasilia belt of Brazil. Precambrian Res. 251, 164–180.

Babinski, M., Vieira, L.C., Trindade, R.I.F., 2007. Direct dating of the Sete Lagoas cap carbonate (Bambuí Group, Brazil) and implications for the Neoproterozoic glacial events. Terra Nov. 19, 401–406.

Bergmann, K.D., Grotzinger, J.P., Fischer, W.W., 2013. Biological Influences on Seafloor Carbonate Precipitation. Palaios 28, 99–115.

Caetano-Filho, S., Macedo Paula-Santos, G., Guacaneme, C., Babinski, M., Bedoya-Rueda, C., Peloso, M., Amorim, K., Afonso, J., Kuchenbecker, M., Reis, H., Trindade, R.I.F., 2019. Sequence stratigraphy and chemostratigraphy of an Ediacaran-Cambrian foreland-related carbonate ramp (Bambuí Group, Brazil). Precambrian Res. 331, 105365.

Caxito, F. de A., Halverson, G.P., Uhlein, A., Stevenson, R., Gonçalves Dias, T., Uhlein, G.J., 2012. Marinoan glaciation in east central Brazil. Precambrian Res. 200–203, 38–58.

Caxito, F.A., Frei, R., Uhlein, G.J., Gonçalves Dias, T., Árting, T.B., Uhlein, A., 2018. Multiproxy geochemical and isotope stratigraphy records of a Neoproterozoic Oxygenation Event in the Ediacaran Sete Lagoas cap carbonate, Bambuí Group, Brazil. Chem. Geol. 481, 119–132.

Crockford, P.W., Hodgskiss, M.S.W., Uhlein, G.J., Caxito, F., Hayles, J.A., Halverson, G.P., 2017. Linking paleocontinents through triple oxygen isotope anomalies. Geology 46, 179–182.

Cui, H., Kaufman, A.J., Xiao, S., Peek, S., Cao, H., Min, X., Cai, Y., Siegel, Z., Liu, X.-M., Peng, Y., Schiffbauer, J.D., Martin, A.J., 2016. Environmental context for the terminal Ediacaran biomineralization of animals. Geobiology 14, 344–363.

Cui, H., Kaufman, A.J., Xiao, S., Zhou, C., Liu, X.M., 2017. Was the Ediacaran Shuram Excursion a globally synchronized early diagenetic event? Insights from methane-derived authigenic carbonates in the uppermost Doushantuo Formation, South China. Chem. Geol. 450, 59–80.

D'Agrella-Filho, M.S., Babinski, M., Trindade, R.I.F., Van Schmus, W.R., Ernesto, M., 2000. Simultaneous remagnetization and U-Pb isotope resetting in Neoproterozoic carbonates of the Sao Francisco craton, Brazil. Precambrian Res. 99, 179–196.

Dardenne, M.A., 1978. Síntese sobre a estratigrafia do Grupo Bambuí no Brasil Central, in: Anais Do XXX Congresso Brasileiro de Geologia. Recife, pp. 597–610.

Drummond, J.B.R., Pufahl, P.K., Porto, C.G., Carvalho, M., 2015. Neoproterozoic peritidal phosphorite from the Sete Lagoas Formation (Brazil) and the Precambrian phosphorus cycle. Sedimentology 62, 1978–2008.

Gill, B.C., Lyons, T.W., Frank, T.D., 2008. Behavior of carbonate-associated sulfate during meteoric diagenesis and implications for the sulfur isotope paleoproxy. Geochim. Cosmochim. Acta 72, 4699–4711.

Guacaneme, C., Babinski, M., Paula-Santos, G.M., Pedrosa-Soares, A.C., 2017. C, O and Sr isotopic variations in Neoproterozoic-Cambrian rocks from Sete Lagoas Formation (Bambuí Group), in the southern São Francisco Basin, Brazil. Brazilian J. Geol. 47, 521–543.

Hall, M., Kaufman, A.J., Vickers-Rich, P., Ivantsov, A., Trusler, P., Linnemann, U., Hofmann, M., Elliott, D., Cui, H., Fedonkin, M., Hoffmann, K.H., Wilson, S.A., Schneider, G., Smith, J., 2013. Stratigraphy, palaeontology and geochemistry of the late Neoproterozoic Aar Member, southwest Namibia: Reflecting environmental controls on Ediacara fossil preservation during the terminal Proterozoic in African Gondwana. Precambrian Res. 238, 214–232.

Hart, B.S., Plint, A.G., 1995. Gravelly shoreface and beachface deposits, in: Sedimentary Facies Analysis. pp. 75–99.

Higgins, J.A., Schrag, D.P., 2003. Aftermath of a snowball Earth. Geochemistry, Geophys. Geosystems 4, 1–20.

Hippertt, J.P., Caxito, F.A., Uhlein, G.J., Nalini, H.A., Sial, A.N., Abreu, A.T., Nogueira, L.B., 2019. The Fate of a Neoproterozoic Intracratonic Marine Basin: Trace Elements, TOC and IRON Speciation Geochemistry of the Bambuí Basin, Brazil. Precambrian Res. 330, 101–120.

Hoffman, P. F., Rose, B.E.J., Fairchild, I.J., Benn, D.I., Brocks, J.J., Halverson, G.P., Sadler, P.M., Cohen, P.A., Hoffman, Paul F., Voigt, A., Donnadieu, Y., Ferreira, D., Le Hir, G., Macdonald, F.A., Creveling, J.R., Jansen, M.F., Love, G.D., Partin, C.A., Abbot, D.S., Tziperman, E., Cox, G.M., Ramstein, G., Erwin, D.H., Goodman, J.C., Rose, C. V., Maloof, A.C., Ashkenazy, Y., Warren, S.G., 2017. Snowball Earth climate dynamics and Cryogenian geology-geobiology. Sci. Adv. 3, 1–43.

Hoffman, P.F., Macdonald, F. a., Halverson, G.P., 2011. Chemical sediments associated with Neoproterozoic glaciation: iron formation, cap carbonate, barite and phosphorite. Geol. Soc. London, Mem. 36, 67–80.

Hoffman, P.F., Schrag, D.P., 2002. The snowball Earth hypothesis: testing the limits of global change. Terra Nov. 14, 129–155.

Hurtgen, M.T., Arthur, M.A., Suits, N.S., Kaufman, A.J., 2002. The sulfur isotopic composition of Neoproterozoic seawater sulfate: Implications for a snowball Earth? Earth Planet. Sci. Lett. 203, 413–429.

Hurtgen, M.T., Halverson, G.P., Arthur, M.A., Hoffman, P.F., 2006. Sulfur cycling in the aftermath of a 635-Ma snowball glaciation: Evidence for a syn-glacial sulfidic deep ocean. Earth Planet. Sci. Lett. 245, 551–570.

Iyer, S.S., Babinski, M., Krouse, H.R., Chemale, F., 1995. Highly 13C-enriched carbonate and organic matter in the Neoproterozoic sediments of the BambuíGroup, Brazil. Precambrian Res. 73, 271–282.

Jahnert, R.J., Collins, L.B., 2011. Significance of subtidal microbial deposits in Shark Bay, Australia. Mar. Geol. 286, 106–111.

Johnston, D.T., Poulton, S.W., Tosca, N.J., O'Brien, T., Halverson, G.P., Schrag, D.P., Macdonald, F.A., 2013. Searching for an oxygenation event in the fossiliferous Ediacaran of northwestern Canada. Chem. Geol. 362, 273–286.

Kah, L.C., Lyons, T.W., Frank, T.D., 2004. Low marine sulphate and protracted oxygenation of the Proterozoic biosphere. Nature 431, 834–838.

Kuchenbecker, M., Pedrosa-Soares, A.C., Lopes-Silva, L., Babinski, M., Pimenta, F., 2016. Chemostratigraphy of the lower Bambuí Group, southwestern São Francisco Craton, Brazil: insights on Gondwana paleoenvironments. Brazilian J. Geol. 46, 145–162.

Lindsay, J.F., Kennard, J.M., Southgate, P.N., 1993. Application of sequence stratigraphy in an intracratonic setting, Amadeus Basin, central Australia, in: Sequence Stratigraphy and Facies Associations. pp. 605–631.

Loyd, S.J., Sour-Tovar, F., Lyons, T.W., Marenco, P.J., Corsetti, F.A., Kaufman, A.J., Hagadorn, J.W., 2013. Local δ34S variability in ~580Ma carbonates of northwestern Mexico and the Neoproterozoic marine sulfate reservoir. Precambrian Res. 224, 551–569.

Macdonald, F.A., Strauss, J. V., Sperling, E.A., Halverson, G.P., Narbonne, G.M., Johnston, D.T., Kunzmann, M., Schrag, D.P., Higgins, J.A., 2013. The stratigraphic relationship between the Shuram carbon isotope excursion, the oxygenation of Neoproterozoic oceans, and the first appearance of the Ediacara biota and bilaterian trace fossils in northwestern Canada. Chem. Geol. 362, 250–272.

Marenco, P.J., Corsetti, F.A., Hammond, D.E., Kaufman, A.J., Bottjer, D.J., 2008. Oxidation of pyrite during extraction of carbonate associated sulfate. Chem. Geol. 247, 124–132.

Martins, M., Lemos, V., 2007. Análise estratigráfica das seqüências neoproterozóicas da Bacia do São Francisco. Brazilian J. Geol. 37, 156–167.

Martins, Mariela, Lemos, V.B., 2007. Análise estratigráfica das seqüências neoproterozóicas da Bacia do São Francisco. Rev. Bras. Geociências 37, 156–167.

Mazumdar, A., Goldberg, T., Strauss, H., 2008. Abiotic oxidation of pyrite by Fe(III) in acidic media and its implications for sulfur isotope measurements of lattice-bound sulfate in sediments. Chem. Geol. 253, 30–37.

McFadden, K.A., Huang, J., Chu, X., Jiang, G., Kaufman, A.J., Zhou, C., Yuan, X., Xiao, S., 2008. Pulsed oxidation and biological evolution in the Ediacaran Doushantuo Formation. Proc. Natl. Acad. Sci. 105, 3197–3202.

Misi, A., Teixeira, J.B.G., Azmy, K., Veizer, J., Boggiani, P.C., Iyer, S.S.S., Gaucher, C., Kaufman, A.J., Powis, K., Sanches, A.L., 2007. Chemostratigraphic correlation of Neoproterozoic successions in South America. Chem. Geol. 237, 143–167.

Nobre-Lopes, J., 2002. Diagenesis of the dolomites hosting Zn/Ag mineral deposits in the Bambuí Group at Januária region (MG). Unpublished PhD thesis, University of Campinas, Campinas-SP, Brazil. 229p.

Okubo, J., Muscente, A.D., Luvizotto, G.L., Uhlein, G.J., Warren, L.V., 2018. Phosphogenesis, aragonite fan formation and seafloor environments following the Marinoan glaciation. Precambrian Res. 311, 24–36.

Osburn, M.R., Owens, J., Bergmann, K.D., Lyons, T.W., Grotzinger, J.P., 2015. Dynamic changes in sulfate sulfur isotopes preceding the Ediacaran Shuram Excursion. Geochim. Cosmochim. Acta 170, 204–224.

Paula-Santos, G.M., Babinski, M., Kuchenbecker, M., Caetano-Filho, S., Trindade, R.I., Pedrosa-Soares, A.C., 2015. New evidence of an Ediacaran age for the Bambuí Group in southern São Francisco craton (eastern Brazil) from zircon U–Pb data and isotope chemostratigraphy. Gondwana Res. 28, 702–720.

Paula-Santos, G.M., Caetano-Filho, S., Babinski, M., Enzweiler, J., 2018. Rare earth elements of carbonate rocks from the Bambuí Group, southern São Francisco Basin, Brazil, and their significance as paleoenvironmental proxies. Precambrian Res. 305, 327–340.

Paula-Santos, G.M., Caetano-Filho, S., Babinski, M., Trindade, R.I.F., Guacaneme, C., 2017. Tracking connection and restriction of West Gondwana São Francisco Basin through isotope chemostratigraphy. Gondwana Res. 42, 280–305.

Perrela Jr., P., Uhlein, A., Uhlein, G.J., Sial, A.N., Pedrosa-Soares, A.C., Lima, O.N.B., 2017. Facies analysis, sequence stratigraphy and chemostratigraphy of the Sete Lagoas Formation (Bambuí Group), northern Minas Gerais State, Brazil: evidence of a cap carbonate deposited on the Januária basement high. Brazilian J. Geol. 47, 59–77.

Rankey, E.C., Riegl, B., Steffen, K., 2006. Form, function and feedbacks in a tidally dominated ooid shoal, Bahamas. Sedimentology 53, 1191–1210.

Raposo, M.I.B., McReath, I., D'Agrella-Filho, M.S., 2006. Magnetic fabrics, rock magnetism, cathodoluminescence and petrography of apparently undeformed Bambui carbonates from São Francisco Basin (Minas Gerais State, SE Brazil): An integrated study. Tectonophysics 418, 111–130.

Reis, H.L.S., Suss, J.F., 2016. Mixed carbonate-siliciclastic sedimentation in forebulge grabens: An example from the Ediacaran Bambuí Group, São Francisco Basin, Brazil. Sediment. Geol. 339, 83–103.

Reis, H.L.S., Suss, J.F., Fonseca, R.C.S., Alkmim, F.F., 2017. Ediacaran forebulge grabens of the southern São Francisco basin, SE Brazil: Craton interior dynamics during West Gondwana assembly. Precambrian Res. 302, 150–170.

Santos, R.V., Souza de Alvarenga, C.J., Babinski, M., Ramos, M.L.S., Cukrov, N., Fonseca, M.A., da Nóbrega Sial, A., Dardenne, M.A., Noce, C.M., 2004. Carbon isotopes of Mesoproterozoic-Neoproterozoic sequences from Southern São Francisco craton and Araçuaí Belt, Brazil: Paleographic implications. J. South Am. Earth Sci. 18, 27–39.

Saylor, B.Z., Grotzinger, J.P., Germs, G.J.B., 1995. Sequence stratigraphy and sedimentology of the Neoproterozoic Kuibis and Schwarzrand Subgroups (Nama Group), southwestern Namibia. Precambrian Res. 73, 153–171.

Shen, B., Xiao, S., Zhou, C., Kaufman, A.J., Yuan, X., 2010. Carbon and sulfur isotope chemostratigraphy of the Neoproterozoic Quanji Group of the Chaidam Basin, NW China: Basin stratification in the aftermath of an Ediacaran glaciation postdating the Shuram event? Precambrian Res. 177, 241–252.

Simonetti, C., Fairchild, T.R., 2000. Proterozoic microfossils from subsurface siliciclastic rocks of the Sao Francisco Craton, south-central Brazil. Precambrian Res. 103, 1–29.

Smith, E.F., Eyster, A.E., Schrag, D.P., Nelson, L.L., Macdonald, F.A., Rowland, S.M., Strange, M.A., 2016. The end of the Ediacaran: Two new exceptionally preserved body fossil assemblages from Mount Dunfee, Nevada, USA. Geology 44, 911–914.

Tostevin, R., He, T., Turchyn, A. V., Wood, R.A., Penny, A.M., Bowyer, F., Antler, G., Shields, G.A., 2017. Constraints on the late Ediacaran sulfur cycle from carbonate associated sulfate. Precambrian Res. 290, 113–125.

Trindade, R.I.F., D'Agrella-Filho, M.S., Babinski, M., Font, E., Brito Neves, B.B., 2004. Paleomagnetism and geochronology of the Bebedouro cap carbonate: Evidence for continental-scale Cambrian remagnetization in the São Francisco craton, Brazil. Precambrian Res. 128, 83–103.

Uhlein, G.J., Uhlein, A., Pereira, E., Caxito, F.A., Okubo, J., Warren, L.V., Sial, A.N., 2019. Ediacaran paleoenvironmental changes recorded in the mixed carbonate-siliciclastic Bambuí Basin, Brazil. Palaeogeogr. Palaeoclimatol. Palaeoecol. 517, 39–51.

Uhlein, G.J., Uhlein, A., Stevenson, R., Halverson, G.P., Caxito, F.A., Cox, G.M., 2017. Early to late Ediacaran conglomeratic wedges from a complete foreland basin cycle in the southwest São Francisco Craton, Bambuí Group, Brazil. Precambrian Res. 299, 101–116.

Vieira, L.C., Nédélec, A., Fabre, S., Trindade, R.I.F., Almeida, R.P.D.E., 2015. Aragonite Crystal Fans in Neoproterozoic Cap Carbonates : a Case Study From Brazil and Implications for the Post – Snowball Earth Coastal Environment. J. Sediment. Res. 85, 285–300.

Vieira, L.C., Trindade, R.I.F., Nogueira, A.C.R., Ader, M., 2007. Identification of a Sturtian cap carbonate in the Neoproterozoic Sete Lagoas carbonate platform, Bambuí Group, Brazil. Comptes Rendus - Geosci. 339, 240–258.

Warren, L. V., Fairchild, T.R., Gaucher, C., Boggiani, P.C., Poiré, D.G., Anelli, L.E., Inchausti, J.C.G., 2011. Corumbella and in situ Cloudina in association with thrombolites in the Ediacaran Itapucumi Group, Paraguay. Terra Nov. 23, 382–389.

Warren, L. V., Quaglio, F., Riccomini, C., Simões, M.G., Poiré, D.G., Strikis, N.M., Anelli, L.E., Strikis, P.C., 2014. The puzzle assembled: Ediacaran guide fossil Cloudina reveals an old proto-Gondwana seaway. Geology 42, 391–394.

Zhu, M., Lu, M., Zhang, J., Zhao, F., Li, G., Aihua, Y., Zhao, X., Zhao, M., 2013. Carbon isotope chemostratigraphy and sedimentary facies evolution of the Ediacaran Doushantuo Formation in western Hubei, South China. Precambrian Res. 225, 7–28.

6. "Phosphogenesis, aragonite fan formation, and seafloor environments following the Marinoan glaciation", publicado na revista Precambrian Research (2018, 311: 24-36)

(Fosfogênese, formação de leques de aragonite e ambientes de fundo oceânico após a glaciação Marinoana)

J. Okubo [a], A.D. Muscente [b], G.L. Luvizotto [c], G.J. Uhlein [d], L.V. Warren [a]

[a] Department of Applied Geology, Institute of Geosciences and Exact Sciences, São Paulo State University (Unesp), Rio Claro, SP, Brazil
[b] Department of Earth and Planetary Sciences, Harvard University, Cambridge, MA 02138, USA
[c] Department of Petrology and Metallogenesis, Institute of Geosciences and Exact Sciences, São Paulo State University (Unesp), Rio Claro, SP, Brazil
[d] Institute of Geosciences, Federal University of Minas Gerais, Belo Horizonte, MG, Brazil

Alguns modelos geoquímicos indicam que altas concentrações de fosfato na água do mar ocorreram após as glaciações atribuídas aos eventos de *Snowball Earth* ao final do período Neoproterozoico. No entanto, até o presente momento não existia nenhuma evidência inequívoca de fosfogênese (e.g. precipitação e soterramento de fosfato) durante a deposição das capas carbonáticas que recobrem os diamictitos glaciais ao redor do mundo. Neste trabalho publicado no periódico *Precambrian Research*, são apresentados dados petrográficos e geoquímicos da porção basal da Formação Sete Lagoas com o objetivo de discutir o significado da associação mineral (aragonita + barita + apatita + pirita) nos ambientes marinhos rasos desenvolvidos após a glaciação Marinoana (~635 Ma).

O novo modelo proposto neste trabalho ilustra um ambiente em que a fosfogênese e a formação de leques de aragonita são concomitantes e discute o papel da ferro-redução na formação destes dois minerais. Neste modelo, os leques de aragonita são formados próximo à interface sedimento-água, logo abaixo do limite aeróbio-anóxico. Neste ambiente, o processo de ferro-redução libera Fe^{2+}, que inibe a nucleação de carbonato e favorece a precipitação de aragonita diretamente no fundo oceânico. Ao mesmo tempo, a dissolução dos particulados de óxido de ferro abaixo deste limite libera fosfato, criando condições para a formação da apatita. Outros dois minerais, como a pirita e barita, substituem a apatita, indicando que tais minerais são posteriores à formação dos leques carbonáticos e dos cimentos de apatita. Vale ressaltar que o processo de ferro-redução está envolvido na formação tanto da apatita quanto da aragonita. Tanto a presença de ferro quanto a alta alcalinidade favorecem a formação dos leques de aragonita. Além disso, a alta alcalinidade remove o cálcio da água do mar durante a precipitação da calcita e limita a precipitação de fosfato, pois ambos os minerais precisam de cálcio para a sua formação.

Considerando o exposto, tem-se que a principal contribuição deste artigo consiste na descrição inédita de cimentos de apatita em um contexto de capa carbonática Marinoana em nível global. Da mesma forma, é inovador também o modelo que explica sua relação com os demais minerais autigênicos presentes na capa carbonática da Formação Sete Lagoas.

Precambrian Research 311 (2018) 24–36

Contents lists available at ScienceDirect

Precambrian Research

journal homepage: www.elsevier.com/locate/precamres

Phosphogenesis, aragonite fan formation and seafloor environments following the Marinoan glaciation

J. Okubo[a,*], A.D. Muscente[b], G.L. Luvizotto[c], G.J. Uhlein[d], L.V. Warren[a]

[a] Department of Applied Geology, Institute of Geosciences and Exact Sciences, São Paulo State University (Unesp), Rio Claro, SP, Brazil
[b] Department of Earth and Planetary Sciences, Harvard University, Cambridge, MA 02138, USA
[c] Department of Petrology and Metallogenesis, Institute of Geosciences and Exact Sciences, São Paulo State University (Unesp), Rio Claro, SP, Brazil
[d] Institute of Geosciences, Federal University of Minas Gerais, Belo Horizonte, MG, Brazil

ABSTRACT

Carbonates in the Sete Lagoas Formation (São Francisco craton, Brazil) preserve a record of chemical, biological, and oceanographic changes that occurred during the Ediacaran Period. The base of this formation constitutes a post-glacial cap carbonate, which contains seafloor precipitates (carbonate and barite crystal fans) as well as various authigenic and diagenetic minerals (apatite, pyrite, and barite). Here, we present petrographic and geochemical data on this unit, and discuss the significance of its mineral association for marine environments following the Marinoan ('Snowball Earth') glaciation. For the first time, we report well-developed apatitic cements in a Neoproterozoic cap carbonate. Isopachous and intergranular void-filling cements encrust and surround seafloor-precipitated fan crystals that precipitated as aragonite. We propose a model for the origin of this mineral association, which relates phosphogenesis and aragonite fan formation to a single set of environmental conditions. According to this model, the boundary between oxic and anoxic conditions was located at or just below the sediment-water interface. Burial of iron (oxyhydr)oxides below this boundary liberated phosphate to pore water and provided fuel for iron reduction. Iron reduction released Fe^{2+}, which inhibited nucleation of carbonate and allowed for aragonite growth on the seafloor. Concurrently, 'iron-pumping' shuttled phosphate from the water column to the sediment, and perhaps in conjunction with organic phosphorus remineralization via anaerobic microbial pathways, created conditions conducive to phosphate mineralization. This model corroborates the hypotheses that aragonite crystal fan formation requires the presence of an inhibitor to carbonate nucleation, in addition to high alkalinity, and that Fe^{2+} serves as this inhibitor. Overall, our work documents a close association between aragonite crystal fan formation and phosphogenesis at the beginning of the Ediacaran, illuminates the paleoenvironments of cap carbonates with seafloor precipitates, and contributes to understanding of phosphogenesis following low latitude glaciations.

1. Introduction

The Ediacaran Period witnessed major changes in the Earth system, including a rise in the oxygen level of the atmosphere-ocean system (McFadden et al., 2008; Macdonald et al., 2013; Lenton et al., 2014; Laakso and Schrag, 2017) and the radiation of complex multicellular eukaryotic life (Xiao et al., 2014). Various lines of evidence indicate that these changes followed an intense period of global ('Snowball Earth') glaciation (Kirschvink, 1992; Hoffman et al., 1998). Glacial diamictites occur worldwide in the Neoproterozoic. In general, three glacial episodes—the Sturtian, Marinoan and Gaskiers glaciations—are recognized in this interval (Halverson et al., 2005), and a combination of geochronologic and paleomagnetic data (Evans & Raub, 2011) indicate that the Sturtian and Marinoan glaciations extended to tropical latitudes (Meert and van der Voo, 1994; Trindade and Macouin, 2007). Although some glacial deposits show faceted and striated clasts and contain deformation structures caused by glacial flow (Deynoux, 1985; Hoffman & Schrag, 2002; McMechan, 2000; Hoffman, 2011), some of the 'glaciomarine' units likely represent syntectonic mass-flow deposits (Eyles and Januszczak, 2004; van Loon, 2008).

Cap carbonates are continuous units of pure dolostone (and locally limestone), up to tens of meters thick (James et al., 2001; Hoffman & Schrag, 2002; Corsetti & Lorentz, 2006; Hoffman et al., 2007), which commonly overlie sharp contacts with glacial deposits and subaqueous mass flow deposits around the world. These units are interpreted as the primary sedimentary records of deglaciation (Hoffman et al., 1998;

* Corresponding author.
E-mail address: juokubo@rc.unesp.br (J. Okubo).

https://doi.org/10.1016/j.precamres.2018.04.002
Received 29 May 2017; Received in revised form 27 February 2018; Accepted 5 April 2018
Available online 06 April 2018
0301-9268/

Fairchild & Kennedy, 2007). Sturtian cap carbonates are generally dark, finely laminated, organic- and iron-rich units with rhythmic and anastomosing laminae (Hoffman and Schrag, 2002). These successions sometimes contain roll-up structures, and generally have $\delta^{13}C$ values > 0 (Kennedy et al., 1998; Corsetti & Lorentz, 2006). Marinoan cap carbonates, in contrast, are typically less than 10 m thick and their representative features include macropeloids, stromatolites, barite crystals and tubestone structures (Kennedy, 1996; James et al., 2001; Hoffman & Schrag, 2002; Jiang et al., 2006a). These features are commonly overlain by limestones rich in aragonite crystal fans and/or by deep-water fine-grained siliciclastics. A regional (Gaskiers) glaciation is dated at 580 Ma, but the geographic extent of this event remains a subject of debate (Myrow and Kaufman, 1999; Pu et al., 2016; Spence et al., 2016).

Three non-exclusive models can account for the origin of the cap carbonates. First, assuming that high atmospheric pCO_2 levels were responsible for deglaciation (the Snowball Earth model), such conditions may have driven intense chemical weathering on the continents, which in turn, enhanced seawater alkalinity and promoted rapid precipitation of cap carbonates around the world (Hoffman et al., 1998; Hoffman & Schrag, 2002; Higgins & Schrag, 2003). Second, assuming that glaciation caused physical stratification in the ocean and created a strong surface-to-deep water carbon isotope gradient, post glacial upwelling or flooding may have delivered alkalinity-rich deep water to continental shelves and interior basins (the overturn or upwelling model), resulting in carbonate precipitation (Grotzinger & Knoll, 1995; Kaufman et al., 1997; Ridgwell et al., 2003). Lastly, if extreme cold fostered inorganic carbon supersaturation in the ocean (methane model), methane oxidation could account for deposition of cap carbonates and their associated low carbon isotopic values (Kennedy et al., 2001; Jiang et al., 2003). Overall, these models provide insights into the possible oceanographic conditions associated with low latitude glaciation and illustrate the extreme environmental shifts associated with climate change.

Authigenic minerals provide invaluable information on the evolution of seawater, as they contain direct and indirect evidence of chemical inputs into the ocean and recycling within it (Kastner, 1999). Seafloor-precipitated carbonate crystal fans, generally pseudomorphs after aragonite, occur in many Neoproterozoic cap carbonates (Peryt et al., 1990; Kennedy, 1996; Hoffman et al., 1998; James et al., 2001; Hoffman & Schrag, 2002; Nogueira et al., 2003; Lorentz et al., 2004; Pruss et al., 2008; Vieira et al., 2015). The environmental conditions that fostered their formation remain poorly understood. In general, aragonite fans form in conditions with neutral to alkaline seawater pH, low average sedimentation rates, and low influx of detrital clastic material (Sumner & Grotzinger, 2004). During deposition of cap carbonates, high alkalinity and the presence of inhibitors to carbonate nucleation (perhaps Fe^{2+} under anoxic conditions) may have also contributed to aragonite fan formation. By limiting nucleation, the inhibitors promote a buildup of alkalinity. Under these conditions, mineral growth is localized to preexisting surfaces on the seafloor, where aragonite incorporates dissolved inorganic carbon (DIC) and develops into encrusting cements.

Barite represents another major component of Neoproterozoic cap carbonates. Dolostone units overlying Marinoan glacial diamictites around the world contain barite crystal fans as well as various forms of diagenetic barite (Kennedy, 1996; Jiang et al., 2006a,b; Shields et al., 2007; Macdonald et al., 2009; Zhou et al., 2010; Hoffman & Halverson, 2011; Macdonald & Jones, 2011; Bergmann et al., 2013). These barites variably signify primary seafloor cements and chemical sediments, which formed in deep-water settings (below storm wave base) during marine transgression (Kennedy, 1996; Hoffman & Halverson, 2011) as well as products of fluid mixing in sedimentary sulfate-methane transition zones influenced by gas-hydrate destabilization (Kennedy et al., 2001; Jiang et al., 2003, 2006a,b; Shields et al., 2007; Cui et al., 2017).

Notably, the cap carbonate record of authigenic minerals does not extend to calcium phosphate minerals (Hoffman et al., 2011), even though P:Fe ratios in iron formations and geochemical models suggest that high dissolved phosphate concentrations developed during and/or in the aftermath of low-latitude glaciations (Planavsky et al., 2010; Laakso & Schrag, 2017). The dearth of phosphorite in cap carbonates stands at odds with the cap carbonate models. Riverine input and ocean upwelling constitute the major fluxes of phosphorus to shelf settings conducive to phosphogenesis, the authigenic and early diagenetic precipitation of phosphate with sediment (Glenn & Arthur, 1990; Glenn et al., 1994; Papineau, 2010). As cap carbonate deposition may have resulted from enhanced post-glacial continental weathering and deep water upwelling, the absence of phosphorite is striking. High alkalinity—which sequesters Ca via $CaCO_3$ precipitation and generally limits the rate of phosphate precipitation (Briggs & Wilby, 1996)—may account for this pattern.

In this contribution, we describe the association of seafloor precipitates (carbonate and barite crystal fans) and authigenic and diagenetic minerals (apatite and barite) within the cap carbonate unit in the lower part of the Sete Lagoas Formation (central São Francisco craton) near Januária, central Brazil. In addition, we discuss its significance for global seawater chemistry and sedimentary environments following Neoproterozoic glaciations. Overall, the presence of apatite in this cap carbonate has direct implications for the origin of the seafloor precipitates as well as indirect implications for the phosphorus cycle during the Cryogenian-Ediacaran critical transition.

2. Geological setting, stratigraphy, and depositional age

In east-central Brazil, the São Francisco craton (SFC) is related to the Brasiliano-Pan African orogenies (Trompette, 1994; Brito Neves et al., 1999; see Fig. 1A). The cratonic cover Bambuí basin is surrounded by the late Neoproterozoic Araçuaí and Brasília fold belts in its central portion, and was formed at the end of the Neoproterozoic (Chang et al., 1988; Pimentel et al., 2001, 2011; Martins-Neto, 2009; Reis & Suss, 2016). Overall, the Bambuí Group constitutes a thick (up to 2000 m) succession of carbonate and siliciclastic rocks (Fig. 1B and C), which is subdivided, from base to top, into the Sete Lagoas (SLF), Serra de Santa Helena, Lagoa do Jacaré, Serra da Saudade, and Três Marias formations (Dardenne et al., 1978; Fig. 1C). In some places, the SLF is underlain by the glaciogenic Jequitaí Formation. Regardless, the SLF is comprised of limestone and dolostone (containing well preserved stromatolites) interbedded with shale and mudstone (Vieira et al., 2007). Above the SLF, the Serra de Santa Helena Formation contains shale, siltstone, and sandstone with subordinate limestone, and the Lagoa do Jacaré Formation consists of abundant black and grey limestone, marl, and shale, marking a resumption of carbonate production. Siliciclastic units predominate near the top of the Bambuí Group succession, represented by siltstone and shale of the Serra da Saudade Formation and the sandstone of the uppermost Três Marias Formation (Chiavegatto, 1992).

The carbonates of the SLF were deposited within a shallow carbonate platform just above an erosive discordance with cratonic basement rocks or in conformity with glaciogenic deposits of the Jequitaí Formation. In the vicinity of Januária (Fig. 1A and B) in the central portion of SFC, the Bambuí succession overlies Paleoproterozoic migmatites and gneisses that constitute the Januária high (Fig. 1B). In this region, the SLF consists mainly of grainstone, microbialite, dolostone, and mudstone. Intraformational and hydrothermal breccias are present in the middle part of the unit and rare black chert occurs as thin (less than 5 cm) layers and nodules within the grainstone. In general, black chert likely precipitated during diagenesis in anoxic sedimentary microenvironments influenced by microbial activity (Xiao et al., 2010; Muscente et al., 2015).

The lowermost portion of the SLF resembles a typical post-glacial cap carbonate succession (Vieira et al., 2007), and despite absence of the glaciogenic Jequitaí Formation in some sections of the São Francisco craton, geochronological and paleontological data constrain the

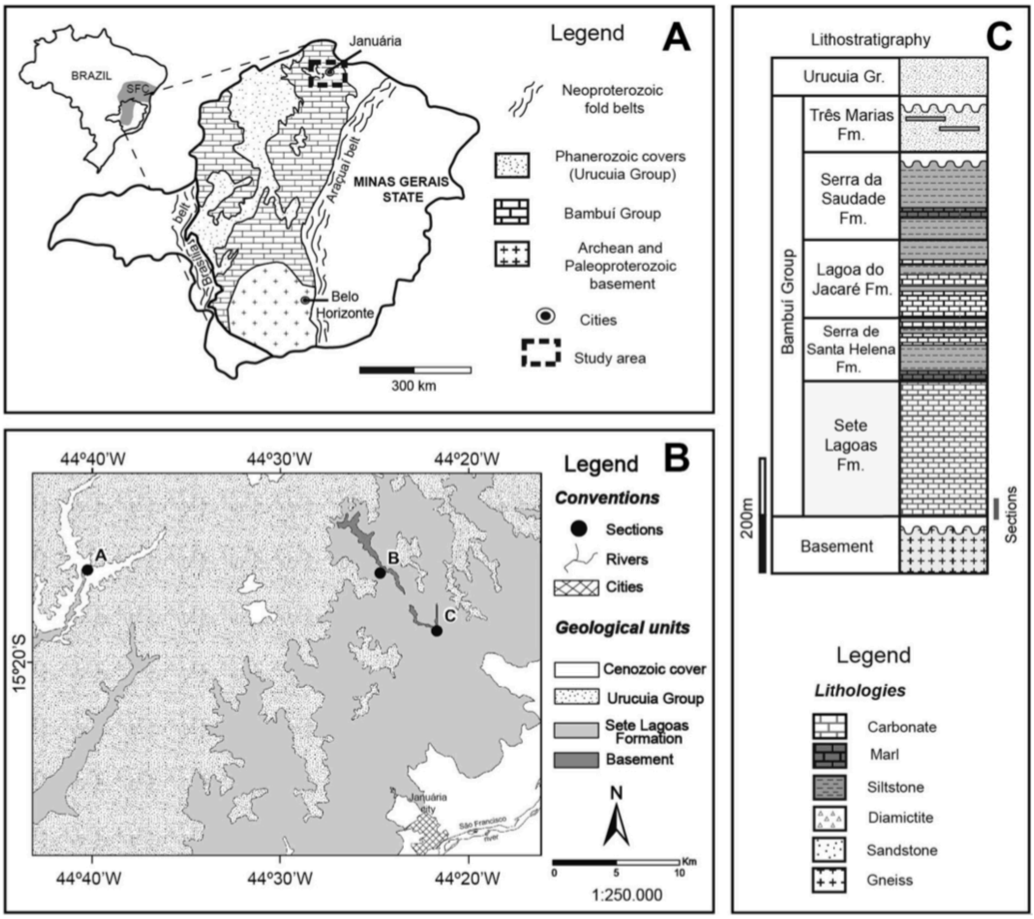

Fig. 1. A) Location of the SFC and the Bambuí Group in the Januária region. B) Geologic map of the SLF in the study area. The sections are presented in Fig. 2. A: Borrachudo section; B: Sapé section; C: Riacho da Cruz section. C) Stratigraphic section of the Bambuí Group in the SFC with the location of the sections presented in Fig. 2. Gr. – Group, Fm. – Formation.

age of the cap carbonate to the Late Neoproterozoic. U-Pb LA-ICP-MS dating of detrital zircon populations collected above the cap carbonate provide a maximum depositional age between 610 Ma (Rodrigues, 2008) and 550 Ma (Paula-Santos et al., 2015) for the middle part of the SLF. In addition, the tubular shelly fossil *Cloudina*—a potential Ediacaran index fossil (Xiao et al., 2016)—occurs in the middle portion of the SLF in the Januária region (Warren et al., 2014), confirming a terminal Ediacaran age for that part of the unit. Occurrence of the fossil *Corumbella*—known from upper Ediacaran strata in Brazil, Paraguay, and the US (Hahn et al., 1982; Hagadorn & Waggoner, 2000; Warren et al., 2011)—likewise corroborates this age. Lastly, planktonic acritarchs with external morphological projections and ornamentation suggest an Ediacaran age for the base of the Bambuí Group (Cruz and Nobre-Lopes, 1992). Other biotic elements in the SLF—microbialites (e.g., Conophyton and thrombolites), silicified microbial mats, and prokaryotic and algal microfossils—do not help to further refine this age (Marchese, 1974; Fairchild & Subacius, 1986; Fairchild et al., 1996; Nobre & Coimbra, 2000), but do represent common elements in terminal Neoproterozoic successions worldwide (Xiao et al., 2014; Muscente et al., 2015).

The maximum depositional age of the cap carbonate and its relative stratigraphic position remain uncertain. In general, the lithological features (e.g., crystal fans and basal pink dolomites), carbon and oxygen isotope profiles, and $^{87}Sr/^{86}Sr$ ratios (0.7074–0.7076) of the unit best match those of Marinoan cap carbonates (Halverson et al., 2005; Hoffman et al., 2007; Caxito et al., 2012). A controversial Pb-Pb isochron age of 740 ± 22 Ma taken from the base of the SLF suggests that the formation was deposited following the Sturtian event (Babinski et al., 2007; Misi et al., 2007; Kaufman et al., 2009). However, the data associated with this age may reflect alteration of the original Pb isotope signal (Caxito et al., 2012) in response to widespread post-burial remagnetization during a large-scale fluid percolation event in the São Francisco craton (Babinski et al., 1999; D'Agrella-Filho et al., 2000). If so, the Pb-Pb age may not be reliable. Regardless, the succession likely contains an unconformity between the lower and upper portions of the SFL (Paula-Santos et al., 2015; Uhlein et al., 2016). Although field surveys have not yet convincingly documented such a feature, a shorter rather than a longer hiatus would account for the limited variation observed in the Bambuí Group strontium isotope curve through the SLF succession (Caxito et al., 2012). Thus, the best available data supports an Ediacaran age for the cap carbonate. The lithology of the cap carbonate—particularly, the presence of crystal fans—points to a Marinoan age, and no substantial carbonate units with similar features occur over Gaskiers glaciogenic deposits. Also, reports of anomalous $\Delta^{17}O$ isotope values within the Sete Lagoas cap carbonate, similar to those found in South China and Mauritania, reinforce the post-

Marinoan context (Crockford et al., 2017). For these reasons, we infer the existence of an unconformity between the base and the middle portion of the sequence, representing an 85 million-year hiatus.

Phosphatic rocks, minerals, and biosedimentary structures occur in the SLF and in the Salitre Formation (Una Group) of the Irecê Basin, which is correlated with the SLF on the basis of chemostratigraphic data (Misi and Veizer, 1998). Vieira et al. (2015) reported apatite as an accessory diagenetic mineral phase in the SLF cap carbonate, but did not describe its petrography or origin. The most substantial phosphatic deposit in the unit occurs in its middle part, where microbial laminated mud-rich siltstone and intraclastic grainstone contain pristine and reworked phosphorite, including discontinuous phosphatic laminae and *in situ*, fine to medium sand-size, ellipsoidal peloids (Drummond et al., 2015). This phosphorite purportedly formed in response to windblown delivery of phosphorus adsorbed on aeolian iron (oxyhydr)oxide and clay (Drummond et al., 2015). In the correlated Salitre Formation, phosphate digitate stromatolites are found at the top of peritidal carbonate cycles, and likely formed when microbial organisms inhabiting intertidal flats created redox and sedimentological conditions conducive to phosphorus mineralization, for instance, by storing and releasing phosphate (Caird et al., 2017). Regardless of the exact processes involved in phosphogenesis in each of these cases, the data are suggestive of high phosphate availability through deposition of the Sete Lagoas and Salitre formations.

3. Material and methods

Three stratigraphic sections were measured in the central part of the SFC near Januária city (Figs. 1B and 2). In all sections, the SLF directly overlies the Paleoproterozoic basement. Rock samples from the Borrachudo and Riacho da Cruz sections were prepared as slabs and thin sections, which were then analyzed via polarized light microscopy and scanning electron microscopy (SEM). All SEM analyses were conducted at an accelerating voltage of 15 keV and a working distance of 10 mm and resulted in secondary electron (SE) and backscattered electron (BSE) images with compositional contrast (Muscente and Xiao, 2015). In addition, several samples were carbon-coated for electron probe microanalysis (EPMA) with X-ray energy dispersive X-ray spectroscopy (EDS) and X-ray wavelength dispersive spectroscopy (WDS). The EPMA work was conducted at the Department of Petrology and Metallogeny (São Paulo State University), using a JEOL JXA 8230 superprobe equipped with 5 WDS spectrometers and a panchromatic cathodoluminescence system (XM-26730PCL). All WDS and EDS data (including elemental maps) were acquired at accelerating voltages of 15 keV and probe currents of 20nA in order to identify major elements: Fe (Kα), Ca (Kα), Mg (Kα), Ba (Lα), S (Kα), Si (Kα) and Al (Kα).

For carbon and oxygen isotopic analyses, carbonate powders were obtained via microdrilling of homogeneous samples (fractured, weathered, and mineral-filled zones were avoided). These powders were reacted with 100% H_3PO_4 under He atmospheric conditions. The carbon and oxygen isotopic compositions of the CO_2 extracted through the process were then measured in a Delta Advantage mass spectrometer in the Federal University of Paraná. Isotopic results are reported in the conventional per-mil delta notation ($\delta^{13}C_{carb}$ and $\delta^{18}O_{carb}$) with respect to Vienna Pee Dee Belemnite (VPDB).

4. Results

Seafloor-precipitated cements were discovered in all studied sections (Figs. 2 and 3). Combined field, petrographic, and *in situ* geochemical analysis show that these fans variably consist of calcium carbonate (Figs. 3–5) and barite (Figs. 3 and 6). The precipitates evidently grew as radiating crystals (i.e., fans) oriented sub-parallel relative to the seafloor as well as upward-oriented (seafloor perpendicular) bed-forming crystals. Carbonate and barite crystal fans occur in rocks of the same facies near the base of the Sete Lagoas Formation. Beginning a few meters above the base of the succession, carbonate fans occur in parallel-laminated beds, which vary from millimeters to decimeters in thickness (Fig. 3A and B). Barite fans, conversely, occur as irregular layers within microbial carbonate and laminated grainstone. These layers extend over laterally continuous areas between 10 and 15 square-meters, are generally 1–2 cm thick, and reach 15 cm thick in some strata exposed in the Borrachudo section (Fig. 2). With the exception of one layer in the Riacho da Cruz section, which bifurcates along the bedding plane (Fig. 3E), the strata containing barite fans are typically stratiform and have flat tops and bases (Fig. 3D).

The calcium carbonate and barite cements occur in close stratigraphic association. However, the relative succession of carbonate- and barite-containing layers varies among sections (Fig. 2). In the Borrachudo section, layers containing carbonate and barite cements alternate in the succession. Conversely, in the Sapé section, seafloor carbonate occurs exclusively within strata below those with barite fans, and in the Riacho da Cruz section, carbonate fans occur in strata ($\delta^{13}C_{carb,}$ $-3.76‰$; $\delta^{18}O_{carb,}$ $-12.77‰$) above those with barite precipitates ($\delta^{13}C_{carb,}$ $-3.15‰$; $\delta^{18}O_{carb,}$ $-8.68‰$).

Electron imaging and *in situ* geochemical analysis generated mineralogical and geochemical data on the various minerals in the unit. As observed from cross sections of bedding surfaces, the fan-forming crystals emanate within horizontal and irregular clay layers (Fig. 3F) with high Al and Si contents relative to the Ca- and Mg-rich calcite matrix of the limestone (Fig. 6). The seafloor barite cements consist of radiating blade-shaped crystals, which are generally between 200 µm and 3 cm in length and about 50 µm in thickness (Figs. 3F and 6). In contrast, the carbonate cements consist of (sub-)acicular (needle-like) crystal units with hexagonal (~200 µm diameter) cross sections (Figs. 3B, C and 4A) and square terminations (Fig. 5D), like aragonite crystals. Each crystal unit, however, consists of mosaic calcite, and is comprised of numerous small equant crystals (Fig. 4B). Polysynthetic twinning of the mosaic crystal units is common. In some layers, the calcite contains a markedly higher concentration of Mg than the surrounding limestone matrix (Fig. 8). Elsewhere, the mosaic units are surrounded by a high-Mg calcite matrix (Fig. 5C).

Besides assorted detrital (quartz, zircon, rutile, and clay – similar to those described by Bergmann et al., 2013) grains and barite and carbonate crystal fans, the matrix of the Sete Lagoas cap carbonate contains three conspicuous forms of sedimentary minerals: apatitic cements, microcrystalline barite, and pyrite (including pseudomorphs of iron oxide after pyrite, Fig. 7). The apatitic cements occur exclusively in layers with carbonate fan crystals (Fig. 4). In these layers, the phosphate minerals occur as isopachous cements encrusting detrital grains (Fig. 4D), as void-filling cements in intergranular spaces (Fig. 4C–E), and as thin laminae within Mg-calcite layers (Fig. 4C and E). The phosphate minerals also rarely occur as cements within rounded aggregates of quartz, calcite, and barite (Fig. 4F). In contrast to these cements, barite and pyrite were found in microcrystalline forms in virtually all samples. Both minerals fill void spaces and encrust apatite (Fig. 4D). In some places, the minerals occur in close association with each other, as exemplified by barite mixed with nodular pyrite/iron oxide (Fig. 7). Elsewhere, the minerals occur in relative isolation (Figs. 6, 7 and 9). Microcrystals of both types are found albeit rarely as inclusions within the mosaic calcite making up the carbonate fan crystals (Fig. 4).

5. Discussion

Petrographic and *in situ* geochemical analyses of the lower SLF near Januária corroborate previous studies, which documented aragonite and barite as major sedimentary minerals within Neoproterozoic cap carbonates (Hoffman et al., 2011). Carbonate crystal fans have been reported from other sections of the SLF (Caxito et al., 2012; Vieira et al., 2015; Kuchenbecker et al., 2016), and in general, are common sedimentary features of cap carbonates around the world (Corsetti et al.,

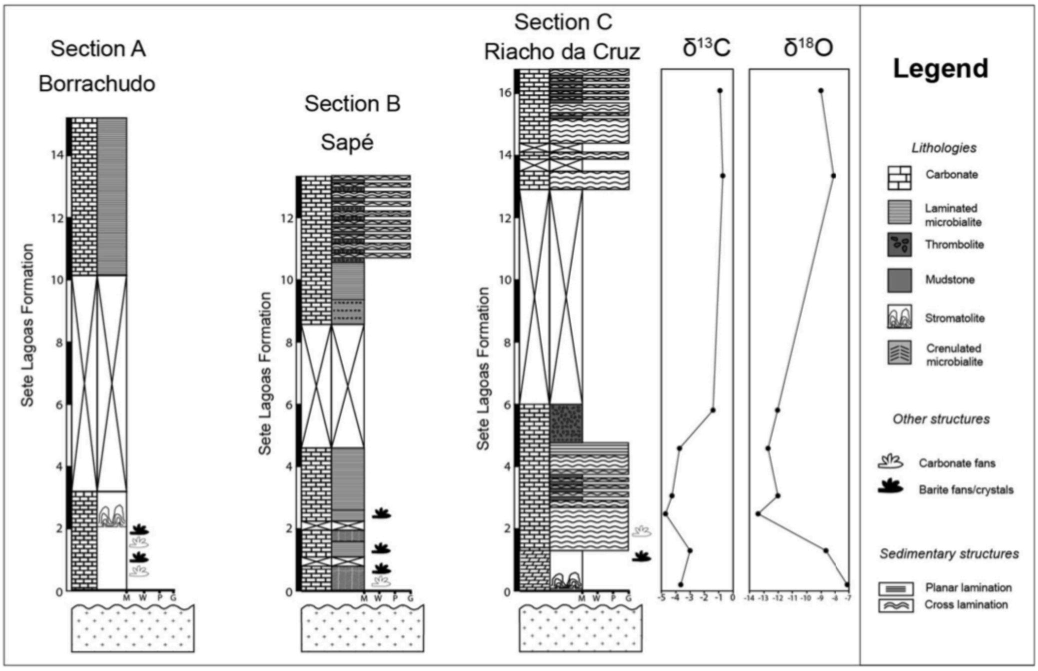

Fig. 2. Measured stratigraphic sections of the lower Sete Lagoas Formation. The columns show the stratigraphic positions of the aragonite fans and barite-bearing strata in relation to various lithologies. Note the prominent negative excursions in the carbon and oxygen isotopic curves near the base of the Sete Lagoas Formation. M = mudstone, W = wackestone, P = packstone, G = grainstone.

2004; Lorentz et al., 2004; Pruss et al., 2008), particularly those overlying Marinoan age glacial diamictites (Hoffman et al., 2011). The presence of well-preserved clusters of aragonite crystals (Figs. 3B, 8) suggests that fan formation in the SLF took place below storm wave base or in protected marine environments, where wave action did not exert a destructive influence, as previously suggested by Vieira et al. (2015). The pseudohexagonal habit of the crystals in these fans indicates that they originally precipitated on the seafloor as aragonite, which was altered to calcite during post-burial diagenesis (Pruss et al., 2008).

Marinoan cap dolostones commonly contain two types of barite (Hoffman et al., 2011)—primary seafloor precipitated crystal fans (Kennedy, 1996; Hoffman and Halverson, 2011) and early diagenetic barites often associated with tepee and tepee-like brecias (Jiang et al., 2006a, 2006b; Shields et al., 2007)—corresponding to the bladed crystals and microcrystalline forms of barite found in the Januária section of SLF, though we did not observe any demonstrable tepees or tepee-like structures. Detrital barite grains (Figs. 4 and 7) may represent products of reworking of fan crystals on the seafloor. In the Riacho da Cruz section, the barite fan crystals emanate within a clay layer (Figs. 3F and 6), affirming that the crystals grew on the seafloor. This millimetric layer could represent a stylolite (Jiang et al., 2006a), produced by pressure-solution during compaction burial, or a pause in the sedimentation, leading to the decantation of the clay over a previous surface in low energy conditions.

Various processes contribute to barite formation and diagenetic alteration, each affecting the morphology and isotopic composition of the resulting crystals (Griffith and Paytan, 2012). In modern marine environments, barite generally forms via hydrothermal/cold seep, biogenic, and diagenetic pathways (Paytan et al., 2002; Shields et al., 2007). Whereas biogenic barite crystals that form in proximity to sinking particular matter and within organisms are typically smaller than 5 μm and ellipsoidal in shape, hydrothermal barite generally consists of rosette-forming tabular crystals 20–70 μm in diameter, and diagenetic barite occurs at tabular crystals 20–700 μm in diameter (Paytan et al., 2002). Biogenic barite generally has a low preservation potential, as diagenetic dissolution in the sulfate-methane transition zone of the sedimentary column destroys biogenic crystals and precipitates barite with a diagenetic overprint (Zhou et al., 2015). Accordingly, the cap carbonate barites most likely represent hydrothermal, cold seep, and/or diagenetic minerals. The processes that promoted widespread precipitation of barite cements on the seafloor during deposition of the cap carbonates remain a subject of debate (Crockford et al., 2016).

For the first time, we report well-developed apatitic cements in a Neoproterozoic cap carbonate. We interpret the phosphatic minerals as products of penecontemporaneous authigenic mineralization for the following reasons. First, pyrite and microcrystalline barite encrust the apatite and fill voids within the phosphatic matrix, indicating that those minerals formed later in diagenesis within the sulfate reduction and sulfate-methane transition zones of the sedimentary column (Fig. 4D). Second, isopacheous phosphate cements encrusting detrital quartz grains and carbonate fan crystals affirm that the phosphate minerals formed prior to the later pyrite and barite (Fig. 4D). Lastly, apatitic cements bind quartz, calcite, and barite in rounded aggregates, which suggest that phosphate mineralization occurred at depths near the sediment-water interface permissive to sedimentary reworking and rounding of material (Fig. 4F), as exemplified by authigenic phosphoclasts in Ediacaran phosphorites (Muscente et al., 2015). Supplementary to these interpretations, subsequent to cementation of the intergranular space between aragonite fan crystals, phosphate mineralization evidently produced several thin laminae within Mg-rich calcite (Fig. 4C and E). These thin laminae point to restriction of phosphate mineralization to a particular depth in the sedimentary column, where sedimentary and geomicrobiological processes concentrated phosphate beyond ordinary supersaturation levels and drove

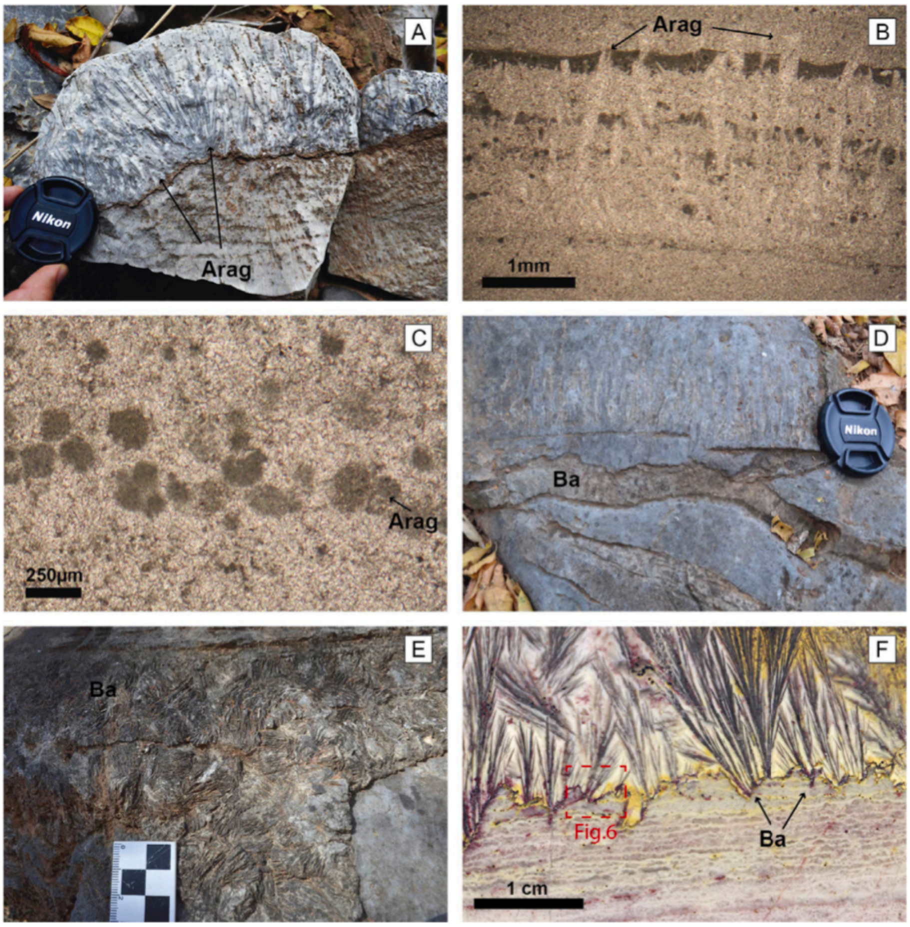

Fig. 3. Photographs and photomicrographs of barite- and aragonite-bearing layers of the lower Sete Lagoas Formation. A) Decimetric aragonite fans in the Borrachudo section. B–C) Thin sections of samples from the Riacho da Cruz section. Scale: 5 cm. B) Millimetric-scale acicular/needlelike crystals forming centimetric aragonite crystal fans. Paralell nicols, 2.5 ×. C) Cross section of aragonite fans, showing pseudohexagonal prisms. Paralell nicols, 10 ×. D) Lateral view of barite (light grey) and aragonite (dark grey) bearing layers (Borrachudo section). Scale: 5 cm. E) Detail of barite fans in the Riacho da Cruz section. F) Rock slab from the Riacho da Cruz section containing barite fans on a surface developed in carbonate/thrombolite substrate (Fig. 4). Arag: aragonite, Ba: barite.

phosphogenesis (Glenn et al., 1994). Overall, in terms of their sedimentology and petrography, the phosphate minerals in the SLF cap carbonate resemble authigenic and early diagenetic phosphatic features in typical phosphatic carbonates and phosphorites of Ediacaran and Cambrian ages (Creveling et al., 2014; Muscente et al., 2015).

This occurrence of apatite supplements other reports of phosphatic rocks, minerals, and biosedimentary structures in the SLF and correlated Salitre Formation (Drummond et al., 2015; Caird et al., 2017). Vieira et al. (2015) previously reported apatite as an accessory diagenetic mineral phase in the SLF cap carbonate, but those author did not describe substantial sedimentary phosphatization of the unit, and they not investigate the petrography of the apatite in any detail. Hence, phosphate mineralization constitutes a widespread but unexplored aspect of the SLF cap carbonate, which merits detailed discussion.

5.1. Model of formation of these authigenic and diagenetic minerals

The petrographic and geochemical data in this original report as well as data from other studies (Jiang et al., 2006a; Shields et al., 2007; Pruss et al., 2008) provide a basis for assessing the origin of the carbonate crystal fans and apatitic cements in the Marinoan cap carbonate at the base of the SLF. As we argue below, the minerals mutually illuminate the localized sedimentary and geobiologic processes involved in their formation as well as provide insights into their stratigraphic and geographic distribution. In addition, from a global to regional perspective, the co-occurrence of carbonate crystal fans and phosphate cements makes sense in terms of the cap carbonate formation and Ediacaran phosphogenic episode models, which attribute high seawater DIC, phosphorus, and calcium concentrations to enhanced continental weathering and ocean upwelling. Therefore, our work provides data pertinent to a variety of hypotheses (Grotzinger and Knoll, 1995; Kaufman et al., 1997; Hoffman et al., 1998; Hoffman and Schrag, 2002; Higgins and Schrag, 2003; Ridgwell et al., 2003; Muscente et al., 2015; Laakso and Schrag, 2017) regarding the low latitude glaciations of the Neoproterozoic.

Aragonite growing on the seafloor may have incorporated DIC from the water column, sediment, or both. Explanations for post-glacial cap carbonate formation generally implicate enhanced alkalinity in benthic marine environments, making the seawater DIC pool the plausible if not likely source of alkalinity. Remineralization of organic carbon via anaerobic microbial processes (iron, manganese, nitrate, and/or sulfate reduction) in the sediment may have further elevated bicarbonate

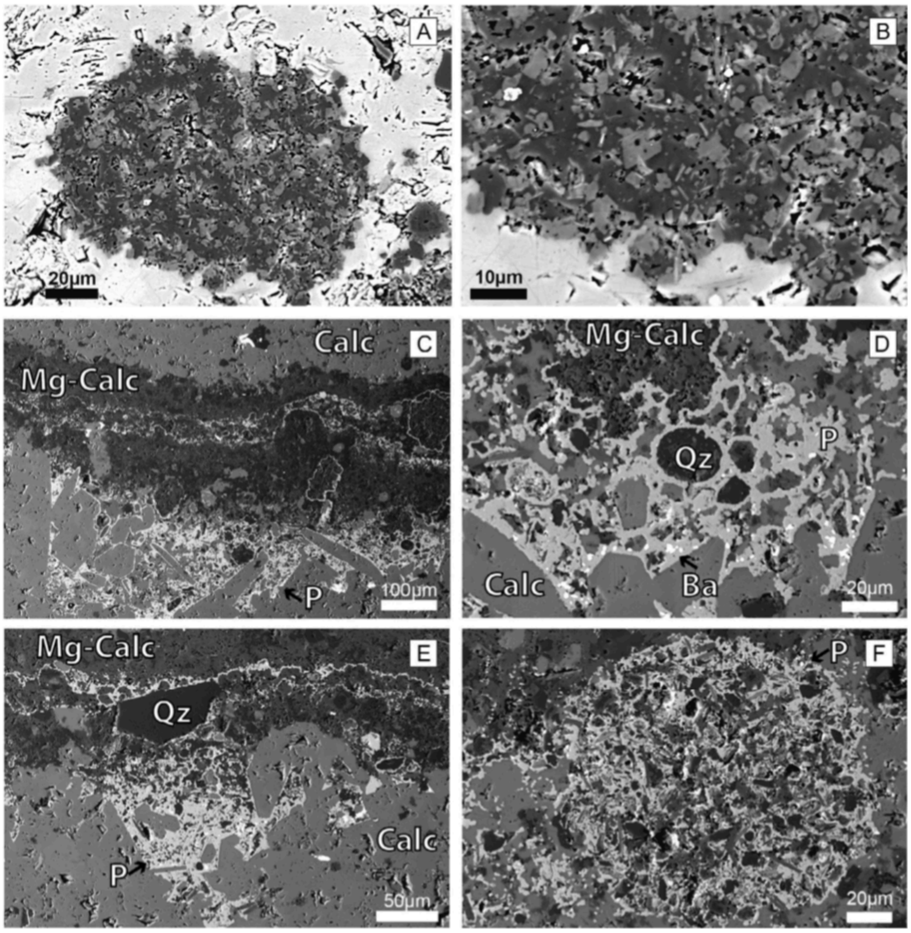

Fig. 4. BSE-SEM images of aragonite fan crystals and encrusting apatitic cements. A) Pseudohexagonal cross-sectional shape of the crystals units, composed of mosaic calcite, a pseudomorph after aragonite. B) Small equant crystal units making up the larger mosaic calcite pseudomorphs after aragonite. C) Phosphate minerals (P) filling the intergranular space and occurring as thin laminae within a Mg-calcite layer. D) Phosphate minerals occurring as isopachous cements on quartz (Qz) and calcite (Calc) grains and filling void spaces between them. Note that barite (Ba) in this image is encrusting the phosphate cement, indicating that it formed later than the cement. E) Phosphate minerals occurring as void-filling cements in intergranular spaces and as thin laminae within a Mg-calcite layer. F) Phosphatic rounded aggregate, composed of quartz, calcite and barite grains.

concentrations beyond supersaturation with respect to aragonite, and thereby, promoted formation of the mineral at the sediment-water interface. If so, the DIC contribution of organic carbon remineralization to aragonite crystal fan growth may have been most significant in seafloor environments, where the oxic-anoxic redox boundary was located near the sediment-water interface. Isotopic data, nonetheless, suggest that carbonate fans in other late Neoproterozoic carbonates principally derived alkalinity from isotopically well-mixed DIC reservoirs, most likely seawater (Pruss et al., 2008). Thus, the sedimentary DIC contribution to growth of the SLF aragonite may have been minor. Regardless of the alkalinity source, formation and growth of aragonite may additionally require the presence of transient inhibitors to carbonate (micrite) nucleation (Sumner and Grotzinger, 1996; De Leeuw, 2002; Pruss et al., 2008). The presence of iron minerals in interstices of fan units (Pruss et al., 2008)—like the pyrite and iron oxides (pyrite pseudomorphs) reported in this study—suggests that Fe^{2+} may have served this role during periods of cap carbonate deposition.

Phosphate follows a number of paths from the water column to sediment, and phosphogenesis may involve precipitation of dissolved pore water phosphate derived from one or more sources. The major fluxes of phosphate to the water column in modern marine shelf environments include upwelling of nutrient-rich seawater and riverine input of phosphate derived from continental weathering (Glenn et al., 1994; Föllmi, 1996). Given hypotheses regarding the source of alkalinity in cap carbonate deposition (Grotzinger and Knoll, 1995; Kaufman et al., 1997; Hoffman et al., 1998; Hoffman and Schrag, 2002; Higgins and Schrag, 2003; Ridgwell et al., 2003), we cannot exclude either of these possibilities or the possibility of aeolian input (Drummond et al., 2015). In any case, phosphorus burial occurs through burial of organic matter, iron (oxyhydr)oxide particulates, phosphatic skeletons, and detrital apatite (Glenn et al., 1994; Föllmi, 1996). The SLF cap carbonate contains no skeletal or detrital apatite grains besides the rounded aggregates of quartz, calcite, and barite (Fig. 4F), which are cemented by authigenic phosphate and likely formed via local reworking of phosphatized sediment. Phosphate mineral cements in the SLF, therefore, likely precipitated from pore water phosphate derived from two sources: remineralization of organically bound phosphorus and desorption of phosphate from surfaces of iron (oxyhydr)oxide particulates.

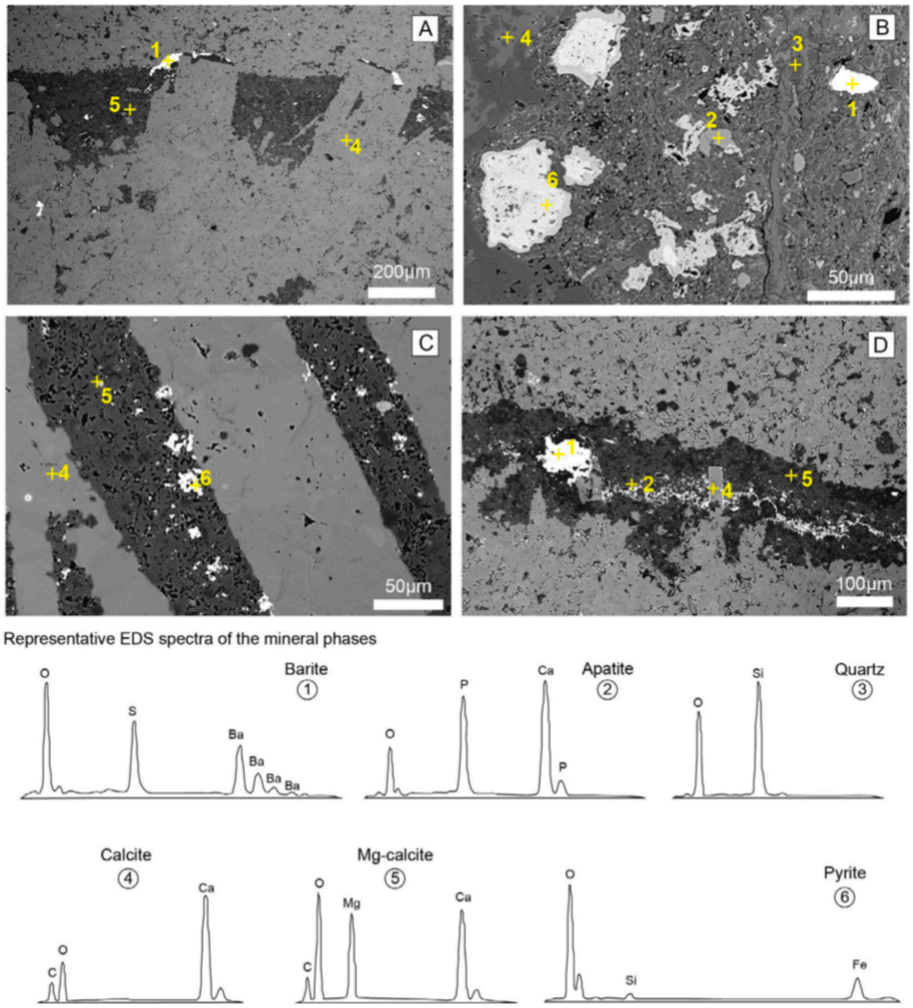

Fig. 5. BSE-SEM images and EDS spectra of the aragonite and barite fans. A) Barite crystals (1) encrusting pseudomorphed aragonite fan crystals. B) Clay surface between the matrix and the barite fans, which is composed of pyrite (6), phosphate (2), and barite (1). C) Details of carbonate fan crystals and inter-crystal spaces containing pyrite grains. D) Surface above the aragonite fans containing barite, diagenetic calcite, and phosphate cement. Numbers in the figure indicate the spot analysis.

In modern phosphogenic settings, the most efficient process of organic phosphorus remineralization is microbial sulfate reduction under anoxic conditions (Arning et al., 2009). The presence of pyrite and iron oxide (pyrite pseudomorphs) provide some evidence for this process. Likewise, these iron minerals affirm that dissolved iron was present during diagenesis, and is consistent with the inference that burial of iron (oxyhydr)oxide particulates below the oxic-anoxic boundary liberated phosphate to pore water. Thus, in general, the data suggest that phosphogenesis occurred near the redox boundary, where both processes maximally contributed to pore water phosphate supersaturation. This hypothesis is consistent with interpretations of other examples of Precambrian phosphogenesis (Nelson et al., 2010; Drummond et al., 2015; Muscente et al., 2015).

Iron (oxyhydr)oxide availability influences both aragonite fan formation and phosphogenesis. Dissolution of iron (oxyhydr)oxide particulates below the redox boundary liberates phosphate for phosphogenesis; microbial iron reduction fueled by these particulates produces DIC for aragonite growth; and both processes result in production of reduced iron (Fe^{2+}), which inhibits carbonate nucleation, and thereby, creates alkaline conditions conducive to aragonite growth on the seafloor. Despite these interrelated aspects of the mineralization processes, marine environments typically favor carbonate over phosphate mineralization, as high ambient bicarbonate concentrations limit the amount of calcium available for reaction with phosphate (Briggs and Wilby, 1996). Correspondingly, pH exerts a strong influence, as acidity destabilizes carbonate minerals, enhances calcium availability, and allows for phosphate precipitation under some circumstances (Allison, 1988).

In this context, a dichotomy presents itself. On the one hand, iron (oxyhydr)oxide burial and microbial metabolisms (carbon and phosphorus remineralization) create conditions conducive to both aragonite fan formation and phosphogenesis. Yet, on the other, microbial remineralization of carbon generates alkalinity, which generally precludes phosphate precipitation and prevents the two mineralization processes from occurring at the same time. A sedimentary model for the mineral association in the SLF cap carbonate must take this dichotomy into consideration. We infer (1) that aragonite crystal fan formation and

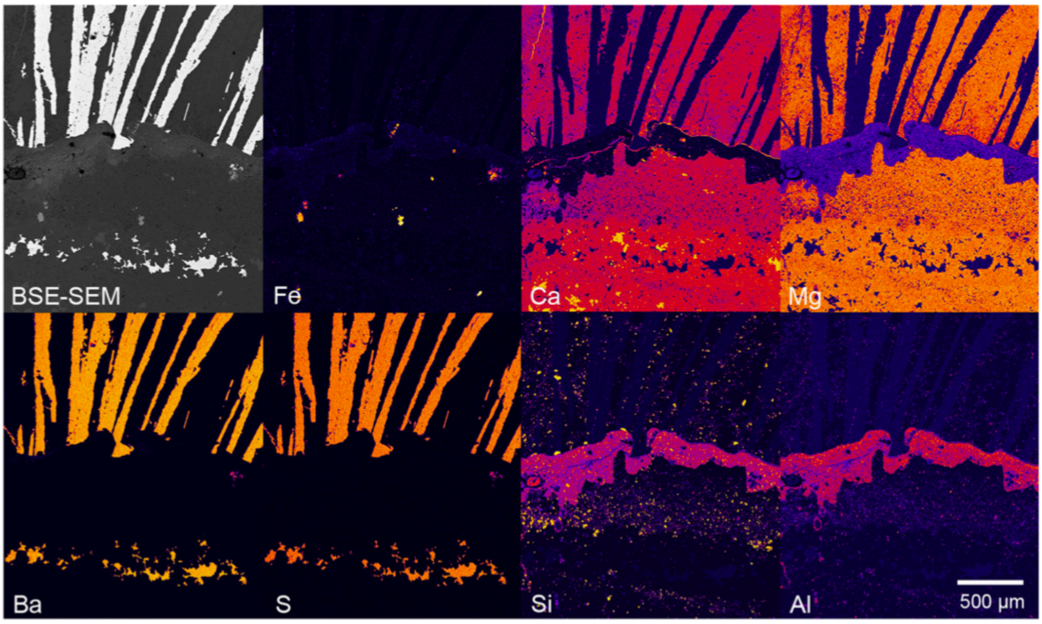

Fig. 6. BSE-SEM image and WDS elemental maps of the contact between the barite fans and the underlying microbialite (Riacho da Cruz section). This contact layer is rich in clays, accounting for its high Al, Si and Mg contents. Detrital barite crystals are commonly found in the matrix of the microbialite facies, as seen below the clay contact layer.

phosphogenesis occurred in an environment, where the oxic-anoxic boundary was located near the sediment-water interface (Fig. 9), and (2) that burial of iron (oxyhydr)oxides below this boundary drove both phenomena through its influence on phosphate and Fe^{2+} concentrations. In the presence of Fe^{2+} generated via reduction of iron (oxyhydr) oxides, carbonate precipitation was largely restricted to preexisting surfaces of aragonitic crystals, which grew on seafloor cements. Following burial of these crystals within sediment with phosphate-rich pore water, phosphate precipitated on the crystals and in the intergranular spaces between them. The contributions of carbon and phosphorus remineralization to mineral growth were likely minor, at least following burial of the aragonite crystals fans, as those microbial

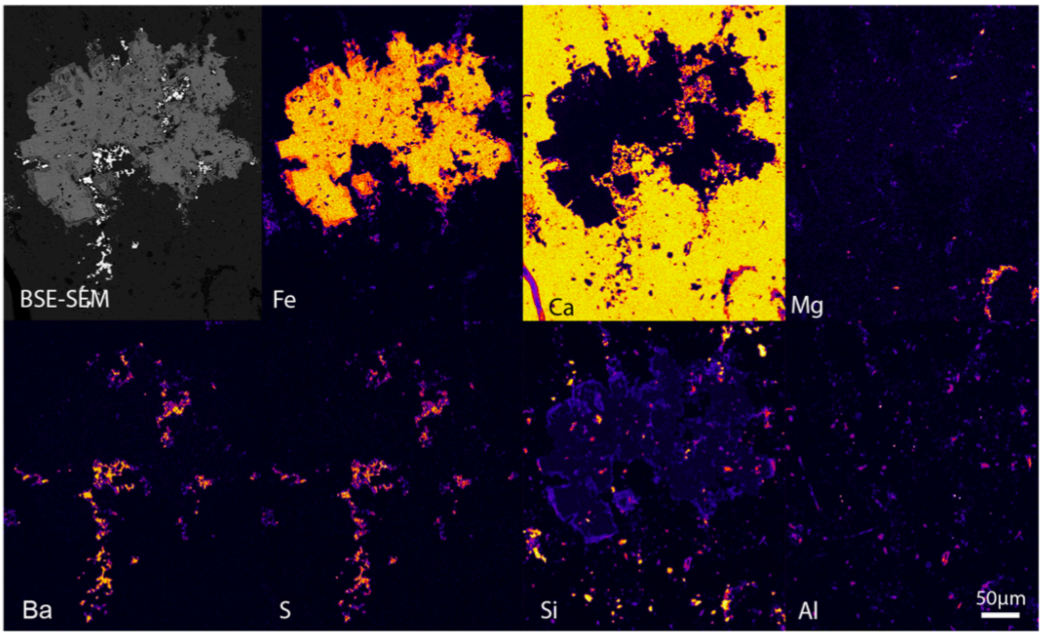

Fig. 7. BSE-SEM image and WDS elemental maps of barite associated with iron oxide pseudomorph of pyrite in microbialites (Borrachudo section).

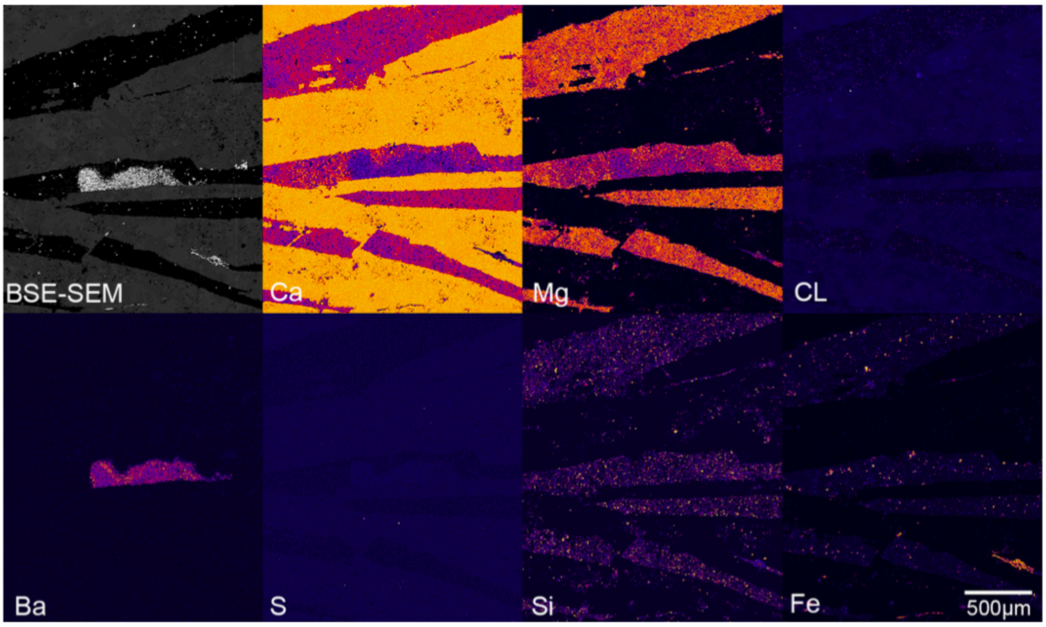

Fig. 8. BSE-SEM image and WDS elemental maps of aragonite fans from the Borrachudo section, showing barite inclusions with carbonate fan crystals.

processes produce alkalinity that kinetically limits phosphate precipitation. In any event, pyrite subsequently formed in the sulfate reduction zone. Diagenetic microcrystalline barite also formed after prolonged burial, most likely in the sulfate-methane transition zone (Zhou et al., 2015), though the origins of cap carbonate barite remain controversial (Crockford et al., 2016). The presence of pyrite and barite inclusions (and absence of apatite inclusions) within the carbonate fan crystals (Figs. 5 and 8; Vieira et al., 2015) corroborate this paragenetic sequence, affirming that the inversion of aragonite to calcite occurred concurrently with barite and pyrite formation in the sulfate reduction and/or methanogenesis zones (Fig. 9).

5.2. Seawater phosphate in the aftermath of glaciation

The discovery of apatite in the SLF represents a striking outcome of this study. Although P:Fe ratios in iron formations and geochemical models suggest continental weathering during and following low latitude glaciations contributed to high dissolved phosphate concentrations in the ocean (Planavsky et al., 2010; Laakso and Schrag, 2017), and enhanced post-glacial seawater phosphate availability could partly account for the inferred rise in oxygen levels in the Neoproterozoic (Lenton et al., 2014; Laakso and Schrag, 2017), cap carbonates have provided little support for a connection between glaciation and enhanced phosphorus burial (Hoffman et al., 2011). Putative evidence for

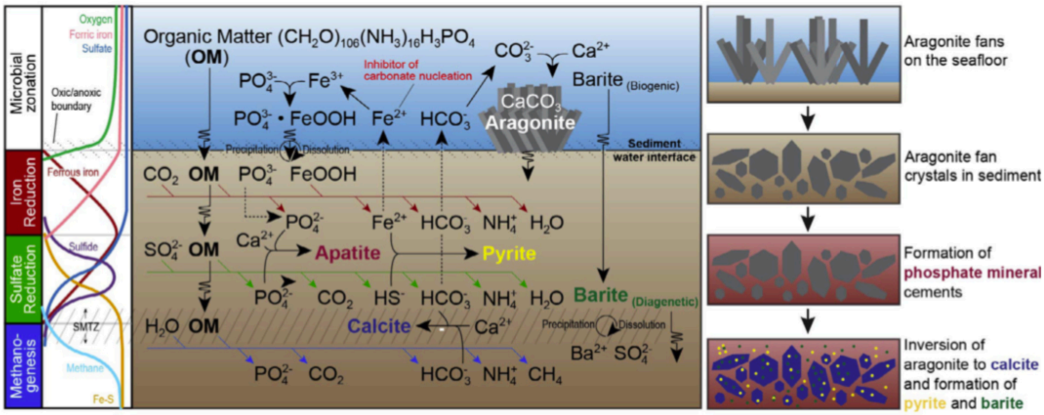

Fig. 9. Sedimentary model for aragonite crystal fan formation and phosphogenesis in the Sete Lagoas Formation, depicting sedimentary and redox-dependent microbial processes. Reactions, microbial zonation, and geochemical gradients provided in sediment profile. The minerals formed near the sediment-water interface just below the oxic-anoxic boundary. Iron reduction below this boundary released Fe^{2+}, which inhibited nucleation of carbonate, thereby allowing for growth of aragonite. Concurrently, dissolution of iron (oxyhydr)oxide particulates liberated phosphate, and in conjunction with remineralization of organic phosphorus via sulfate reduction deeper in the sediment, created conditions conducive to formation of authigenic and/or early diagenetic apatite. Deeper in the sediments, sulfate reduction and methanogenesis led to the formation of pyrite, diagenetic microcrstyalline barite, and calcite. OM, organic matter.

a relationship includes phosphorite overlying cap carbonates in West Africa (Trompette et al., 1980; Bertrand-Sarfati et al., 1997; Shields et al., 2007), South China (Xiao et al., 1998; Zhang et al., 1998; Zhou et al., 2002; Muscente et al., 2015), and Mongolia (Sheldon, 1984; Ilyin et al., 1986; Ilyin, 2009; Macdonald and Jones, 2011). In most cases, however, stratigraphic continuity between cap carbonate and phosphorite remains tenuous (Hoffman et al., 2011). The absence of phosphorite and phosphatic minerals in cap carbonates is therefore conspicuous, given the supposedly high seawater phosphate concentrations that developed in association with low latitude glaciation. Unfortunately, the newly discovered apatitic cements in the SLF do not fill this knowledge gap, as they may reflect local or regional phenomena, like many other phosphatic rocks in Neoproterozoic successions (She et al., 2014; Drummond et al., 2015; Muscente et al., 2015; Cui et al., 2016; Caird et al., 2017). High ocean alkalinity during deposition of cap carbonates likely limited development of the broad and long-lived phosphogenic conditions that became established later in the Ediacaran (Cook and Shergold, 1986; Cook, 1992; Drummond et al., 2015; Muscente et al., 2015; Caird et al., 2017). Even so, phosphate mineral cements in the SLF cap carbonate indicate that such circumstances did not preclude the formation of localized phosphate deposits within cap carbonates. Consequently, future studies may begin to fill the knowledge gap by targeting particular cap carbonate microfacies for petrographic and *in situ* geochemical analyses. Given the roles that iron (oxyhydr)oxides play in the aragonite fan formation and phosphogenesis, microfacies containing carbonate fan crystals merit particular attention in future investigations.

6. Conclusions

The base of the Sete Lagoas Formation cap carbonate (São Francisco craton, Brazil) preserves a record of geochemical, biological, and oceanographic changes that occurred during the Ediacaran Period and contains seafloor precipitates as well as distinct authigenic and diagenetic minerals. Our work explores the significance of these minerals for global seawater chemistry and sedimentary environments following Neoproterozoic glaciations.

- For the first time, this study documents isopachous and void-filling apatitic cements in a Neoproterozoic cap carbonate. These cements occur with carbonate fan crystals within strata correlated with the base of the Sete Lagoas Formation, which contains lithological features (e.g., aragonite and barite crystal fans and basal pink dolostone), carbon and oxygen isotope profiles, and $^{87}Sr/^{86}Sr$ ratios (0.7074–0.7076) consistent with Marinoan cap carbonates (Halverson et al., 2005; Hoffman et al., 2007; Caxito et al., 2012).
- The carbonate fan crystals consist of pseudohexagonal calcite units, representing pseudomorphs after aragonite. These minerals formed near the sediment-water interface below the boundary between oxic seawater and anoxic pore water. Iron reduction at this boundary released Fe^{2+}, which inhibited nucleation of micritic carbonate, thereby allowing for formation of aragonite. Concurrently, dissolution of iron (oxyhydr)oxide particulates liberated phosphate bound to their surfaces, and perhaps in conjunction with remineralization of organic phosphorus via sulfate reduction deeper in the sediment, created conditions conducive to formation of the authigenic and/or early diagenetic phosphate minerals.
- Taken altogether, this model suggests that aragonite crystal fans in Neoproterozoic cap carbonates primarily incorporated alkalinity from well-mixed seawater rather than microbially and diagenetically influenced pore water, and corroborates the hypothesis that, in addition to high alkalinity, the presence of inhibitors to carbonate nucleation (Fe^{2+}) was a prerequisite for their formation. In addition, given the inferred role of iron reduction, the model suggests that aragonite fans may track seafloors intersected by oxic-anoxic redox boundaries through stratigraphic and geographic space.
- Lastly, this study records a rare but expected occurrence of phosphogenesis following a low latitude Neoproterozoic glaciation. Cap carbonates generally provide little support for a connection between glaciation and phosphorus burial. Nonetheless, future studies may begin to fill this knowledge gap by targeting cap carbonate microfacies containing carbonate fan crystals, given the role that iron reduction played in the origins of both apatite and aragonite in the Sete Lagoas Formation.

Acknowledgements

We would like to thank Hamilton dos Reis Sales for his support in the field and Andy Knoll for helpful comments that helped us to improve the quality of this manuscript. We would also like to thank the State of São Paulo Research Foundation (FAPESP grant 2015/07391-0), the State of Minas Gerais Research Foundation (FAPEMIG project APQ-01711-14), National Council for Scientific and Technological Development (CNPq grants 444070/2014-1 and 447449/2014-1) and Petrobras (Sigitec 2014/-00519-9) for financial support. We additionally thank Huan Cui for the constructive comments that helped us to improve this manuscript. Randall Parrish is also acknowledged for handling the manuscript and for giving insightful comments on the manuscript. This research was conducted with institutional support of the São Paulo State University-UNESP, Brazil. L.V. Warren is fellow of the CNPq. A. D. Muscente is supported by the Keck Foundation-funded project "The Co-Evolution of the Geo- and Biospheres: An Integrated Program for Data-Driven Abductive Discovery in Earth Sciences."

References

Agrella-Filho, M.S.D., Babinski, M., Trindade, R.I.F., Van Schmus, W.R., Ernesto, M., 2000. Simultaneous remagnetization and U–Pb isotope resetting in Neoproterozoic carbonates of the São Francisco craton, Brazil. Precambr. Res. 99, 179–196.
Allison, P.A., 1988. Konservat-Lagerstätten: cause and classification. Paleobiology 14, 331–344.
Arning, E.T., Birgel, D., Brunner, B., Peckmann, J., 2009. Bacterial formation of phosphatic laminites off Peru. Geobiology 7, 295–307. http://dx.doi.org/10.1111/j.1472-4669.2009.00197.x.
Babinski, M., Van Schmus, W.R., Chemale, F., 1999. Pb-Pb dating and Pb isotope geochemistry of Neoproterozoic carbonate rocks from the Sao Francisco basin, Brazil: implications for the mobility of Pb isotopes during tectonism and metamorphism. Chem. Geol. 160, 175–199. http://dx.doi.org/10.1016/S0009-2541(99)00067-4.
Babinski, M., Vieira, L.C., Trindade, R.I.F., 2007. Direct dating of the Sete Lagoas cap carbonate (Bambuí Group, Brazil) and implications for the Neoproterozoic glacial events. Terra Nova 19, 401–406. http://dx.doi.org/10.1111/j.1365-3121.2007.00764.x.
Bergmann, K.D., Grotzinger, J.P., Fischer, W.W., 2013. Biological influences on seafloor carbonate precipitation. Palaios 28, 99–115. http://dx.doi.org/10.2110/palo.2012.p12-088r.
Bertrand-Sarfati, J., Flicoteaux, R., Moussine-Pouchkine, A., Ahmed, A.A.K., 1997. Lower Cambrian apatitic stromatolites and phospharenites related to the glacio-eustatic cratonic rebound (Sahara, Algeria). J. Sediment. Res. 67.
Briggs, D.E.G., Wilby, P.R., 1996. The role of calcium carbonate-calcium phosphate switch in the mineralization of soft-bodied fossils. J. Geol. Soc., London 153, 665–668.
Brito Neves, B.B.D., da Costa Campos Neto, M., Fuck, R.A., 1999. From Rodinia to western Gondwana; an approach to the Brasiliano-Pan African cycle and orogenic collage. Episodes 22, 155–166.
Caird, R.A., Pufahl, P.K., Hiatt, E.E., Abram, M.B., Dourado, A.R., Kyser, T.K., 2017. Ediacaran stromatolites and intertidal phosphorite of the Salitre formation, Brazil: phosphogenesis during the Neoproterozoic oxygenation event. Sed. Geol. 350, 55–71. http://dx.doi.org/10.1016/j.sedgeo.2017.01.005.
Caxito, F.de A., Halverson, G.P., Uhlein, A., Stevenson, R., Gonçalves Dias, T., Uhlein, G.J., 2012. Marinoan glaciation in east central Brazil. Precambr. Res. 200–203, 38–58. http://dx.doi.org/10.1016/j.precamres.2012.01.005.
Chang, H.K., Miranda, F.P., Magalhães, L., Alkmim, F.F., 1988. Considerações sobre a evolução tectônica da bacia do São Francisco. In: Proceedings of the 35th Congresso Brasileiro de Geologia. Sociedade Brasileira de Geologia (SBG), Belém, pp. 2076–2090.
Chiavegatto, J.R.S., 1992. Análise estratigráfica das sequências tempestíticas da Fm. Três Marias (Proterozoico Superior) na porção meridional da bacia do São Francisco.
Cook, P.J., 1992. Phosphogenesis around the Proterozoic-Phanerozoic transition. Journal of the Geological Society 149, 615–620.
Cook, P.J., Shergold, J.H., 1986. Phosphate deposits of the world Vol. 1 Cambridge University Press, Cambridge.

Corsetti, F.A., Lorentz, N.J., 2006. On Neoproterozoic Cap Carbonates as Chronostratigraphic Markers. In: Xiao, S., Kaufman, A.J. (Eds.), Neoproterozoic Geobiology and Paleobiology. pp. 273–294.
Corsetti, F.A., Lorentz, N.J., Pruss, S.B., 2004. Formerly-Aragonite Seafloor Fans from Neoproterozoic Strata, Death Valley and Southeastern Idaho, United States: Implications for "Cap Carbonate" Formation and Snowball Earth. The Extreme Proterozoic: Geology, Geochemistry, and Climate, pp. 33–44. doi: 10.1029/146GM04.
Creveling, J.R., Johnston, D.T., Poulton, S.W., Kotrc, B., März, C., Schrag, D.P., Knoll, A.H., 2014. Phosphorus sources for phosphatic Cambrian carbonates. Bull. Geol. Soc. Am. 126, 145–163. http://dx.doi.org/10.1130/B30819.1.
Crockford, P.W., Cowie, B., Johnston, D.T., Macdonald, F.A., 2016. Triple oxygen and multiple sulfur isotope constraints on the evolution of the post-Marinoan sulfur cycle. Earth Planet. Sci. Lett. 435, 74–83. http://dx.doi.org/10.1016/j.epsl.2015.12.017.
Crockford, P.W., Hodgskiss, M.S.W., Uhlein, G.J., Caxito, F., Hayles, J.A., Halverson, G.P., 2017. Linking paleocontinents through triple oxygen isotope anomalies. Geology 46 (2), 179–182. http://dx.doi.org/10.1130/G39470.1 |.
Cruz, N.M.C., Nobre-Lopes, J., 1992. Microfósseis do Grupo Bambuí na região de Arcos, Minas Gerais. An. Acad. Bras. Cienc. 64, 420.
Cui, H., Xiao, S., Zhou, C., Peng, Y., Kaufman, A.J., Plummer, R.E., 2016. Phosphogenesis associated with the Shuram Excursion: petrographic and geochemical observations from the Ediacaran Doushantuo formation of South China. Sediment. Geol. 341, 134–146. http://dx.doi.org/10.1016/j.sedgeo.2016.05.008.
Cui, H., Kaufman, A.J., Xiao, S., Zhou, C., Liu, X.-M., 2017. Was the Ediacaran Shuram Excursion a globally synchronized early diagenetic event? Insights from methane-derived authigenic carbonates in the uppermost Doushantuo Formation, South China. Chem. Geol. 450, 59–80. http://dx.doi.org/10.1016/j.chemgeo.2016.12.010.
Dardenne, M.A., 1978. Síntese sobre a estratigrafia do Grupo Bambuí no Brasil Central. In: Congresso Brasileiro de Geologia, 30°. Anais, Recife, Brazil, pp. 597–610.
De Leeuw, N.H., 2002. Molecular dynamics simulations of the growth inhibiting effect of $Fe2+$, $Mg2+$, $Cd2+$, and $Sr2+$ on calcite crystal growth. J. Phys. Chem. B 106, 5241–5249.
Deynoux, M., 1985. Terrestrial or waterlain glacial diamictites? Three case studies from the Late Precambrian and Late Ordovician glacial drifts in West Africa. Palaeogeogr. Palaeoclimatol. Palaeoecol. 51, 97–141.
Drummond, J.B.R., Pufahl, P.K., Porto, C.G., Carvalho, M., 2015. Neoproterozoic peritidal phosphorite from the Sete Lagoas Formation (Brazil) and the Precambrian phosphorus cycle. Sedimentology 62, 1978–2008. http://dx.doi.org/10.1111/sed.12214.
Evans, D.A.D., Raub, T.D., 2011. Neoproterozoic glacial palaeolatitudes: a global update. Geol. Rec. Neoproter. Glaciat. 93–112. http://dx.doi.org/10.1144/M36.7.
Eyles, N., Januszczak, N., 2004. "Zipper-rift": a tectonic model for Neoproterozoic glaciations during the breakup of Rodinia after 750 Ma. Earth Sci. Rev. 65, 1–73. http://dx.doi.org/10.1016/S0012-8252(03)00080-1.
Fairchild, I.J., Kennedy, M.J., 2007. Neoproterozoic glaciation in the Earth System. J. Geol. Soc., London 164, 895–921. http://dx.doi.org/10.1144/0016-76492006-191.
Fairchild, T.R., Schopf, J.W., Shen-Miller, J., Guimarães, E.M., Edwards, M.D., Lagstein, A., Xiao, L., Pabst, M., Melo-Filho, L.S., 1996. Recent discoveries of Proterozoic microfossils in south-central Brazil. Precambr. Res. 80, 125–152. http://dx.doi.org/10.1016/S0301-9268(96)00009-5.
Fairchild, T.R., Subacius, S.M.R., 1986. Microfossils associated with silicified Stratifera undata Komar 1966 from the Late Proterozoic Bambuí Group, south-central Brazil. Precambr. Res. 33, 323–339.
Föllmi, K.B., 1996. The phosphorus cycle, phosphogenesis and marine phosphate-rich deposits. Earth Sci. Rev. 40, 55–124.
Glenn, C.R., Arthur, M.A., 1990. Anatomy and origin of a Cretaceous phosphorite-greensand giant, Egypt. Sedimentology 37, 123–154. http://dx.doi.org/10.1111/j.1365-3091.1990.tb01986.x.
Glenn, C.R., Föllmi, K.B., Grimm, K.A., Sadaqah, R.M.Y., Schidlowski, M., Sheldon, R.E., Siegmund, H., 1994. Phosphorus and phosphorites: sedimentology and environments of formation. Eclog. Geol. Helv. 87, 747–788.
Griffith, E.M., Paytan, A., 2012. Barite in the ocean – occurrence, geochemistry and palaeoceanographic applications. Sedimentology 59, 1817–1835. http://dx.doi.org/10.1111/j.1365-3091.2012.01327.x.
Grotzinger, J.P., Knoll, A.H., 1995. Anomalous carbonate precipitates: is the Precambrian the key to the Permian? Palaios 10, 578–596.
Hagadorn, J.W., Waggoner, B., 2000. Ediacaran fossils from the Southwestern Great Basin, United States. J. Paleontol. 74, 349–359. http://dx.doi.org/10.1666/0022-3360(2000) 074<0349:EFFTSG>2.0.CO;2.
Hahn, G., Hahn, R., Leonardos, O.H., Pflug, H.D., Walde, D.H.G., 1982. Körperlich erhaltene Scyphozoen-Reste aus dem Jungpräkambrium Brasiliens. Geol. Paleontol. 16, 1–18.
Halverson, G.P., Hoffman, P.F., Schrag, D.P., Maloof, A.C., Rice, A.H.N., 2005. Toward a Neoproterozoic composite carbon-isotope record. Bull. Geol. Soc. Am. 117, 1181–1207. http://dx.doi.org/10.1130/B25630.1.
Higgins, J.A., Schrag, D.P., 2003. Aftermath of a snowball earth. Geochem. Geophys. Geosyst. 4, 1–20. http://dx.doi.org/10.1029/2002GC000403.
Hoffman, P.F., 2011. Strange bedfellows: Glacial diamictite and cap carbonate from the Marinoan (635Ma) glaciation in Namibia. Sedimentology 58, 57–119. http://dx.doi.org/10.1111/j.1365-3091.2012.01360.x.
Hoffman, P.F., Halverson, G.P., 2011. Neoproterozoic glacial record in the Mackenzie Mountains, northern Canadian Cordillera. Geol. Soc., London Memoirs 36, 397–412.
Hoffman, P.F., Halverson, G.P., Domack, E.W., Husson, J.M., Higgins, J.A., Schrag, D.P., 2007. Are basal Ediacaran (635 Ma) post-glacial "cap dolostones" diachronous? Earth Planet. Sci. Lett. 258, 114–131. http://dx.doi.org/10.1016/j.epsl.2007.03.032.
Hoffman, P.F., Kaufman, A.J., Halverson, G.P., Schrag, D.P., 1998. A Neoproterozoic snowball earth. Science 281, 1342–1346. http://dx.doi.org/10.1126/science.281.5381.1342.
Hoffman, P.F., Macdonald, F.a., Halverson, G.P., 2011. Chemical sediments associated with Neoproterozoic glaciation: iron formation, cap carbonate, barite and phosphorite. Geol. Soc., London Memoirs 36, 67–80. http://dx.doi.org/10.1144/M36.5.
Hoffman, P.F., Schrag, D.P., 2002. The snowball Earth hypothesis: testing the limits of global change. Terra Nova 14, 129–155. http://dx.doi.org/10.1080/713604466.
Ilyin, A.V., 2009. Neoproterozoic banded iron formations. Lithol. Min. Resour. 44, 78–86.
Ilyin, A.V., Zaitsev, N.S., Bjamba, Z., 1986. Khubsugul, Mongolia people's republic. In: Cook, P.J., Sheldon, J.H. (Eds.), Phosphate Deposits of the World. Proterozoic and Cambrian Phosphorites. Cambridge University Press, Cambridge.
James, N.P., Narbonne, G.M., Kyser, T.K., 2001. Late Neoproterozoic cap carbonates: Mackenzie Mountains, northwestern Canada: precipitation and global glacial meltdown. Can. J. Earth Sci. 38, 1229–1262. http://dx.doi.org/10.1139/cjes-38-8-1229.
Jiang, G., Kennedy, M.J., Christie-Blick, N., 2003. Stable isotopic evidence for methane seeps in Neoproterozoic postglacial cap carbonates. Nature 426, 822–826. http://dx.doi.org/10.1038/nature02201.
Jiang, G., Kennedy, M.J., Christie-Blick, N., Wu, H., Zhang, S., 2006a. Stratigraphy, sedimentary structures, and textures of the late Neoproterozoic Doushantuo Cap carbonate in South China. J. Sediment. Res. 76, 978–995. http://dx.doi.org/10.2110/jsr.2006.086.
Jiang, G., Shi, X., Zhang, S., 2006b. Methane seeps, methane hydrate destabilization, and the late Neoproterozoic postglacial cap carbonates. Chin. Sci. Bull. 51, 1152–1173. http://dx.doi.org/10.1007/s11434-006-1152-y.
Kastner, M., 1999. Oceanic minerals: their origin, nature of their environment, and significance. PNAS 96, 3380–3387. http://dx.doi.org/10.1073/pnas.96.7.3380.
Kaufman, A.J., Knoll, A.H., Narbonne, G.M., 1997. Isotopes, ice ages, and terminal Proterozoic earth history. Geology 94, 6600–6605. http://dx.doi.org/10.1073/pnas.94.13.6600.
Kaufman, A.J., Sial, A.N., Frimmel, H.E., Misi, A., 2009. Neoproterozoic to Cambrian palaeoclimatic events in southwestern Gondwana. In: Gaucher, C., Sial, A.N., Frimmel, H.E., Halverson, G.P. (Eds.), Developments in Precambrian Geology. Elsevier, Amsterdam, Netherlands, pp. 369–388. http://dx.doi.org/10.1016/s0166-2635(09)01626-0.
Kennedy, M.J., 1996. Stratigraphy, sedimentology, and isotopic geochemistry of Australian Neoproterozoic postglacial cap dolostones: deglaciation, D13C excursions, and carbonate precipitation. J. Sediment. Res. 66, 1050–1064.
Kennedy, M.J., Christie-Blick, N., Sohl, L.E., 2001. Are Proterozoic cap carbonates and isotopic excursions a record of gas hydrate destabilization following Earth's coldest intervals? Geology 29, 443–446. http://dx.doi.org/10.1130/0091-7613(2001)029<0443:APCCAI>2.0.CO.
Kennedy, M.J., Runnegar, B., Prave, A.R., Hoffman, K.-H., Arthur, M.A., 1998. Two or four Neoproterozoic glaciations? Geology 26, 1059–1063.
Kirschvink, J.L., 1992. Late Proterozoic low-latitude global glaciation: the snowball Earth. In: Schopf, J.W., Klein, C. (Eds.), The Proterozoic Biosphere. Cambridge University Press, Cambridge, pp. 51–52.
Kuchenbecker, M., Babinski, M., Pedrosa-Soares, A.C., Lopes-Silva, L., Pimenta, F., 2016. Chemostratigraphy of the lower Bambuí Group, southwestern São Francisco Craton, Brazil: insights on Gondwana paleoenvironments. Braz. J. Geol. 46, 145–162. http://dx.doi.org/10.1590/2317-488920160030285.
Laakso, T.A., Schrag, D.P., 2017. A theory of atmospheric oxygen. Geobiology 15, 366–384. http://dx.doi.org/10.1111/gbi.12230.
Lenton, T.M., Boyle, R.A., Poulton, S.W., Shields-zhou, G.A., Butterfield, N.J., 2014. Co-evolution of eukaryotes and ocean oxygenation in the Neoproterozoic era. Nat. Geosci. 7, 257–265. http://dx.doi.org/10.1038/NGEO2108.
Lorentz, N.J., Corsetti, F.A., Link, P.K., 2004. Seafloor precipitates and C-isotope stratigraphy from the Neoproterozoic Scout Mountain Member of the Pocatello Formation, southeast Idaho: Implications for Neoproterozoic earth system behavior. Precambr. Res. 130, 57–70. http://dx.doi.org/10.1016/j.precamres.2003.10.017.
Macdonald, F.A., Jones, D.S., 2011. The Khubsugul Group, Northern Mongolia. In: The Geological Record of Neoproterozoic Glaciations. pp. 339–345.
Macdonald, F.A., Mcclelland, W.C., Schrag, D.P., Macdonald, W.P., Macdonald, F.A., Mcclelland, W.C., Schrag, D.P., Macdonald, W.P., 2009. Neoproterozoic glaciation on a carbonate platform margin in Arctic Alaska and the origin of the North Slope subterrane. GSA Bull. 121, 448–473. http://dx.doi.org/10.1130/B26401.1.
Macdonald, F.A., Strauss, J.V., Sperling, E.A., Halverson, G.P., Narbonne, G.M., Johnston, D.T., Kunzmann, M., Schrag, D.P., Higgins, J.A., 2013. The stratigraphic relationship between the Shuram carbon isotope excursion, the oxygenation of Neoproterozoic oceans, and the first appearance of the Ediacara biota and bilaterian trace fossils in northwestern Canada. Chem. Geol. 362, 250–272. http://dx.doi.org/10.1016/j.chemgeo.2013.05.032.
Marchese, H.G., 1974. Estromatólitos "Gymnosolenideos" em el lado oriental de Minas Gerais, Brasil. Revista Brasileira de Geociências 4, 257–271.
Martins-Neto, M.A., 2009. Sequence stratigraphic framework of Proterozoic successions in eastern Brazil. Mar. Pet. Geol. 26, 163–176. http://dx.doi.org/10.1016/j.marpetgeo.2007.10.001.
McFadden, K.A., Huang, J., Chu, X., Jiang, G., Kaufman, A.J., Zhou, C., Yuan, X., Xiao, S., 2008. Pulsed oxidation and biological evolution in the Ediacaran Doushantuo Formation. Proc. Natl. Acad. Sci. U.S.A. 105, 3197–3202. http://dx.doi.org/10.1073/pnas.0708336105.
McMechan, M.E., 2000. Vreeland Diamictites – Neoproterozoic glaciogenic slope deposits, Rocky Mountains, northeast British Columbia. Bull. Can. Pet. Geol. 48, 246–261.
Meert, J.G., van der Voo, R., 1994. The Neoproterozoic (1000–540 Ma) glacial intervals: No more snowball earth? Earth Planet. Sci. Lett. 123, 1–13. http://dx.doi.org/10.1016/0012-821X(94)90253-4.
Misi, A., Veizer, J., 1998. Neoproterozoic carbonate sequences of the Una Group, Irecê

Basin, Brazil: chemostratigraphic, age and correlations. Precambr. Res. 89, 87–100.
Misi, A., Kaufman, A.J., Veizer, J., Powis, K., Azmy, K., Boggiani, P.C., Gaucher, C., Teixeira, J.B.G., Sanches, A.L., Iyer, S.S., 2007. Chemostratigraphic correlation of Neoproterozoic successions in South America. Chem. Geol. 237, 143–167. http://dx.doi.org/10.1016/j.chemgeo.2006.06.019.
Muscente, A.D., Hawkins, A.D., Xiao, S., 2015. Fossil preservation through phosphatization and silicification in the Ediacaran Doushantuo Formation (South China): A comparative synthesis. Palaeogeogr. Palaeoclimatol. Palaeoecol. 434, 46–62. http://dx.doi.org/10.1016/j.palaeo.2014.10.013.
Muscente, A.D., Xiao, S., 2015. Resolving three-dimensional and subsurficial features of carbonaceous compressions and shelly fossils using backscattered electron scanning electron microscopy (BSE-SEM). Palaios 30, 462–481. http://dx.doi.org/10.2110/palo.2014.094.
Myrow, P.M., Kaufman, A.J., 1999. A newly discovered cap carbonate above Varanger-age glacial deposits in Newfoundland, Canada. J. Sediment. Res. 69, 784–793. http://dx.doi.org/10.2110/jsr.69.784.
Nelson, G.J., Pufahl, P.K., Hiatt, E.E., 2010. Paleoceanographic constraints on Precambrian phosphorite accumulation, Baraga Group, Michigan, USA. Sed. Geol. 226, 9–21. http://dx.doi.org/10.1016/j.sedgeo.2010.02.001.
Nobre-Lopes, J., Coimbra, A.M., 2000. Microfitólitos associados a construções estromatolíticas do Grupo Bambuí, Proterozóico Superior, na região de Arcos – MG. Rev. Bras. Geocien. 30, 589–592.
Nogueira, A.C.R., Riccomini, C., Nóbrega Sial, A., Veloso Moura, C.A., Fairchild, T.R., 2003. Soft-sediment deformation at the base of the Neoproterozoic Puga cap carbonate (southwestern Amazon craton, Brazil): Confirmation of rapid icehouse to greenhouse transition in snowball Earth. Geology 31, 613–616. http://dx.doi.org/10.1130/0091-7613(2003) 031<0613:SDATBO>2.0.CO;2.
Papineau, D., 2010. Global biogeochemical changes at both ends of the proterozoic: insights from phosphorites. Astrobiology 10, 165–181. http://dx.doi.org/10.1089/ast.2009.0360.
Paula-Santos, G.M., Babinski, M., Kuchenbecker, M., Caetano-Filho, S., Trindade, R.I., Pedrosa-Soares, A.C., 2015. New evidence of an Ediacaran age for the Bambuí Group in southern São Francisco craton (eastern Brazil) from zircon U-Pb data and isotope chemostratigraphy. Gondwana Res. 28, 702–720. http://dx.doi.org/10.1016/j.gr.2014.07.012.
Paytan, A., Mearon, S., Cobb, K., Kastner, M., 2002. Origin of marine barite deposits: Sr and S isotope characterization. Geology 30, 747–750. http://dx.doi.org/10.1130/0091-7613(2002) 030<0747:OOMBDS>2.0.CO;2.
Peryt, T.M., Hoppe, A., Bechstädt, T., Koster, J., Pierre, C., Richter, D.K., 1990. Late Proterozoic aragonitic cement crusts, Bambui Group, Minas Gerais, Brazil. Sedimentology 37, 279–286. http://dx.doi.org/10.1111/j.1365-3091.1990.tb00959.x.
Pimentel, M.M., Dardenne, M.A., Fuck, R.A., Viana, M.G., Junges, S.L., Fischel, D.P., Seer, H.J., Dantas, E.L., 2001. Nd isotopes and the provenance of detrital sediments of the Neoproterozoic Brasília Belt, central Brazil. J. S. Am. Earth Sci. 14, 571–585.
Pimentel, M.M., Rodrigues, J.B., DellaGiustina, M.E.S., Junges, S., Matteini, M., Armstrong, R., 2011. The tectonic evolution of the Neoproterozoic Brasília Belt, central Brazil, based on SHRIMP and LA-ICPMS U-Pb sedimentary provenance data: A review. J. S. Am. Earth Sci. 31, 345–357. http://dx.doi.org/10.1016/j.jsames.2011.02.011.
Planavsky, N.J., Rouxel, O.J., Bekker, A., Lalonde, S.V., Konhauser, K.O., Reinhard, C.T., Lyons, T.W., 2010. The evolution of the marine phosphate reservoir. Nature 467, 1088–1090. http://dx.doi.org/10.1038/nature09485.
Pruss, S.B., Corsetti, F.A., Fischer, W.W., 2008. Seafloor-precipitated carbonate fans in the Neoproterozoic Rainstorm Member, Johnnie formation, Death Valley Region, USA. Sed. Geol. 207, 34–40. http://dx.doi.org/10.1016/j.sedgeo.2008.03.005.
Pu, J.P., Bowring, S.A., Ramezani, J., Myrow, P., Raub, T.D., Landing, E., Mills, A., Hodgin, E., Macdonald, F.A., 2016. Dodging snowballs: Geochronology of the Gaskiers glaciation and the first appearance of the Ediacaran biota. Geology 44, 955–958. http://dx.doi.org/10.1130/G38284.1.
Reis, H.L.S., Suss, J.F., 2016. Mixed carbonate-siliciclastic sedimentation in forebulge grabens: An example from the Ediacaran Bambuí Group, São Francisco Basin, Brazil. Sed. Geol. 339, 83–103. http://dx.doi.org/10.1016/j.sedgeo.2016.04.004.
Ridgwell, A.J., Kennedy, M.J., Caldeira, K., 2003. Carbonate Deposition, Climate Stability, and Neoproterozoic Ice Ages. Science 302, 859–862. http://dx.doi.org/10.1126/science.1088342.
Rodrigues, J.B., 2008. Proveniência de sedimentos dos grupos Canastra, Ibiá, Vazante e Bambuí – Um estudo de zircões detríticos e Idades Modelo Sm-Nd. Universidade de Brasília.
She, Z.B., Strother, P., Papineau, D., 2014. Terminal Proterozoic cyanobacterial blooms and phosphogenesis documented by the Doushantuo granular phosphorites II: Microbial diversity and C isotopes. Precambr. Res. 251, 62–79. http://dx.doi.org/10.1016/j.precamres.2014.06.004.
Sheldon, R.P., 1984. Ice-ring origin of the Earth's atmosphere and hydrosphere and Late Proterozoic-Cambrian hypothesis. Geol. Surv. India Spec. Publ. 17, 17–21.
Shields, G.A., Deynoux, M., Strauss, H., Nahon, D., 2007. Barite-bearing cap dolostones of the Taoudéni Basin, northwest Africa: Sedimentary and isotopic evidence for methane seepage after a Neoproterozoic glaciation. Precambr. Res. 153, 209–235. http://dx.doi.org/10.1016/j.precamres.2006.11.011.
Spence, G.H., Heron, D. Le, Fairchild, I., 2016. Sedimentological perspectives on climatic, atmospheric and environmental change in the Neoproterozoic Era. Sedimentology 63, 253–306. http://dx.doi.org/10.1111/sed.12261.
Sumner, D.Y., Grotzinger, J.P., 2004. Implications for Neoarchean ocean chemistry from primary carbonate mineralogy of the Campbell-Malmani Platform, South Africa. Sedimentology 51, 1–27.
Sumner, D.Y., Grotzinger, J.P., 1996. Herringbone calcite: petrology and environmental significance. J. Sediment. Res. 66.
Trindade, R.I.F., Macouin, M., 2007. Palaeolatitude of glacial deposits and palaeogeography of Neoproterozoic ice ages. C. R. Geosci. 339, 200–211. http://dx.doi.org/10.1016/j.crte.2007.02.006.
Trompette, R., Affaton, P., Joulia, F., Marchand, J., 1980. Stratigraphic and structural controls of late Precambrian phosphate deposits of the northern Volta Basin in Upper Volta, Niger, and Benin, West Africa. Econ. Geol. 75, 62–70.
Trompette, R.R., 1994. Geology of Western Gondwana (2000–500 Ma): Pan-African – Brasiliano aggregation of South America and Africa.
Uhlein, G.J., Uhlein, A., Halverson, G.P., Stevenson, R., Caxito, F.A., Cox, G.M., Carvalho, J.F.M.G., 2016. The Carrancas formation, Bambuí Group: a record of pre-Marinoan sedimentation on the southern São Francisco craton, Brazil. J. S. Am. Earth Sci. 71, 1–16. http://dx.doi.org/10.1016/j.jsames.2016.06.009.
van Loon, A.J., 2008. Could "Snowball Earth" have left thick glaciomarine deposits? Gondwana Res. 14, 73–81. http://dx.doi.org/10.1016/j.gr.2007.05.009.
Vieira, L.C., Nédélec, A., Fabre, S., Trindade, R.I.F., Almeida, R.P.D.E., 2015. Aragonite crystal fans in Neoproterozoic cap carbonates: a case study from Brazil and implications for the post – snowball earth coastal environment. J. Sediment. Res. 85, 285–300. http://dx.doi.org/10.2110/jsr.2015.21.
Vieira, L.C., Trindade, R.I.F., Nogueira, A.C.R., Ader, M., 2007. Identification of a Sturtian cap carbonate in the Neoproterozoic Sete Lagoas carbonate platform, Bambuí Group, Brazil. C. R. Geosci. 339, 240–258. http://dx.doi.org/10.1016/j.crte.2007.02.003.
Warren, L.V., Fairchild, T.R., Gaucher, C., Boggiani, P.C., Poiré, D.G., Anelli, L.E., Inchausti, J.C.G., 2011. Corumbella and in situ Cloudina in association with thrombolites in the Ediacaran Itapucumi Group, Paraguay. Terra Nova 23, 382–389. http://dx.doi.org/10.1111/j.1365-3121.2011.01023.x.
Warren, L.V., Quaglio, F., Riccomini, C., Simões, M.G., Poiré, D.G., Strikis, N.M., Anelli, L.E., Strikis, P.C., 2014. The puzzle assembled: Ediacaran guide fossil Cloudina reveals an old proto-Gondwana seaway. Geology 42, 391–394. http://dx.doi.org/10.1130/G35304.1.
Xiao, S., Muscente, A.D., Chen, L., Zhou, C., Schiffbauer, J.D., Wood, A.D., Polys, N.F., Yuan, X., 2014. The Weng'an biota and the Ediacaran radiation of multicellular eukaryotes. Natl. Sci. Rev. 1, 498–520. http://dx.doi.org/10.1093/nsr/nwu061.
Xiao, S., Narbonne, G.M., Zhou, C., Laflamme, M., Grazhdankin, D.V., Moczydlowska-Vidal, M., Cui, H., 2016. Towards an Ediacaran time scale: problems, protocols, and prospects. Episodes 39, 540. http://dx.doi.org/10.18814/epiiugs/2016/v39i4/103886.
Xiao, S., Schiffbauer, J.D., McFadden, K.A., Hunter, J., 2010. Petrographic and SIMS pyrite sulfur isotope analyses of Ediacaran chert nodules: implications for microbial processes in pyrite rim formation, silicification, and exceptional fossil preservation. Earth Planet. Sci. Lett. 297, 481–495. http://dx.doi.org/10.1016/j.epsl.2010.07.001.
Xiao, S., Zhang, Y., Knoll, A.H., 1998. Three-dimensional preservation of algae and animal embryos in a Neoproterozoic phosphorite. Nature 391, 553–558. http://dx.doi.org/10.1038/35318.
Zhang, Y., Yin, L., Xiao, S., Knoll, A.H., 1998. Permineralized fossils from the terminal proterozoic Doushantuo. J. Paleontol. 72, 1–52.
Zhou, C., Yuan, X., Xiao, S., 2002. Phosphatized biotas from the Neoproterozoic Doushantuo Formation on the Yangtze Platform. Chin. Sci. Bull. 47, 1918–1924. http://dx.doi.org/10.1360/02tb9419.
Zhou, C., Bao, H., Peng, Y., Yuan, X., 2010. Timing the deposition of 17O-depleted barite at the aftermath of Nantuo glacial meltdown in South China. Geology 38, 903–906. http://dx.doi.org/10.1130/g31224.1.
Zhou, X., Chen, D., Dong, S., Zhang, Y., Guo, Z., Wei, H., Yu, H., 2015. Diagenetic barite deposits in the Yurtus formation in Tarim Basin, NW China: implications for barium and sulfur cycling in the earliest Cambrian. Precambr. Res. 263, 79–87. http://dx.doi.org/10.1016/j.precamres.2015.03.006.

7. "Hydrothermal influence on barite precipitates in the basal Ediacaran Sete Lagoas cap carbonate, São Francisco Craton, central Brazil", artigo submetido a um volume especial da revista Precambrian Research

(Influência hidrotermal em precipitados de barita na capa carbonática eoediacarana Sete Lagoas, Cráton São Francisco, Brasil central)

Juliana Okubo [a, c], Yury Igorevich Klyukin [b, c], Lucas Veríssimo Warren [a], Robert J. Bodnar [c], Benjamin Gill, [c] Shuhai Xiao [c]

[a] Department of Applied Geology, Institute of Geosciences and Exact Sciences, São Paulo State University (Unesp), Rio Claro-SP, Brazil
[b] Department of Earth & Atmospheric Sciences, University of Alberta, Edmonton, Canada
[c] Department of Geosciences, Virginia Tech, Blacksburg, Virginia 24061, USA

Buscando o melhor entendimento do ambiente em que se depositou a capa carbonática Marinoana da Formação Sete Lagoas, este trabalho explora a origem da barita descrita no artigo intitulado "*Phosphogenesis, aragonite fan formation, and seafloor environments following the Marinoan glaciation*", publicado na revista *Precambrian Research (2018, 311: 24-36; ver Capítulo 6)*. Baritas pré-cambriana podem ser interpretadas como de origem diagenética, hidrotermal ou associada à precipitação *in situ* por emanação de metano (*cold seep*). Precipitados de barita de fundo oceânico e cimentos de barita preenchendo cavidades em capas carbonáticas têm sido usualmente interpretados como sinsedimentares ou eodiagenéticos, e têm sido utilizados para aferir a geoquímica dos paleoceanos durante a deglaciação pós- *Snowball Earth*. A ocorrência de barita associada à anomalia negativa de oxigênio triplo na base da Formação Sete Lagoas (Crockford et al., 2017), constitui uma das principais evidências de idade Marinoana para a capa carbonática da Formação Sete Lagoas. Devido à ocorrência de mineralizações do tipo *Mississippi Valley* (MVT) na área estudada (norte de Minas Gerais abarcando os munícipios de Januária, Montalvânia e Morro do Itacarambi), é importante testar se a barita (mineral comum em depósitos MVT) associada aos carbonatos de capa ainda preserva o sinal isotópico primário, ou seja, ainda representa as condições geoquímicas originais da água do mar Ediacarano.

A utilização de técnicas como a espectroscopia Raman e análises de inclusões fluidas, possibilitou compreender como e porque o evento hidrotermal que afetou as rochas da região norte da Bacia Bambuí modificou a evolução térmica da barita. A mineralização MVT na Formação Sete Lagoas apresenta características semelhantes a outros depósitos no Cráton São Francisco (Misi et al., 2005), cujas estimativas de temperatura em inclusões fluidas de sulfetos mostram temperaturas variando entre 100 e 250ºC e salinidades moderadas (3 a 20% NaCl). Devido à influência hidrotermal localizada nas rochas da Formação Sete Lagoas, este tipo de estudo mostra que muitos cuidados analíticos devem ser adotados ao utilizar o mineral barita como indicador geoquímico da composição da paleo-água do mar Ediacarano.

Abstract

Most Precambrian sediment-hosted barites have been interpreted to be diagenetic, hydrothermal exhalation, or methane-seepage in origin. However, seafloor barite precipitates and void-filling barite cements in basal Ediacaran cap carbonates have been interpreted as sedimentary and early diagenetic in origin, and they have been used to infer ocean geochemistry in the aftermath of the terminal Cryogenian (or Marinoan) Snowball Earth glaciation. Barite crystals precipitated syndepositionally from seawater or authigenically from porewaters in direct communication with seawater can potentially offer insights into Neoproterozoic ocean geochemistry. In this study, we analyzed void-filling barite cements from the basal Ediacaran Sete Lagoas cap dolostone to determine whether the barite records seawater geochemical signatures (i.e., early diagenetic in origin) and whether it experienced post-depositional hydrothermal alteration. Sete Lagoas barite occurs as veins and as major void-filling cement in multiple horizons, sometimes interbedded with carbonate fans. Barite crystals, commonly forming rosettes, grew both upwards and downwards. Barite is present as radiating bladed crystals, isolated crystals in the matrix, inclusions within carbonate fan crystals and minor void-filling cements, sometimes partially replacing carbonate fans. Sulfur isotope compositions of coexisting barite and carbonate-associated sulfate show similar values, suggesting a similar source, perhaps both derived from seawater sulfate. Assuming that CAS was sourced from seawater sulfate, we infer that the Sete Lagoas barite was precipitated from porewaters in connection with seawater and hence the source of sulfate ultimately came from the seawater. Carbonaceous material (CM) and fluid inclusions in barite crystals share a similar thermal history with a peak temperature in the range of 206–257°C. CM was not detected in the host rock, possibly due to pervasive dolomitization, thermodegradation of CM or the fine-grained nature of the host rock. Estimated temperatures and salinity based on fluid inclusions are both higher than seawater, suggesting that hydrothermal activities, perhaps those related to MVT mineralization in the São Francisco Craton, may have influenced the Sete Lagoas barite. Thus, although the Sete Lagoas barite may have originally precipitated from seawater or porewaters in communication with seawater, it may have been subsequently influenced by hydrothermal activities and thorough diagenetic assessment must be done before the Sete Lagoas barite can be used to infer seawater geochemistry and environment in the aftermath of Marinoan Snowball Earth.

7.1 Introduction

Modern barite precipitates from a variety of fluids, including hydrothermal fluids, cold seeps, seawater, and pore water within sediments (Griffith and Paytan, 2012). While most Precambrian sedimentary barites are interpreted to be derived from hydrothermal exhalation (Huston and Logan, 2004), diagenetic and methane-seepage origins have been proposed for Archean barite (Heinrichs and Reimer, 1977; Reimer, 1980) and barites in basal Ediacaran cap carbonates (Shields et al., 2007; Zhou et al., 2010).

Griffith and Paytan (2012) identified four models of barite precipitation: (i) marine barite forms when barium is released during degradation of organic material, creating microenvironments that are supersaturated with respect to barite and leading to the precipitation of barite in the water column; (ii) hydrothermal barite precipitates from Ba-rich hydrothermal fluids ascending from depth and mixing with seawater near the seafloor; (iii) cold-seep barite precipitates at the sediment-water interface when Ba-rich fluids are driven out of the sediment by tectonic and hydrological processes not related to volcanic or hydrothermal activity; and (iv) diagenetic barite usually forms through barite dissolution mediated by sulfate reduction in sediments, followed by re-precipitation of barite. This latter process occurs when Ba-rich pore fluids interact with pore water enriched in sulfate at redox boundaries within the sediment.

Two types of barite have been described from basal Ediacaran cap dolostones: syngenetic seafloor barite formed at the water-sediment interface and occurring as laterally continuous barite layers in the upper few centimeters of the cap dolostones (Hoffman and Halverson, 2011; Kennedy, 1996) and early diagenetic barite formed as void-filling isopachous crustose cements associated with tepee-like structures and sheet cracks (Jiang et al., 2006; Shields et al., 2007). Anomalies in $\Delta^{17}O$ have been reported from these barites (Crockford et al., 2017, 2016; Peng et al., 2011; Zhou et al., 2010). These anomalies are thought to represent a global signature and, as such, can be used to correlate cap dolostones from different paleocontinents (Crockford et al., 2017) and to constrain the temporal duration of the cap dolostone deposition based on the time scale at which $\Delta^{17}O$ anomalies come and go (Crockford et al., 2018). However, late diagenetic or hydrothermal barites have also been reported from some basal Ediacaran cap dolostones (Bristow et al., 2011; Zhou et al., 2017), and these barites do not show $\Delta^{17}O$ anomalies (Bao et al., 2008; Killingsworth et al., 2013). Thus, the interpretation of $\Delta^{17}O$ data requires a solid understanding of the origin and diagenetic history of barite in basal Ediacaran cap dolostone.

Three conceptual models have been proposed for the origin of syngenetic and early diagenetic barite in the basal Ediacaran cap dolostone (Crockford et al., 2016): (i) upwelling of anoxic, barium-rich, sulfide-rich, but sulfate-poor deep waters into an oxygenated surface ocean (Hurtgen et al., 2006), (ii) barium sequestration during the oxidation of methane seeping from permafrost that was flooded during rapid marine transgression (Shields et al., 2007), and (iii) upwelling of sulfate-free and Ba^{2+}-rich deep water to shallow platform environments where Ba^{2+} mixed with sulfate from riverine input to precipitate barite (Peng et al., 2011). Thus, there is no consensus about the sources of Ba and sulfate that drove barite precipitation in the cap dolostone. Ba could come from deep water (Hurtgen et al., 2006; Zhou et al., 2010) or groundwater seepage (Shields et al., 2007), whereas the sulfate can be associated with seawater (Hurtgen et al., 2006; Zhou et al., 2010) or riverine input (Peng et al., 2011). Understanding the source of sulfate is critical to deciphering the origin and diagenetic history of the barite, which in turn helps constrain the sulfur and oxygen cycles in the aftermath of terminal Cryogenian glaciation.

In this study, we investigated void-filling barite cements in the basal Ediacaran cap dolostone of the Sete Lagoas Formation, Bambuí Group, central Brazil. Our goal was to test several hypotheses about the origin and diagenetic history of the Sete Lagoas barite by addressing the following questions: (i) whether the barite precipitated from porewaters in direct connection with seawater and hence sulfate was ultimately sourced from seawater, (ii) whether barite cements experienced any subsequent hydrothermal alteration, and (iii) if hydrothermal alteration did occur, what is the nature of the hydrothermal fluids.

We first conducted a detailed petrographic analysis to define the morphology and mode of occurrence of the barite crystals. We then analyzed the sulfur isotope compositions of barite ($\delta^{34}S_{barite}$) and carbonate associated sulfate ($\delta^{34}S_{CAS}$) of the Sete Lagoas Formation, and compared these values with published $\delta^{34}S$ values of Mississippi-Valley type (MVT) sulfide minerals in the São Francisco Craton, in order to test whether the Sete Lagoas barite precipitated from pore fluids that were isotopically similar to seawater or to MVT hydrothermal fluids. Raman spectroscopy and fluid inclusion analysis were used to characterize the thermal history of the Sete Lagoas barite. Raman spectra of carbonaceous material (CM) present in barite crystals and in fluid inclusions hosted in barite crystals were used to estimate temperatures, and Raman spectra of O-H stretching bands of fluid inclusions were used to calculate the salinity of the hydrothermal fluids.

7.2 Geological Setting

The São Francisco Craton (SFC) in central Brazil consists of an Archean-Paleoproterozoic igneous and metamorphic basement covered with Meso- and Neoproterozoic sedimentary strata. The Bambuí Group is part of the sedimentary cover of the SFC. The Bambuí Group (Fig. 7.1A) in the São Francisco basin and the Una Group in the Irecê and Una-Utinga basins consist of glaciogenic diamictites overlain by thick carbonate successions (Misi et al., 2011, 2007). These glaciogenic units include the Jequitaí Fm. and Carrancas Fm. (Bambuí Group) and the Bebedouro Fm. (Una Group) in the Irecê and Una-Utinga basins. The Vazante Group in São Francisco Basin (Fig. 7.1A) is also accumulated in a passive margin setting and rest directly on a glaciogenic unit (Santo Antonio do Bonito Formation, Dardenne et al., 1998). However, at least part of the Vazante Group possibly predates the Bambuí Group (Geboy et al., 2013; Misi et al., 2011). The detailed correlation among these carbonate successions (Fig. 7.1B) is tentatively supported by regional stratigraphic and chemostratigraphic data (Azmy et al., 2001; Misi et al., 2011; Misi and Veizer, 1998), but it remains a matter of intense debate (Misi et al., 2014).

The Bambuí Group is subdivided into five units (Dardenne, 1978). From the base to the top, these units include the Sete Lagoas (SLF), Serra de Santa Helena, Lagoa do Jacaré, Serra da Saudade, and Três Marias formations. The SLF is the basal unit of the Bambuí Group and consists of limestone and dolostone, overlying glaciogenic diamictites or resting unconformably on Paleoproterozoic basement. In the studied area in the vicinity of the town of Januária (central Brazil), the SLF is in sharp contact with the basement (Fig. 7.1C). The lowermost 2.5 meters of the SLF represents the basal Ediacaran cap dolostone, with aragonite fans and barite cements (Caxito et al., 2012; Crockford et al., 2017; Okubo et al., 2018). In the upper part of the SLF, small and localized Mississippi Valley type (MVT) mineralization has been described. The sulfide ores consist primarily of sphalerite, pyrite, and galena with barite, quartz, and minor calcite as associated minerals (Misi et al., 2014, 2005).

The age of the MVT event in the São Francisco Craton is still matter of debate. Misi et al. (2014) claimed the hydrothermal event that affect the craton was Neoproterozoic. However, some authors claimed that the mineralization could be younger. Rock paleomagnetism, U-Pb and Pb isotope data in the undeformed carbonates of the Bambuí Group provided independent evidence for a strong event of remagnetization and resetting of the isotopic system between 530-500Ma (D'Agrella-Filho et al., 2000). Similarly, Trindade et al. (2004) suggested that carbonates from the Salitre Formation in the Irecê basin recorded a regional-scale fluid migration event close to ~520Ma. These authors also interpreted that Pb signatures in both carbonates and sulfides indicates a common source for the fluids responsible for the Pb-Zn mineralization and remagnetization. Thus, mineralization and remagnetization events must overlap in time. More recently, Gonçalves and others (2019) pointed out that this massive fluid flow event that affected the eastern border of the São Francisco Craton could have been even younger (between 515 Ma and 495 Ma).

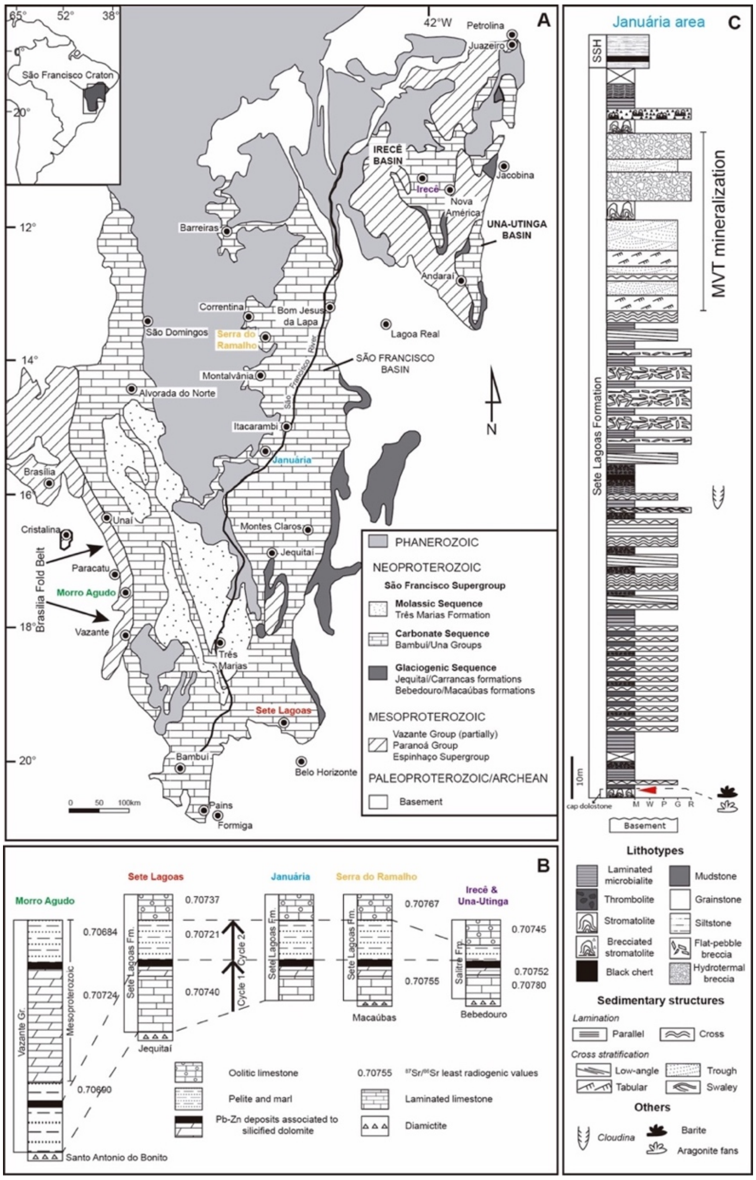

Figure 7.1: Simplified geological map (A) and generalized schematic stratigraphic columns of the carbonate units (B) of the São Francisco Craton and their tentative stratigraphic correlation with coeval successions. The upper strata of Morro Agudo deposit (Mesoproterozoic) are thrusted over the Neoproterozoic successions (modified after Misi et al., 2005, 2014). C) Composite section of the Sete Lagoas Formation at Januária area. Red arrow in (C) denotes stratigraphic horizon where barite samples were collected for this study. SSH: Serra de Santa Helena Formation, MVT: Mississippi-Valley type mineralization.

Pb-Zn deposits and prospects were found in different units (e. g. Morro Agudo and Vazante (Vazante Gr.), Serra do Ramalho (Sete Lagoas Fm.), Três Irmãs (Salitre Fm.) and others, see Fig. 1A) (Cordeiro et al., 2018; Kyle and Misi, 1997; Misi et al., 2014, 2005). These deposits are all similar in terms of stratigraphic position (Fig. 7.1B), association with contemporaneous normal faults, the relatively high temperatures of formation, and the massive nature of the mineral deposits. These features corroborate the interpretation of flow of metal-bearing hydrothermal fluids along fractures and fault zones, probably related to the complex polycyclic Brasiliano orogeny and diagenetic evolution of the host basins (Misi et al., 2014, 2005, 1999).

7.3 Methods

Barite and carbonate samples were collected from a horizon 2.5 meters above the base of the Sete Lagoas cap dolostone, the same stratigraphic horizon studied by Crockford et al. (2017, 2019) and Okubo et al. (2018).

Standard petrographic thin sections were prepared and examined using a transmitted light microscope. Doubly polished thick sections of barite were prepared for Raman and microthermometry analyses of fluid inclusions. The fluid inclusions were classified according into fluid inclusion assemblages based on their origins (primary, pseudosecondary, and secondary) following Goldstein and Reynolds (1994). The inclusions were also examined under UV-light microscopy to assess the presence of hydrocarbons (Bodnar, 1990).

A barite-bearing hand samples was scanned using X-ray computed tomography (X-ray CT) at the University of Texas High-Resolution X-ray CT Facility, in order to reconstruct the three-dimensional shape, orientation, and relative volume of the barite crystals. The sample was scanned at a voltage and current of 220 kV and 0.3 μA, respectively. Barite crystals and the dolostone matrix have high contrast in X-ray attenuation so that they can be easily differentiated in X-ray CT scans: barite crystals are much brighter than the dolostone matrix. The X-ray CT data were processed using Avizo (version 9.0; Visualisation Centre Group) to segment and estimate the relative volume of the barite crystals from the dolostone matrix. Because of the high contrast, segmentation was achieved using simple thresholding techniques.

In order to understand the origin of barite in the Sete Lagoas Formation, we analyzed the sulfur isotope compositions of both the barite ($\delta^{34}S_{barite}$) and carbonate-associated sulfate ($\delta^{34}S_{CAS}$) of subjacent dolostones. All sample preparation and geochemical analyses were performed in the Department of Geosciences at Virginia Tech. Sulfur isotope compositions are reported in standard delta notation as per mil (‰) deviations from the Vienna Canyon Diablo Troilite (V-CDT) and calibrated using international standards (IAEA-SO-5, IAEA-SO-6 and NBS-17).

Carbonate-associated sulfate (CAS) was extracted using the method described in Gill et al. (2011). Approximately 100 g of sample was powdered and treated with a 10% sodium chloride solution to remove soluble sulfate. These samples were rinsed three times with deionized water between each leach. After each rinse, the sample was allowed to settle, and the overlying water was carefully decanted. The carbonate was then dissolved in 4N HCl, the supernatant solution was separated and allowed to react with saturated $BaCl_2$ solution, and the acid-leachable sulfate was precipitated as barite. The barite was then filtered from the solution using a 0.45 μm membrane filter and allowed to dry. The filter with barite precipitate was then dried and weighed. The $BaSO_4$ precipitates were then homogenized and loaded into tin capsules with excess V_2O_5 and analyzed for their $^{34}S/^{32}S$ isotope ratio on an Isoprime 100 isotope ratio mass spectrometer (IRMS) coupled with a vario ISOTOPE Cube EA.

Fluid inclusions in barite crystals were examined under a petrographic microscope. They vary in size from <1 μm to 10 μm. They are usually rounded to irregular in shape. The fluid inclusions form inter- and intragranular inclusion trails, generally parallel to the cleavage planes of the host crystal; these are considered as secondary fluid inclusions. Some intragranular inclusions are randomly distributed in barite crystals, and these are probably primary fluid inclusions.

Raman analysis was performed at Virginia Tech using a JY Horiba LabRam Raman microprobe system equipped with 600 grooves/mm gratings. Excitation was provided by a 514.57 nm (green) laser focused onto the sample through a 100× objective. The targets for Raman analysis were carbonaceous material (CM) in barite crystals and fluid inclusions, which sometimes also contain CM. Raman spectra were recorded in the 1000–4000 cm^{-1} range, avoiding the barite peak (988 cm^{-1}) that can sometimes overwhelm the CM peaks. Raman spectra of CM can be used as a geothermometer to estimate the peak metamorphic temperature of the host rock (Aoya et al., 2010; Beyssac et al., 2002; Kouketsu et al., 2014; Lahfid et al., 2010; Rahl et al., 2005). Raman spectra were processed using the Fityk software for baseline correction, spectral deconvolution, and peak fitting (Wojdyr, 2010). Spectra were reduced using the pseudo-Voigt function for the following peaks: G-band (a minor peak at ~1593 cm^{-1}), D1 (a broad peak at ~1350 cm^{-1}), D2 (a sharp and prominent peak at ~1610 cm^{-1}), D3 (a minor shoulder at ~1470 cm^{-1}), and D4 (a minor broad peak with fixed position at 1245 cm^{-1}). Raman carbonaceous material thermometry was performed following the procedure described in Kouketsu et al. (2014), using fitting cases F and G shown in the Fig. 7.3.

The conventional method of determining the salinity of fluids in inclusions is to measure the ice melting temperature and then determine the salinity based on the known relationship between salinity and ice-melting temperature (Bodnar, 1993). However, if the inclusions are too small or do not contain a vapor bubble when frozen, the ice melting temperature cannot be measured with precision. Fortunately, the salinity of such inclusions can also be estimated based on Raman analysis of the H_2O band owing to the fact that the "shape" of the broad H_2O band changes systematically with salinity (Mernagh and Wilde, 1989; Moncada and Bodnar, 2012; Sun et al., 2010). The shape of the water band is partly dependent on the ionic environment of the water molecules and the variation in Raman-band shape can be used to determine the salinity of inclusions that are as small as 1 micron, which are too small for conventional microthermometric analysis.

7.4 Results

7.4.1 Petrography, microCT, and sulfur isotope data

The Sete Lagoas cap dolostone is interpreted as post-Marinoan or basal Ediacaran deposits on the basis of its sedimentological and geochemical similarities with other post-Marinoan cap carbonates, including the presence of aragonite fans, pink dolostones, and comparable $^{87}Sr/^{86}Sr$ ratios and $\delta^{13}C_{carbonate}$ profiles (Caxito et al., 2012; Halverson et al., 2005; Hoffman et al., 2007). In the study area, the ~2.5-m-thick cap dolostone rests directly on the Paleoproterozoic basement rocks and contains void-filling barite cement in the domal stromatolite facies. Barite occurs as veins and as major void-filling cement in multiple layers, sometimes interbedded with aragonite fans. Barite crystals, commonly forming rosettes, grew both upwards and downwards in stratigraphic orientation (Figs. 7.2A, B), suggesting that they precipitated from pore fluids in the sediment and not on the seafloor, i.e., they were post-depositional precipitates. Barite is present as radiating bladed crystals, isolated crystals in the matrix, and inclusions within carbonate fan crystals and minor void-filling carbonate cements. Microcrystalline barite and pyrite also fill void space and encrust apatite cement.

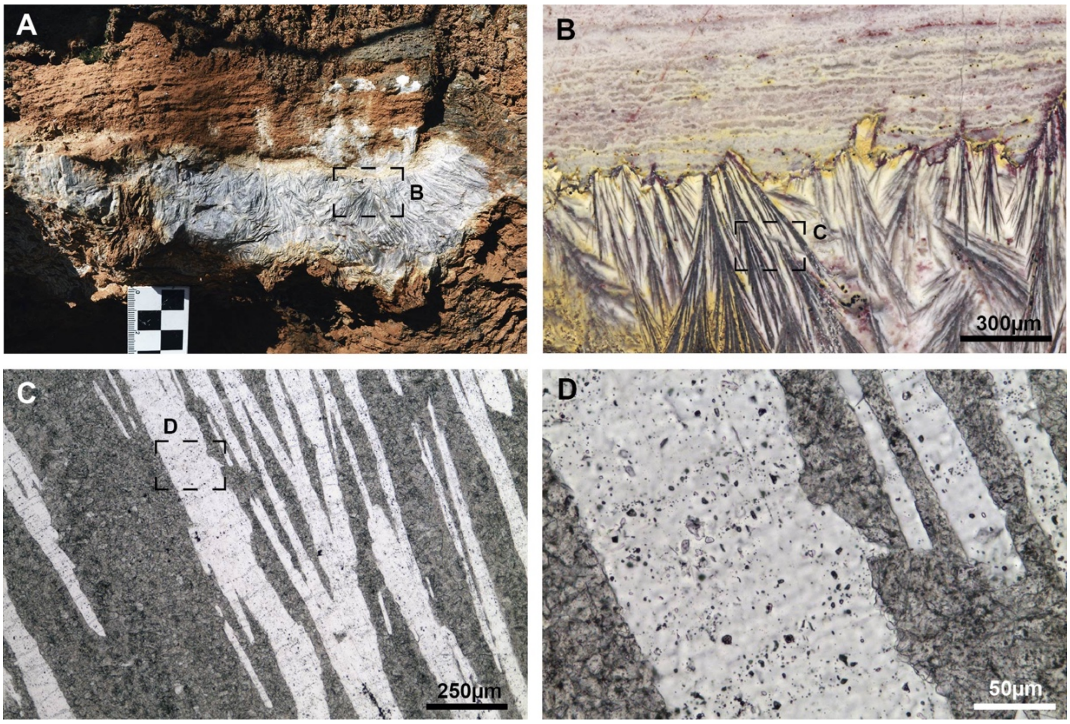

Figure 7.2: Mesoscopic and microscopic features of the barite layer. A) Void-filling barite in the outcrop, commonly forming rosettes, growing inward from both the top and bottom of the vug. B) Dolomitic matrix (top) and radiating bladed barite crystals (bottom). C) Secondary (?) fluid inclusion trails perpendicular to growth direction of barite crystals. Plane polarized light microscopy (PPL). D) Enlarged view of (C), showing trails of intergranular and intragranular secondary (?) fluid inclusions perpendicular to the growth direction of barite crystals. PPL.

X-ray CT analysis of a Sete Lagoas specimen shows a layer of void-filling barite crystals and a layer of the host rock. The barite layer (bottom half of Fig. 7.3) accounts for 66% of the total volume of the specimen, whereas the host rock (top half in Fig. 7.3) accounts for 34%. In the barite layer, bladed barite crystals (green color in bottom half of Fig. 3) occur densely in a micritic carbonate matrix (pink color in bottom half of Fig. 7.3), with the former representing volumetrically 76% of the barite layer and the latter 23%. In the host rock layer, a small amount of microcrystalline barite (green color in top half of Fig. 7.3) is present in the dolostone (blue color in Fig. 7.3) of the host rock.

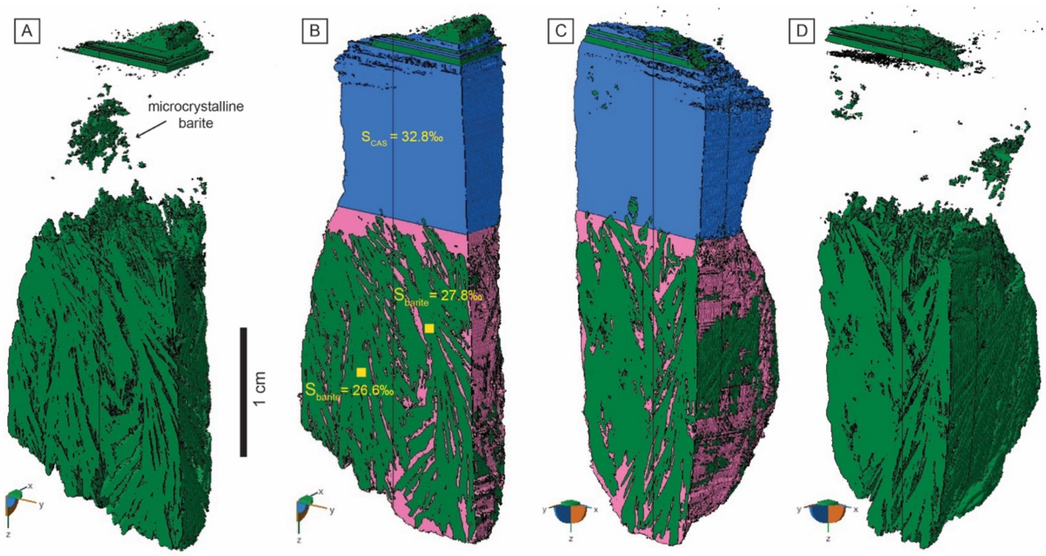

Figure 7.3: X-ray CT three-dimensional reconstruction of a Sete Lagoas sample that contains a layer of void-filling barite crystals (bottom half of the specimen) and a layer of the host rock (top half of the specimen). Barite is segmented as blue color, micritic matrix in the barite layer as pink color, and dolostone in the host rock as blue color. (A–B) and (C–D) are two different views of the same specimen, with (A) and (D) showing only the barite component of the specimen. Microcrystalline barite corresponds to small crystals that grew within the dolostone. $\delta^{34}S_{CAS}$ and $\delta^{34}S_{barite}$ values are marked on the specimen. The specimen is oriented in stratigraphic up direction.

The results of sulfur isotope compositions of barite crystals and CAS are marked on Fig. 3, with $\delta^{34}S_{CAS}$ = 32.8‰ CDT, and two measurements of $\delta^{34}S_{barite}$ gave values of 26.6 and 27.8‰ CDT. For comparison, $\delta^{34}S_{barite}$ values from the same unit reported by Crockford et al. (2017) range from 25.7 to 32.2‰ CDT. Thus, our measurements of $\delta^{34}S_{CAS}$ and $\delta^{34}S_{barite}$ overlap with Crockford et al.'s (2017) $\delta^{34}S_{barite}$ measurements. Arguably, this can be taken as evidence that the barite and CAS were ultimately sourced from the same reservoir, namely seawater sulfate, although this interpretation needs to further tested using additional $\delta^{34}S_{CAS}$ data to determine whether it captures the entire range of $\delta^{34}S_{barite}$ data reported in Crockford et al. (2017).

7.4.2 Raman spectroscopy and fluid inclusions

The petrographic observations and sulfur isotope data described above suggest that the Sete Lagoas barite crystals were post-depositional but record seawater $\delta^{34}S$ values. Thus, it is likely that they were precipitated during early diagenesis from porewaters in connection with seawater. In this section, we describe petrographic observations of fluid inclusions (FI) and Raman data of carbonaceous material (CM) to evaluate the diagenetic and thermal history of the Sete Lagoas barite.

Petrographic observations show that FI and CM are present in void-filling barite crystals (Fig. 7.2C, D); they may also be present in the dolostone matrix, but the micritic nature of the matrix sediment makes it difficult to discern them under a petrographic microscope. Fluid inclusions are mainly less than 5 μm in size (Fig. 7.5). Two-phase fluid inclusions (Fig. 7.5D) are common, and one-phase and three-phase fluid inclusions containing solid phases (Fig. 7.5A, C) are rare. Most fluid inclusions occur as linear trails (Fig. 7.5B, D) that are nearly perpendicular to the long crystal direction (Fig. 7.2D). Considering that barite crystals have perfect {001} cleavages, it is likely that these FI trails follow the cleavages, with the slight deviation from an orthogonal relationship with the long axis of the crystal being a result of two-dimensional thin sections. However, there are some randomly distributed intragranular fluid inclusions (Fig. 7.5A), and these could be primary fluid inclusions.

Because CM is present in both barite crystals and fluid inclusions, it offers opportunity for Raman CM geothermometric analysis. Furthermore, independent temperature estimates can be obtained from FI homogenization temperatures. Result of peak fitting and resolved peaks shown on Fig. 4 for CM trapped in the barite crystal (top) and fluid inclusion (bottom). Raman CM geothermometric data, based on CM in barite crystals, suggest that the barite crystals experienced a peak temperature of 238±10 ºC (calibrated using the D1 peak; n = 9) and 210±10 ºC (calibrated using the D2 peak; n = 9) (Fig. 7.4A–B). Raman CM geothermometric data, based on CM in fluid inclusions trapped barite crystals, gave a peak temperature of 257±12 ºC (calibrated using the D1 peak; n = 6) and 206±12 ºC (calibrated using the D2 peak; n = 6) (Fig. 7.4C–D). The maximum homogenization temperature of fluid inclusions was ~150 ºC (Bodnar, personal communication). Considering that the homogenization temperatures of the fluid inclusions represent minimum trapping temperatures (Roedder and Bodnar, 1980), the three sets of temperatures are broadly consistent with one another.

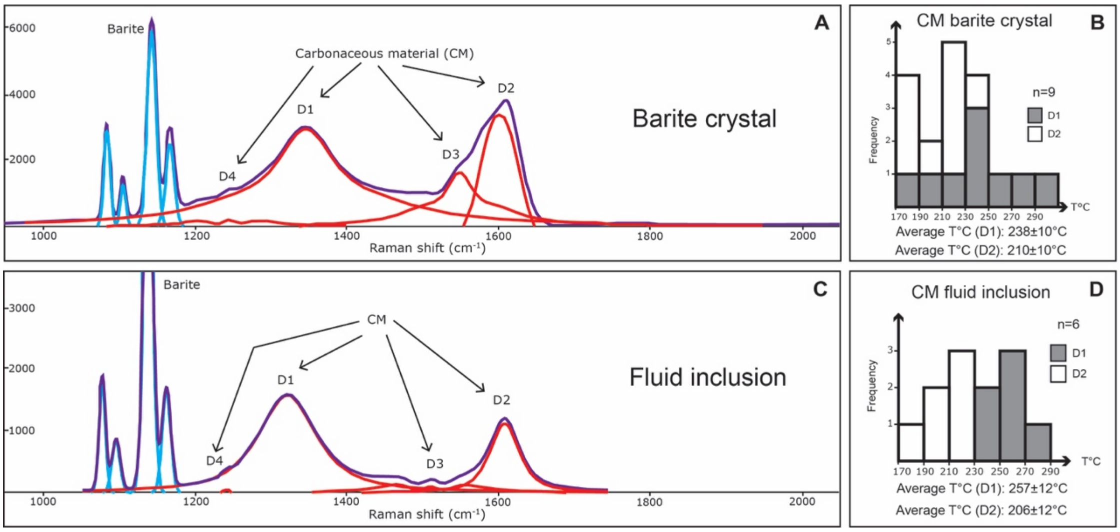

Figure 7.4: CM Raman spectra and CM Raman temperatures. A-B) Representative Raman spectrum and histogram of CM Raman temperatures based on CM in barite crystals. C-D) Representative Raman spectrum and histogram of CM Raman temperatures based on CM in fluid inclusions trapped in barite crystals. Blue and red lines in (A) and (C) mark Raman peaks for barite and CM (D1-D4).

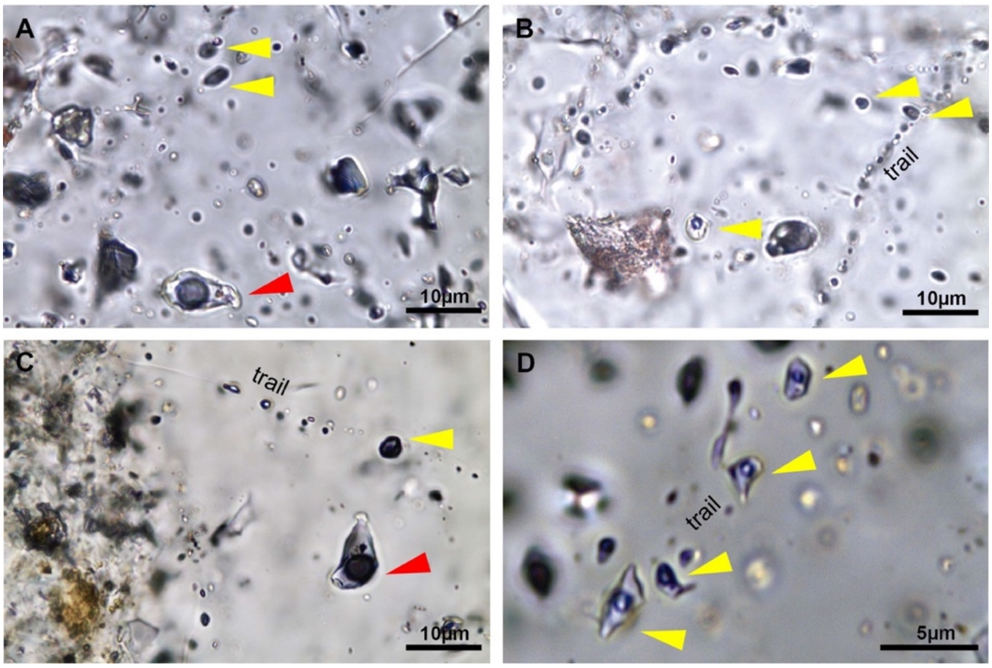

Figure 7.5: Fluid inclusions in barite crystals, showing secondary trails and some primary fluid inclusions. Most of them are two-phase liquid-rich fluid inclusions (liquid + vapor, yellow arrows). A) Primary fluid inclusions randomly distributed and some secondary fluid inclusions. At the bottom, there is a three-phase fluid inclusion (red arrow). B) Secondary trails of two-phase fluid inclusions. C) Matrix (left) – barite crystal (right) interface, showing trails of secondary fluid inclusions cutting the barite crystal. Note that the large fluid inclusion at the center is three-phase fluid inclusion (red arrow). D) Trail of two-phase secondary fluid inclusions showing stretching.

Table 7.1: CM Raman peak parameters and CM Raman temperatures based on CM in barite crystals and CM in fluid inclusions hosted in barite crystals. CM Raman temperatures were calculated using geothermometers from Kouketsu et al. (2014).

Spectra	D1 FWHM (cm^{-1})	D2 FWHM (cm^{-1})	D3 FWHM (cm^{-1})	D4 FWHM (cm^{-1})	T-D1 (ºC)	T-D2 (ºC)
Barite crystals						
CM-B1	91.2	45.1	76.5	29.9	282	229
CM-B2	106.2	52.9	62.7	2.3	250	176
CM-B4	86.7	42.3	87.8	40.3	292	248
CM-B5	138.8	48.8	73.6	83.5	180	204
CM-B6	113.7	46.0	102.2	1038.6	234	223
CM-B7	122.1	45.5	98.5	202.2	215	226
CM-B8	112.4	52.7	56.6	40.7	236	177
CM-B9	131.3	46.8	123.0	9.6	196	217
CM-B10	103.0	51.5	69.2	33.9	257	186
Fluid inclusions						
CM-FI-S4	102.1	45.2	200.8	58.1	258	228
CM-FI-S17	115.1	50.7	160.4	139.7	231	191
CM-FI-S1	106.7	53.3	59.6	13.0	249	174
CM-FI-S5	90.2	45.7	46.0	13.0	284	225
CM-FI-S8	100.2	50.6	72.7	5.4	263	192
CM-FI-S9	103.1	45.6	78.4	87.0	256	226

Petrographic and Raman spectroscopic analyses of fluid inclusions also reveal the presence of hydrocarbons. Some FIs are fluorescent under UV epifluorescence (Fig. 7.6A), indicating that these inclusions contain organic hydrocarbon molecules. This inference is consistent with Raman spectroscopic analysis, which reveals a peak near 2918 cm^{-1} characteristic of methane (Lin et al., 2007) (Fig. 7.6B) and suggests the presence of methane dissolved in the liquid phase.

Finally, Raman spectra of the aqueous phase in FIs allowed estimates of salinity. Based on calibrated relationships between salinity and variations in the O-H stretching band (Sun et al., 2010), the salinity of FIs in Sete Lagoas barite crystals is determined to be ~10%wt NaCl (Fig. 7.7B), higher than that of normal seawater (3.5% wt NaCl).

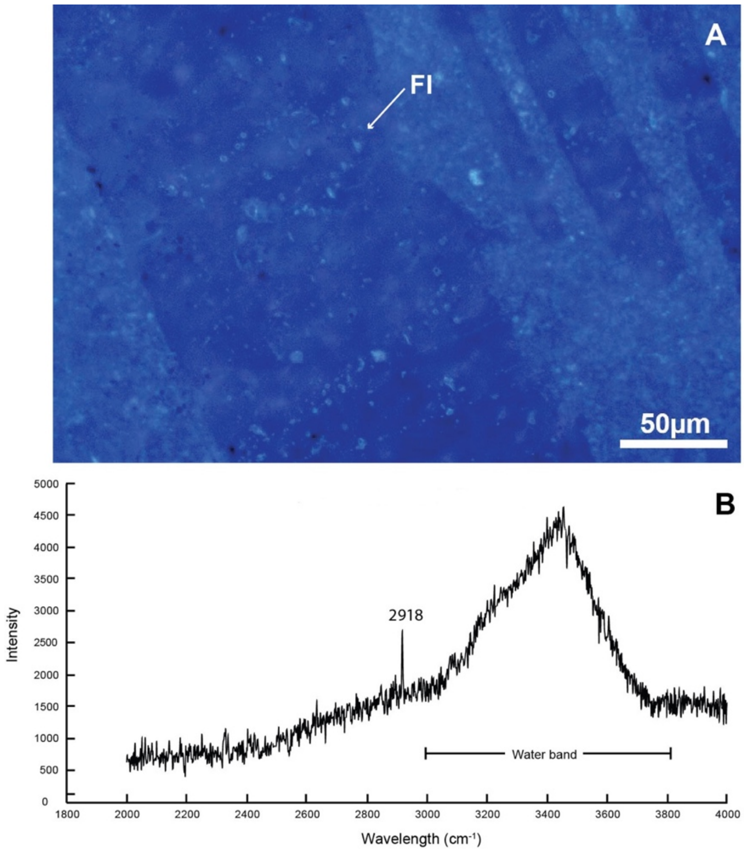

Figure 7.6: Methane-bearing fluid inclusions (FI). A) Blue UV-fluorescence of primary and secondary fluid inclusions; B) Raman spectrum of two-phase fluid inclusion, showing the presence of hydrocarbon (CH_4 – 2918 cm-1) and water.

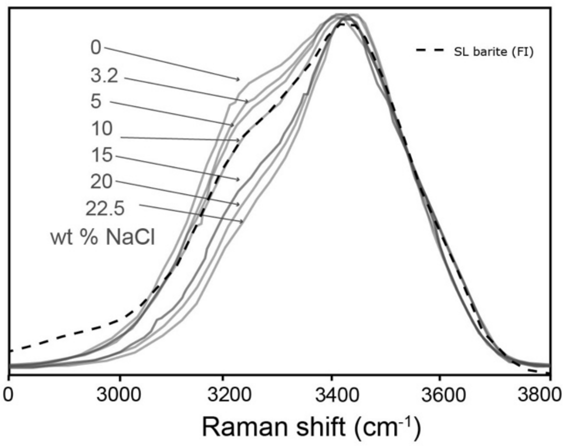

Figure 7.7: Representative Raman spectrum of fluid inclusions in barite crystals of the Sete Lagoas Formation (dashed line; SL barite FI) and calibration Raman spectra showing Raman O-H stretching bands for water with known salinities (solid gray lines; Sun et al., 2010). The salinity of Sete Lagoas fluid inclusions is estimated to be ~10 wt% NaCl.

7.5 Discussions

Although modern barite deposits forms in cold seeps, diagenetic, hydrothermal, and pelagic environments (Griffith and Paytan, 2012; Paytan et al., 2002), most documented occurrences of Proterozoic barites represent stratiform deposits that are of hydrothermal or cold seep origins (e.g. Clark et al., 2004; Crockford et al., 2019; Deb et al., 1991; Huston and Logan, 2004). Geochemical data offer a useful tool to test the different origins of barite. For example, strontium and sulfur isotopic compositions of barite can help to constrain the source of sulfate and the geochemical processes that act upon the sulfate prior to its precipitation as barite. By comparing the Sr isotope compositions of barite and carbonate in the basal Ediacaran Doushantuo cap dolostone, Peng et al. (2011) attributed the source of sulfate for barite precipitation to a mixture of riverine and seawater sulfate. Turchyn et al. (2009) suggested that similar $\delta^{34}S$ values of coexisting barite and CAS indicate that they both formed in equilibrium with seawater. Following the same reasoning, the similarity in sulfur isotopic compositions between the barite and CAS of the host rock in the Sete Lagoas cap dolostone suggests that sulfate for barite precipitation was ultimately sourced from the seawater. Recently, Crockford et al. (2019) presented the Ba isotope variation obtained for different environments (cold seep, terrestrial, hydrothermal, pelagic) and discussed some lines of evidence in considering if post-Marinoan barites were deposited in seep-like environments. They also concluded that the source of barium was seawater.

Assuming that the barite and CAS were ultimately sourced from the same reservoir (seawater sulfate), we can also compare the $\delta^{34}S_{CAS}$ and $\delta^{34}S_{barite}$ values from the Sete Lagoas Formation with $\delta^{34}S_{barite}$ values from other supposedly correlative units in the São Francisco Craton (Fig. 7.8). $\delta^{34}S_{CAS}$ and $\delta^{34}S_{barite}$ values from the Sete Lagoas Formation range from 25.7‰ to 32.2‰ CDT (Crockford et al., 2017; this paper), broadly similar to values from the Salitre Formation of the Irecê Basin, where $\delta^{34}S_{barite}$ range from +25.2‰ to +32.8‰ CDT (Kyle and Misi, 1997). However, these values are different from $\delta^{34}S_{barite}$ values from the Salitre Formation at Nova Redenção (+33.6‰ to +41.0‰ CDT; Misi et al., 2005), and those from the Sete Lagoas Formation in the Montalvânia region (48.2‰ to 50‰ CDT; Gomes, 2005). Such differences could result from incomplete stratigraphic coverage, stratigraphic miscorrelation, regional variation due to basin restriction, diagenetic alteration, or different origins for barite in different units. For example, the high $\delta^{34}S_{barite}$ values from the Salitre Formation at Nova Redenção reflect a more restricted environment in a semi-isolated basin (Misi et al., 2005). The same may be said of the relatively high $\delta^{34}S_{barite}$ values from the Sete Lagoas Formation in the Montalvânia region (Gomes, 2005).

Sulfur isotopic data of sulfide minerals ($\delta^{34}S_{pyrite}$, $\delta^{34}{}_{sphalerite}$ and $\delta^{34}S_{galena}$) have also been reported from the Sete Lagoas Formation and other supposedly correlative stratigraphic units (Salitre Formation - Irecê basin and Nova Redenção deposit) in the São Francisco Craton (Fig. 8). Like the $\delta^{34}S_{barite}$ data, the $\delta^{34}S_{pyrite}$ data also show significant variations within and between stratigraphic units. $\delta^{34}S_{pyrite}$ values have not been reported for the Sete Lagoas Formation, but $\delta^{34}S_{pyrite}$ values are 19.1–22.6‰ in the Salitre Formation in the Irecê Basin (Kyle and Misi, 1997), 17.2 – 17.6‰ in the Salitre Formation at Nova Redenção (Misi et al., 2005) and 1.5–29.58‰ in the Morro Agudo deposit (Misi et al., 2005). $\delta^{34}S_{galena}$ values are 18 – 35.5‰ in the Sete Lagoas Formation in the study area (Iyer et al., 1992),17.3–32.4‰ in the Sete Lagoas Formation in the Montalvânia region (Iyer et al., 1992; Gomes, 2005), 19.4 – 26.2 in the Sete Lagoas Formation in the Serra do Ramalho region (Gomes, 2005), 7.1 – 39.36‰ in the Irecê basin (Misi et al., 2005), 0.1 – 16.2‰ at Nova Redenção deposit (Misi et al., 2005), 1.7 – 33.9‰ in the Morro Agudo deposit (Iyer et al., 1992). $\delta^{34}S_{sphalerite}$ values are 25.4 – 30.4‰ in the Sete Lagoas Formation in the Serra do Ramalho region (Gomes, 2005), 21.1 – 22.6‰ in the Salitre Formation in the Irecê basin (Misi et al., 2005), 16.5 – 18.6‰ in the Salitre Formation at Nova Redenção (Misi et al., 2005) and 0.3 – 38.8‰ in the Morro Agudo deposit (Misi et al., 2005).

The isotopic difference between sulfate and co-existing sulfide can be used to infer the origin of sulfide, with greater fractionations (>20‰) suggesting sulfide formation by bacterial reduction of sulfates (BSR) and small fractionations (<10‰) suggesting sulfides production through thermochemical reduction of sulfates (TSR) (Cui et al., 2018; Machel et al., 1995; Worden et al., 2000). The difference between mean $\delta^{34}S_{sulfate}$ and mean $\delta^{34}S_{sulfide}$ values (= average $\delta^{34}S_{sulfate}$ – average $\delta^{34}S_{sulfide}$) is 1.9‰, 25 ‰, 8.2‰, 20.1‰ and 11.3‰ at Januária locality (Sete Lagoas Formation), Montalvânia locality (Sete Lagoas Formation) Irecê Basin (Salitre Formation), Nova Redenção (Salitre Formation) and Morro Agudo deposit (Vazante Group), respectively. Thus, some authors have proposed that sulfides in the Salitre Formation at Nova Redenção locality was derived from BSR (Gomes, 2005), whereas sulfides in the Salitre Formation in the Irecê Basin may have derived from TSR (Kyle and Misi, 1997), likely at temperatures higher than 110°C (Machel, 2001; Machel et al., 1995). A more systematic petrographic and isotopic study between barite, pyrite and the hydrothermal base metal sulfides would improve the understanding of the paragenetic relationship between these minerals, as well as the processes involving the barite formation (e.g. Magnall et al., 2016).

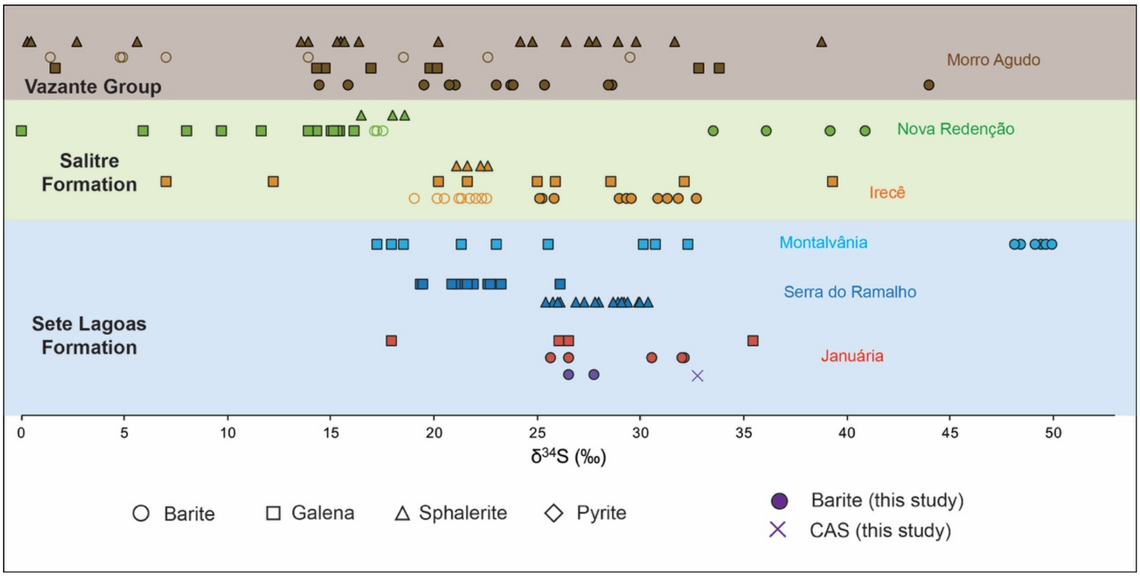

Figure 7.8: Sulfur isotope data of sulfides and sulfates from Sete Lagoas Formation (Januária, Serra do Ramalho and Montalvânia localities) and other supposedly correlative units, Salitre Formation (Irecê and Nova Redenção localities) and Vazante Group (Morro Agudo locality), of the São Francisco Craton. See Fig. 1 for location. Januária: barite and CAS (Crockford et al., 2017; this study), galena (Iyer et al., 1992); Serra do Ramalho: sphalerite and galena (Gomes, 2005); Montalvânia: barite and galena (Iyer et al., 1992; Gomes, 2005); Irecê Basin: barite and pyrite (Kyle and Misi, 1997), galena and sphalerite (Misi et al., 2005); Nova Redenção: barite, galena, sphalerite and pyrite (Misi et al., 2005). Morro Agudo: barite, pyrite, galena and sphalerite (Misi et al., 2005).

Indeed, Raman CM paleotemperatures based on CM in barite crystals (180ºC to 292ºC for T-D1 and 176ºC to 248ºC for T-D2) and fluid inclusions of the Sete Lagoas cap dolostone (231ºC to 284ºC for T-D1 and 191ºC to 228ºC for T-D2) suggest that the Sete Lagoas Formation did experience temperatures greater than 110ºC (Table 1). These temperatures are also consistent with the temperatures reported for limited fluid inclusions in sphalerite from the Salitre Formation and quartz and dolomite from the Vazante Group in the SFC (Carvalho et al., 2017; Kyle and Misi, 1997; Misi et al., 2005). In the Sete Lagoas Formation, Gomes (2005) reported primary fluid inclusions in fluorite from 120 °C to 310 °C at Montalvânia locality, 140 °C to 240 °C at Serra do Ramalho locality and ~190 °C at Januária locality. In the Irecê Basin, primary fluid inclusions in sphalerite indicate a range of homogenization temperatures from ~ 140°C – 200 °C (Gomes et al., 2000; Kyle and Misi, 1997). In the Morro Agudo deposit (Vazante Group), the mineralization is related to a main fault zone, showing paleotemperatures ranging from 100°C to 300 °C that decrease as they move away from the fault (Cunha et al., 2000).

It is possible that the thermal alteration of CM and secondary fluid inclusion trails in barite crystals of the Sete Lagoas Formation were related to Mississippi-Valley-type Pb-Zn mineralization in the São Francisco Craton. Indeed, independent evidence for MVT hydrothermal activities, including the presence of saddle dolomite and fluorite, dissolution and collapse brecciation (Coelho et al., 2005; Nobre-Lopes, 2002), have been reported from the Sete Lagoas Formation in the Januária region. In addition, the presence of methane in fluid inclusions trapped in Sete Lagoas barite crystals, as evidenced by Raman data (Fig. 6B), may have been product of thermodegradation related to MVT mineralization. Crockford et al. (2019) also interpreted that organic matter degradation or hydrothermal circulation could have played a role in the barite precipitation.

Although the chemical diversity between individual MVT deposits is large and requires each deposit or ore-district to be addressed separately, the salinity of MVT fluids is typically 16 to 26 wt% NaCl equivalent (Basuki and Spooner, 2002). In the Irecê Basin, limited determinations of final ice-melting temperatures suggest that the fluid inclusions have a salinity of 3–10 wt. % NaCl equivalent, reaching almost ~25 % NaCl equivalent in the Nova Redenção deposit (Gomes et al., 2000; Kyle and Misi, 1997). In the Morro Agudo deposit (Vazante Group), primary and pseudosecondary fluid inclusions in sphalerite crystals indicate moderate saline solutions (~14 % wt NaCl) (Cunha et al., 2000). Importantly, the salinity of fluid inclusions in Sete Lagoas barite crystals (~10% NaCl equivalent) is similar to that of MVT fluids determined previously (~10–24.3% NaCl equivalent; Gomes et al., 2000; Cunha et al., 2000).

According to Leach et al. (2001), radiometric dating of MVT ore minerals has been difficult due to the low abundances of the natural radioactive isotopes of dated minerals (fluorite, calcite and sphalerite) and the selection of cogenetic minerals that represent an isotopically homogeneous isotopic composition. In the São Francisco Craton, no direct dating of MVT ore minerals have been reported yet. However, paleomagnetic studies of MVT deposits (D'Agrella-Filho et al., 2000; Trindade et al., 2004) have argued that the MVT deposits in the Sete Lagoas and Salitre formations are related to a regional fluid-flow event in the early Cambrian (~520Ma). Also, younger rocks, such as the Cretaceous Urucuia Group that covers the Bambuí Group, does not seem to host MVT mineralization, either because these rocks did not record the mineralization or the MVT mineralization is older than the deposition of these rocks.

An important implication of this study is that Sete Lagoas barite may have altered by hydrothermal activities such as MVT mineralization event in the São Francisco Craton. Although major elements in the barite, such as sulfur and oxygen, may be buffered against hydrothermal alteration and may still be useful in the study of ocean geochemistry and paleoenvironments in the aftermath of the Marinoan glaciation (Crockford et al., 2017, 2016; Hoffman and Halverson, 2011), caution must be exercised when using trace elements such as strontium concentrations and isotopes to infer paleoceanographic and environmental conditions. Such hydrothermal activities can also affect the geochemistry of any primary fluid inclusions present in the Sete Lagoas barite, because barite-hosted fluid inclusions are particularly susceptible to necking, stretching, leaking or decrepitation and re-equilibration, which can lead to large variability in homogenization temperature (Ulrich and Bodnar, 1988).

7.6 Conclusions

We carried out integrative petrographic, sulfur isotopic, Raman spectroscopic, and fluid inclusion analyses to understand the origin and hydrothermal alteration of void-filling barite crystals in the basal Ediacaran Sete Lagoas Formation in the São Francisco Craton, central Brazil. Petrographic observations indicate that the barite was post-depositional cement precipitated from porewaters. Co-existing barite and carbonate-associated sulfate (CAS) have marginally overlapping $\delta^{34}S$ values ($\delta^{34}S_{barite}$ = 25.7–32.2‰ CDT; $\delta^{34}S_{CAS}$ = 32.8‰ CDT), suggesting that they were sourced from the same sulfate pool. Assuming that CAS was sourced from seawater sulfate, we infer that the Sete Lagoas barite was precipitated from porewaters in connection with seawater and hence the source of sulfate ultimately came from the seawater. Fluid inclusion and Raman spectroscopic analyses suggest that carbonaceous material (CM) in barite crystals and in fluid inclusions trapped in the barite crystals share a similar thermal history, with a peak temperature in the range of 206–257°C. Raman spectroscopic analysis also reveals that the salinity of the fluid inclusions is ~10 wt% NaCl equivalent, higher than that of seawater but similar to that of fluids in the early Cambrian Mississippi Valley Type (MVT) mineralization in the São Francisco Craton (~3–20 wt% NaCl equivalent; Misi et al., 2005). These results suggest that the Sete Lagoas barite was affected by hydrothermal activities, and we hypothesize that these hydrothermal activities were related the MVT mineralization event in the São Francisco Craton (Cordeiro et al., 2018; Misi et al., 2005). Although the major element geochemistry of void-filling barite cements in the Sete Lagoas Formation has been used to infer seawater geochemistry and paleoenvironments in the aftermath of the Marinoan Snowball Earth glaciation (Crockford et al., 2017; Hoffman and Halverson, 2011), data presented here indicate that the Sete Lagoas barite was affected by hydrothermal activities related to MVT mineralization, and caution must be taken when using Sete Lagoas barite (particularly its trace element geochemistry) to infer seawater geochemistry and paleoenvironments.

ACKNOWLEDGEMENTS

This study was funded by Fundação de Amparo à Pesquisa do Estado de São Paulo (FAPESP 2015/07391-0 and 2017/19023-1). S.X. acknowledges funding from the NASA Exobiology and Evolutionary Biology Program (80NSSC18K1086). The authors are grateful to Charles Farley for assistance in Raman analysis and Khanh To for assistance in X-ray CT data processing. L.V. Warren is fellow of the CNPq, Brazil.

7.7 REFERENCES

Aoya, M., Kouketsu, Y., Endo, S., Shimizu, H., Mizukami, T., Nakamura, D., Wallis, S., 2010. Extending the applicability of the Raman carbonaceous-material geothermometer using data from contact metamorphic rocks. J. Metamorph. Geol. 28, 895–914.

Azmy, K., Veizer, J., Misi, A., De Oliveira, T.F., Sanches, A.L., Dardenne, M.A., 2001. Dolomitization and isotope stratigraphy of the Vazante Formation, São Francisco Basin, Brazil. Precambrian Res. 112, 303–329.

Bao, H., Lyons, J.R., Zhou, C., 2008. Triple oxygen isotope evidence for elevated CO2 levels after a Neoproterozoic glaciation. Nature 453, 504–506.

Basuki, N.I., Spooner, E.T.C., 2002. A review of fluid inclusion temperatures and salinities in Mississippi Valley-type Zn-Pb deposits: identifying thresholds for metal transport. Explor. Min. Geol. 11, 1–17.

Beyssac, O., Goffé, B., Chopin, C., Rouzaud, J.N., 2002. Raman spectra of carbonaceous material in metasediments: a new geothermometer. J. Metamorph. Geol. 20, 859–871.

Bodnar, R.J., 1993. Revised equation and table for determining the freezing point depression of H2O-Nacl solutions. Geochim. Cosmochim. Acta 57, 683–684.

Bodnar, R.J., 1990. Petroleum migration in the Miocene Monterey Formation, California, USA: constraints from fluid-inclusion studies. Mineral. Mag. 54, 295–304.

Bristow, T.F., Bonifacie, M., Derkowski, A., Eiler, J.M., Grotzinger, J.P., 2011. A hydrothermal origin for isotopically anomalous cap dolostone cements from south China. Nature 474, 68–71.

Carvalho, I.A.K., Olivo, G.R., Moura, M.A., Oliveira, G.D., 2017. Fluid evolution in the southern part of the Proterozoic Vazante Group, Brazil: Implications for exploration of sedimentary-hosted base metal deposits. Ore Geol. Rev. 91, 588–611.

Caxito, F. de A., Halverson, G.P., Uhlein, A., Stevenson, R., Gonçalves Dias, T., Uhlein, G.J., 2012. Marinoan glaciation in east central Brazil. Precambrian Res. 200–203, 38–58.

Clark, S.H.B., Poole, F.G., Wang, Z., 2004. Comparison of some sediment-hosted, stratiform barite deposits in China, the United States, and India. Ore Geol. Rev. 24, 85–101.

Coelho, C.E.S., Misi, A., Cunha, I. de A., Gomes, A.S.R., Martins, V. de S., 2005. Composição e geotermometria dos fluidos mineralizantes em depósitos de Zn-Pb das coberturas neoproterozoicas do Cráton São Francisco: implicações metalogenéticas. Rev. Bras. Geociências 35, 35–46.

Cordeiro, P.F.O., Oliveira, C.G., Paniago, L.N., Romagna, G., Santos, R. V., 2018. The carbonate-hosted MVT Morro Agudo Zn-Pb deposit, central Brazil. Ore Geol. Rev. 101, 437–452.

Crockford, P.W., Cowie, B.R., Johnston, D.T., Hoffman, P.F., Sugiyama, I., Pellerin, A., Bui, T.H., Hayles, J., Halverson, G.P., Macdonald, F.A., Wing, B.A., 2016. Triple oxygen and multiple sulfur isotope constraints on the evolution of the post-Marinoan sulfur cycle. Earth Planet. Sci. Lett. 435, 74–83.

Crockford, P.W., Hayles, J.A., Bao, H., Planavsky, N.J., Bekker, A., Fralick, P.W., Halverson, G.P., Bui, T.H., Peng, Y., Wing, B.A., 2018. Triple oxygen isotope evidence for limited mid-Proterozoic primary productivity. Nature 559, 613–616.

Crockford, P.W., Hodgskiss, M.S.W., Uhlein, G.J., Caxito, F., Hayles, J.A., Halverson, G.P., 2017. Linking paleocontinents through triple oxygen isotope anomalies. Geology 46, 179–182.

Crockford, P.W., Kunzmann, M., Bekker, A., Hayles, J., Bao, H., Halverson, G.P., Peng, Y., Bui, T.H., Cox, G.M., Gibson, T.M., Wörndle, S., Rainbird, R., Lepland, A., Swanson-Hysell, N.L., Master, S., Sreenivas, B., Kuznetsov, A., Krupenik, V., Wing, B.A., 2019. Claypool continued: Extending the isotopic record of sedimentary sulfate. Chem. Geol. 513, 200–225.

Cui, H., Kitajima, K., Spicuzza, M.J., Fournelle, J.H., Denny, A., Ishida, A., Zhang, F., Valley, J.W., 2018. Questioning the biogenicity of Neoproterozoic superheavy pyrite by SIMS. Am. Mineral. 103, 1362–1400.

D'Agrella-Filho, M.S., Babinski, M., Trindade, R.I.F., Van Schmus, W.R., Ernesto, M., 2000. Simultaneous remagnetization and U-Pb isotope resetting in Neoproterozoic carbonates of the Sao Francisco craton, Brazil. Precambrian Res. 99, 179–196.

Dardenne, M.A., 1978. Síntese sobre a estratigrafia do Grupo Bambuí no Brasil Central, in: Anais Do XXX Congresso Brasileiro de Geologia. Recife, pp. 597–610.

Dardenne, M.A., Freitas-Silva, F.H., Souza, J.C.F., Campos, J.E.G., 1998. Evolução tectono-sedimentar do Grupo Vazante no contexto da Faixa de Dobramentos Brasília, in: Proceedings of the Congresso Brasileiro de Geologia. Belo Horizonte-MG.

Deb, M., Hoefs, J., Bauman, A., 1991. Isotopic composition of two Precambrian stratiform barite deposits from the Indian shield. Geochim. Cosmochim. Acta 55, 303–308.

Geboy, N.J., Kaufman, A.J., Walker, R.J., Misi, A., de Oliviera, T.F., Miller, K.E., Azmy, K., Kendall, B., Poulton, S.W., 2013. Re-Os age constraints and new observations of Proterozoic glacial deposits in the Vazante Group, Brazil. Precambrian Res. 238, 199–213.

Gill, B.C., Lyons, T.W., Young, S.A., Kump, L.R., Knoll, A.H., Saltzman, M.R., 2011. Geochemical evidence for widespread euxinia in the later Cambrian ocean. Nature 469, 80–83.

Goldstein, R.H., Reynolds, T.J., 1994. Systematics of Fluid Inclusions in Diagenetic Minerals, in: SEPM Short Course 31. p. 213p.

Gomes, A.S.R., 2005. Modelagem Metalogenética das Mineralizações de Pb-Zn Hospedadas em Carbonatos Neoproterozóicos de Irecê (BA), Serra do Ramalho (BA) e Montalvânia (MG). Unpublished PhD thesis, Federal University of Bahia, Salvador-BA, Brazil. 169p.

Gonçalves, G.O., Lana, C., Buick, I.S., Alkmim, F.F., Scholz, R., Queiroga, G., 2019. Twenty million years of post-orogenic fluid production and hydrothermal mineralization across the external Araçuaí orogen and adjacent São Francisco craton, SE Brazil. Lithos 342–343, 557–572.

Griffith, E.M., Paytan, A., 2012. Barite in the ocean - occurrence, geochemistry and palaeoceanographic applications. Sedimentology 59, 1817–1835.

Halverson, G.P., Hoffman, P.F., Schrag, D.P., Maloof, A.C., Rice, A.H.N., 2005. Toward a Neoproterozoic composite carbon-isotope record. Bull. Geol. Soc. Am. 117, 1181–1207.

Halverson, G.P., Wade, B.P., Hurtgen, M.T., Barovich, K.M., 2010. Neoproterozoic chemostratigraphy. Precambrian Res. 182, 337–350.

Heinrichs, T.K., Reimer, T.O., 1977. A sedimentary barite deposit from the Archean Fig Tree Group of the Barbeton Mountain Land (South Africa). Econ. Geol. 72, 1426–1441.

Hoffman, P.F., Halverson, G.P., 2011. Chapter 36 Neoproterozoic glacial record in the Mackenzie Mountains, northern Canadian Cordillera. Geol. Soc. London, Mem. 36, 397–412.

Hoffman, P.F., Halverson, G.P., Domack, E.W., Husson, J.M., Higgins, J.A., Schrag, D.P., 2007. Are basal Ediacaran (635 Ma) post-glacial "cap dolostones" diachronous? Earth Planet. Sci. Lett. 258, 114–131.

Hurtgen, M.T., Halverson, G.P., Arthur, M.A., Hoffman, P.F., 2006. Sulfur cycling in the aftermath of a 635-Ma snowball glaciation: Evidence for a syn-glacial sulfidic deep ocean. Earth Planet. Sci. Lett. 245, 551–570.

Huston, D.L., Logan, G.A., 2004. Barite, BIFs and bugs: Evidence for the evolution of the Earth's early hydrosphere. Earth Planet. Sci. Lett. 220, 41–55.

Jiang, G., Kennedy, M.J., Christie-Blick, N., Wu, H., Zhang, S., 2006. Stratigraphy, Sedimentary Structures, and Textures of the Late Neoproterozoic Doushantuo Cap Carbonate in South China. J. Sediment. Res. 76, 978–995.

Kennedy, M.J., 1996. Stratigraphy, sedimentology, and isotopic geochemistry of Australian Neoproterozoic postglacial cap dolostones; deglaciation, delta ^{13}C excursions, and carbonate precipitation. J. Sediment. Res. 66, 1050–1064.

Killingsworth, B.A., Hayles, J.A., Zhou, C., Bao, H., 2013. Sedimentary constraints on the duration of the Marinoan Oxygen-17 Depletion (MOSD) event. Proc. Natl. Acad. Sci. 110, 17686–17690.

Kouketsu, Y., Mizukami, T., Mori, H., Endo, S., Aoya, M., Hara, H., Nakamura, D., Wallis, S., 2014. A new approach to develop the Raman carbonaceous material geothermometer for low-grade metamorphism using peak width. Isl. Arc 23, 33–50.

Kyle, J.R., Misi, A., 1997. Origin of Zn-Pb-Ag sulfide mineralization within upper Proterozoic phosphate-rich carbonate strata, Irecê basin, Bahia, Brazil. Int. Geol. Rev. 39, 383–399.

Lahfid, A., Beyssac, O., Deville, E., Negro, F., Chopin, C., Goffé, B., 2010. Evolution of the Raman spectrum of carbonaceous material in low-grade metasediments of the Glarus Alps (Switzerland). Terra Nov. 22, 354–360.

Lin, F., Bodnar, R.J., Becker, S.P., 2007. Experimental determination of the Raman CH4 symmetric stretching (ν1) band position from 1-650 bar and 0.3-22 °C: Application to fluid inclusion studies. Geochim. Cosmochim. Acta 71, 3746–3756.

Machel, H.G., 2001. Bacterial and thermochemical sulfate reduction in diagenetic settings - old and new insights. Sediment. Geol. 140, 143–175.

Machel, H.G., 1987. Saddle dolomite as a by-product of stylolitization and thermochemical sulfate reduction. Geology 15, 936–940.

Machel, H.G., Krouse, H.R., Sassen, R., 1995. Products and distinguishing criteria of bacterial and thermochemical sulfate reduction. Appl. Geochemistry 10, 373–389.

Magnall, J.M., Gleeson, S.A., Stern, R.A., Newton, R.J., Poulton, S.W., Paradis, S., 2016. Open system sulphate reduction in a diagenetic environment - Isotopic analysis of barite (δ34S and δ18O) and pyrite (δ34S) from the Tom and Jason Late Devonian Zn-Pb-Ba deposits, Selwyn Basin, Canada. Geochim. Cosmochim. Acta 180, 146–163.

McFadden, K.A., Huang, J., Chu, X., Jiang, G., Kaufman, A.J., Zhou, C., Yuan, X., Xiao, S., 2008. Pulsed oxidation and biological evolution in the Ediacaran Doushantuo Formation. Proc. Natl. Acad. Sci. 105, 3197–3202.

Mernagh, T.P., Wilde, A.R., 1989. The use of the laser Raman microprobe for the determination of salinity in fluid inclusions. Geochim. Cosmochim. Acta 53, 765–771.

Misi, A., Azmy, K., Kaufman, A.J., de Oliveira, T.F., Dardenne, M.A., Sial, A.N., 2011. Neoproterozoic successions of the São Francisco Craton, Brazil: the Bambuí, Una, Vazante and Vaza Barris/Miaba groups and their glaciogenic deposits, in: Geological Society, London, Memoirs. pp. 509–522.

Misi, A., Azmy, K., Kaufman, A.J., Oliveira, T.F., Sanches, A.L., Oliveira, G.D., 2014. Review of the geological and geochronological framework of the Vazante sequence, Minas Gerais, Brazil: Implications to metallogenic and phosphogenic models. Ore Geol. Rev. 63, 76–90.

Misi, A., Iyer, S.S., Tassinari, C.C.G., Kyle, J.R., Coelho, C.E.S., Franca-Rocha, W.J.S., Gomes, A.S.R., Cunha, I.A., Carvalho, I.G., 1999. Geological and Isotopic Constraints on the Metallogenic Evolution of the Proterozoic Sediment-Hosted Pb-Zn (Ag) Deposits of Brazil. Gondwana Res. 2, 47–65.

Misi, A., Iyer, S.S.S., Coelho, C.E.S., Tassinari, C.C.G., Franca-Rocha, W.J.S., de Abreu Cunha, I., Rocha Gomes, A.S., de Oliveira, T.F., Teixeira, J.B.G., Filho, V.M.C., 2005. Sediment hosted lead-zinc deposits of the Neoproterozoic Bambuí Group and correlative sequences, São Francisco Craton, Brazil: A review and a possible metallogenic evolution model. Ore Geol. Rev. 26, 263–304.

Misi, A., Teixeira, J.B.G., Azmy, K., Veizer, J., Boggiani, P.C., Iyer, S.S.S., Gaucher, C., Kaufman, A.J., Powis, K., Sanches, A.L., 2007. Chemostratigraphic correlation of Neoproterozoic successions in South America. Chem. Geol. 237, 143–167.

Misi, A., Veizer, J., 1998. Neoproterozoic carbonate sequences of the Una Group, Irecê Basin: chemostratigraphy, age and correlations. Precambrian Res. 89, 87–100.

Moncada, D., Bodnar, R.J., 2012. Raman spectroscopic technique to determine the salinity of fluid inclusions, in: 11th Pan-American Current Research on Fluid Inclusions (PACROFI) Conference. Abstract Volume with Program, Windsor, Ontario, pp. 67–68.

Nobre-Lopes, J., 2002. Diagenesis of the dolomites hosting Zn/Ag mineral deposits in the Bambui Group at Januaria region-MG. Unpublished PhD thesis, University of Campinas, Campinas-SP, Brazil. 229p.

Okubo, J., Muscente, A.D., Luvizotto, G.L., Uhlein, G.J., Warren, L.V., 2018. Phosphogenesis, aragonite fan formation and seafloor environments following the Marinoan glaciation. Precambrian Res. 311, 24–36.

Paytan, A., Mearon, S., Cobb, K., Kastner, M., 2002. Origin of marine barite deposits: Sr and S isotope characterization. Geology 30, 747–750.

Peng, Y., Bao, H., Zhou, C., Yuan, X., 2011. 17O-depleted barite from two Marinoan cap dolostone sections, South China. Earth Planet. Sci. Lett. 305, 21–31.

Rahl, J.M., Anderson, K.M., Brandon, M.T., Fassoulas, C., 2005. Raman spectroscopic carbonaceous material thermometry of low-grade metamorphic rocks: Calibration and application to tectonic exhumation in Crete, Greece. Earth Planet. Sci. Lett. 240, 339–354.

Reimer, T.O., 1980. Archean sedimentary baryte deposits of the Swaziland Supergroup (Barberton Mountain Land, South Africa). Precambrian Res. 12, 393–410.

Roedder, E., Bodnar, R.J., 1980. Geologic pressure determinations from fluid inclusion studies. Annu. Rev. Earth Planet. Sci. 8, 263–301.

Shields, G.A., Deynoux, M., Strauss, H., Paquet, H., Nahon, D., 2007. Barite-bearing cap dolostones of the Taoudéni Basin, northwest Africa: Sedimentary and isotopic evidence for methane seepage after a Neoproterozoic glaciation. Precambrian Res. 153, 209–235.

Sun, Q., Zhao, L., Li, N., Liu, J., 2010. Raman spectroscopic study for the determination of Cl- concentration (molarity scale) in aqueous solutions: Application to fluid inclusions. Chem. Geol. 272, 55–61.

Trindade, R.I.F., D'Agrella-Filho, M.S., Babinski, M., Font, E., Brito Neves, B.B., 2004. Paleomagnetism and geochronology of the Bebedouro cap carbonate: Evidence for continental-scale Cambrian remagnetization in the São Francisco craton, Brazil. Precambrian Res. 128, 83–103.

Turchyn, A. V., Schrag, D.P., Coccioni, R., Montanari, A., 2009. Stable isotope analysis of the Cretaceous sulfur cycle. Earth Planet. Sci. Lett. 285, 115–123.

Ulrich, M.R., Bodnar, R.J., 1988. Systematics of strecthing of fluid inclusions II: barite at 1 atm confining pressure. Econ. Geol. 83, 1037–1046.

Wojdyr, M., 2010. Fityk: A general-purpose peak fitting program. J. Appl. Crystallogr. 43, 1126–1128.

Worden, R.H., Smalley, P.C., Cross, M.M., 2000. The influence of rock fabric and mineralogy on thermochemical sulfate reduction: Khuff Formation, Abu Dhabi. J. Sediment. Res. 70, 1210–1221.

Zhou, C., Bao, H., Peng, Y., Yuan, X., 2010. Timing the deposition of 17O-depleted barite at the aftermath of Nantuo glacial meltdown in South China. Geology 38, 903–906.

Zhou, G., Luo, T., Zhou, M., Xing, L., Gan, T., 2017. A ubiquitous hydrothermal episode recorded in the sheet-crack cements of a Marinoan cap dolostone of South China: Implication for the origin of the extremely ^{13}C-depleted calcite cement. J. Asian Earth Sci. 134, 63–71.

8. "The enigmatic flat-pebble breccia of the Sete Lagoas Formation (Bambuí Group, Brazil): evidences of seismic-induced deformation in an Ediacaran carbonate platform", submetido para o periódico Journal of South American Earth Sciences

(A enigmática *flat-pebble breccia* da Formação Sete Lagoas, Grupo Bambuí, Brasil: evidências de deformação induzida por sismos em uma plataforma carbonática ediacarana)

J. Okubo[a], L.V. Warren[a], G.L. Luvizotto [b], F.G. Varejão[a], F. Quaglio [c], G.J. Uhlein [d], M.L. Assine [a]

[a] Department of Applied Geology, Institute of Geosciences and Exact Sciences, São Paulo State University (Unesp), Rio Claro, SP, Brazil

[b] Department of Petrology and Metallogenesis, Institute of Geosciences and Exact Sciences, São Paulo State University (Unesp), Rio Claro, SP, Brazil

[c] Departament of Ecology and Evolutionary Biology, Universidade Federal de São Paulo, Diadema, SP, Brazil

[d] Institute of Geosciences, Federal University of Minas Gerais, Belo Horizonte, MG, Brazil

Brechas intraformacionais são fácies particulares e ocorrem em profusão em plataformas carbonáticas neoproterozoicas. Estes depósitos têm sido comumente descritos como: 1) olistoestromas (Formação Doushantuo, China); 2) *edgewise conglomerates* (Formação Buah, Omã); 3) *molar tooth strutures* (noroeste do Canadá), 4) tsunamitos; 5) tempestitos; 6) escorregamentos submarinos; 7) exposição subaérea ou até mesmo 8) produtos relacionados a eodiagênese. No entanto, independentemente de sua origem, estas facies sempre representam eventos deposicionais e/ou processos bastante particulares e importantes atuantes nas plataformas carbonáticas antigas. Ainda que pese a existência de poucos exemplos de deformações sedimentares descritas em unidades carbonáticas ediacaranas brasileiras (à exemplo da Formação Mirassol do Oeste, Grupo Araras), esta facies é particularmente comum nas unidades carbonáticas do Grupo Bambuí. Ao longo da sucessão sedimentar da Formação Sete Lagoas na região de Januária, MG, ocorrem brechas de colapso, brechas evaporíticas, brechas hidrotermais e brechas intraformacionais (*flat-pebble breccia*). Especialmente no caso deste último tipo de facies, praticamente inexistem trabalhos na literatura que propõem uma discussão detalhada sobre o mecanismo de formação desses depósitos. Deste modo, neste trabalho, buscou-se caracterizar, descrever e interpretar a origem dos 20 metros de *flat-pebble breccia*, que ocorrem na parte intermediária da sucessão da Formação Sete Lagoas. Estas camadas se caracterizam por apresentarem clastos tabulares muito angulosos, dispostos horizontalmente ao acamamento e comumente encaixados uns aos outros, evidenciando transporte e/ou retrabalhamento reduzidos.

Características intrínsecas a estes depósitos, tais como a presença de clastos verticais e feições de deformação aumentando em direção ao topo das camadas, continuidade lateral das brechas e alternância de camadas brechadas e não-brechadas em contato abrupto, conduziram a uma interpretação que considera a fragmentação *in situ* de camadas de microbialitos laminados precocemente litificadas devido ao impacto de ondas de choque relacionadas à atividade sísmica concomitante à sedimentação.

Abstract

The Sete Lagoas Formation (Ediacaran), located in the central part of the São Francisco Craton (Brazil), consists of limestones and dolostones deposited in very shallow waters in the inner part of a rimmed carbonate platform. Four breccia types occur throughout the stratigraphic succession: evaporitic breccia with tepees, flat-pebble breccia, hydrothermal breccia and brecciated stromatolites. Here we combine a detailed sedimentological and stratigraphic analyses of the flat-pebble breccia in order to determine its origin and the processes and environmental conditions that originated these brecciated facies. The studied interval consists of a 20 m-thick succession of tabular beds composed of flat-pebble breccia interbedded with laminated microbialites. In these breccia beds, the clasts are usually platy or oblate with angular edges and are mainly disposed horizontally within the sedimentary bed, suggesting that they were not transported or reworked. The presence of microbialite clasts with sharp edges and vertices in the Sete Lagoas flat-pebble breccia suggests that the lithification process started very early in diagenesis; even the sediments exposed at the bottom were, at least, partially lithified. Some breccia levels show bidirectional imbrication and the clast size analyze reveal that the higher aspect ratio clasts show a NE-SW orientation whereas square clasts tend to fill the space among oriented clasts. Breccia clasts are vertically oriented and show deformation features increasing upwards, typically of deforming beds formed by ascendant expulsion of liquefied sediment. These features are found both in modern and ancient deposits of seismic influence, which suggests a similar origin for the Sete Lagoas flat-pebble breccia. Thus, the processes that led to the formation of the studied flat-pebble breccia are interpreted as seismically triggered, since: a) the breccia beds are laterally continuous and extend for several kilometers; b) the breccia beds are restricted to a 20m-thick stratigraphic interval; c) the interbedding of breccia beds and laminated microbialite beds is recurrent; d) the breccia beds are subhorizontal and present irregular upper and lower contacts; e) the presence of liquefaction structures and dyke injection. Thus, this seismic-triggered breccia deposits represent the product of the synsedimentary tectonism occurred within the São Francisco Craton during the terminal Ediacaran and correspond to a very well-defined local stratigraphic marker in the Bambuí Basin. The exact location of the epicenter is uncertain, but it could be related to the NW regional faults in the regional Paleoproterozoic basement of the study area, which were reactivated during the deposition of the Sete Lagoas Formation in the Ediacaran Period.

***Keywords*:** Intraformational breccia, carbonate platform, synsedimentary deformation, intraplate seismicity, Ediacaran

8.1 Introduction

Multiple origins have been attributed to the formation of carbonate breccias, including submarine slope deposits, subaerial talus, karstic cavern collapse breccias, intraformational breccias associated with accommodation generation in underlying units and fault-related breccias (Spence and Tucker, 1997; Myrow et al., 2004; Quijada et al., 2014; Madden et al., 2017). These facies have the potential to provide insights into the nature of ancient carbonate systems (Wilson et al., 2012; Madden and Wilson, 2013) and have been documented in several Neoproterozoic and lower Paleozoic shallow water platforms worldwide (Kennedy, 1996; Pratt, 1994, 2002a, b; Myrow et al., 2004; Patil Pillai and Kale, 2011; Hood et al., 2015). A considerable number of unusual brecciated facies have been described in the late Proterozoic Era, such as molar tooth, edgewise breccia and olistostrome breccia (Frank and Lyons, 1998; Cozzi et al., 2004; Vernhet et al., 2006).

A particular category of carbonate breccia refers to “flat-pebble conglomerates” or “pseudoconglomerates”, which correspond to limestones bearing flat to undulated, disc- or plate-shaped pebble- to cobble-sized clasts (Sepkoski et al., 1991; Myrow et al., 2004; Chen et al., 2009a). They represent a striking feature of late Proterozoic to early Ordovician shallow marine carbonate successions, but it is most widespread in the late Cambrian-early Ordovician (Sepkoski, 1982; Myrow et al., 2004; Wright and Cherns, 2016), possibly related to the abundance of microbial facies during this time interval (Riding 2006). Flat-pebble conglomerates are usually, clast-supported deposits that consist of rip-up clasts derived from underlying planar to crinkle microbial beds (Palma et al., 2013). Bed geometries are typically tabular, but some are lenticular (Myrow et al., 2004), and are fairly continuous and can be tracked for long distances, providing considerable resolution in the stratigraphic correlation (Sepkoski, 1982).

The Ediacaran Sete Lagoas Formation (Bambuí Group) is interpreted as a carbonate ramp deposited just above the Proterozoic and Archaean basement of the São Francisco Craton (SFC) and, locally, overlies glaciogenic diamictites of the Jequitaí Formation and its correlative units (Dardenne, 1978; Vieira et al., 2007a; Uhlein et al., 2019). The Sete Lagoas Formation consists of dolostones, limestones, siltstones and mudstones with well-preserved stromatolites (Vieira et al., 2007a). In terms of breccia facies, some authors have described distinct types of carbonate brecciated deposits, related to different mechanisms of formation. In the southern outcrop area of the Sete Lagoas Formation, the breccia bed from the upper part of this unit has been interpreted as a product of collapse of stromatolitic buildings (Vieira et al., 2007). On the other hand, in the central SFC, hydrothermal Pb-Zn mineralized breccias from the upper part of the Sete Lagoas Formation were interpreted as originated from high-pressure injection of hydrothermal fluid during eodiagenesis burial (Nobre-Lopes, 2002).

In this contribution, we distinguish these breccia deposits of the middle part of the Sete Lagoas succession by focusing on the unusual flat-pebble breccia. We also carried out a combined detailed sedimentological and stratigraphic analyses of the flat-pebble breccia in order to determine its origin. Furthermore, the complete understanding of the formation of these brecciated facies provides significant contribution to delineate the evolution of the Sete Lagoas carbonate ramp in the context of the Ediacaran Bambuí Basin.

8.2 Geological Setting

The São Francisco Craton (SFC), central-eastern Brazil, is characterized by an Archean to Paleoproterozoic basement, covered by clastic Paleo- to Mesoproterozoic units (Espinhaço Supergroup, Paranoá and Canastra groups) and Neoproterozoic mixed-carbonate-siliciclastic deposits (Bambuí Group). The SFC is delimited in its eastern and western borders by the Neoproterozoic Araçuaí and Brasília orogenic belts, respectively (Fig. 8.1A). The occurrence of deformational structures, such as folds and reverse faults, as well as metamorphism is rare to absent in the center of the basin (study area), but it increases towards the western and eastern borders (Marshak and Alkmim, 1989).

The Bambuí Group is a 700 to 1500 meters thick mixed carbonate-siliciclastic platform deposited directly over the basement rocks of the SFC (Fig. 1A, C; Misi et al., 2007; Sial et al., 2009). It is the sedimentary expression of a transgressive event over the SFC and the Cryogenian, glacially-influenced Jequitaí unit (Martins-Neto et al., 2001; Figueiredo et al., 2009; Uhlein et al., 2016). The Bambuí Group includes, from base to top, the Sete Lagoas, Serra de Santa Helena, Lagoa do Jacaré, Serra da Saudade and Três Marias formations (Fig. 1C; Dardenne, 1978).

The depositional age of the Bambuí Group, particularly the Sete Lagoas Formation, has been a matter of debate in the last few decades. Based on geochronologic data, previous authors considered the carbonate rocks of the lower part of the Sete Lagoas Formation as correlated to the Sturtian glacial event (Babinski et al., 2007, 2012; Vieira et al., 2007). However, stratigraphic and isotopic evidences suggest a younger post-Marinoan cap carbonate age for the unit (Misi et al., 2007; Caxito et al., 2012; Alvarenga et al., 2014). Despite these inconsistencies, the occurrence of the *Cloudina* index fossil in the lower part of the Sete Lagoas

Formation confirms depositional ages between 549 and 542 Ma at least for this part of the succession (Warren et al., 2014). U-Pb ages obtained in detrital zircon grains from the middle part of the Sete Lagoas Formation indicate a maximum depositional age of 557 Ma (Paula-Santos et al., 2015), coherent with the interval defined by the *Cloudina* fossil (Warren et al., 2014).

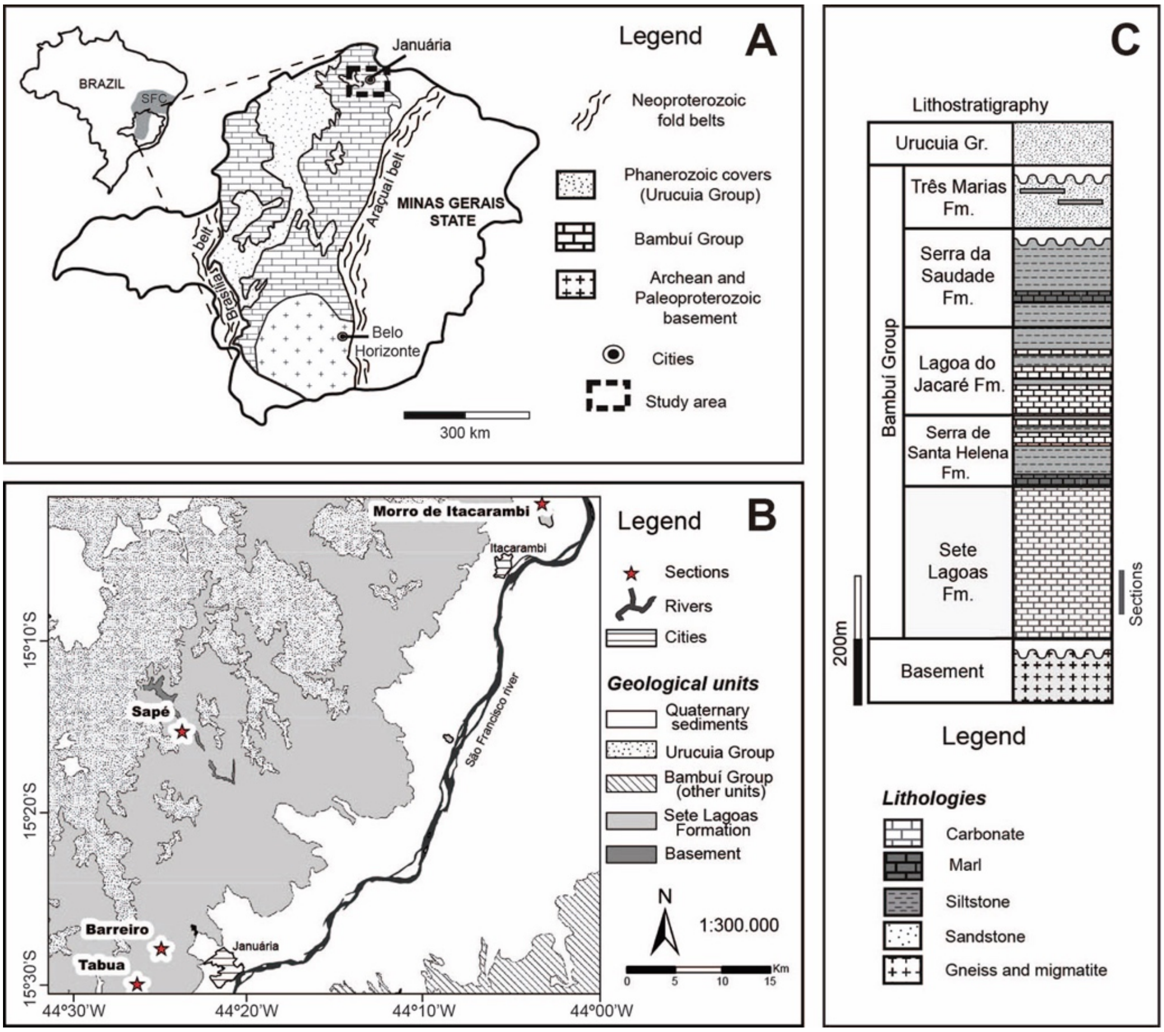

Figure 8.1: Location of the studied area. A: Location of the São Francisco Craton (SFC) and the Bambuí Group in the Minas Gerais State, central Brazil. B: Geological map of Ediacaran Sete Lagoas Formation in the vicinity of the town of Januária, northern Minas Gerais State, and location of the columnar sections. C: Lithostratigraphic column of the Bambuí Group in the study area. Fm. = Formation; Gr. = Group.

In the studied area, the Sete Lagoas Formation occur as a thick carbonate succession (~130m) exposed in the canyons and cliffs located in the left margin of the São Francisco River (Fig. 8.1). The region is characterized by well-developed karstic features, including sink valleys, dolines and caves that tend to develop exclusively in the middle part of the carbonate succession (Nobre-Lopes, 2002). The unit is mainly composed of mudstones, ooid grainstones, peloidal packstones, dolomudstones, microbialites and rare intraformational breccias (Perrella Jr. et al., 2017). Skeletal fossils of the Ediacaran Nama Assemblage, as *Cloudina* and *Corumbella* organisms as well as trace simple fossils, occur in the middle part of the Sete Lagoas section (Warren et al., 2014).

8.2 Material and Methods

We measured four columnar sections in order to estimate the extension and lateral variation of different sedimentary facies, focusing on the flat-pebble breccia deposits. Clast size and orientation measurements were performed on sub-horizontal outcrops from the breccia beds at the Barreiro locality in order to to define the framework of the clasts in the rock fabric. These clast measurements represent two-dimensional orientation (i,e., azimuths) of elongate clasts. Paleocurrent data were exclusively collected from trough cross-stratifications and laminations of the overlying grainstone facies and were statistically analyzed and presented in the form of iso-frequency rose diagrams.

We accessed microstructures of matrix and clasts by examining polished thin sections under both normal and polarized light using a petrographic microscope. Element intensity maps were carried out using wavelength dispersive spectroscopy (WDS) at the Department of Petrology at São Paulo State University (UNESP), Brazil, using a JEOL JXA8230 electron microprobe. The machine is equipped with 5 WDS spectrometers, a solid-state energy dispersive spectroscopy (EDS) detector and a panchromatic cathodoluminescence system (XM-26730PCL). The maps were carried out using an acceleration voltage of 20 kV and a beam current of 20 nA, with a step size and dwell time of 4 µm and 10 ms, respectively. EDS data was collected simultaneously with the WDS data.

8.3 Results

8.3.1 Facies associations of the Sete Lagoas Formation

The Sete Lagoas Formation occurs in the studied area as an irregular NE-SW elongated outcrop at the left margin of the São Francisco River (Fig. 8.1B), as elongated hills separated by NW-SE canyons. The region is characterized by well-developed karstic features, including sink valleys, dolines and caves that tend to develop exclusively in the middle part of the carbonate succession. The Sete Lagoas Formation overlies the local metamorphic basement in regional erosive unconformity (Fig. 8.2A). The contact of the Sete Lagoas Formation with siltstones, marls and mudstones of the overlying Serra de Santa Helena Formation is transitional (Fig. 8.1C).

Near the Januária city, the Sete Lagoas Formation comprises a 130m-thick succession of carbonate and minor dolomite facies. The sedimentary succession described in the study area is characterized by three facies associations, from base to top (Fig. 8.3): (1) peritidal, (2) flat-pebble, and (3) subtidal facies associations (Figure 8.4). Four breccia types are observed in this succession, from the base to top: (1) evaporitic breccia with tepees from peritidal facies; (2) intraformational breccia (i.e., flat-pebble breccia); (3) hydrothermal breccia and, (4) brecciated stromatolites.

8.3.1.1 Peritidal facies association

Description

The peritidal/lagoonal facies association (~30 m thick) occurs mostly in the Tabua and Sapé section (Fig. 8.4) and is mainly composed of centimeter-thick thrombolites and planar microbialites beds interbedded with heterolithic wavy facies (grainstone/mudstone). Occasionally low angle and/or swaley/hummocky cross-stratified, wave/current-rippled grainstones and evaporitic breccia with tepees also occur in this interval. Thrombolites present internal clotted fabric (with clots diameter varying from 0.5 to 1 cm) which may form small thrombolite columns (2 cm height) in association with oncoids (Fig. 8.2B). In some cases, irregular domes and bulbous stromatolites, with metric lateral and vertical extension, are also present (Fig. 8.2C). Evaporitic breccia is relatively common in this facies association and occur with tepees and convoluted (interrupted/curled) and broken microbialitic lamination (Fig. 8.3B). These breccia beds are 10 to 20 cm thick, extending tens of meters laterally.

Interpretation

The association between microbialites and grainstone facies suggests deposition under shallow water conditions, probably in inter to supratidal settings influenced by fair-weather current and waves (Fig. 8.2D). The sporadic presence of swaley and hummocky cross-stratified grainstones suggests some storm influence in the shallow parts of the carbonate ramp with deposition conditioned by storm wave orbitals and rip currents. The presence of evaporitic breccia is interpreted as a result of brecciation by sporadic subaerial exposure of microbial mats and mudstones.

8.3.1.2 Flat-pebble breccias facies association

The peritidal facies association is overlaid in sharp contact by 20 m thick interval of tabular beds composed of flat-pebble breccia (dm to m thick) interbedded with undeformed microbialites (cm thick). Flat-pebble breccia is mostly clast-supported. The clasts are usually platy or oblate with angular edges and are mainly disposed horizontally within the sedimentary bed. The stratigraphic and sedimentological significance of the flat-pebble breccia beds will be detailed further (see section 5 for detailed description and section 6.2 for interpretation).

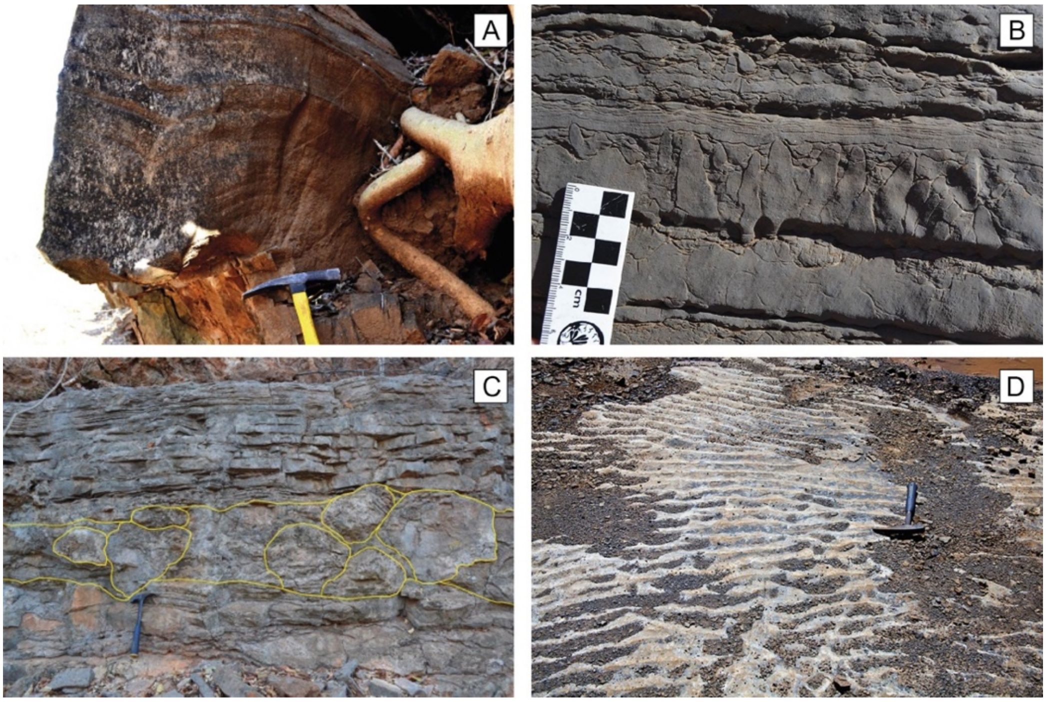

Figure 8.2: Representative sedimentary facies of the Sete Lagoas Formation in the studied area. A: Contact between the domal stromatolite and the gneiss from the Paleoproterozoic basement in the Sapé section; B: Interbedded succession of laminated microbialites and small columnar thrombolites in the Sapé section; C: Biostromes constituted by irregular domes and bulbous stromatolites with meter-scale length in the Tabua section (delimited by yellow lines). D: Fine-grained grainstone with wave and current ripples near the Barreiro section. The hammer in A and C is 25cm long and 33cm in D.

8.3.1.3 Subtidal facies association

Description

The subtidal facies association overlies the flat-pebble facies association and corresponds to middle to upper part of the Sete Lagoas Formation (see Morro de Itacarambi section in Fig. 8.4). These subtidal deposits consist of meter- scale thick sets of trough cross-bedded ooidgrainstones interbedded with tabular beds with normal gradation, low-angle cross-stratified grainstone and wave cross-laminated grainstone. The ooids are 300 μm in diameter, spherical, concentric and often intensely recrystallized.

Two different breccia types occur in this facies association: i) hydrothermal breccia, which is composed of a pink, saccharoidal brecciated dolomite, containing galena, sphalerite and variable proportions of fluorite and subordinated barite ore (Fig. 8.3A, see Nobre-Lopes, 2002 and Misi et al., 2005 for a detailed description of these deposits); ii) brecciated stromatolite, which comprises irregular centimeter fragments of laminated microbialites chaotically dispersed in the rock matrix (Fig. 8.3D). This breccia type occurs few meters below the contact between the Sete Lagoas Formation and the overlying Serra de Santa Helena Formation.

Interpretation

The presence of ooids suggests that these grainstones were formed in shallow subtidal environments with agitated water commonly located in platform margins. The absence of structures indicative of subaerial exposure (e.g. teepes, brecciated microbialites, mud cracks and karstic features) and the association of facies deposited by the migration of 3D dunes and climbing ripples are indicative of tidal currents in subtidal conditions in a shallow to moderately deep ramp. However, grainstones with swaley stratification may indicate that these subtidal deposits were occasionally reworked by storm wave orbitals associated with rip currents.

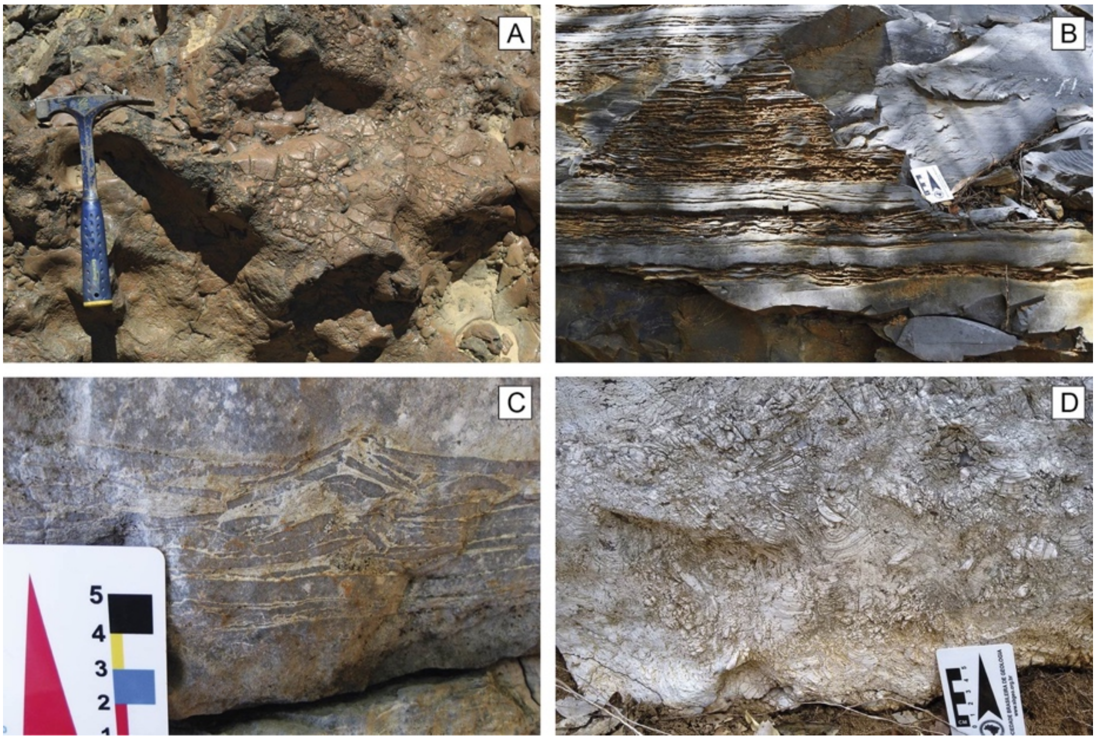

Figure 8.3: Different types of breccia deposits present in the Sete Lagoas Formation succession in the studied area. A: Hydrothermal Pb-Zn mineralized breccia. B: Evaporitic breccia developed from thin laminated microbialitic facies. C: Tepee-like structure associated with the evaporitic breccia shown in B. D: Brecciated stromatolites composed of angular fragments of columnar stromatolites cemented by dolomite. The hammer in A is 25 cm long.

8.3.2 Sedimentary characteristics of the Sete Lagoas flat-pebble breccia deposits

The occurrence of flat-pebble breccia facies association is restricted to a 20 m thick interval in the middle part of the Sete Lagoas succession (Fig. 8.4). These deformed deposits extend laterally for tens of kilometers and are limited vertically by undeformed deposits of carbonate facies deposited in peritidal conditions (Fig. 8.6A). There is no observable gradation between deformed and undeformed beds. Individually, each breccia bed shows tabular geometry with abrupt and irregular contacts with both underlying and overlying undeformed planar microbialite beds.

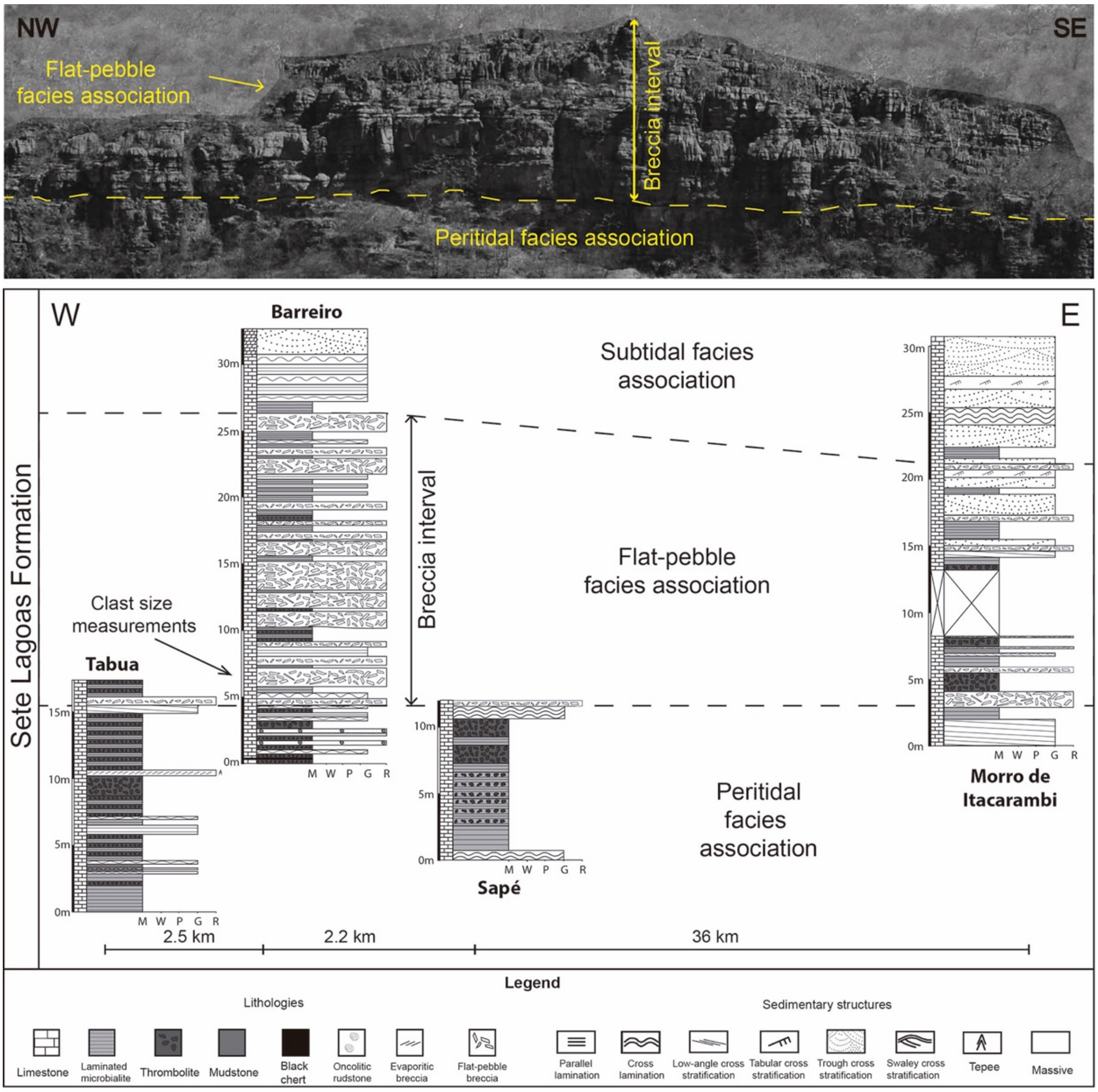

Figure 8.4: Correlation of stratigraphic columnar sections showing the flat-pebble breccia of the Sete Lagoas Formation in the Januária region. The evaporitic breccia occurs only in the lower part of the section and the hydrothermal breccia is not represented in these sections. Note that the breccia interval has lateral extension of tens of kilometers. For the exact location of the columnar sections, please see Fig. 1B. M = mudstone; W = wackestone; P = packstone; G = grainstone; R = rudstone.

In the Barreiro section (see Fig. 8.1B), the breccia interval comprises 13 breccia beds interbedded with tabular laminated microbialites (Fig. 8.4). Breccia beds range from 44 cm to 2.20 m in thickness, whereas microbialite beds range from 10 cm to 2.1 m thick (Fig. 8.4). In the Morro de Itacarambi section, five breccia beds (12 cm to 1.2 m thick) occur within a 17 m thick interval. It is important to note that the brecciated beds have similar composition of the undeformed beds, that is, the clasts are exclusively composed of microbialite fragments immersed in a granular matrix. The thickness of the individual breccia beds tends to decrease towards NE from Tabua to Morro do Itacarambi localities (Figs. 8.1B and 8.4).

The flat-pebble breccia is mostly clast-supported. Their clasts are mainly disposed horizontally in the layer, but some levels show bidirectional imbrication (Fig. 8.5). Few clasts are sub-vertical or chaotically dispersed (Fig. 8.5 and 8.7B). Vertical clasts are not concentrated in specific levels and build up overturned beds (Figs. 8.7C and D). In plan view, clasts are mostly equidimensional, forming a mosaic-like pattern (Fig. 8.7B). The amount of reworked clasts increases upwards (Fig. 8.5).

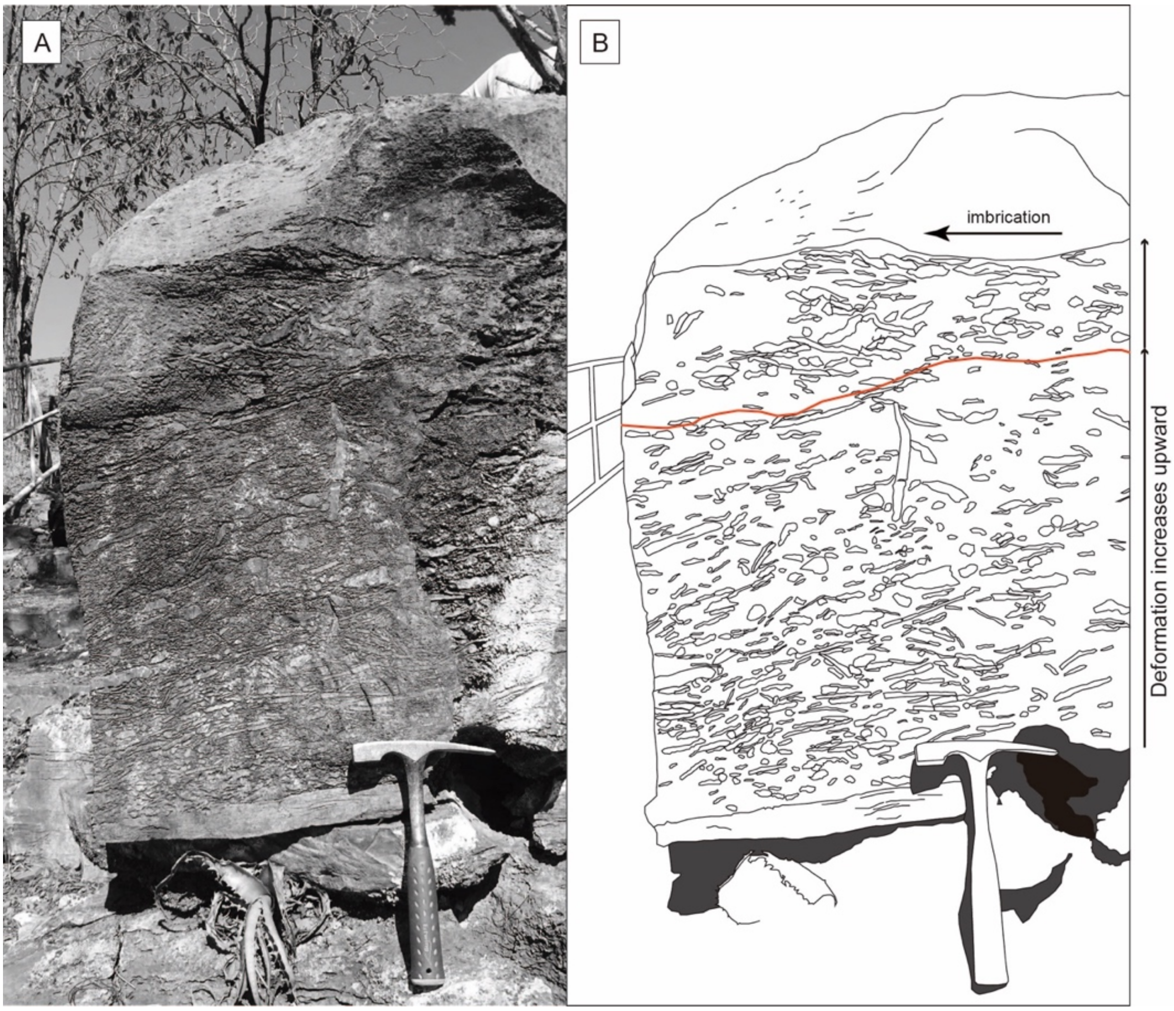

Figure 8.5: A) Outcrop photograph of flat-pebble breccia beds at Barreiro section. B) Representative sketch of A showing the arrange of the clasts. The degree of organization of the clast framework tends to decrease upward, with almost horizontal fitted clasts at base grading to a chaotic, loosely dispersed clasts at the top. Note that the upper breccia bed showing clear imbrication of the clasts apparently erode the underlying bed. The hammer in A and B is 25cm long.

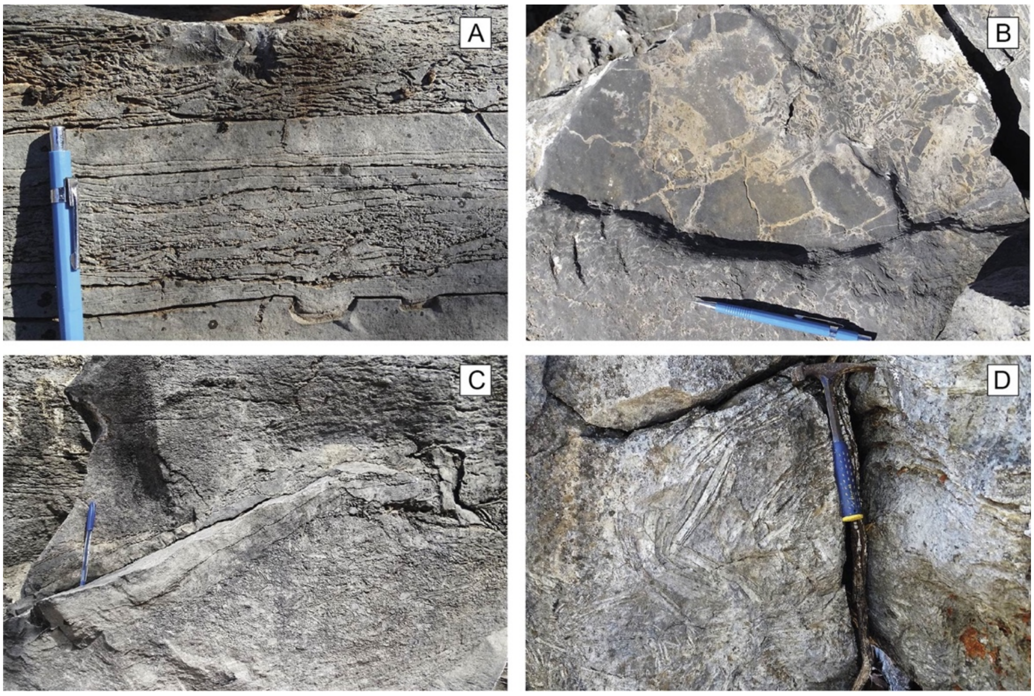

Figure 8.6: Sedimentary features of the flat-pebble breccia and their relationship with underlying and overlying layers. A) Interbedded slightly deformed and undeformed microbialitic beds. Note the perfect adjustment of the clasts in the lower bed. B) Plan view of a mosaic-like pattern constituted by fitted polygonal clasts. Note that the bed is cracked, but not show any evidence of sedimentary transport. C) Microbial sedimentary bed deformed and partially broken between two brecciated beds. D) Open recumbent fold developed from breccia fragments. This deformation structure is interpreted as produced by upward injection related to fluid scape. The automatic pencil and pen in A, B and C is 14 cm long. The hammer in D is 25 cm long.

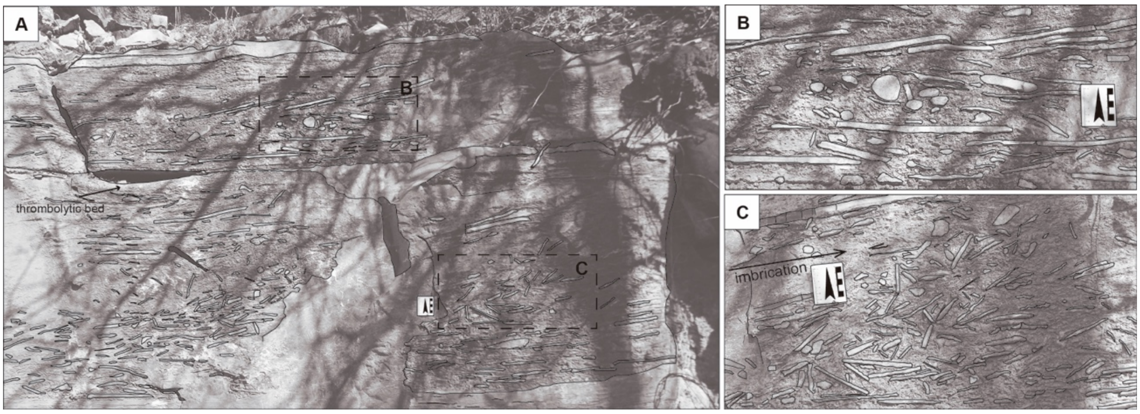

Figure 8.7: A) Representative sketch of flat-pebble breccia beds at the Barreiro section. The breccia framework is composed of loosely packed angular clasts dispersed in a fine-grained carbonate matrix. B) Detail of A showing polygonal clasts disposed horizontally with subordinated occurrence of some rounded clasts. C) Detail of A showing localized imbricated clasts.

Because of their elongated shape, most of clasts have a long aspect ratio (i.e., the ratio between width and height), or elongated shape, resulting in an anisotropic framework (Fig.

8.7). The shorter axis is usually smaller than 2 cm, whereas the longer axis has great dispersion, ranging from 0.5 cm to 16 cm (Fig. 8.8A) and showing different aspect ratios (Fig. 8.8B).

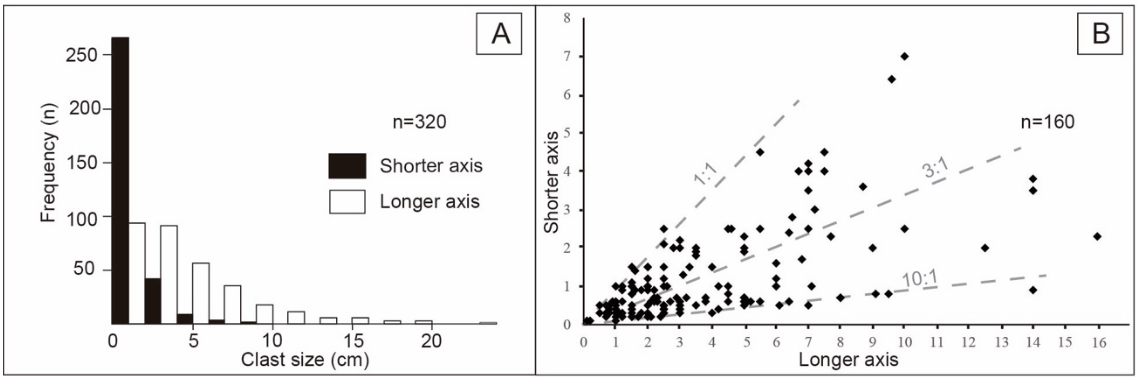

Figure 8.8: Size measurements of clasts in the lower breccia interval at the Barreiro section.A) Frequency size distribution histogram of the longer and shorter axis of clasts. B) Aspect ratio related to the size of clasts. The measurements were acquired from different horizontal plans from the same stratigraphic horizon (see Fig. 8.5 for the precise stratigraphic position).

Although macroscopically clasts are lighter colored than the matrix, petrographic analysis revealed that the texture of the matrix and the clasts are very similar, which makes difficult to distinguish between clast and matrix under the microscope (Fig. 8.9B). They are both microcrystalline, ranging from 10 to 50µm. However, due to the microbialitic composition of the clasts (boundstones), sometimes it is possible to identify relicts of the crenulated microbial lamination in these fragments. Clasts are predominantly calcitic (locally showing silicified portions), whereas matrix is dolomitic with subordinated apatite grains (Fig. 8.9C, D). Locally, millimetric *Cloudina* shell fragments might occur within the clasts. Moreover, there is no evidence of stylolites and/or dissolution features in the margins of the clasts.

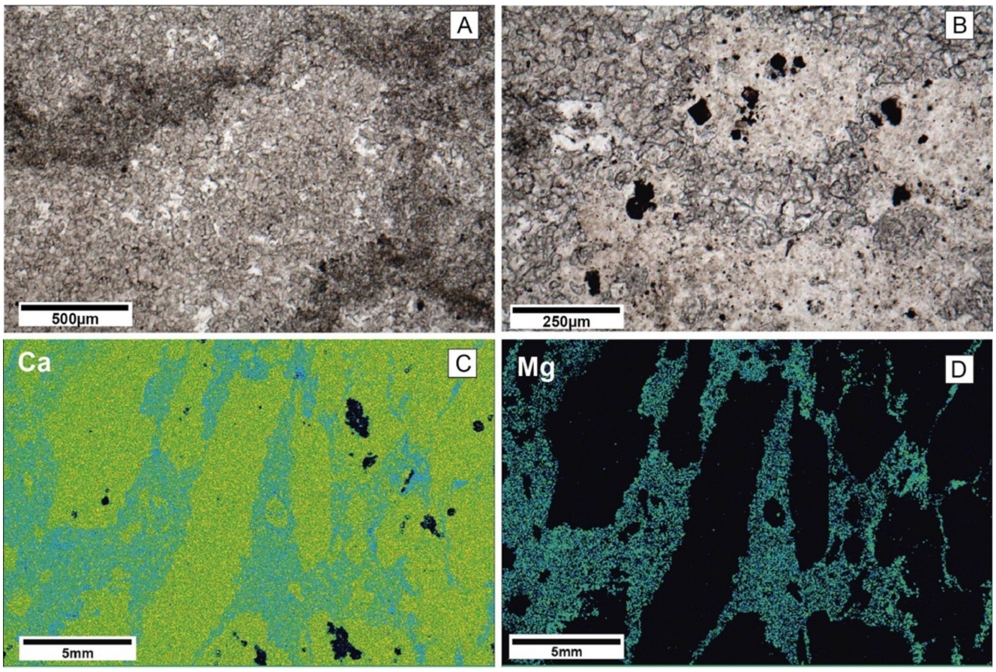

Figure 8.9: Thin section microphotographs and compositional EDS maps of the flat-pebble breccia at the Barreiro section. A) Detail of clasts surrounded by a brown-color calcitic matrix (5x, parallel polarizers). B) Detail of clasts are thinner and lighter in color than the matrix. The edges of the clasts are very smooth (10x, parallel polarizers). C-D) EDS compositional maps for Ca and Mg of the studied breccia deposits.

Another striking feature in some breccia beds is the presence of brittle-to-ductile deformation structures (Fig. 8.10). Disrupted layers or presenting folds and synsedimentary faults commonly occur confined between undeformed beds (Figs. 8.10 A, B and C). Although the folds apparently do not have a preferential orientation in the outcrops analyzed, these structures usually have similar geometry and direction when confined in a single bed. Other evidences of liquefaction and soft-sediment deformation are the punctual presence of injection structures in the base of the brecciated beds (Figs. 8.10 D and E). These structures commonly penetrate the upper bed and disrupt the sedimentary layer immediately above promoting local brecciation (Figs. 8.10 D and E). Injection structures, as flame and load cast-like features, also occur in little deformed microbialitic beds that confine the brecciated beds (Fig. 8.10 F).

Aspect ratio data indicate a slightly NE-SW long-axis clast orientation. This preferential orientation is likely to represent the alignment of the major axis clasts (> 10cm or higher aspect ratios) and the orientation of square clasts tends to fit in the remaining space because they are not elongated (Fig. 8.10B). The square clasts or chip facies (1:1 aspect ratio *sensu* Pruss et al., 2005) are less frequent and may represent flat-pebble conglomerates that underwent additional reworking.

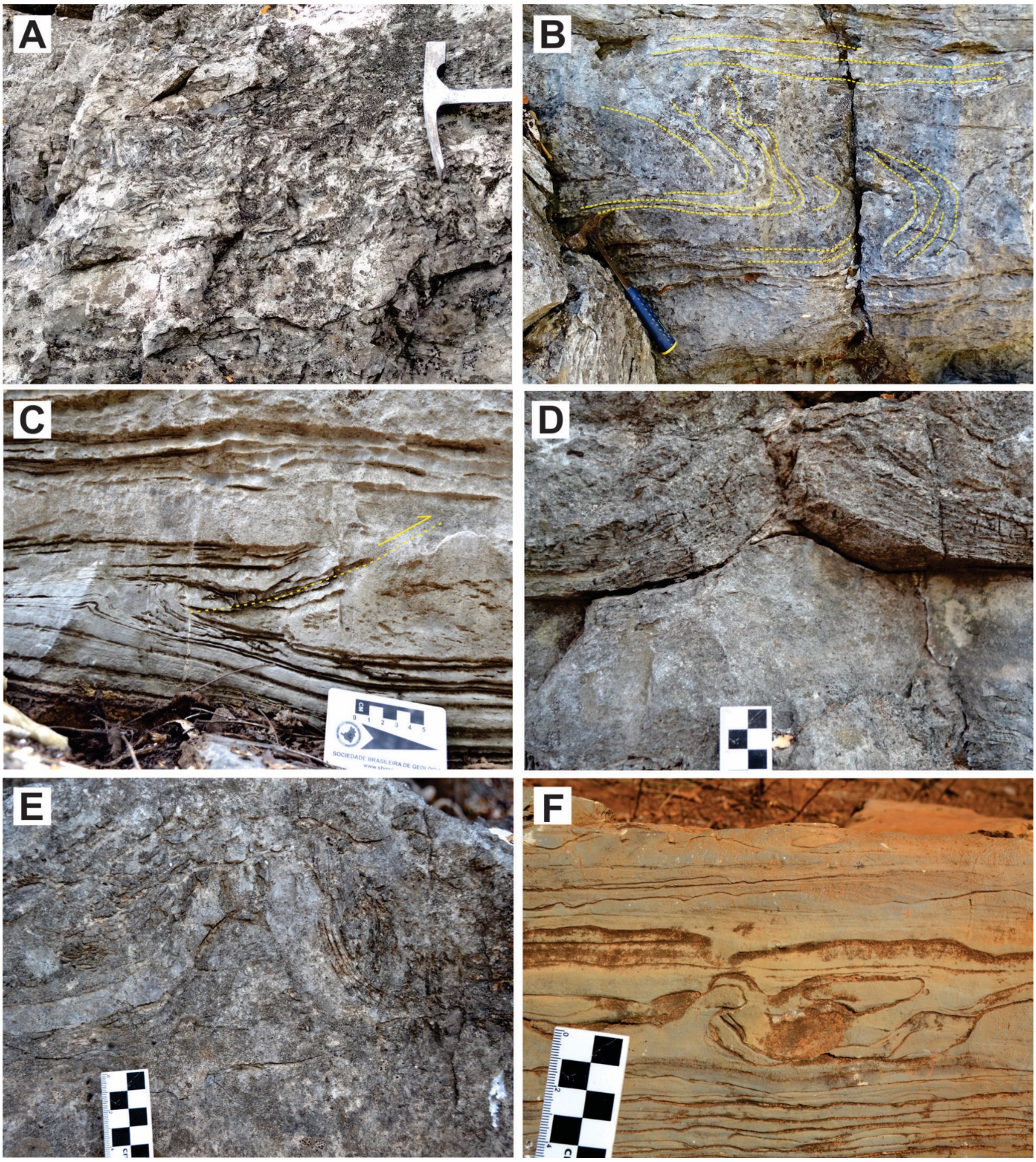

Figure 8.10: A) Deformed bed showing disrupted layers. B) Folded bed (yellow dotted line) confined between two undeformed beds. C and D) Detail of centimeter size injection features at the base of a brecciated bed. E) Folded bed associated with breccia facies (right side of the image). Note that the reclined fold is sectioned by a synsedimentary inverse fault. F) Detail of injection features in the top of brecciated bed. The hammerhead in A is 18cm length.

Additionally, paleocurrent data acquired in cross-stratified grainstones from the overlying subtidal facies association suggest a NE-SW trend for the shoreline during the deposition (Fig. 8.11A). We also observed that the clasts with higher aspect ratio (higher than 10 cm, Fig. 8.11B) seem to be parallel to this interpreted shoreline orientation.

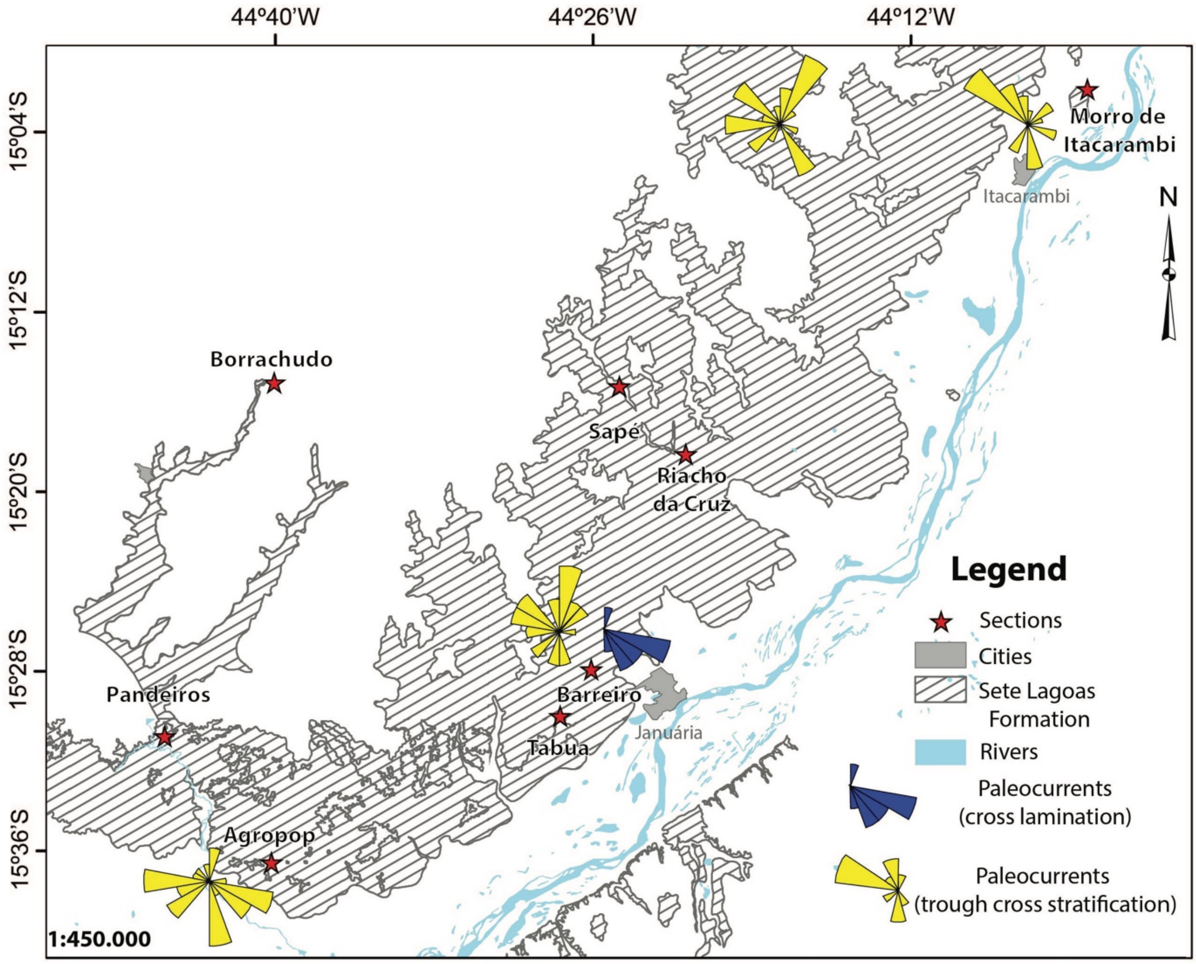

Figure 8.11: Paleocurrents of the Sete Lagoas Formation in the study area. A) Paleocurrents of the subtidal facies association positioned stratigraphically above the flat-pebble breccia interval. B) Rose diagrams of azimuthal orientation of 243 elongate clasts in flat-pebble breccia near Barreiro section.

8.4 Discussions

8.4.1 The flat-pebble breccia problem: distinct triggers, processes and products

Three conditions must occur simultaneously to form soft-sediment deformation (Owen et al., 2011): i) a driving force must deform primary sedimentary features, ii) a deformation mechanism must enable the sediment to deform; iii) a trigger mechanism, a natural agent that initiates the process. Driving forces correspond to stresses that are normally incapable of deforming sedimentary deposits, such as gravity acting on slopes, bedform topography and shear by aqueous or other currents. However, when the stress magnitude exceeds the normal sediment strength, deformation occurs and identifying the means by which sediment deformed has important implications for determining the trigger (Owen and Moretti, 2011).

Syn-depositional flat pebble conglomerates have been usually interpreted as subtidal deposits (Sepkoski, 1982; Wignall and Twitchett, 1999; Pruss et al., 2005), typically formed in offshore settings. Several mechanisms have been evoked as triggers for breccia formation, including: (1) subaerial desiccation (Kendall and Warren, 1987; Pratt, 2002b; Palma et al., 2013), (2) storms and/or tsunamis (Kazmierczak and Goldring, 1978; Sepkoski, 1982; Molina et al., 1998; Chen et al., 2009a; Chen and Lee, 2013), (3) slope-related failure or slumps (Spence and Tucker, 1997; Myrow et al., 2004), (4) seismic shocks (Bhattacharya and Bandyopadhyay, 1998; Rodriguez-Pascua et al., 2000; Kullberg et al., 2001; Nogueira et al., 2003; Montenat et al., 2007; Martín-Chivelet et al., 2011; Patil Pillai and Kale, 2011; Myrow and Chen, 2015), and (5) bed fracturing associated with early-diagenesis processes (Kwon et al., 2002; Chen et al., 2009b). However, a combination of such processes is quite common.

Storm-induced waves and currents are important sedimentary agents that episodically and catastrophically erode, deposit, rework and deform sedimentary strata. The dynamics of storm-induced currents are complex and such currents may form a wide range of sedimentary structures such as swaley and hummocky cross-stratification, flat pebbles, and pots and gutter casts (Bhattacharya and Bandyopadhyay, 1998; Molina et al., 1998; Alfaro et al., 2002; Pratt, 2002a; Chen et al., 2009a). In this context, flat-pebble conglomerate facies have been related to erosion and redeposition by storms of subaerial exposed shallow water facies, as desiccated microbial mats (Palma et al., 2013).

Although tsunamites seem to be relatively rare and difficult to recognize in the geological record, they may constitute an important mechanism to form flat-pebble conglomerates (Pratt, 2002b; Pratt and Bordonaro, 2007). Pratt and Bordonaro (2007) interpreted large tsunamis recorded by Middle Cambrian limestones of western Argentina were able to produce the anomalous degree of scour needed to erode lithified substrate. Strong tsunami waves reach much deeper than storms waves on continental shelves. So, tsunamis are viable alternative to generate erosional events of exceptional magnitude at and beyond storm wave base (Pratt, 2002b). However, distinguishing between a storm or tsunami deposits in the geological record is not an easy task.

Loading, earthquakes, and high-frequency sea-level fluctuations can also trigger the initial break-up and subsequent sliding of a breccia layer (Spence and Tucker, 1997; Gibert et al., 2005; Spatullo et al., 2007). Storm-wave loading and earthquake shock waves have been considered as the most likely trigger for slope failures (Myrow et al., 2004; Gibert et al., 2005; Spalluto et al., 2007), producing slumps, slides and sediment-gravity-flow deposits.

A seismic trigger can also produce previously discussed mechanisms of brecciation (Montenat et al., 2007; Owen and Moretti, 2011; Owen et al., 2011). The following criteria have been used to determine the influence of seismicity in deformational structures of siliciclastic rocks: (1) large area extent, (2) proximity to active fault system during sedimentation, (3) potential liquefiable sediments, (4) absence of slope influence, (5) similar morphology between the described syn-sedimentary features and deformation structures recorded in recent earthquakes or generated experimentally (Sims, 1975; Jones and Omoto, 2000; Owen and Moretti, 2011). Despite some differences, those criteria can also be used to determine a seismic origin for deformation structures in carbonate rocks (Molina et al., 1998; Kahle, 2002).

8.4.2 Flat pebble carbonate breccia as evidence of Ediacaran synsedimentary tectonic activity

The flat pebble breccia from the basal to intermediate part of the Sete Lagoas Formation in the Januária region constitute uncommon deposits that only occur in a well-defined stratigraphic interval that can be laterally tracked by tens of kilometers (see Fig. 8.4). This particular interval is mainly constituted by an intercalation of disrupted/deformed (flat pebble breccia) and non-deformed laminar microbialites deposits. We interpret that this breccia was formed as a result of fragmentation of the underlying peritidal facies association, particularly the laminated microbialites. Besides the absence of ductile deformation of the clasts, the presence of clasts with sharp edges and vertices in the Sete Lagoas flat-pebble breccia suggests that they were deposited as rigid objects and the lithification process started very early in diagenesis; even the sediments exposed at the bottom were, at least, partially lithified. The clasts were formed from the original laminae and rupture of the lamination was a precursor of a liquefied state, where pore pressure exceeds cohesive forces and drives cracks through the sediment (Fig. 8.6B). The dolomitization of the matrix, not the clasts, (Figs. 8.9C and D) is another evidence that each clast was already a cohesive unit before the deformation. Moreover, the presence of large vertical clasts also corroborates the interpretation that the clasts were already lithified when a mechanical force rearranged the breccia framework and the square clasts or chip facies may represent flat-pebble conglomerates that underwent additional reworking.

Most of the clasts are randomly oriented within the same deformed bed (Fig. 8.5), however, rare clast beds with higher aspect ratio show slight imbrication (Fig. 8.10).

The complete absence of fining upward pattern or any internal structure indicative of decrease in flow energy or velocity in the brecciated bed allows us to refute deposition by waves and/or bottom currents. In this way, the massive predominance of sharp-edged clasts also reinforces the hypothesis of brecciation in situ without involving significant sedimentary transport. Because the coarse-grained sediments composed of pebbles and cobbles do not form hummocky and swaley cross-bedding, the recognition of these type of sedimentary structures is not definitive to assign storms as a trigger for breccia deposits.

Several aspects also make it possible to differentiate the breccia beds here detailed from other evaporitic breccias found in the sedimentary succession of the Sete Lagoas Formation. As the most distinctive characteristics between these two deposits, we can cite the lateral extension of the brecciated beds, presence of sin-sedimentary structures associated with the brecciated beds (see Fig. 8.10), the absence of evaporites and/or subaerial exposure structures and the absence of reworking of the bottom layer by the top layer in the brecciated beds. It is important to note that all these features are commonly observed in evaporitic breccias in the entire succession of the Sete Lagoas Formation in Januária area and other localities (Vieira et al. 2007, Perrella et al. 2017).

The breccia layers are sub horizontal, deposited in a shallow water protected lagoon in a carbonate ramp context, and there is no evidence of lateral shear stresses in the beds. Hence, the gravity-driven mass movements can also be ruled out as the main trigger for the break-up of the breccia beds due to the absence of associated deformation structures and lithofacies indicative of a slope environment in the flat-pebble facies association (e.g., slumps, slides and sediment-gravity-flow deposits).

On the other hand, the deposits here studied present several inherent characteristics that are compatible with seismic-induced breccia formation (Kullberg et al., 2001; Montenat et al., 2007; Moretti and Owen, 2011). The most positive evidences are: a) lateral and regional stratigraphic distribution: The breccia interval constitutes a well-defined 20-meters-thick stratigraphic level that can be laterally tracked by tens of kilometers; b) geomorphologic features: The breccia interval occurs as a continuous horizontal package and constitutes a regional geomorphologic surface associated with significant Cenozoic karstification; c) single stratigraphic interval: Deformed beds are restricted to a single stratigraphic interval. In the succession, the flat-pebble facies association, which contain the flat-pebble breccia, is limited below and above by the peritidal facies association and by the coarse-grained subtidal deposits, respectively. The overall breccia interval is composed of interbedded, well-defined, deformed and undeformed microbialitic brecciated deposits, suggesting that the triggering mechanism occurred punctually and not as a day-by-day depositional process; d) vertical repetition: breccia beds occur repeatedly through the vertical succession of the flat-pebble facies association and each one of these decametric to metric beds is a product of a seismic event. The middle part of the breccia interval has the greater thickness and probably represents the highest magnitude of the earthquake event; e) shape and composition: breccia clasts are monomythic and oblate. The clasts are composed of fragments of disrupted laminated microbialites, locally allowing the reconstitution of the original layer. In terms of composition, the clasts are predominantly calcitic and the matrix is dolomitic. There is no evidence of rounding or other feature indicative of sedimentary reworking or transport; f) the predominance of chaotically-dispersed clasts reinforces the absence of sedimentary transport and any granulometry sorting by subaqueous flux; g) association with synsedimentary faults and deformational structures indicatives of tectonic stress that acted on liquefied beds (see Fig. 8.10);

A series of NW trending structures occurring in the studied area could be tentatively associated with the tectonic activity responsible for the sin-sedimentary deformation (Fig. 8.12). These NW faults and fractures may have controlled the emplacement of the Pb-Zn hydrothermal fluids in the carbonates of the upper part of the Sete Lagoas Formation and would represent active structures during the Ediacaran evolution of the carbonate platform. As observed in the measured sections (Fig. 8.4), the thickness of the brecciated stratigraphic interval (and also the individual breccia beds) tends to decrease to NE, as it distances from the Tabua and Barreiro fault system (Fig. 8.11). This reinforces the hypothesis that these structures were active during the sedimentation and were probably related to the seismicity responsible for the brittle deformation that formed the breccia deposits. In this way, the variation in thickness and number of occurrences could be related to distance of epicenter and magnitude of the earthquake.

Similarly to the model of formation of the flat-pebble breccia formed in laminated sequences (Agnon et al. 2006), we propose the following model (illustrated in the Figure 8.12): a) initially, the laminated deposits are disrupted and deformed by ground shaking, motion of the water column, and water escape from the underlying early-lithified sediment; b) the water movement related to the seismic waves shaking the sea floor caused pore pressure and fragmentation to increase. Pressure in the pore fluids of the sediment exceeds the confining pressure of the overlying brine, resulting in liquefaction of the sediment. As a result, the top of the sedimentary succession becomes fluidized and suspended at the sediment-water interface;

c) intraclasts are then deposited. After settling, the breccia is capped by the continuing deposition of microbial laminites.

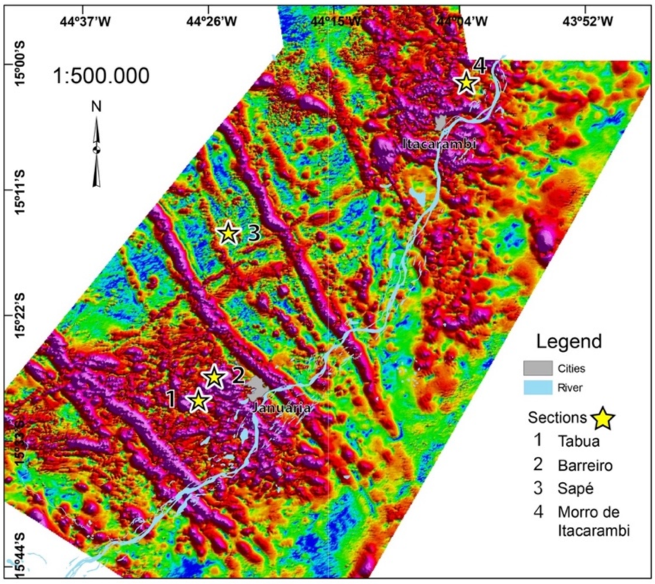

Figure 8.12: Magnetometric map of Januária region. The NW structures are representative of regional discontinuities present in the Paleoproterozoic basement related to dextral transpressive faults. Modified from: CODEMIG (2015).

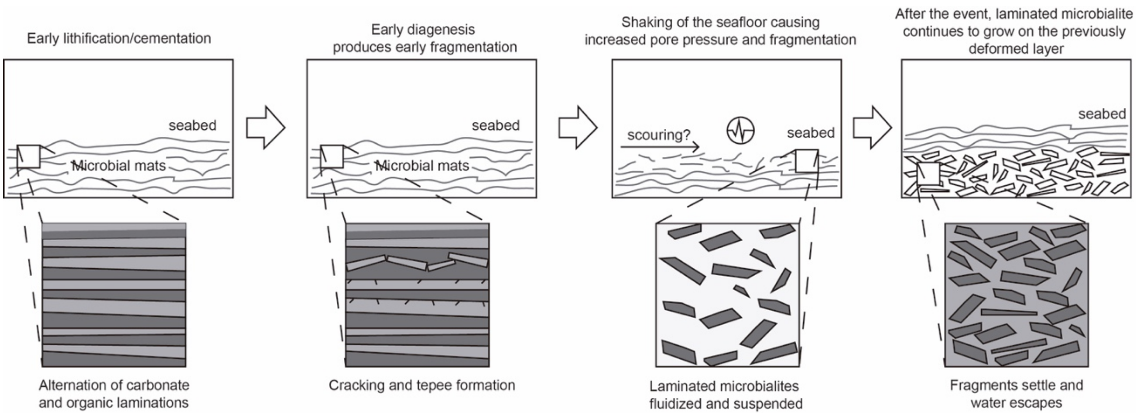

Figure 8.13: Schematic model for the seismic origin of flat-pebble breccia from Sete Lagoas Formation in the Januária region.

8.5 Conclusions

The Sete Lagoas Formation succession in the Januária region is interpreted as deposited in very shallow water conditions in the interior part of a rimmed carbonate ramp. Intraformational limestone breccias described in this unit have been previously interpreted as product of different processes as gravitational instability, dissolution, early dolomitization associated with subaerial exposure and storms during marine flooding (Nobre-Lopes, 2002; Vieira et al. 2007).

The seismic origin of the flat-pebble breccias from middle part the Sete Lagoas Formation is supported by several lines of evidence, such as the breccia framework and internal organization, wide distribution and lateral homogeneity, intercalation with undeformed deposits, association with synsedimentary deformational structures and the geodynamic context of the basin in which they were generated. Thus, this seismic-triggered breccia deposits represent the product of the synsedimentary tectonism occurred within the São Francisco Craton during the terminal Ediacaran and correspond to a very well-defined local stratigraphic marker in the Bambuí basin. The exact location of the epicenter is uncertain, but it could be related to the NW regional faults in the regional Paleoproterozoic basement of the study area, which were reactivated during the deposition of the Sete Lagoas Formation. Thus, at least putatively, the flat-pebble breccia from the base of the Bambuí Group represent the result of the ultimate efforts related to the Brasiliano Cycle and the final consolidation of the SW Gondwana.

Acknowledgements

This study was funded by FAPESP (grants 2015/07391-0, 2018/26230-6), CNPq (grant 444070/2014-1) and Petrobras (Sigitec 2014/-00519-9). GJU acknowledges funding from FAPEMIG (APQ-01711-14), CNPq (grants 301294/2018-6 and 447449/2014-1). This research was made with institutional support of the São Paulo State University-UNESP, Brazil. We also would like to acknowledge the two anonymous reviewers that greatly improved this manuscript. M.L. Assine and L.V. Warren are fellows of the CNPq.

8.6 REFERENCES

Agnon, A., Migowski, C., Marco, S., 2006. Intraclast breccias in laminated sequences reviewed: recorders of paleo-earthquakes. Geological Society of America Special Pa, 195–214. doi:10.1130/2006.2401(13)

Alfaro, P., Delgado, J., Estévez, A., Molina, J., Moretti, M., Soria, J., 2002. Liquefaction and fluidization structures in Messinian storm deposits (Bajo Segura Basin, Betic Cordillera, southern Spain). International Journal of Earth Sciences 91, 505–513. doi:10.1007/s00531-001-0241-z

Alvarenga, C.J.S., Santos, R. V., Vieira, L.C., Lima, B.A.F., Mancini, L.H., 2014. Meso-Neoproterozoic isotope stratigraphy on carbonates platforms in the brasilia belt of Brazil. Precambrian Research 251, 164–180. doi:10.1016/j.precamres.2014.06.011

Babinski, M., Pedrosa-Soares, A.C., Trindade, R.I.F., Martins, M., Noce, C.M., Liu, D., 2012. Neoproterozoic glacial deposits from the Araçuaí orogen, Brazil: age, provenance and correlations with the São Francisco craton and West Congo belt. Gondwana Research 21, 451–465. doi:10.1016/j.gr.2011.04.008

Babinski, M., Vieira, L.C., Trindade, R.I.F., 2007. Direct dating of the Sete Lagoas cap carbonate (Bambuí Group, Brazil) and implications for the Neoproterozoic glacial events. Terra Nova 19, 401–406. doi:10.1111/j.1365-3121.2007.00764.x

Bhattacharya, H.N., Bandyopadhyay, S., 1998. Seismites in a Proterozoic tidal succession, Singhbhum, Bihar, India. Sedimentary Geology 119, 239–252. doi:10.1016/S0037-0738(98)00051-7

Caxito, F. de A., Halverson, G.P., Uhlein, A., Stevenson, R., Gonçalves Dias, T., Uhlein, G.J., 2012. Marinoan glaciation in east central Brazil. Precambrian Research 200–203, 38–58. doi:10.1016/j.precamres.2012.01.005

Chen, J., Chough, S.K., Chun, S.S., Han, Z., 2009a. Limestone pseudoconglomerates in the Late Cambrian Gushan and Chaomidian Formations (Shandong Province, China): Soft-sediment deformation induced by storm-wave loading. Sedimentology 56, 1174–1195. doi:10.1111/j.1365-3091.2008.01028.x

Chen, J., Loon, A.J. Van, Han, Z., Chough, S.K., 2009b. Funnel-shaped , breccia- filled clastic dykes in the Late Cambrian Chaomidian Formation (Shandong Province , China). Sedimentary Geology 221, 1–6. doi:10.1016/j.sedgeo.2009.09.006

Chen, J., Lee, H.S., 2013. Soft-sediment deformation structures in Cambrian siliciclastic and carbonate storm deposits (Shandong Province , China): differential liquefaction and fluidization triggered by storm-wave loading. Sedimentary Geology 288, 81–94. doi:10.1016/j.sedgeo.2013.02.001

Cozzi, A., Grotzinger, J. P., Allen, P. A., 2004. Evolution of a terminal Neoproterozoic carbonate ramp system (Buah Formation, Sultanate of Oman): Effects of basement paleotopography. Geological Society of America Bulletin 116,11-12: 1367-1384.

Dardenne, M.A., 1978. Síntese sobre a estratigrafia do Grupo Bambuí no Brasil Central, in: Congresso Brasileiro de Geologia, 30º, Anais, Recife, Brazil. pp. 597–610.

Figueiredo, F.T., de Almeida, R.P., Tohver, E., Babinski, M., Liu, D., Fanning, C.M., 2009. Neoproterozoic glacial dynamics revealed by provenance of diamictites of the Bebedouro Formation, São Francisco Craton, Central Eastern Brazil. Terra Nova 21, 375–385. doi:10.1111/j.1365-3121.2009.00893.x

Frank, T. D., Lyons, T. W.,1998). "Molar-tooth" structures: A geochemical perspective on a Proterozoic enigma. Geology 26, 8: 683-686.

Gibert, L., Galdeano, C.S. De, Alfaro, P., Scott, G., Lo, A.C., Catalunya, D., 2005. Seismic-induced slump in Early Pleistocene deltaic deposits of the Baza Basin (SE Spain). Sedimentary Geology 179, 279–294. doi:10.1016/j.sedgeo.2005.06.003

Hood, A.V.S., Wallace, M.W., Reed, C.P., Hoffmann, K.H., Freyer, E.E., 2015. Enigmatic carbonates of the Ombombo Subgroup, Otavi Fold Belt, Namibia: A prelude to extreme Cryogenian anoxia? Sedimentary Geology 324, 12–31. doi:10.1016/j.sedgeo.2015.04.007

Jones, A.P., Omoto, K., 2000. Towards establishing criteria for identifying trigger mechanisms for soft-sediment deformation: A case study of late pleistocene lacustrine sands and clays, Onikobe and Nakayamadaira Basins, Northeastern Japan. Sedimentology 47, 1211–1226. doi:10.1046/j.1365-3091.2000.00355.x

Kahle, C.F., 2002. Seismogenic deformation structures in microbialites and mudstones, Silurian Lockport Dolomite, northwestern Ohio, U.S.A. Journal of Sedimentary Research 72, 201–216. doi:10.1306/051501720201

Kazmierczak, J., Goldring, R., 1978. Subtidal flat-pebble conglomerate from the Upper Devonian of Poland: a multiprovenant high-energy product. Geological Magazine 115, 359–366.

Kendall, C.G.C., Warren, J.K., 1987. A review of the origin and setting of tepees and their associated fabrics. Sedimentology 34, 1007–1027.

Kennedy, M.J., 1996. Stratigraphy, sedimentology, and isotopic geochemistry of Australian Neoproterozoic postglacial cap dolostones: deglaciation, D13C excursions, and carbonate precipitation. Journal of Sedimentary Research 66, 1050–1064.

Kullberg, J.C., Olóriz, F., Marques, B., Caetano, P.S., Rocha, R.B., 2001. Flat-pebble conglomerates: A local marker for early jurassic seismicity related to syn-rift tectonics in the Sesimbra area (Lusitanian Basin, Portugal). Sedimentary Geology 139, 49–70. doi:10.1016/S0037-

0738(00)00160-3

Kwon, Y.K., Chough, S.K., Choi, D.K., Lee, D.J., 2002. Origin of limestone conglomerates in the Choson Supergroup (Cambro – Ordovician), mid-east Korea. Sedimentary Geology 146, 265–283. doi:10.1016/S0037-0738(01)00128-2

Madden, R.H.C., Wilson, M.E.J., 2013. Diagenesis of a SE Asian Cenozoic carbonate platform margin and its adjacent basinal deposits. Sedimentary Geology 286–287, 20–38. doi:10.1016/j.sedgeo.2012.11.006

Madden, R.H.C., Wilson, M.E.J., Mihaljevi, M., Pandol, J.M., Welsh, K., 2017. Unravelling the depositional origins and diagenetic alteration of carbonate breccias. Sedimentary Geology 357, 33–52. doi:10.1016/j.sedgeo.2017.05.002

Marshak, S., Alkmim, F.F., 1989. Proterozoic contraction/extension tectonics of the southern São Francisco Craton region, Minas Gerais, Brazil. Tectonics 8, 555–571.

Martín-Chivelet, J., Palma, R.M., López-Gómez, J., Kietzmann, D.A., 2011. Earthquake-induced soft-sediment deformation structures in Upper Jurassic open-marine microbialites (Neuquén Basin, Argentina). Sedimentary Geology 235, 210–221. doi:10.1016/j.sedgeo.2010.09.017

Martins-Neto, M.A., Pedrosa-Soares, A.C., Lima, S.A.., 2001. Tectono-sedimentary evolution of sedimentary basins from Late Paleoproterozoic in the São Francisco craton and Araçuaí fold belt, eastern Brazil. Sedimentary Geology 141–142, 343–370.

Misi, A., Kaufman, A.J., Veizer, J., Powis, K., Azmy, K., Boggiani, P.C., Gaucher, C., Teixeira, J.B.G., Sanches, A.L., Iyer, S.S.S., 2007. Chemostratigraphic correlation of Neoproterozoic successions in South America. Chemical Geology 237, 161–185. doi:10.1016/j.chemgeo.2006.06.019

Molina, J.M., Alfaro, P., Moretti, M., Soria, J.M., 1998. Soft-sediment deformation structures induced by cyclic stress of storm waves in tempestites (Miocene, Guadalquivir Basin, Spain). Terra Nova 10, 145–150. doi:10.1046/j.1365-3121.1998.00183.x

Montenat, C., Barrier, P., Ott dEstevou, P., Hibsch, C., 2007. Seismites: An attempt at critical analysis and classification. Sedimentary Geology 196, 5–30. doi:10.1016/j.sedgeo.2006.08.004

Myrow, P.M., Chen, J., 2015. Estimates of large magnitude Late Cambrian earthquakes from seismogenic soft-sediment deformation structures : Central Rocky Mountains. Sedimentology 62, 621–644. doi:10.1111/sed.12154

Myrow, P.M., Tice, L., Archuleta, B., Clark, B., Taylor, J.F., Ripperdan, R.L., 2004. Flat-pebble conglomerate: Its multiple origins and relationship to metre-scale depositional cycles. Sedimentology 51, 973–996. doi:10.1111/j.1365-3091.2004.00657.x

Nobre-Lopes, J., 2002. Diagenesis of the dolomites hosting Zn/Ag mineral deposits in the Bambuí Group at Januária region (MG). Unpublished dissertation, University of Campinas, Campinas-SP, Brazil. 229p.

Nogueira, A.C.R., Riccomini, C., Nóbrega Sial, A., Veloso Moura, C.A., Fairchild, T.R., 2003. Soft-sediment deformation at the base of the Neoproterozoic Puga cap carbonate (southwestern Amazon craton, Brazil): Confirmation of rapid icehouse to greenhouse transition in snowball Earth. Geology 31, 613–616. doi:10.1130/0091-7613(2003)031<0613:SDATBO>2.0.CO;2

Owen, G., Moretti, M., 2011. Identifying triggers for liquefaction-induced soft-sediment deformation in sands. Sedimentary Geology 235, 141–147. doi:10.1016/j.sedgeo.2010.10.003

Owen, G., Moretti, M., Alfaro, P., 2011. Recognising triggers for soft-sediment deformation: Current understanding and future directions. Sedimentary Geology 235, 133–140. doi:10.1016/j.sedgeo.2010.12.010

Palma, R.M., Kietzmann, D.A., Bressan, G.S., Martín-Chivelet, J., López-Gómez, J., Farias, M.E., Llanos, M.P.I., 2013. Peritidal cyclic sedimentation from La Manga Formation (Oxfordian), Neuquén Basin, Mendoza, Argentina. Journal of South American Earth Sciences 47, 1–11.

Patil Pillai, S., Kale, V.S., 2011. Seismites in the Lokapur Subgroup of the Proterozoic Kaladgi Basin, South India: A testimony to syn-sedimentary tectonism. Sedimentary Geology 240, 1–13. doi:10.1016/j.sedgeo.2011.06.013

Paula-Santos, G.M., Babinski, M., Kuchenbecker, M., Caetano-Filho, S., Trindade, R.I., Pedrosa-Soares, A.C., 2015. New evidence of an Ediacaran age for the Bambuí Group in southern São Francisco craton (eastern Brazil) from zircon U-Pb data and isotope chemostratigraphy. Gondwana Research 28, 702–720. doi:10.1016/j.gr.2014.07.012

Perrella Jr., P., Uhlein, A., Uhlein, G.J., Sial, A.N., Pedrosa-Soares, A.C., Lima, O.N.B., 2017. Facies analysis , sequence stratigraphy and chemostratigraphy of the Sete Lagoas Formation (Bambui Group), northern Minas Gerais State , Brazil : evidence of a cap carbonate deposited on the Januária basement high. Brazilian Journal of Geology 47, 59–77. doi:10.1590/2317

Pratt, B.R., 1994. Seismites in the Mesoproterozoic Altyn Formation (Belt Supergroup), Montana: a test for tectonic control of peritidal carbonate cyclicity. Geology 22, 1091–1094.

Pratt, B.R., 2002a. Tepees in peritidal carbonates: Origin via earthquake-induced deformation, with example from the Middle Cambrian of western Canada. Sedimentary Geology 153, 57–64. doi:10.1016/S0037-0738(02)00318-4

Pratt, B.R., 2002b. Storms versus tsunamis: Dynamic interplay of sedimentary, diagenetic, and tectonic processes in the Cambrian of Montana. Geology 30, 423–426. doi:10.1130/0091-7613(2002)030<0423:SVTDIO>2.0.CO;2

Pratt, B. R., Bordonaro, O. L., 2007. Tsunamis in a stormy sea: Middle Cambrian inner-shelf limestones of western Argentina. Journal of Sedimentary Research 77, 4: 256-262.

Pruss, S.B., Corsetti, F.A., Bottjer, D.J., 2005. The unusual sedimentary rock record of the Early Triassic: A case study from the southwestern United States. Palaeogeography, Palaeoclimatology, Palaeoecology 222, 33–52. doi:10.1016/j.palaeo.2005.03.007

Quijada, I.E., Suarez-Gonzalez, P., Benito, M.I., Lugli, S., Mas, R., 2014. From carbonate-sulphate interbeds to carbonate breccias: The role of tectonic deformation and diagenetic processes (Cameros Basin, Lower Cretaceous, N Spain). Sedimentary Geology 312, 76–93. doi:10.1016/j.sedgeo.2014.07.006

Riding, R., 2006. Microbial carbonate abundance compared with fluctuations in metazoan diversity over geological time. Sedimentary Geology 185(3-4), 229-238.

Rodriguez-Pascua, M.A., Calvo, J.P., De Vicente, G., Gómez-gras, D., 2000. Soft-sediment deformation structures interpreted as seismites in lacustrine sediments of the Prebetic Zone, SE Spain, and their potential use as indicators of earthquake magnitudes during the Late Miocene. Sedimentary Geology 135, 117–135. doi:10.1016/S0037-0738(00)00067-1

Sepkoski, J.J., 1982. Flat-Pebble Conglomerates, Storm Deposits, and the Cambrian Bottom Fauna, in: Einsele, G., Seilacher, A. (Eds.), Cyclic and Event Stratification. Springer-Verlag, Berlin, pp. 371–385.

Sepkoski, J.J., Bambach, R.K., Droser, M.L., 1991. Secular changes in Phanerozoic event bedding and the biological overprint, in: Einsele, G., Richen, W., Seilacher, A. (Eds.), Cycles and Events in Stratigraphy. Springer-Verlag, Berlin, pp. 298–312.

Sial, A.N., Dardenne, M.A., Misi, A., Pedreira, A.J., Gaucher, C., Ferreira, V.P., Silva Filho, M.A., Uhlein, A., Pedrosa-Soares, A.C., Santos, R. V., Egydio-Silva, M., Babinski, M., Alvarenga, C.J.S., Fairchild, T.R., Pimentel, M.M., 2009. The São Francisco Palaeocontinent, in: Developments in Precambrian Geology. pp. 31–69. doi:10.1016/S0166-2635(09)01603-X

Sims, J., 1975. Determining eartquake recurrence intervals from defomational structres in young lacustrine sediments. Tectonophysics 29, 141–152.

Spalluto, L., Moretti, M., Festa, V., Tropeano, M., 2007. Seismically-induced slumps in Lower-Maastrichtian peritidal carbonates of the Apulian Platform (southern Italy). Sedimentary Geology 196, 81–98. doi:10.1016/j.sedgeo.2006.06.009

Spence, G.H., Tucker, M.E., 1997. Genesis of limestone megabreccias and their significance in carbonate sequence stratigraphic models: a review. Sedimentary Geology 112, 163–193. doi:10.1016/S0037-0738(97)00036-5

Uhlein, G.J., Uhlein, A., Halverson, G.P., Stevenson, R., Caxito, F.A., Cox, G.M., Carvalho, J.F.M.G., 2016. The Carrancas Formation, Bambuí Group: A record of pre-Marinoan sedimentation on the southern São Francisco craton, Brazil. Journal of South American Earth Sciences 71, 1–16. doi:10.1016/j.jsames.2016.06.009

Vernhet, E., Heubeck, C., Zhu, M. Y., & Zhang, J. M. (2006). Large-scale slope instability at the southern margin of the Ediacaran Yangtze platform (Hunan province, central China). Precambrian Research 148, 1-2: 32-44.

Vieira, L.C., Trindade, R.I.F., Nogueira, A.C.R., Ader, M., 2007. Identification of a Sturtian cap carbonate in the Neoproterozoic Sete Lagoas carbonate platform, Bambuí Group, Brazil

Warren, L. V., Quaglio, F., Riccomini, C., Simões, M.G., Poiré, D.G., Strikis, N.M., Anelli, L.E., Strikis, P.C., 2014. The puzzle assembled: Ediacaran guide fossil Cloudina reveals an old proto-Gondwana seaway. Geology 42, 391–394. doi:10.1130/G35304.1

Wignall, P.B., Twitchett, R.J., 1999. Unusual intraclastic limestones in Lower Triassic carbonates and their bearing on the aftermath of the end-Permian mass extinction. Sedimentology 46, 303–316.

Wilson, M.E.J., Chambers, J.L.C., Manning, C., Nas, D.S., 2012. Spatio-temporal evolution of a Tertiary carbonate platform margin and adjacent basinal deposits. Sedimentary Geology 271–272, 1–27. doi:10.1016/j.sedgeo.2012.05.002

Wright, V.P., Cherns, L., 2016. Leaving no stone unturned : the feedback between increased biotic diversity and early diagenesis during the Ordovician. Journal of the Geological Society 173, 241–244. doi:10.1144/jgs2015-043

9. Conclusões

Na presente pesquisa, materializada em artigos científicos e na presente tese de doutoramento, buscou-se compreender de forma integrada como se deu a evolução sedimentar da Formação Sete Lagoas e a variação paleoambiental durante sua deposição. Para isso, teve-se como principais objetivos: i) descrever as associações de fácies e definir os sistemas deposicionais da Formação Sete Lagoas. Adicionalmente, buscou-se detalhar os processos formadores de facies e sucessões de fácies incomuns, tais como a capa carbonática da base da unidade e brechas presentes na porção intermediária da sucessão; ii) definir padrões arquiteturais e de empilhamento das sucessões estudadas, bem como caracterizar superfícies estratigráficas chave a fim de compor um quadro estratigráfico adequado para a Formação Sete Lagoas na região de Januária, MG; iii) caracterizar em detalhe os aspectos sedimentares e geoquímicos dos precipitados de fundo oceânico presentes na capa carbonática da porção inferior da unidade iv) identificar variações nos padrões isotópicos de carbono e oxigênio visando detalhar aspectos paleoambientais, identificar mudanças de padrão associadas a variação de fácies e superfícies estratigráficas e auxiliar na correlação da unidade com outras porções da bacia e unidades coevas ao redor do mundo; e finalmente, v) estabelecer uma inédita curva isotópica de enxofre para a unidade, cujo significado está intimamente relacionado com a composição da água do mar e a oxigenação dos oceanos no Período Ediacarano.

Na área estudada, a Formação Sete Lagoas apresenta espessura total de 130 metros e é composta por três sequências deposicionais distintas (S1, S2 e S3). Da base para o topo, foram definidas cinco associações de fácies: i) capa dolomítica (AF1), ii) carbonatos de perimaré (AF2), iii) rampa carbonática influenciada por sismos (AF3), iv) cordão oolítico (AF4) e v) planície de maré com microbialitos (AF5).

A sequência basal S1 se inicia com a deposição da capa dolomitíca com valores de ^{13}C em torno de -5 ‰ PDB, contendo precipitados de fundo oceânico incomuns, como leques de aragonita e barita. O limite inferior desta sequência corresponde à discordância erosiva regional entre o embasamento Paleoproterozoico e a Formação Sete Lagoas, e o limite superior corresponde a discordância local que marca o topo da sucessão de rampa carbonática influenciada por sismos.

Precipitados de fundo oceânico sobrepondo estromatólitos dômicos da AF1 constituem um empilhamento retrogradacional, representando a migração do onlap costeiro devido à deglaciação e transgressão pós-Marinoana. Estes depósitos de carbonatos de capa foram interpretados como representativos dos estágios iniciais do trato de sistema transgressivo

(TST1), similar às capas carbonáticas na Namíbia, Canadá e China. A superfície de máxima inundação (MFS1) foi posicionada na camada que contém os precipitados de fundo oceânico devido ao fato de os leques estarem preservados e, por isso, terem sido formados abaixo do nível de ondas de tempo bom e tempestade.

Minerais autigênicos como por aragonita e barita já haviam sido descritos anteriormente por outros autores. No entanto, a identificação e descrição destes leques de aragonita e barita junto à cimentos apatíticos permitiu uma melhor compreensão dos seus mecanismos de formação no contexto da capa carbonática da Formação Sete Lagoas. Outros minerais diagenéticos também foram interpretados, como pirita e calcita. Ressalta-se aqui que a fosfatização em capas carbonáticas é descrita pela primeira vez neste trabalho (Capítulo 6, artigo "Phosphogenesis, aragonite fan formation and seafloor environments following the Marinoan glaciation"), bem como o processo que controla a precipitação de aragonita e apatita por ferro-redução na interface sedimento-água, permitindo a coexistência destas duas fases minerais.

O outro mineral que compõe os precipitados de fundo oceânico típicos de capa carbonática é a barita e, devido a sua importância na definição da idade Marinoana para os carbonatos de capa estudados, considerou-se discutir a origem e a história termal deste mineral (Capítulo 7, artigo "Hydrothermal influence on barite precipitates in the basal Ediacaran Sete Lagoas cap carbonate, São Francisco Craton, central Brazil"). Com base na análise de isótopos de enxofre no carbonato e na barita, espectroscopia Raman e análise de inclusões fluidas, foi constatado que a barita ainda preserva o sinal isotópico da água do mar, mesmo registrando temperaturas e salinidades condizentes com eventos de percolação de fluidos (e.g. hidrotermalismo). Desta forma, ainda que este mineral preserve o sinal isotópico original, é preciso cuidado analítico ao utilizar a barita da Fm. Sete Lagoas (e de outras unidades de mesma idade) para aferir condições geoquímicas e paleoambientais da água do mar.

Na seção Borrachudo, localizada no alto estrutural de Januária, não foram reconhecidas as associações de fácies AF2, AF3 e AF4, o que nos leva a interpretar um expressivo espessamento de seção na direção E-NE, possivelmente relacionado a um aumento expressivo na taxa de subsidência nesta porção da bacia (depocentro).

Fácies de perimaré (AF2) formadas principalmente por microbialitos laminados, trombólitos e grainstones finos laminados, correspondem a uma sucessão típica de trato de mar alto (HST1) nesta porção da bacia. Neste ambiente de águas rasas, proliferaram-se os metazoários Cloudina e Corumbella associados à trombólitos e esteiras microbianas. Estes depósitos de perimaré são recobertos por brechas intraformacionais, interpretadas como flat-pebble breccia. Tal depósito é clasto-suportado, apresenta clastos angulosos e alongados ou oblatos. Não há evidências de deformação dúctil, o que sugere que estes clastos foram depositados como objetos rígidos praticamente na mesma posição em que originalmente se formaram. A presença de clastos em posição vertical, deformação aumentando para o topo, continuidade lateral das camadas brechadas e alternância de camadas deformadas e não-deformadas com contato abrupto sugerem fragmentação in situ de camadas de microbialitos previamente litificados devido ao impacto de ondas de choque relacionadas à atividade sísmica concomitante à sedimentação. Dados de direção dos clastos alongados da flat-pebble breccia da AF3 e de paleocorrentes dos grainstones oolíticos da AF4 indicam que a linha de costa original estava posicionada na direção NE-SW, com abertura oceânica para SE (quadrante E).

Barras e dunas oolíticas do cordão oolítico (AF4) recobrem a flat-pebble breccia e as fácies de perimaré, configurando um padrão retrogradacional representativo dos estágios iniciais do segundo trato transgressivo (TST2). Embora a sucessão contendo grainstones oolíticos apresente 20-30 metros de espessura nas áreas de Arcos e Januária, tal sucessão pode alcançar centenas de metros na região de Montalvânia, sugerindo que a bacia era progressivamente mais profunda na direção E-NE (quadrante E). Este intervalo provavelmente reflete a produção carbonática máxima relacionada com o crescente aumento no espaço de acomodação no depocentro.

No topo da Formação Sete Lagoas, a fácies de brecha estromatolítica representa a exposição subaérea de microbialitos e corresponde ao limite inferior da sequência S3. Este intervalo é marcado pelo decréscimo na produção carbonática, desenvolvimento de uma superfície regional paleocárstica, seguida por um aumento de input terrígeno associado a uma transgressão representativa do início da sedimentação dos siltitos e margas da Fm. Serra de Santa Helena.

As amostras da Fm. Sete Lagoas submetidas às análises de isótopos de C e O tiveram seus valores originais aferidos a partir da relação ^{13}C vs. ^{18}O e razões Mn/Sr, sendo que a grande maioria delas foi considerada não alterada. As curvas isotópicas de ^{13}C variam de -4.33 até 4.77 ‰ PDB, condizentes com valores previamente obtidos por outros autores, exceto pelos valores fortemente positivos do topo da unidade, que não foram encontrados no presente trabalho.

Por fim, uma das principais contribuições deste trabalho consiste na obtenção e interpretação de uma inédita curva isotópica de enxofre (S_{CAS}) para a Formação Sete Lagoas, a qual associada com dados isotópicos de C e O obtidos para as mesmas seções, permitiram delinear algumas condições paleoambientais. Na seção composta estudada, os valores isotópicos de $^{34}S_{CAS}$ mostram co-variância com os valores de $^{13}C_{carb}$, indicando que a pirita e o carbono orgânico foram oxidados e soterrados a uma mesma taxa. Este padrão é comumente encontrado em rochas do início do Fanerozoico. Além disso, as concentrações de CAS medidas mostram um pico de oxigenação na porção basal da unidade seguida por condições anóxicas, semelhante às estimativas anteriores do reservatório de sulfato em outras unidades do final do Ediacarano. Este pico de oxigenação precede estratigraficamente (local) e temporalmente (global) o surgimento dos organismos pertencentes à assembleia de Nama (*Cloudina*, *Namacalathus*, *Corumbella*, entre outros), considerada o último grande evento evolutivo antes da grande explosão de vida Cambriana.

10. Referências bibliográficas

Abreu Lima, S.A., 1997. Fácies, ambiente deposicional e aspectos diagenéticos da Formação Sete Lagoas na região norte de Minas Gerais, Bacia do São Francisco. UFOP.

Alkmim, F.F., Brito Neves, B.B., Castro Alves, J.A., 1993. Arcabouço tectônico do Cráton do São Francisco - Uma revisão, in: Dominguez, J.M.L., Misi, A. (Eds.), O Cráton São Francisco. SBG/Núcleo BA/SE, pp. 45–62.

Alkmim, F.F., Chemale Jr, F., Endo, I., 1996. A deformação das coberturas proterozóicas do Cráton do São Francisco e o seu significado tectônico. Rev. Esc. Minas 49, 22–38.

Alkmim, F.F., Marshak, S., Pedrosa-Soares, A.C., Peres, G.G., Cruz, S.C.P., Whittington, A., 2006. Kinematic evolution of the Araçuaí-West Congo orogen in Brazil and Africa: Nutcracker tectonics during the Neoproterozoic assembly of Gondwana. Precambrian Res. 149, 43–64.

Alkmim, F.F., Martins-Neto, M.A., 2012. Proterozoic first-order sedimentary sequences of the São Francisco craton, eastern Brazil. Mar. Pet. Geol. 33, 127–139.

Alkmim, F.F., Martins-Neto, M.A., 2001. A bacia intracratônica do São Francisco: arcabouço estrutural e cenários evolutivos, in: Pinto, C.P., Martins-Neto, M.A. (Eds.), Bacia Do São Francisco: Geologia e Recursos Minerais. SBG/MG, Belo Horizonte-MG, pp. 9–30.

Allen, P.A., Hoffman, P.F., 2005. Extreme winds and waves in the aftermath of a Neoproterozoic glaciation. Nature 433, 123–127.

Allen, P.A., Leather, J., Brasier, M.D., 2004. The Neoproterozoic Fiq glaciation and its aftermath, Huqf supergroup of Oman. Basin Res. 16, 507–534.

Alvarenga, C.J.S., Dardenne, M.A., Vieira, L.C., Martinho, C.T., Guimarães, E.M., Santos, R.V., Santana, R.O., 2012. Estratigrafia da borda ocidental da Bacia do São Francisco. Bol. Geociências Petrobrás 20, 145–164.

Babinski, M., Pedrosa-Soares, A.C., Trindade, R.I.F., Martins, M., Noce, C.M., Liu, D., 2012. Neoproterozoic glacial deposits from the Araçuaí orogen, Brazil: age, provenance and correlations with the São Francisco craton and West Congo belt. Gondwana Res. 21, 451–465.

Babinski, M., Vieira, L.C., Trindade, R.I.F., 2007. Direct dating of the Sete Lagoas cap carbonate (Bambuí Group, Brazil) and implications for the Neoproterozoic glacial events. Terra Nov. 19, 401–406.

Banner, J.A.Y.L., Hanson, G.N., 1990. Calculation of simultaneous isotopic and trace element variations during water-rock interaction with applications to carbonate diagenesis. Geochim. Cosmochim. Acta 54, 3123–3137.

Bengtson, S., Morris, S.C., 1992. Early Radiation of Biomineralizing Phyla 447–481.

Buatois, L.A., Mángano, M.G., 2018. The other biodiversity record: Innovations in animal-substrate interactions through geologic time. GSA Today 28, 4–10.

Burdett, J.W., Arthur, M.A., Richardson, M., 1989. A Neogene seawater sulfur isotope age curve from calcareous pelagic microfossils. Earth Planet. Sci. Lett. 94, 189–198.

Caetano-Filho, S., Macedo Paula-Santos, G., Guacaneme, C., Babinski, M., Bedoya-Rueda, C., Peloso, M., Amorim, K., Afonso, J., Kuchenbecker, M., Reis, H., Trindade, R.I.F., 2019. Sequence stratigraphy and chemostratigraphy of an Ediacaran-Cambrian foreland-related carbonate ramp (Bambuí Group, Brazil). Precambrian Res. 331, 105365.

Canfield, D.E., Poulton, S.W., Knol, A.H., Narbonne, G.M., Ross, G., Goldberg, T., Strauss, H., 2008. Ferruginous conditions dominated later neoproterozoic deep-water chemistry. Science (80-.). 321, 949–952.

Canfield, D.E., Poulton, S.W., Narbonne, G.M., 2007a. Late-Neoproterozoic Deep-Ocean Oxygenation and the Rise of Animal Life. Science (80-.). 315, 92–95.

Canfield, D.E., Poulton, S.W., Narbonne, G.M., Science, S., Series, N., Jan, N., Canfield, E., Narbonne, G.M., 2007b. Late-Neoproterozoic oxygenation and the rise of animal life. Science (80-.). 315, 92–95.

Castro, A., Dardenne, M., 2000. The sedimentology, stratigraphy and tectonic context of the São Francisco Supergroup at the southwestern domain of the São Francisco Craton, Brazil. Rev. Bras. Geociências 30, 439–441.

Castro, P.T.A., 1997. Os conglomerados associados ao Grupo Bambuí na porção sudoeste do Cráton do São Francisco: sedimentologia, estratigrafia e implicações tectônicas. Universidade de Brasília.

Catuneanu, O., 2006. Principles of Sequence Stratigraphy, Changes.

Caxito, F. de A., Halverson, G.P., Uhlein, A., Stevenson, R., Gonçalves Dias, T., Uhlein, G.J., 2012. Marinoan glaciation in east central Brazil. Precambrian Res. 200–203, 38–58.

Chang, H.K., Miranda, F.P., Magalhães, L., Alkmim, F.F., 1988. Considerações sobre a evolução tectônica da bacia do São Francisco, in: Proceedings of the 35th Congresso Brasileiro de Geologia, Sociedade Brasileira de Geologia (SBG), Belém. pp. 2076–2090.

Chiavegatto, J.R.S., 1992. Análise estratigráfica das sequências tempestíticas da Fm. Três Marias (Proterozoico Superior) na porção meridional da bacia do São Francisco.

Chiavegatto, J.R.S., Gomes, N.S., Dardenne, M.A., Delgado, C.E.R., 2003. Estratigrafia do Grupo Bambuí nas regiões do norte de Minas Gerais: uma nova unidade estratigráfica em um contexto de inversão de bacia, in: XXII Simpósio de Geologia de Minas Gerais. SBG, Ouro Preto-MG.

Clapham, M.E., Narbonne, G.M., 2002. Ediacaran epifaunal tiering. Geology 30, 627–630.

Clapham, M.E., Narbonne, G.M., Gehling, J.G., 2003. Paleoecology of the oldest known animal communities: Ediacaran assemblages at Mistaken Point, Newfoundland. Paleobiology 29, 527–544.

Coelho, J.C.C., Martins-Neto, M.A., Marinho, M.S., 2008. Estilos estruturais e evolução tectônica da porção mineira da bacia proterozóica do São Francisco. Rev. Bras. Geociências 38, 149–165.

Corsetti, F.A., Lorentz, N.J., 2006. On Neoproterozoic Cap Carbonates as Chronostratigraphic Markers, in: Xiao, S., Kaufman, A.J. (Eds.), Neoproterozoic Geobiology and Paleobiology. pp. 273–294.

Corsetti, F.A., Lorentz, N.J., Pruss, S.B., 2004. Formerly-Aragonite Seafloor Fans from Neoproterozoic Strata, Death Valley and Southeastern Idaho, United States: Implications for "Cap Carbonate" Formation and Snowball Earth. Extrem. Proterozoic Geol. Geochemistry, Clim. 33–44.

Corsetti, F.A., Olcott, A.N., Bakermans, C., 2006. The biotic response to Neoproterozoic snowball earth. Palaeogeogr. Palaeoclimatol. Palaeoecol. 232, 114–130.

Costa, M.T., Branco, J.J.R., 1961. Roteiro para a excursão Belo Horizonte-Brasília, in: Congresso Brasileiro de Geologia. pp. 15–25.

Cox, G.M., Halverson, G.P., Minarik, W.G., Le, D.P., Macdonald, F.A., Bellefroid, E.J., Strauss, J. V, 2013. Neoproterozoic iron formation: An evaluation of its temporal, environmental and tectonic significance. Chem. Geol. 362, 232–249.

Cox, G.M., Halverson, G.P., Poirier, A., Le, D., Strauss, J. V, Stevenson, R., 2016. A model for Cryogenian iron formation. Earth Planet. Sci. Lett. 433, 280–292.

Crockford, P.W., Hodgskiss, M.S.W., Uhlein, G.J., Caxito, F., Hayles, J.A., Halverson, G.P., 2017. Linking paleocontinents through triple oxygen isotope anomalies. Geology 46, 179–182.

Cruz, N.M.C., Nobre-Lopes, J., 1992. Microfósseis do Grupo Bambuí na região de Arcos, Minas Gerais. An. Acad. Bras. Cienc. 64, 420.

D'Agrella-Filho, M.S., Babinski, M., Trindade, R.I.F., Van Schmus, W.R., Ernesto, M., 2000. Simultaneous remagnetization and U-Pb isotope resetting in Neoproterozoic carbonates of the Sao Francisco craton, Brazil. Precambrian Res. 99, 179–196.

da Silva, L.C., Pedrosa-Soares, A.C., Armstrong, R., Noce, C.M., 2011. Determinando a duração do período colisional do Orógeno Araçuaí com base em geocronologia U-Pb de alta resolução em zircão : uma contribuição para a história da amalgamação do Gondwana Ocidental. Geonomos 19, 180–197.

Dardenne, M.A., 2000. The Brasília Fold Belt, in: Cordani, U.G., Milani, A.J., Thomaz-Filho, A., Campos, D.A. (Eds.), Tectonic Evolution of South America. Rio de Janeiro, Brazil, pp. 231–264.

Dardenne, M.A., 1978. Síntese sobre a estratigrafia do Grupo Bambuí no Brasil Central, in: Anais Do XXX Congresso Brasileiro de Geologia. Recife, pp. 597–610.

Derry, L.A., 2010. A burial diagenesis origin for the Ediacaran Shuram-Wonoka carbon isotope anomaly. Earth Planet. Sci. Lett. 294, 152–162.

Deynoux, M., 1985. Terrestrial or waterlain glacial diamictites? Three case studies from the Late Precambrian and Late Ordovician glacial drifts in West Africa. Palaeogeogr. Palaeoclimatol. Palaeoecol. 51, 97–141.

Drummond, J.B.R., Pufahl, P.K., Porto, C.G., Carvalho, M., 2015. Neoproterozoic peritidal phosphorite from the Sete Lagoas Formation (Brazil) and the Precambrian phosphorus cycle. Sedimentology 62, 1978–2008.

Dunham, R.J., 1962. Classification of carbonate rocks according to depositional textures 108–121.

Embry, A.F., Klovan, J.E., 1971. A late Devonian reef tract on northeastern Banks Island, NWT. Bull. Can. Pet. Geol. 19, 730–781.

Evans, D.A.D., 2000. Stratigraphic, geochronological and paleomagnetic constraints upon the Neoproterozoic climatic paradox. Am. J. Sci. 347–433.

Evans, D.A.D., Raub, T.D., 2011. Neoproterozoic glacial palaeolatitudes: a global update, in: The Geological Record of Neoproterozoic Glaciations. pp. 93–112.

Eyles, N., Januszczak, N., 2004. "Zipper-rift": A tectonic model for Neoproterozoic glaciations during the breakup of Rodinia after 750 Ma. Earth-Science Rev. 65, 1–73.

Fairchild, I.J., Kennedy, M.J., 2007. Neoproterozoic glaciation in the Earth System. J. Geol. Soc. London 164, 895–921.

Fairchild, T.R., Schopf, J.W., Shen-Miller, J., Guimarães, E.M., Edwards, M.D., Lagstein, A., Xiao, L., Pabst, M., Melo-Filho, L.S., 1996. Recent discoveries of Proterozoic microfossils in south-central Brazil. Precambrian Res. 80, 125–152.

Fairchild, T.R., Subacius, S.M.R., 1986. Microfossils associated with silicified Stratifera undata Komar 1966 from the Late Proterozoic Bambuí Group, south-central Brazil. Precambrian Res. 33, 323–339.

Fanning, C.M., Link, P.K., 2004. U-Pb SHRIMP ages of Neoproterozoic (Sturtian) glaciogenic Pocatello Formation, southeastern Idaho. Geology 32, 881–884.

Fike, D.A., Grotzinger, J.P., Pratt, L.M., Summons, R.E., 2006. Oxidation of the Ediacaran ocean. Nature 444, 744–747.

Frei, R., Gaucher, C., Poulton, S.W., Canfield, D.E., 2009. Fluctuations in Precambrian atmospheric oxygenation recorded by chromium isotopes. Nature 461, 250–253.

Frimmel, H.E., Fo, P.G., 2002. Chemostratigraphic correlation of carbonate successions in the Gariep and Saldania Belts , Namibia and South Africa. Basin Res.

Gehling, J.G., Rigby, J.K., 1996. Long expected sponges from the Neoproterozoic Ediacara Fauna of South Australia. J. Paleontol. 70, 185–195.

Gellatly, A.M., Lyons, T.W., 2005. Trace sulfate in mid-Proterozoic carbonates and the sulfur isotope record of biospheric evolution. Geochim. Cosmochim. Acta 69, 3813–3829.

Germs, G.J.B., 1972. New shelly fossils from Nama Group, South West Africa. Am. J. Sci. 272, 752–761.

Glenn, C.R., Föllmi, K.B., Grimm, K.A., Sadaqah, R.M.Y., Schidlowski, M., Sheldon, R.E., Siegmund, H., 1994. Phosphorus and Phosphorites: Sedimentology and Environments of Formation. Eclogae Geol. Helv. 87, 747–788.

Grant, S.W., 1992. Carbon isotopic vital effect and organic diagenesis, Lower Cambrian Forteau Formation, northwest Newfoundland: Implications for δ13C chemostratigraphy. Geology 20, 243–246.

Grant, S.W., 1990. Shell structure and distribution of Cloudina, a potential index fossil for the terminal Proterozoic. Am. J. Sci. 290-A, 261–294.

Grazhdankin, D., Seilacher, A., 2005. A re-examination of the Nama-type Vendian organism Rangea schneiderhoehni. Geol. Mag. 142, 571.

Grazhdankin, D., Seilacher, A., 2002. Underground Vendobionta from Namibia. Palaeontology 45, 57–78.

Grotzinger, J.P., Knoll, A.H., 1995. Anomalous carbonate precipitates : Is the Precambrian the key to the Permian? Palaios 10, 578–596.

Grotzinger, J.P., Watters, W.A., Knoll, A.H., 2000. Calcified metazoans in thrombolite-stromatolite reefs of the terminal Proterozoic Nama Group, Namibia. Paleobiology 26, 334–359.

Guimarães, E.M., 1997. Estudos de proveniência e diagênese, com ênfase na caracterização dos filossilicatos dos grupos Paranoá e Bambuí, na região de Bezerra e Cabeceiras-GO. Universidade de Brasília.

Halverson, G.P., Hoffman, P.F., Schrag, D.P., Maloof, A.C., Rice, A.H.N., 2005. Toward a Neoproterozoic composite carbon-isotope record. Bull. Geol. Soc. Am. 117, 1181–1207.

Halverson, G.P., Wade, B.P., Hurtgen, M.T., Barovich, K.M., 2010. Neoproterozoic chemostratigraphy. Precambrian Res. 182, 337–350.

Hemming, N.G., Meyers, W.J., Grams, J.C., 1989. Cathodoluminescence in diagenetic calcites: the roles of Fe and Mn as deduced from electron probe and spectrophotometric measurements. J. Sediment. Res. 59, 404–411.

Hidalgo, R., 2007. Vida após glaciações globais neoproterozóicas: um estudo microfossilífero de capas carbonáticas dos crátons do São Francisco e Amazônico.

Higgins, J.A., Schrag, D.P., 2003. Aftermath of a snowball Earth. Geochemistry, Geophys.

Geosystems 4, 1–20.
Hoffman, P.F., 1999. The break-up of Rodinia, birth of Gondwana, true polar wander and the snowball Earth. J. African Earth Sci. 28, 17–33.
Hoffman, P.F., Halverson, G.P., 2011. Chapter 36 Neoproterozoic glacial record in the Mackenzie Mountains, northern Canadian Cordillera. Geol. Soc. London, Mem. 36, 397–412.
Hoffman, P.F., Halverson, G.P., Domack, E.W., Husson, J.M., Higgins, J.A., Schrag, D.P., 2007. Are basal Ediacaran (635 Ma) post-glacial "cap dolostones" diachronous? Earth Planet. Sci. Lett. 258, 114–131.
Hoffman, P.F., Kaufman, A.J., Halverson, G.P., Schrag, D.P., 1998. A Neoproterozoic Snowball Earth. Science (80-.). 281, 1342–1346.
Hoffman, P.F., Li, Z.X., 2009. A palaeogeographic context for Neoproterozoic glaciation. Palaeogeogr. Palaeoclimatol. Palaeoecol. 277, 158–172.
Hoffman, P.F., Macdonald, F. a., Halverson, G.P., 2011. Chemical sediments associated with Neoproterozoic glaciation: iron formation, cap carbonate, barite and phosphorite. Geol. Soc. London, Mem. 36, 67–80.
Hoffman, P.F., Schrag, D.P., 2002. The snowball Earth hypothesis: testing the limits of global change. Terra Nov. 14, 129–155.
Hoffmann, K.H., Condon, D.J., Bowring, S.A., Crowley, J.L., 2004. U-Pb zircon date from the Neoproterozoic Ghaub Formation Namibia: Constraints on Marinoan glaciation. Geology 32, 817–820.
Huang, J., Chu, X., Lyons, T.W., Sun, T., Feng, L., Zhang, Q., Chang, H., 2013. The sulfur isotope signatures of Marinoan deglaciation captured in Neoproterozoic shallow-to-deep cap carbonate from South China. Precambrian Res. 238, 42–51.
James, N.P., Narbonne, G.M., Kyser, T.K., 2001. Late Neoproterozoic cap carbonates : Mackenzie Mountains, northwestern Canada: precipitation and global glacial meltdown. Can. J. Earth Sci. 38, 1229–1262.
Jensen, S., 2006. The Proterozoic and Earliest Cambrian Trace Fossil Record; Patterns, Problems and Perspectives. Integr. Comp. Biol. 43, 219–228.
Jensen, S., Droser, M.L., Gehling, J.G., 2006. A critical look at Ediacaran trace fossil record, in: Neoproterozoic Geobiology and Paleobiology. pp. 115–157.
Jiang, G., Kaufman, A.J., Christie-Blick, N., Zhang, S., Wu, H., 2007. Carbon isotope variability across the Ediacaran Yangtze platform in South China: Implications for a large surface-to-deep ocean δ13C gradient. Earth Planet. Sci. Lett. 261, 303–320.
Jiang, G., Kennedy, M.J., Christie-Blick, N., 2003. Stable isotopic evidence for methane seeps in Neoproterozoic postglacial cap carbonates. Nature 426, 822–826.
Jiang, G., Kennedy, M.J., Christie-Blick, N., Wu, H., Zhang, S., 2006. Stratigraphy, Sedimentary Structures, and Textures of the Late Neoproterozoic Doushantuo Cap Carbonate in South China. J. Sediment. Res. 76, 978–995.
Johnston, D.T., Poulton, S.W., Tosca, N.J., O'Brien, T., Halverson, G.P., Schrag, D.P., Macdonald, F.A., 2013. Searching for an oxygenation event in the fossiliferous Ediacaran of northwestern Canada. Chem. Geol. 362, 273–286.
Kaufman, A.J., Hayes, J.M., Knoll, A.H., Germs, G.J.B., 1991. Isotopic compositions of carbonates and organic carbon from upper Proterozoic successions in Namibia: stratigraphic variation and the effects of diagenesis and metamorphism. Precambrian Res. 49, 301–327.
Kaufman, A.J., Jacobsen, S.B., Knoll, A.H., 1993. The Vendian record of Sr and C isotopic variations in seawater: Implications for tectonics and paleoclimate. Earth Planet. Sci. Lett. 120, 409–430.

Kaufman, A.J., Knoll, A.H., 1995. Neoproterozoic variations in the C-isotopic composition of seawater: stratigraphic and biogeochemical implications. Precambrian Res. 73, 27–49.

Kaufman, A.J., Knoll, A.H., Narbonne, G.M., 1997. Isotopes, ice ages, and terminal Proterozoic earth history. Geology 94, 6600–6605.

Kennedy, M.J., 1996. Stratigraphy, sedimentology, and isotopic geochemistry of Australian Neoproterozoic postglacial cap dolostones; deglaciation, delta 13 C excursions, and carbonate precipitation. J. Sediment. Res. 66, 1050–1064.

Kennedy, M.J., Christie-Blick, N., Sohl, L.E., 2001. Are Proterozoic cap carbonates and isotopic excursions a record of gas hydrate destabilization following Earth's coldest intervals? Geology 29, 443–446.

Kennedy, M.J., Runnegar, B., Prave, A.R., Hoffman, K.-H., Arthur, M.A., 1998. Two or four Neoproterozoic glaciations? Geology 26, 1059–1063.

Kerans, C., Tinker, S.W., 1997. Sequence stratigraphy and characterization of carbonate reservoirs, in: SEPM Short Course Notes. p. 10p.

Kirschvink, J.L., 1992. Late Proterozoic low-latitude global glaciation: the snowball Earth. Proterozoic Biosph. 52, 51–52.

Knoll, A.H., Hayes, J.M., Kaufman, A.J., Swett, K., Lambert, I.B., 1986. Secular variation in carbon isotope ratios from Upper Proterozoic successions of Svalbard and East Greenland. Nature 321, 832–838.

Kontorovich, A.E., Varlamov, A.I., Grazhdankin, D. V., Karlova, G.A., Klets, A.G., Kontorovich, V.A., Saraev, S. V., Terleev, A.A., Belyaev, S.Y., Varaksina, I. V., Efimov, A.S., Kochnev, B.B., Nagovitsin, K.E., Postnikov, A.A., Filippov, Y.F., 2008. A section of Vendian in the east of West Siberian Plate (based on data from the Borehole Vostok 3). Russ. Geol. Geophys. 49, 932–939.

Kruse, P.D., Zhuravlev, A.Y., James, N.P., 1995. Primordial metazoan-calcimicrobial reefs: Tommotian (Early Cambrian) of the Siberian Platform. Palaios 10, 291–321.

Kuchenbecker, M., 2011. Quimioestratigrafia e proveniência sedimentar da porção basal do Grupo Bambuí em Arcos (MG).

Kuchenbecker, M., Atman, D., Da Costa, R.D., Pedrosa-Soares, A.C., Babinski, M., 2016a. A Formação Gorutuba: Sedimentação litorânea a continental na margem leste da Bacia Bambuí (MG). Geol. USP - Ser. Cient. 16, 67–81.

Kuchenbecker, M., Pedrosa-Soares, A.C., Lopes-Silva, L., Babinski, M., Pimenta, F., 2016b. Chemostratigraphy of the lower Bambuí Group, southwestern São Francisco Craton, Brazil: insights on Gondwana paleoenvironments. Brazilian J. Geol. 46, 145–162.

Lamb, M.P., Fischer, W.W., Raub, T.D., Taylor Perron, J., Myrow, P.M., 2012. Origin of giant wave ripples in snowball earth cap carbonate. Geology 40, 827–830.

Le Heron, D.P., Cox, G., Trundley, A., Collins, A.S., 2011. Two Cryogenian glacial successions compared: Aspects of the Sturt and Elatina sediment records of South Australia. Precambrian Res. 186, 147–168.

Li, C., Love, G.D., Lyons, T.W., Fike, D.A., Sessions, A.L., Chu, X., 2010. A stratified redox model for the Ediacaran ocean. Science (80-.). 328, 80–83.

Lima, O.N.B., 2005. Grupo Bambuí: estratigrafia regional no Alto Rio São Francisco e geologia dos depósitos fosfáticos da Serra da Saudade. Universidade Federal de Minas Gerais.

Ling, H.F., Chen, X., Li, D., Wang, D., Shields-Zhou, G.A., Zhu, M., 2013. Cerium anomaly variations in Ediacaran-earliest Cambrian carbonates from the Yangtze Gorges area, South China: Implications for oxygenation of coeval shallow seawater. Precambrian Res. 225, 110–127.

Linnemann, U., Ovtcharova, M., Schaltegger, U., Gärtner, A., Hautmann, M., Geyer, G., Vickers-Rich, P., Rich, T., Plessen, B., Hofmann, M., Zieger, J., Krause, R., Kriesfeld, L.,

Smith, J., 2019. New high-resolution age data from the Ediacaran–Cambrian boundary indicate rapid, ecologically driven onset of the Cambrian explosion. Terra Nov. 31, 49–58.
Lorentz, N.J., Corsetti, F.A., Link, P.K., 2004. Seafloor precipitates and C-isotope stratigraphy from the Neoproterozoic Scout Mountain Member of the Pocatello Formation, southeast Idaho: Implications for Neoproterozoic earth system behavior. Precambrian Res. 130, 57–70.
Macdonald, F.A., Strauss, J. V., Sperling, E.A., Halverson, G.P., Narbonne, G.M., Johnston, D.T., Kunzmann, M., Schrag, D.P., Higgins, J.A., 2013. The stratigraphic relationship between the Shuram carbon isotope excursion, the oxygenation of Neoproterozoic oceans, and the first appearance of the Ediacara biota and bilaterian trace fossils in northwestern Canada. Chem. Geol. 362, 250–272.
Marchese, H.G., 1974. Estromatólitos "Gymnosolenideos" em el lado oriental de Minas Gerais, Brasil. Rev. Bras. Geociências 4, 257–271.
Marshak, S., Alkmim, F.F., 1989. Proterozoic contraction/extension tectonics of the southern São Francisco Craton region, Minas Gerais, Brazil. Tectonics 8, 555–571.
Martins-Neto, M.A., 2009. Sequence stratigraphic framework of Proterozoic successions in eastern Brazil. Mar. Pet. Geol. 26, 163–176.
Martins, M., 1999. Análise estratigráfica das sequências mesoproterozóicas (borda oeste) e neoproterozóicas da Bacia do São Francisco. Universidade Federal do Rio Grande do Sul.
Martins, M., Lemos, V., 2007. Análise estratigráfica das seqüências neoproterozóicas da Bacia do São Francisco. Brazilian J. Geol. 37, 156–167.
McFadden, K. A., Huang, J., Chu, X., Jiang, G., Kaufman, A.J., Zhou, C., Yuan, X., Xiao, S., 2008. Pulsed oxidation and biological evolution in the Ediacaran Doushantuo Formation. Proc. Natl. Acad. Sci. 105, 3197–3202.
McFadden, Kathleen A., Huang, J., Chu, X., Jiang, G., Kaufman, A.J., Zhou, C., Yuan, X., Xiao, S., 2008. Pulsed oxidation and biological evolution in the Ediacaran Doushantuo Formation. Proc. Natl. Acad. Sci. 105, 3197–3202.
McMechan, M.E., 2000. Vreeland Diamictites - Neoproterozoic glaciogenic slope deposits, Rocky Mountains, northeast British Columbia. Bull. Can. Pet. Geol. 48, 246–261.
Misi, A., Teixeira, J.B.G., Azmy, K., Veizer, J., Boggiani, P.C., Iyer, S.S.S., Gaucher, C., Kaufman, A.J., Powis, K., Sanches, A.L., 2007. Chemostratigraphic correlation of Neoproterozoic successions in South America. Chem. Geol. 237, 143–167.
Mitchum, R.M., Van Wagoner, J.C., 1991. High-frequency sequences and their stacking patterns: sequence-stratigraphic evidence of high-frequency eustatic cycles. Sediment. Geol. 70, 1–2.
Morris, S.C., Mattes, B.W., Chen Menge, 1990. The early skeletal organism Cloudina: new occurrences from Oman and possibly China. Am. J. Sci. 290 A, 245–260.
Myrow, P.M., Kaufman, A.J., 2012. A newly discovered cap carbonate above Varanger-age glacial deposits in Newfoundland, Canada. J. Sediment. Res. 69, 784–793.
Narbonne, G.M., 2005. The Ediacara Biota: Neoproterozoic origin of animals and their ecosystems. Annu. Rev. Earth Planet. Sci. 33, 421–442.
Narbonne, G.M., Gehling, J.G., 2003. Life after snowball: The oldest complex Ediacaran fossils. Geology 31, 27–30.
Narbonne, G.M., Saylor, B.Z., Grotzinger, J.P., 1997. The youngest Ediacaran fossils from Southern Africa. J. Paleontol. 71, 953–967.
Nelson, G.J., Pufahl, P.K., Hiatt, E.E., 2010. Paleoceanographic constraints on Precambrian phosphorite accumulation, Baraga Group, Michigan, USA. Sediment. Geol. 226, 9–21.
Nobre-Lopes, J., 2002. Diagenesis of the dolomites hosting Zn/Ag mineral deposits in the

Bambuí Group at Januária region (MG). Unpublished PhD thesis, University of Campinas, Campinas-SP, Brazil. 229p.
Nobre-Lopes, J., 1995. Faciologia e gênese dos carbonatos do Grupo Bambuí na região de Arcos, estado de Minas Gerais.
Nobre-Lopes, J., Coimbra, A.M., 2000. Microfitólitos associados a construções estromatolíticas do Grupo Bambuí, Proterozóico Superior, na região de Arcos - MG. Rev. Bras. Geociências 30, 589–592.
Nogueira, A.C.R., 2003. A plataforma carbonática Araras no sudoeste do cráton Amazônico, Mato Grosso: estratigrafia, contexto paleoambiental e correlação com os eventos glaciais do Neoproterozóico.
Nogueira, A.C.R., Riccomini, C., Nóbrega Sial, A., Veloso Moura, C.A., Fairchild, T.R., 2003. Soft-sediment deformation at the base of the Neoproterozoic Puga cap carbonate (southwestern Amazon craton, Brazil): Confirmation of rapid icehouse to greenhouse transition in snowball Earth. Geology 31, 613–616.
Och, L.M., Shields-Zhou, G.A., 2012. The Neoproterozoic oxygenation event: Environmental perturbations and biogeochemical cycling. Earth-Science Rev. 110, 26–57.
Papineau, D., 2010. Global Biogeochemical Changes at Both Ends of the Proterozoic: Insights from Phosphorites. Astrobiology 10, 165–181.
Paula-Santos, G.M., 2012. Quimioestratigrafia isotópica (C, O, Sr) e geocronologia (U-Pb, Sm-Nd) das rochas da Formação Sete Lagoas, Grupo Bambuí.
Paula-Santos, G.M., Babinski, M., Kuchenbecker, M., Caetano-Filho, S., Trindade, R.I., Pedrosa-Soares, A.C., 2015. New evidence of an Ediacaran age for the Bambuí Group in southern São Francisco craton (eastern Brazil) from zircon U–Pb data and isotope chemostratigraphy. Gondwana Res. 28, 702–720.
Peryt, T.M., Hoppe, a, Bechstädt, T., Koster, J., Pierre, C., Richter, D.K., 1990. Late Proterozoic aragonitic cement crusts, Bambui Group, Minas Gerais, Brazil. Sedimentology 37, 279–286.
Pimentel, M.M., Rodrigues, J.B., DellaGiustina, M.E.S., Junges, S., Matteini, M., Armstrong, R., 2011. The tectonic evolution of the Neoproterozoic Brasília Belt, central Brazil, based on SHRIMP and LA-ICPMS U-Pb sedimentary provenance data: A review. J. South Am. Earth Sci. 31, 345–357.
Posamentier, H.W., Jervey, M.T., Vail, P.R., 1988. Eustatic controls on clastic deposition I - Conceptual framework, in: Wilgus, C.K., Hastings, B.J., Posamentier, H.W., Van Wagoner, J.C., Ross, C.A., Kendall, C.G. (Eds.), Sea-Level Changes: An Integrated Approach. Society of Economic Paleontologists and Mineralogists Special Publications 42, pp. 109–124.
Potter, P.E., Pettijohn, F.J., 1977. Paleocurrents and basin analysis, 2nd ed. ed. Springer-Verlag, New York.
Poulton, S.W., Butterfield, N.J., Shields-Zhou, G.A., Lenton, T.M., Boyle, R.A., 2014. Co-evolution of eukaryotes and ocean oxygenation in the Neoproterozoic era. Nat. Geosci. 7, 257–265.
Pruss, S.B., Corsetti, F.A., Fischer, W.W., 2008. Seafloor-precipitated carbonate fans in the Neoproterozoic Rainstorm Member, Johnnie Formation, Death Valley Region, USA. Sediment. Geol. 207, 34–40.
Pu, J.P., Bowring, S.A., Ramezani, J., Myrow, P., Raub, T.D., Landing, E., Mills, A., Hodgin, E., Macdonald, F.A., 2016. Dodging snowballs: Geochronology of the Gaskiers glaciation and the first appearance of the Ediacaran biota. Geology 44, 955–958.
Ridgwell, A.J., Kennedy, M.J., Caldeira, K., 2003. Carbonate Deposition, Climate Stability, and Neoproterozoic Ice Ages. Science (80-.). 302, 859–862.

Rodrigues, J.B., 2008. Proveniência de sedimentos dos grupos Canastra, Ibiá, Vazante e Bambuí – Um estudo de zircões detríticos e Idades Modelo Sm-Nd. Universidade de Brasília.

Romeiro-Silva, P.C., Zalán, P.V., 2005. Contribuição da sísmica de reflexão na determinação do limite oeste do cráton São Francisco, in: Simpósio Sobre o Cráton Do São Francisco. pp. 44–47.

Rothman, D.H., Hayes, J.M., Summons, R.E., 2003. Dynamics of the Neoproterozoic carbon cycle. Proc. Natl. Acad. Sci. 100, 8124–8129.

Sahoo, S.K., Planavsky, N.J., Jiang, G., Kendall, B., Owens, J.D., Wang, X., Shi, X., Anbar, A.D., Lyons, T.W., 2016. Oceanic oxygenation events in the anoxic Ediacaran ocean. Geobiology 14, 457–468.

Sanchez, E.A.M., 2014. Microbialitos e microfósseis da Formação Sete Lagoas, Neoproterozoico, Brasil: implicações geomicrobiológicas em um contexto de mudanças climáticas e evolutivas. Universidade de São Paulo.

Schöll, W.U., 1976. Sedimentologia e geoquímica do Grupo Bambuí na parte sudeste da Bacia do São Francisco, in: Congresso Brasileiro de Geologia, v.29, Anais. pp. 207–231.

Seer, H.J., Moraes, L.C., Fogaça, A.C.C., 1987. Faciologia e estruturação tectônica dos metassedimentos com diamictitos e jaspilitos da região de Lagoa Formosa, MG (Grupo Bambuí?), in: Simpósio de Geologia de Minas Gerais. SBG/Núcleo Minas Gerais, Belo Horizonte-MG, pp. 199–213.

Shen, B., Xiao, S., Kaufman, A.J., Bao, H., Zhou, C., Wang, H., 2008. Stratification and mixing of a post-glacial Neoproterozoic ocean: Evidence from carbon and sulfur isotopes in a cap dolostone from northwest China. Earth Planet. Sci. Lett. 265, 209–228.

Shields, G.A., Deynoux, M., Strauss, H., Paquet, H., Nahon, D., 2007. Barite-bearing cap dolostones of the Taoudéni Basin, northwest Africa: Sedimentary and isotopic evidence for methane seepage after a Neoproterozoic glaciation. Precambrian Res. 153, 209–235.

Sial, A.N., Gaucher, C., Misi, A., Boggiani, P.C., Alvarenga, C.J.S. de, Ferreira, V.P., Pimentel, M.M., Pedreira, J.A., Warren, L.V., Fernández-Ramírez, R., Geraldes, M., Pereira, N.S., Chiglino, L., Cezario, W. dos S., 2016. Correlations of some Neoproterozoic carbonate-dominated successions in South America based on high-resolution chemostratigraphy, Brazilian Journal of Geology.

Simonetti, C., Fairchild, T.R., 1989. Paleobiologia de uma nova microflórula silicificada do Grupo Bambuí (Proterozoico Superior) da região de Unaí, MG, in: Boletim IG-USP. pp. 1–25.

Sommer, F.W., 1982. Mais oncólitos do Calcário Bambuí de Minas Gerais. An. Acad. Bras. Cienc. 54, 343–349.

Sommer, F.W., 1981. Oncólitos do Calcário Bambuí de Minas Gerais. An. Acad. Bras. Cienc. 53, 785–791.

Sommer, F.W., 1971. Microfósseis do Calcário Bambuí, de Pedro Leopoldo, Estado de Minas Gerais. An. Acad. Bras. Cienc. 43, 135–139.

Spence, G.H., Heron, D. Le, Fairchild, I., 2016. Sedimentological perspectives on climatic, atmospheric and environmental change in the Neoproterozoic Era. Sedimentology 63, 253–306.

Sumner, D.Y., Grotzinger, J.P., 2004. Implications for Neoarchean ocean chemistry from primary carbonate mineralogy of the Campbell-Malmani Platform, South Africa. Sedimentology 51, 1–27.

Tostevin, R., Clarkson, M.O., Gangl, S., Shields, G.A., Wood, R.A., Bowyer, F., Penny, A.M., Stirling, C.H., 2019. Uranium isotope evidence for an expansion of anoxia in terminal Ediacaran oceans. Earth Planet. Sci. Lett. 506, 104–112.

Tostevin, R., He, T., Turchyn, A. V., Wood, R.A., Penny, A.M., Bowyer, F., Antler, G., Shields, G.A., 2017. Constraints on the late Ediacaran sulfur cycle from carbonate associated sulfate. Precambrian Res. 290, 113–125.

Trindade, R.I.F., Macouin, M., 2007. Palaeolatitude of glacial deposits and palaeogeography of Neoproterozoic ice ages. Comptes Rendus - Geosci. 339, 200–211.

Uchio, Y., Isozaki, Y., Buslov, M.M., Maruyama, S., 2008. Occurrence of phosphatic microfossils in an Ediacaran-Cambrian mid-oceanic paleo-atoll limestone of southern Siberia. Gondwana Res. 14, 183–192.

Uhlein, A., Alvarenga, C.J.S., Dardenne, M.A., Trompette, R., 2011a. The glaciogenic Jequitaí Formation, southeastern Brazil, in: Arnaud, E., Halverson, G.P., Shields-Zhou, G. (Eds.), The Geological Record of Neoproterozoic Glaciations. Geological Society of London Memoir 36, London, pp. 51–66.

Uhlein, A., Alvarenga, C.J.S., Trompette, R., Dupont, H.S.J.B., Egydio-Silva, M., Cukrov, N., Lima, O.N.B., 2004. Glaciação neoproterozóica sobre o Cráton do São Francisco e faixas dobradas adjacentes, in: Mantesso-Neto, V., Bartorelli, A., Carneiro, C.D.R., Brito Neves, B.B. (Eds.), Geologia Do Continente Sul-Americano. Editora Beca, pp. 539–553.

Uhlein, A., Baptista, M.C., Seer, H.J., Caxito, F. de A., Uhlein, G.J., Dardenne, M.A., 2011b. A Formação Lagoa Formosa, Grupo Bambuí (MG): sistema deposicional de leque submarino em bacia de antepaís. Geonomos 19, 163–172.

Uhlein, A., Baptista, M.C., Seer, H.J., Caxito, F.D.A., Uhlein, G.J., Dardenne, M.A., 2011c. A Formação Lagoa Formosa , Grupo Bambuí (MG): sistema deposicional de leque submarino em bacia de antepaís. Geonomos 19, 163–172.

Uhlein, G.J., Uhlein, A., Pereira, E., Caxito, F.A., Okubo, J., Warren, L.V., Sial, A.N., 2019. Ediacaran paleoenvironmental changes recorded in the mixed carbonate-siliciclastic Bambuí Basin, Brazil. Palaeogeogr. Palaeoclimatol. Palaeoecol. 517, 39–51.

Uhlein, G.J., Uhlein, A., Stevenson, R., Halverson, G.P., Caxito, F.A., Cox, G.M., 2017. Early to late Ediacaran conglomeratic wedges from a complete foreland basin cycle in the southwest São Francisco Craton, Bambuí Group, Brazil. Precambrian Res. 299, 101–116.

Vail, P.R., Audemard, F., Bowman, S.A., Eisner, P.N., Perez-Cruz, G., 1991. The stratigraphic signatures of tectonics, eustasy and sedimentation: an overview, in: Einsele, G., Riken, W., Seilacher, A. (Eds.), Cycles and Events in Stratigraphy. Springer-Verlag, pp. 617–659.

Vail, P.R., Mitchum, R.M., Thompson, S., 1977. Seismic stratigraphy and global changes in sea level, in: Payton, C.E. (Ed.), Seismic Stratigraphy Applications to Hydrocarbon Exploration. AAPG Memoir 26, pp. 63–97.

Valeriano, C.M., 1992. Evolução tectônica da extremidade meridional da Faixa Brasília, região da Represa de Furnas, sudoeste de Minas Gerais. Universidade de São Paulo.

Valeriano, C.M., Teixeira, W., Heilbron, M., Simões, L.S.A., 2000. Southern Brasília belt (SE Brazil): tectonic discontinuities , K-Ar data and evolution during the Neoproterozoic Brasiliano orogeny. Rev. Bras. Geociências 30, 195–199.

van Loon, A.J., 2008. Could “Snowball Earth” have left thick glaciomarine deposits? Gondwana Res. 14, 73–81.

Van Wagoner, J.C., Posamentier, H.W., Mitchum, R.M., Vail, P.R., Sarg, J.F., Loutitt, T.S., Handerbo, J., 1988. An overview of the fundamentals of sequence stratigraphy and key definitions, in: Wilgus, C.K., Hastings, B.J., Posamentier, H.W., Van Wagoner, J.C., Ross, C.A., Kendall, C.G. (Eds.), Sea-Level Changes: An Integrated Approach. Society of Economic Paleontologists and Mineralogists Special Publications 42, pp. 30–45.

Vieira, L.C., 2007. A Formação Sete Lagoas (Grupo Bambuí) e as variações paleoambientais no final do Proterozóico. Universidade de São Paulo.

Vieira, L.C., Almeida, R.P., Trindade, R.I.F., 2007a. A Formação Sete Lagoas em sua área-

tipo: fácies, estratigrafia e sistemas deposicionais. Brazilian J. Geol. 37, 1–14.
Vieira, L.C., Nédélec, A., Fabre, S., Trindade, R.I.F., Almeida, R.P.D.E., 2015. Aragonite Crystal Fans in Neoproterozoic Cap Carbonates : a Case Study From Brazil and Implications for the Post – Snowball Earth Coastal Environment. J. Sediment. Res. 85, 285–300.
Vieira, L.C., Trindade, R.I.F., Nogueira, A.C.R., Ader, M., 2007b. Identification of a Sturtian cap carbonate in the Neoproterozoic Sete Lagoas carbonate platform, Bambuí Group, Brazil. Comptes Rendus - Geosci. 339, 240–258.
Walker, R.G., 2006. Facies models revisited: Introduction, in: Posamentier, H.W., Walker, R.G. (Eds.), Facies Models Revisited. Society of Sedimentary Geology, pp. 1–18.
Walker, R.G., 1992. Facies, facies models and modern stratigraphic concepts, in: Walker, R.G., James, N.P. (Eds.), Facies Models - Response to Sea Level Change. Geological Association of Canada, pp. 1–14.
Warren, L.V., 2011. Tectônica e sedimentação do Grupo Itapucumi (Neoproterozoico, Paraguai Setentrional). Universidade de São Paulo.
Warren, L. V., Fairchild, T.R., Gaucher, C., Boggiani, P.C., Poiré, D.G., Anelli, L.E., Inchausti, J.C.G., 2011. Corumbella and in situ Cloudina in association with thrombolites in the Ediacaran Itapucumi Group, Paraguay. Terra Nov. 23, 382–389.
Warren, L. V., Quaglio, F., Riccomini, C., Simões, M.G., Poiré, D.G., Strikis, N.M., Anelli, L.E., Strikis, P.C., 2014. The puzzle assembled: Ediacaran guide fossil Cloudina reveals an old proto-Gondwana seaway. Geology 42, 391–394.
Wei, H., Wang, X., Shi, X., Jiang, G., Tang, D., Wang, L., An, Z., 2019. Iodine content of the carbonates from the Doushantuo Formation and shallow ocean redox change on the Ediacaran Yangtze Platform, South China. Precambrian Res. 322, 160–169.
Williams, G.E., 1975. Late Precambrian glacial climate and the Earth's obliquity. Geol. Mag. 112, 441–465.
Williams, G.E., Gostin, V.A., McKirdy, D.M., Preiss, W. V., 2008. The Elatina glaciation, late Cryogenian (Marinoan Epoch), South Australia: Sedimentary facies and palaeoenvironments. Precambrian Res. 163, 307–331.
Wood, R.A., 2011. Paleoecology of the earliest skeletal metazoan communities: Implications for early biomineralization. Earth-Science Rev. 106, 184–190.
Wood, R.A., Grotzinger, J.P., Dickson, J.A.D., 2002. Proterozoic modular biomineralized metazoan from the Nama Group, Namibia. Science (80-.). 296, 2383–2386.
Xiao, S., Knoll, A.H., 1999. Fossil preservation in the Neoproterozoic Doushantuo phosphorite Lagerstatte , South China. Lethaia 32, 219–240.
Xiao, S., Laflamme, M., 2009. On the eve of animal radiation: phylogeny, ecology and evolution of the Ediacara biota. Trends Ecol. Evol. 24, 31–40.
Xiao, S., Narbonne, G.M., Zhou, C., Laflamme, M., Grazhdankin, D. V., Moczydlowska-Vidal, M., Cui, H., 2016. Towards an Ediacaran Time Scale: Problems, Protocols, and Prospects. Episodes 39, 540.
Xiao, S., Zhang, Y., Knoll, A.H., 1998. Three-dimensional preservation of algae and animal embryos in a neoproterozoic phosphorite. Nature 391, 553–558.
Xiao, S., Zhou, C., Liu, P., Wang, D., Yuan, X., 2014. Phosphatized Acanthomorphic Acritarchs and Related Microfossils from the Ediacaran Doushantuo Formation at Weng'an (South China) and their Implications for Biostratigraphic Correlation. J. Paleontol. 88, 1–67.
Yuan, X., Xiao, S., Zhang, L., Hua, H., Chen, Z., 2005. Skeletogenesis and asexual reproduction in the earliest biomineralizing animal Cloudina. Geology 33, 277.
Zhang, F., Xiao, S., Kendall, B., Romaniello, S.J., Meyer, M., Cui, H., Gilleaudeau, G.J.,

Kaufman, A.J., Anbar, A.D., 2018. Extensive marine anoxia during the terminal Ediacaran Period. Sci. Adv. 4, eaan8983.

Zhang, S., Jiang, G., Han, Y., 2008. The age of the Nantuo formation and Nantuo glaciation in South China. Terra Nov. 20, 289–294.

Zhou, C., Yuan, X., Xiao, S., 2002. Phosphatized biotas from the Neoproterozoic Doushantuo Formation on the Yangtze Platform. Chinese Sci. Bull. 47, 1918–1924.

Zhuravlev, A.Y., Liñán, E., Vintaned, J.A.G., Debrenne, F., Fedorov, A.B., 2011. New Finds of Skeletal Fossils in the Terminal Neoproterozoic of the Siberian Platform and Spain. Acta Palaeontol. Pol. 57, 205–224.

Apêndice A: Dados isotópicos e geoquímicos referentes às amostras estudadas

Tabela 1: Dados isotópicos e razões geoquímicas dos carbonatos da Fm. Sete Lagoas na área de Januária.

Sample		Facies	FA	^{13}C	^{18}O	[CAS]	$^{34}S_{CAS}$	Sr/Ca	Mg/Ca	Mn/Sr	Rb/Sr	Fe/Sr
JI 5X	MX	laminated microbialite	FA5	4.54	-6.41	21.24	48	0.00046	0.46	1.86	0.052	35.77
SB3/TS3 – amalgamated sequence boundary and transgressive surface												
JI 05 VA	MV	brecciated stromatolite	FA4	4.77	-4.45	34.12	-	0.00064	0.46	1.08	0.043	11.13
JI 5 U	MU	stromatolite	FA4	4.67	-6.19	49.95	44.70	0.00070	0.51	21.58	0.071	1.30
JI 5 T	MT	hydrothermal breccia	FA4	4.41	-4.59	105.35	-	0.00053	0.55	10.24	0.047	133.97
JI 5 S	MS	dolomitized trough cross stratified grainstone	FA4	4.12	-7.03	52.47	-	0.00050	0.56	3.33	0.036	66.44
JJ 17 M	AM	trough cross stratified ooidgrainstone	FA4	3.78	-5.41	42.13	33.40	-	-	-	-	-
JJ 17 L	AL	trough cross stratified grainstone	FA4	1.50	-4.72	13.12	-	0.00054	0.40	2.42	0.033	11.25
JI 05 R	MR	hydrothermal breccia	FA4	5.08	-6.95	1.51	-	-	-	-	-	-
JJ 17 K	AK	brecciated stromatolite	FA4	2.22	-7.19	9.20	-	0.00056	0.54	3.86	0.034	21.97
JI 5 Q	MQ	hydrothermal breccia	FA4	4.46	-9.82	31.55	-	0.00063	0.45	1.66	0.049	24.65
JJ 17 J	AJ	brecciated stromatolite	FA4	2.15	-6.97	9.20	-	-	-	-	-	-
JJ 17 I	AI	trough cross stratified grainstone	FA4	3.10	-5.49	20.34	-	-	-	-	-	-
JJ 17 H	AH	trough cross stratified grainstone	FA4	2.74	-6.98	19.02	-	0.00057	0.56	16.28	0.036	2.92
JI 5 P	MP	hydrothermal breccia	FA4	5.17	-6.45	5.56	-	-	-	-	-	-
JJ 17 G	AG	trough cross stratified grainstone	FA4	2.37	-6.71	12.83	-	-	-	-	-	-
JI 05 O	MO	planar cross stratified grainstone	FA4	4.60	-8.51	11.97	-	0.00033	0.13	0.77	0.041	14.70
JJ 17 F	AF	trough cross stratified ooidgrainstone	FA4	0.68	-6.87	30.55	36.30	-	-	-	-	-
JJ 17 E	AE	trough cross stratified grainstone	FA4	0.92	-9.63	12.63	-	-	-	-	-	-
JJ 17 D	AD	trough cross stratified grainstone	FA4	0.31	-10.43	15.06	-	-	-	-	-	-
JI 5 NB	MN	trough cross stratified grainstone	FA4	3.34	-8.43	32.66	-	0.00062	0.27	1.40	0.032	18.47
JJ 4 R	BR	dolomitized trough cross stratified grainstone	FA4	2.06	-7.39	11.69	-	-	-	-	-	-
JI 5 M	MM	cross-laminated grainstone	FA4	2.30	-9.67	10.37	-	-	-	-	-	-
JJ 17 C	AC	trough cross stratified grainstone	FA4	0.43	-9.97	17.44	-	0.00108	0.11	0.45	0.017	2.73
JJ 4 Q	BQ	dolomitized trough cross stratified grainstone	FA4	2.19	-8.66	9.47	-	-	-	-	-	-
JI 05 L	ML	trough cross stratified grainstone	FA4	1.89	-8.85	21.63	-	-	-	-	-	-
JJ 17 B	AB	grainstone?	FA4	0.43	-7.49	8.22	-	-	-	-	-	-
JJ 4 PA	BP	dolomitized laminated grainstone	FA4	0.42	-8.32	64.63	38.90	0.00158	0.03	0.07	0.013	2.46
JJ 17 A	AA	laminated grainstone	FA4	0.59	-7.26	15.49	-	-	-	-	-	-
JI 5 K	MK	cross-laminated grainstone	FA4	1.79	-8.53	78.07	-	0.00072	0.05	0.32	0.016	2.73
JI 5 J	MJ	trough cross stratified grainstone	FA4	1.96	-7.94	4.56	-	-	-	-	-	-
JI 5 I	MI	planar cross stratified grainstone	FA4	1.81	-7.76	20.70	-	0.00115	0.02	0.22	0.016	3.29
JJ 4 O	BO	laminated microbialite	FA4	0.03	-5.96	30.90	-	-	-	-	-	-
JI 5 H	MH	trough cross stratified grainstone	FA4	1.57	-7.66	9.89	-	-	-	-	-	-
JI 5 G	MG	laminated microbialite	FA4	1.45	-7.59	2.38	-	0.00082	0.14	0.31	0.024	4.29
JI 5 F	MF	low-angle stratified grainstone	FA4	1.51	-6.77	36.69	35.60	-	-	-	-	-
SB2/TS2 – amalgamated sequence boundary and transgressive surface												
JJ 4 N	BN	flat-pebble breccia	FA3	0.55	-7.40	18.92	-	-	-	-	-	-
JJ 4 M	BM	laminated microbialite	FA3	0.60	-6.71	40.67	43.90	-	-	-	-	-
JI 5 E	ME	laminated microbialite	FA3	1.20	-8.22	45.81	-	0.00074	0.04	0.31	0.026	4.87
JI 5 D	MD	laminated microbialite	FA3	1.13	-8.02	9.58	-	-	-	-	-	-
JJ 4 L	BL	flat-pebble breccia	FA3	0.70	-6.27	34.46	48.20	0.00245	0.02	0.05	0.009	0.69
JI 5 C	MC	trough cross stratified grainstone	FA4	1.18	-7.60	10.61	-	-	-	-	-	-
JI 5 B	MB	laminated microbialite	FA2	1.64	-7.04	12.43	-	0.00093	0.13	0.41	0.033	7.74
JI 05-A	MA	low-angle stratified grainstone	FA2	1.36	-6.87	2.16	-	0.00080	0.01	0.28	0.026	2.90
JJ 4 K	BK	thrombolite	FA2	0.50	-6.69	86.95	44.70	-	-	-	-	-
JJ 4 J	BJ	chert	-	-	-	-	-	-	-	-	-	-
JJ 4 I	BI	laminated microbialite	FA2	0.47	-4.75	26.04	42.00	-	-	-	-	-
JJ 4 H	BH	laminated microbialite	FA2	0.31	-6.28	24.14	-	0.00220	0.004	0.05	0.009	1.30
JJ 4 G	BG	oncolitic rudstone?	FA2	0.51	-6.41	88.48	43.20	-	-	-	-	-
JJ 4 F	BF	low-angle stratified grainstone	FA2	0.46	-6.28	-	-	0.00163	0.005	2.79	0.0141	0.07
JJ 4 E	BE	laminated grainstone	FA2	0.34	-6.62	50.18	41.50	-	-	-	-	-
JJ 4 D	BD	laminated grainstone	FA2	0.50	-6.73	23.75	44.90	0.00175	0.004	0.69	0.01298	0.06
JJ 4 C	BC	laminated grainstone	FA2	0.76	-6.36	15.15	-	-	-	-	-	-
JJ 4 B	BB	laminated grainstone or thrombolite	FA2	0.81	-5.87	42.90	47.10	0.00175	0.01	1.78	0.01301	0.06
JJ 4 A	BA	laminated grainstone	FA2	0.59	-6.41	44.78	48.60	-	-	-	-	-
JJ 7 M	RM	thrombolite	FA2	0.06	-6.82	127.00	36.60	0.00103	0.07	0.30	0.059	23.04
JJ 7 L	RL	cross-laminated grainstone	FA2	-0.30	-6.88	117.13	-	0.00091	0.02	0.29	0.04921	13.078
JJ 7 K	RK	cross-laminated grainstone	FA2	-0.97	-7.86	105.34	44.10	0.00079	0.03	0.99	0.076	21.41
JJ 7 J	RJ	thrombolite	FA2	-0.94	-8.54	124.29	45.10	0.00078	0.02	0.55	0.072	21.60
JJ 7 I	RI	cross-laminated grainstone	FA2	-0.88	-8.70	172.88	41.90	0.00066	0.02	0.82	0.077	20.75
JJ 7H	RH	cross-laminated grainstone w/ mudstone	FA2	-4.33	-11.94	125.80	37.20	0.00077	0.03	0.74	0.073	30.58
JJ 7G	RG	cross-laminated grainstone	FA2	-0.84	-8.15	172.24	42.80	0.00078	0.02	21.24	0.072	0.73
MFS 1- maximum flooding surface												
JJ 7F	RF	thrombolite	FA2	-1.30	-12.05	287.50	44.90	0.00060	0.02	1.24	0.069	11.82
JJ 7E	RE	aragonite fans	FA1	-3.76	-12.77	334.44	26.00	0.00050	0.02	8.13	0.092	27.02
JJ 7D	RD	cross-laminated grainstone w/ mudstone	FA1	-4.33	-11.94	332.41	27.50	-	-	-	-	-
JJ 7C	RC	cross-laminated grainstone	FA1	-4.71	-13.36	310.65	22.20	-	-	-	-	-
JJ 7B	RB	barite fans above carbonate	FA1	-3.15	-8.68	367.28	32.80	-	-	-	-	-
JJ 7A	RA	cap dolostone	FA1	-3.58	-7.09	167.45	22.80	0.00041	0.42	6.14	0.055	37.00
SB1/TS1 – amalgamated sequence boundary and transgressive surface												

Tabela 2: Elementos maiores e traço das amostras analisadas da Fm. Sete Lagoas. * = (ppm)

Sample	SiO_2	TiO_2	Al_2O_3	Fe_2O_3	MnO	MgO	CaO	Na_2O	K_2O	P_2O_5	LOI	Total	Ni*	Cu*	V*	Zn*	Ba*	Rb*	Sr*
JI 5X	0.06	0.02	0.25	0.57	0.03	20.88	38.03	-0.16	0.05	0.04	40.22	99.99	1	4	21	17	1	7	125
JI 05 VA	1.13	0.03	0.24	0.23	0.02	18.98	34.74	-0.15	0.03	0.03	44.74	100.01	2	13	23	48	25	7	158
JI 5 U	0.92	0.05	0.71	0.45	0.03	19.48	32.34	0.16	0.01	0.04	45.82	100.02	3	11	21	18	24	12	162
JI 5 T	0.32	0.02	0.17	2.14	0.16	21.20	32.55	-0.14	0.05	0.12	43.28	99.86	3	22	23	21	19	6	124
JI 5 S	0.10	0.01	0.02	0.99	0.05	21.58	32.25	-0.15	-0.01	0.04	44.94	99.82	4	2	19	15	3	4	115
JJ 17L	0.43	0.02	0.03	0.20	0.04	17.45	36.93	-0.15	0.01	0.19	44.70	99.86	2	12	21	269	7	5	141
JJ 17K	0.45	0.02	0.03	0.37	0.07	20.85	32.51	-0.17	-0.01	0.08	45.71	99.91	0	0	17	139	<2	5	131
JI 5Q	1.13	0.04	0.29	0.49	0.03	18.58	34.65	-0.12	0.08	0.05	44.81	100.04	2	6	25	21	15	8	155
JJ 17H	0.53	0.01	0.01	0.27	0.05	21.36	31.92	0.01	0.01	0.04	45.84	100.03	2	16	17	2323	16	5	129
JI 05 O	0.22	0.02	0.08	0.23	0.01	8.27	51.70	-0.13	-0.01	0.05	39.65	100.08	0	8	22	26	9	5	121
JI 5 NB	0.00	0.03	0.03	0.44	0.03	13.19	41.74	-0.11	0.00	0.04	44.48	99.88	6	8	29	36	16	6	185
JJ 17 C	0.04	0.01	0.04	0.13	0.02	6.27	49.55	-0.07	-0.01	0.09	43.95	100.04	6	8	39	74	24	7	383
JJ 4 PA	0.26	0.01	0.06	0.19	0.01	2.14	54.52	0.02	-0.01	0.09	42.70	99.98	6	4	45	42	21	8	616
JI 5 K	-0.07	0.02	0.02	0.10	0.01	3.26	53.35	0.02	-0.01	0.03	43.39	100.12	1	0	25	18	5	5	274
JI 5 I	6.60	0.01	0.07	0.18	0.01	1.14	51.74	0.08	0.00	0.04	40.13	100.01	7	8	42	32	28	7	424
JI 5 G	0.35	0.02	0.10	0.17	0.01	7.92	52.74	-0.04	0.01	0.09	39.28	100.63	6	8	38	30	17	8	308
JI 5 E	0.41	0.02	0.08	0.18	0.01	2.73	55.19	0.02	0.01	0.10	41.09	99.84	6	11	41	31	34	8	291
JJ 4 L	0.41	0.02	0.24	0.09	0.01	1.40	54.91	0.05	0.01	0.09	42.72	99.95	4	-4	42	31	44	9	963
JI 5 B	0.23	0.02	0.15	0.26	0.01	6.21	39.00	-0.06	0.00	0.12	53.97	99.92	7	9	38	29	21	9	259
JI 05-A	0.25	0.02	0.03	0.12	0.01	0.42	56.16	0.07	-0.01	0.06	42.83	99.97	6	11	44	33	22	9	322
JJ 4 H	-0.12	0.01	0.10	0.15	0.01	0.24	56.73	0.15	0.01	0.07	42.82	100.15	6	3	47	34	17	8	891
JJ 4 F	1.25	0.03	0.36	0.23	0.01	0.30	54.00	0.36	0.09	0.07	43.36	100.06	6	5	46	33	25	9	631
JJ 4 D	-0.11	0.02	0.07	0.06	0.01	0.29	56.04	0.08	0.01	0.05	43.51	100.02	8	5	46	38	36	9	701
JJ 4 B	0.13	0.02	0.15	0.16	0.01	0.97	55.25	0.06	0.00	0.05	43.40	100.19	7	3	47	34	34	9	692
JJ 7 M	12.09	0.09	1.69	0.94	0.01	3.73	43.33	0.04	0.60	0.06	37.47	100.07	8	10	42	34	40	19	319
JJ 7 L	7.75	0.08	1.15	0.54	0.01	1.19	49.58	0.09	0.20	0.08	39.32	99.99	8	12	46	38	56	19	252
JJ 7 K	14.97	0.10	1.70	0.69	0.03	1.40	44.40	0.10	0.63	0.06	35.86	99.96	8	11	48	38	51	16	321
JJ 7 J	11.33	0.11	1.75	0.73	0.02	0.85	47.39	0.14	0.35	0.05	37.35	100.09	9	11	48	36	41	19	264
JJ 7 I	8.62	0.09	1.54	0.62	0.02	1.04	49.06	0.11	0.26	0.08	38.71	100.16	8	9	45	30	34	18	232
JJ 7H	10.07	0.10	1.87	1.02	0.02	1.61	47.14	0.09	0.35	0.09	37.89	100.25	12	13	46	35	63	19	259
JJ 7G	10.65	0.12	1.81	0.75	0.03	1.05	49.24	0.12	0.48	0.06	35.69	100.00	9	12	47	34	41	20	273
JJ 7F	4.47	0.08	1.16	0.37	0.04	1.27	57.04	0.15	0.39	0.05	34.97	99.99	8	12	45	35	138	17	244
JJ 7E	5.26	0.09	1.28	0.64	0.19	0.99	50.97	0.10	0.38	0.07	39.86	99.84	7	13	50	36	141	17	183
JJ 7A	2.14	0.01	0.16	0.55	0.09	19.26	39.08	-0.16	0.06	0.04	38.80	100.03	4	37	19	14	17	6	116

Apêndice B: Co-autoria em artigos científicos relacionados ao tópico da tese: Inglez et al. (2019) Discs and discord: The paleontological record of Ediacaran discoidal structures in the South American continent. Journal of South America Earth Sciences, 89: 319-336.

Journal of South American Earth Sciences 89 (2019) 319–336

Contents lists available at ScienceDirect

Journal of South American Earth Sciences

journal homepage: www.elsevier.com/locate/jsames

Discs and discord: The paleontological record of Ediacaran discoidal structures in the south American continent

L. Inglez[a,*], L.V. Warren[a], J. Okubo[a], M.G. Simões[b], F. Quaglio[c], M.J. Arrouy[d], R.G. Netto[e]

[a] Departamento de Geologia Aplicada, Instituto de Geociências e Ciências Exatas, Universidade Estadual Paulista, Avenida 24A, 1515, Rio Claro 13506-900, Brazil
[b] Departamento de Zoologia, Instituto de Biociências, Universidade Estadual Paulista, Distrito de Rubião Júnior, Botucatu 18618-000, Brazil
[c] Departamento de Ecologia e Biologia Evolutiva, Universidade Federal de São Paulo, Rua Professor Artur Riedel, 275, Diadema, 09972-270, Brazil
[d] Centro de Investigaciones Geológicas, UNLP-CONICET, calle 1, n. 644, La Plata 1900, Argentina
[e] Programa de Pós-Graduação em Geologia, Universidade do Vale do Rio dos Sinos - UNISINOS, São Leopoldo, RS, Brazil

ARTICLE INFO

Keywords:
Ediacaran biotas
Ediacaran geobiology
Biogenicity criteria
Dubiofossils

ABSTRACT

Discoidal sedimentary structures are commonly described in Proterozoic strata, and even more common in Ediacaran to lower Cambrian sedimentary successions. Many abiotic processes are able to produce such circular or discoidal structures in bedding planes, however, their abundance in Ediacaran strata suggests a possible correlation with the evolution and preservation of epibenthic metazoans that emerged at the end of this period. In the South American paleontological record, studies regarding the Ediacaran soft-bodied organisms are meager and restricted to few reports in Brazil, Paraguay, and Argentina. In many cases, such "fossils" were only tentatively characterized in terms of their general morphology and putative taxonomic affinity. Thus, considering the almost absence of work on these enigmatic structures in South America, this paper aims to make a critical analysis on the main occurrences of Ediacaran-Cambrian discoidal structures described in this continent. Based on a detailed review and unpublished data, it was possible to provide a general picture concerning the main paleoenvironmental and sedimentary significance of this structures, as well as on the most promising prospects in terms of the paleontological record of Ediacaran soft-bodied metazoans in South American. In this sense, it was settled that occurrences such as those in the Jaibaras and Itajaí basins should be reassessed in order to establish reliable criteria of biogenicity. In the case of the material from the Sete Lagoas and Tagatiya Guazu formations, it is considered more parsimonious to interpret the discoidal features as resulting from microbial processes. Similarly, the discoidal structures of the Cerro Negro Formation presents a series of internal laminations and textures that resembles those developed by processes of microbial grain binding and trapping suggesting that, at least part of this material, can be related to microbially induced sedimentary structures. Finally, for the ichnologically diversified Puncoviscana and Camaquã basins, two different scenarios were identified. The first presents an ichnological assemblage strongly indicative of lower Paleozoic, and possibly Cambrian affinity. Thus, the discs in association with these traces, should be viewed with caution and interpretations made in light of a Paleozoic context. The second possesses an ichnological association typical of that expected for the Ediacaran-Cambrian transition, and the diversity of discoidal forms can potentially represent imprints of macroorganisms on a microbially bounded substrate, thus deserving a more detailed approach.

1. Introduction

Sedimentary structures of discoidal or circular morphology (in plan view) are considerably common in the geological record. When resulted from abiotic processes they may represent raindrop impressions (Moussa, 1974; Metz, 1981) or fluid escape features (Pringle et al., 2007; Põldsaar and Ainsaar, 2014), among other structures. When related to the direct or indirect effect of biological activity they represent trace fossils (e.g., Actiniarian resting traces, Alpert, 1973, or invertebrate feeding radial structures, Strzebonski and Uchman, 2015), microbial structures (Grazhdankin and Gerdes, 2007; Menon et al., 2016) or even impressions of macrofossils (see for example, the revision of MacGabhann, 2007, on "Ediacaran discoidal fossils"). They are commonly described in Proterozoic rocks (e.g., Callow et al., 2011; El Albani et al., 2014; Anderson et al., 2016), especially in Ediacaran strata, where they are often interpreted as molds and/or impressions of

* Corresponding author.
E-mail address: lucas.inglez@unesp.br (L. Inglez).

https://doi.org/10.1016/j.jsames.2018.11.023
Received 5 July 2018; Received in revised form 20 November 2018; Accepted 26 November 2018
Available online 27 November 2018
0895-9811/

soft-bodied macroscopic organisms of Ediacaran biotas (e.g., Glaessner and Walter, 1975; Hofmann, 1971; Narbonne and Hofman, 1987; Waggoner, 2003; Clapham et al., 2003; McCall, 2006; Macgabhann, 2007, 2014). Soft-bodied macroorganisms of these biotas are usually preserved under exceptional taphonomic conditions, in distinct sedimentary marine settings (Seilacher et al., 2005; Waggoner, 2003; Shen et al., 2008; Arrouy et al., 2016, but see Retallack, 2012a,b, for a distinct interpretation). Although including forms with a high degree of morphological disparity, they are anatomically simple and lack common stem-group synapomorphies, making it difficult to establish clear phylogenetic relationships with Phanerozoic clades (Seilacher, 1992; Buss and Seilacher, 1994; Droser and Gehling, 2015), though petalonamid forms are pointed as sister-group to Eumetazoa (Hoyal Cuthill and Han, 2018). However, evidences demonstrated that some of the forms previously identified as Ediacaran discs, are in fact related to the interaction of benthic microbial populations with physical sedimentary processes (Seilacher et al., 2005; Van Loon, 2008; Hagadorn and Miller, 2011; Menon et al., 2015, 2016) or even the structuring of microbial colonies as pristine multicellular aggregates (Grazhdankin and Gerdes, 2007; Bobrovskiy et al., 2018).

In the South American continent, studies regarding the Ediacaran soft-bodied fossils are meager and restricted to preliminary reports (see the revision of Kerber et al., 2013, on the record of South American Ediacaran Metazoan) of occurrences in Brazil (Paim et al., 1997; Zucatti da Rosa, 2005; Drefahl and Silva, 2007; Netto, 2012; Barroso et al., 2014), Paraguay (Warren et al., 2011), and Argentina (Acenolaza and Acenolaza, 2007; Arrouy et al., 2016). Indeed, in many cases the “fossils” were only tentatively characterized in terms of their general morphology, with putative taxonomic classification made by comparison with typical specimens from classic localities of the Ediacaran biota (Zucatti da Rosa, 2005; Acenolaza and Acenolaza, 2007; Drefahl and Silva, 2007; Barroso et al., 2014). Hence, key issues concerning these “fossils”, such as the modes of occurrences, their biotic *vs.* abiotic origin, and stratigraphical distribution and correlation were not explored in its full potential.

Considering the relevance of these data to unveil key paleobiological issues of the Ediacaran-Cambrian transition, critical revisions are particularly worthy in the light of new discoveries and interpretations (see Fairchild et al., 2012 and Becker-Kerber et al., 2013 for revisions with different emphasis within this theme). In this sense, this contribution aims to make a critical review on the main occurrences of discoidal structures of the Ediacaran-Cambrian transition described in the sedimentary record of the South American terrains. The main goal is to provide a general picture of what has been described and presented as occurrences of members of Ediacaran soft-bodied clades, especially discoidal forms. Since the abiological origin of these structures cannot be ruled out, in this contribution we (a) discuss the appropriate biogenicity criteria to be applied in the description and interpretation of these problematic structures; (b) raise critical questions concerning the interpretations of those structures, by discussing their relevance as tools for paleoenvironmental and paleoecological reconstitutions of the South American Ediacaran-Cambrian successions, and (c) identify sites with great potential for future scientific prospects concerning the Ediacaran-Cambrian paleontology in this continent.

2. The discoidal structures in the Ediacaran record: a historical review

Structures interpreted as fossils of discoidal morphology are relatively common in some Ediacaran successions, as those from the classical Avalon and White Sea assemblages (McCall, 2006). Despite of that, their significance in terms of evolutionary affinities and the preservational taphonomic pathways are far from being fully understood (McCall, 2006; MacGabhann, 2007). Advances in the past two decades paved the idea that the discoidal structures are mainly molds and impressions of a bulbous-like holdfast of a group of benthic sessile metazoans (Gehling et al., 2000; MacGabhann, 2007; Tarhan et al., 2010, 2015; Dzik and Martyshyn, 2017), mainly referred to the *Aspidella*-plexus, and the genera *Charniodicus* sp. and *Eoporpita* sp., among others.

The first descriptions of Ediacaran discoidal structures date back to the 19th century, with the discovery of simple circular impressions on Proterozoic successions in Long Mynd (Salter, 1856) and Charnwood Forest, United Kingdom (Eskrigge, 1868), and in Newfoundland, Canada (Billings, 1872). These authors described the specimens in terms of general morphology, highlighting their possible biological origin, and interpreting them as either putative worm burrows (Salter, 1856), impressions of holdfasts of some sort of macroalgae (Eskrigge, 1868, but see Howe et al., 2012, for further discussion regarding the first descriptions of such enigmatic features) or even possible invertebrate fossils of uncertain biological affinity (Billings, 1872). However, these findings and interpretations were viewed as very unlikely, given the dominant idea at that time that macrofossils should be absent in Precambrian strata (Howe et al., 2012). Therefore, subsequent studies either ignored the presence of these structures, or considered them non-organic (Hill and Bonney, 1877; Weston, 1892; Watts, 1947).

The views above started to change with further discoveries of discoidal structures in the Ediacaran-Cambrian successions from the Flinders Ranges and Mount John, Australia. Based on their external morphology, the Australian discs were considered as impressions of pelagic, soft-bodied cnidarian scyphozoans (or possibly hydrozoans) (Sprigg, 1947, 1949). Therefore, this interpretation introduced new ideas and issues to the discussion about the biological meaning of those discoidal structures (Sprigg, 1947, 1949). In this context, Sprigg (1947, 1949) proposed several new taxa to accommodate such structures, including: *Beltanella gilesi*, *Cyclomedusa davidi*, *Ediacaria flindersi*, *Protodipleurosoma wardi*, and *Tateana inflata.* All these taxonomic names would be extensively applied to morphologically similar discoidal structures in the upcoming literature regarding these Ediacaran fossils not only in Australia (Glaessner and Wade, 1966; Wade, 1969, 1972), but also in Canada (Hofmann et al., 1983, 1985; Narbonne and Hofman, 1987), and Russia (Fedonkin, 1978, 1980). Standing on the occurrences from these localities new species were erected based on slight morphological variations of the discoidal structures referred to already established genera (e.g., *Beltanella*, *Cyclomedusa*, *Ediacaria*).

Another advance regarding the nature of the discoidal structures was made with the discovery (or more properly, re-description, Howe et al., 2012) of the Precambrian fossils in the region of Charnwood Forest, England (Ford, 1958). At this locality, as well as in Australia and South Africa, discoidal fossils were observed in association with frond-like structures (foliate or leaf-like structures composed of segmented lobe sets that alternates on either side of a central axis) (Glaessner, 1959; Glaessner and Wade, 1966; Jenkins and Gehling, 1978). In some specimens the fronds appeared to be attached to a circular or discoidal structure by a stalk (Ford, 1958; Glaessner, 1959). This suggested that the two elements were, indeed, different anatomical parts of the same organism, providing the fossils a general body plan similar to that of modern pennatulaceans (Glaessner, 1959; Glaessner and Wade, 1966). Nevertheless, only a few specimens showed the connection between these two structures and, in some assemblages, discoidal taxa were described without any association to fronds of any type (e.g., *Beltanneliformis* sp., Menner, 1963; *Nemiana* sp. Palij, 1976), suggesting that many of these discs could represent distinct biological entities (MacGabhann, 2007).

As more material was being uncovered, new evidences came up and helped to explain the nature and affinities of those discoidal fossils. Descriptions of specimens from the Ediacaran succession of the Mackenzie Mountains, Canada, allowed the proposal of new taxonomic entities, and novel paleobiological hypotheses (Hofmann et al., 1981; 1983, 1985). Researchers started questioning the cnidarian affinity of discoidal forms, as well as their pelagic mode of life (Seilacher, 1984; McMenamin, 1986; Narbonne and Hofman, 1987). In a critical review, Sun (1986) suggested that many occurrences previously interpreted as metazoan fossils could be possibly reinterpreted as abiotic structures. Yet, the author also proposed that numerous specimens would represent taphonomic variants of the same given group of medusoid organisms. Based on this plea, Sun (1986) erected the *Cyclomedusa*-plexus (Sun, 1986).

This interpretation was only reconsidered recently with the erection of the *Aspidella*-plexus by Gehling et al. (2000). This proposal is in accordance with the taxonomic nomenclature and considers the first genus described by Billings (1872), namely *Aspidella terranovica.* Alike the *Cyclomedusa*-plexus, the *Aspidella*-plexus comprises a series of taphonomically-derived morphological variants (*i.e.*, taphotaxons, *sensu* Lucas, 2001), which does not necessarily represent distinct taxa. Furthermore, the *Aspidella*-plexus includes various previously described genera (e.g. *Cyclomedusa*, *Ediacaria*, *Spriggia*) that are junior synonyms of *Aspidella* (see Gehling et al., 2000). Still, the current interpretations recognize that most discoidal fossils would represent molds and impressions of attachment structures (*e.g.*, holdfasts) of sessile benthic organisms (Gehling et al., 2000; Tarhan et al., 2010, 2015). This same interpretation was given to some taxa, such as *Charniodiscus* sp., and other frond-like fossils (Ford, 1958; Glaessner, 1959). However, the *Aspidella*-plexus should include specimens with no preserved fronds, or other structures that allow a more precise taxonomic assignment (Gehling et al., 2000).

In the last two decades, some studies focused on this new taphonomic/taxonomic paradigm, by proposing new models for the preservation of the discoidal structures (Mapstone and McIlroy, 2006; Liu, 2016; Tarhan et al., 2010, 2015; Retallack, 2016) also discussing their nature and morphological variants (Tarhan et al., 2010, 2015).

Following the definition of the *Aspidella* plexus, some important taxonomic or paleobiological interpretations were presented for these Ediacaran discoidal fossils. One example is the evidence of horizontal and vertical movement described in *Aspidella terranovic*a in the type locality (Menon et al., 2013). Fossils include short traces, with crescent ridges and raised margins terminating in discs with radial grooves and central elevated pimp typical of *Aspidella* (Menon et al., 2013). In addition, polished slabs revealed a laminated patter above the plane where fossils are preserved (as hyporelief features), similarly to meniscus-like structures produced during vertical adjustments of an organism. Both observations point to an eumetazoan affinity for the originally described taxon *Aspidella terranovica* (Menon et al., 2013).

Nevertheless, once the *plexus* (as suggested by Gehling et al., 2000) would assemble forms of different localities and ages, as well as distinct environments, it is very unlike that they all represent only one biological group (see MacGabhann, 2007, for a detailed discussion). Therefore, the extensive use of the term *Aspidella* to refer to discoidal fossils and interpret them as holdfasts of frondose organisms should be made with caution (see MacGabhann, 2007). On the other hand, recent analysis focused on biometrical comparisons between discs preserved with distinct styles in distinct assemblages (Burzynski and Narbonne, 2015). Their results demonstrated a positive correlation between disc size and frond size (when preserved), suggesting that the majority of discoidal markings (even when dissociated from fronds or stem-like features) probably functioned as tethering structures to frondose organisms (Burzynski and Narbonne, 2015).

Finally, the advances in the last years regarding the dynamics of benthic microbial communities have widened the array of possible sedimentary structures developed and/or preserved in modern and ancient depositional environments (Noffke et al., 1996, 2001, 2003, 2009; Hagadorn and Bottjer, 1997; Noffke and Krumbein, 1999, but see Davies et al., 2016, for a recent revision and discussion). Considering the influence of bio-stabilization by microbial communities, diverse physical and/or biological processes are able to produce (or enhance) the preservation of circular or discoidal structures in distinct sedimentary settings. Such structures can include gas or fluid escape structures (Callow et al., 2011; Van Loon and Maulik, 2011; Taj et al., 2014; Menon et al., 2015, 2016; Tu et al., 2016), liquefaction or overload features (Kahle, 2009), as well as microbial constructions (Grazhdankin and Gerdes, 2007; Ivantsov et al., 2014; Bobrovskiy et al., 2018). This led various authors to reinterpret many discoidal structures originally interpreted as fossils, as inorganic or microbially-induced sedimentary structures (Seilacher et al., 2005; Van Loon, 2008; Hagadorn and Miller, 2011; Menon et al., 2015, 2016).

The advances in the study of Ediacaran discoidal forms, and the changing trend on the study of this enigmatic group of fossils or abiotic structures over the last 150 years are summarized in Table 1.

Table 1
Interpretation of discoidal structures through time.

Authors	Interpretations
Eskrigge (1868) Billings (1872)	First descriptions of discoidal fossils in Precambrian strata
Hill and Bonney (1877) Weston, 1892 Watts, 1947	Denial of a biological origin for the discoidal features
Sprigg (1947), 1949 Ford (1958) Glaessner (1959)	Description of fossils from the Flinders Ranges, Australia and interpretation of discs as impressions of medusoid cnidarians.
Glaessner and Wade (1966) Wade (1969), 1972	Description of frond-like fossils in association to discoidal features. Proposal of taxa such as *Charnia* and *Charnioduscus* Ford
Seilacher (1984) McMenamin (1986) Sun (1986)	Questioning about the cnidarian affinity of discoidal fossils, their biogenicity and taxonomic significance of morphological variation among them.
Noffke, 2009 Hagadorn and Bottjer (1997) Noffke et al. (2001)	Proposition of microbially induced features (MISS - microbially induced sedimentary structures) as a new class of sedimentary structures
Gehling et al. (2000) MacGabhann (2007) Tarhan et al., (2010), 2015	Proposition of the *Aspidella* -plexus. Synonymization of several taxa as taphonomic variations among a diversified group of organisms.
Seilacher et al. (2005) Grazhdankin and Gerdes, 2007 Van Loon, 2008 Hagadorn and Miller (2011) Menon et al., (2015), 2016	Reinterpretation of many taxa as microbially influenced sedimentary structures

3. Ediacaran-Cambrian discs of the South American continent

Occurrences of Ediacaran-Cambrian discoidal structures in South America are known from various localities from Brazil, Paraguay, and Argentina. The most diverse one is that from the Jaibaras Basin, Brazil, including discoidal structures as well as supposed fossil impressions of other groups also found in classical marine Ediacaran assemblages as the White Sea assemblage, Russia (Barroso et al., 2014). Discoidal structures from Argentina are found in the Cerro Negro Formation, La Providencia Group, where they occur in great numbers and variable sizes in some strata (Arrouy et al., 2016). Despite the recent advances in our knowledge of these discoidal structures in Argentina, their origin is still under discussion (Inglez, 2018). On the other hand, the Paraguayan record is limited to the occurrences of the Tagatiya Guazu Formation (Warren et al., 2011).

A brief overview on the Ediacaran-Cambrian discs of South America continent is presented below. The occurrences are listed according to the present geographical distribution of the disc-bearing lithostratigraphic units and are summarized in Table 2, which includes additional biostratigraphical and geochronological data for each localitiy. Fig. 1 illustrates the geographical location of each of these units, while in Fig. 2 schematic columns with the tentative age correlation among localities are shown.

Table 2
–The record of Ediacaran discoidal structures in the South America terrains. Data for each basin and locality is correlated with their aging constraint, their putative fossil record along with general depositional settings described for disc bearing units.

Occurrences	Unit	Age (method)	Sedimentary facies	Depositional system	Type of discoidal structure	Fossil Assemblage	References
Punconviscana Basin, Argentina	Puncoviscana Fm.	530-560 Ma (detritic zircon) 536 -534 Ma (plutonic intrusions)	Conglomerates, sandstones, turbidites, shales and limestones	Shelf, shelf-edge and slope deposits	*Beltanelliformis* sp., *Sekwia* sp., *Nemiana* sp., *Selkirkia* sp., (=*Sphenotallus*? sp.) revised as belonging to *Beltanelloides* sp.	*Archaeonassa* isp., *Asaphoidichnus* sp., *Cochlichnus* isp., *Didymaulichnus* isp, *Dimorphichnus* isp., *Diplichnites* sp., *Glockerichnus* sp., *Helminthoidichnites* isp., *Monomorphichnus* isp., cf. *Multipodichnus* isp., *Nereites* isp., *Oldhamia* isp., cf. *Thalassinoides* isp., *Palaeophycus* isp., *Protochnites* isp., *Protovirgularia* isp., *Tasmanadia* isp., *Treptichnus* isp.	Aceñolaza (2004); Aceñolaza and Aceñolaza (2007)
Tandilla system, La Providencia Group, Argentina	Cerro Negro Fm.	580 - 542 Ma (Leiosphaeridia Palynoflora)	Massive fluidized sandstone beds	Sub to infra tidal flats environment	*Aspidella*-plexus (?)	*Synsphaeridium* sp., *Trachysphaeridium* sp., *Leiosphaeridia* sp.	Gaucher et al. (2005); Arrouy (2015); Arrouy et al. (2016)
Itapucumi Group	Tagatiya Guazu Fm.	550-542 Ma (Cloudina biozone)	Thrombolites	Carbonatic ramp, inner laggon	Gas domes (?)/cf. *Nimbia* sp.	*Cloudina* sp., *Corumbella* sp., *Namacalathus* sp., Archaeonassa isp, non identified tubular structures.	Warren et al. (2011, 2012, 2014, 2017)
Camaquã Basin, Brazil	Santa Bárbara Allogroup	559-540 Ma	Sandstone beds of braidplain delta facies association	Progradation of braidplain deltas and fandeltas into shallow, most lacustrine environments	*Beltanelliformis* isp., *Aspidella* sp., *Intrites* sp., *Sekwia* sp.	*Cochlicnus* isp., *Planolites* isp., *Palaeophycus* isp., *Treptichnus* isp., *Arthraria* isp.	Paim et al. (2000); Netto (2012)
Itajaí Basin, Brazil	Sequence 2B?	581 ± 48 Ma (Rb/Sr)	(0.5 m-thick) Normal graded, thinly-bedded siltstones and claystones	Product of low-density turbidity currents deposited in interchannel areas of a submarine-fan complex	*Aspidella* sp., *Cyclomedusa*? sp., *Charniodiscus*? sp. *Helminthoidichnites* isp.	*Chancelloria* sp., *Choia* sp., *Parvancorina* sp.	Paim et al. (1997); Zucatti da Rosa (2005); Netto (2012)
Camarinha Basin, Brazil	Camarinha Fm.	432.8 ± 6.3 and 437.7 ± 2.5 Ma (Rb/Sr) 505 ± 10 and 478 ± 10 Ma (K/Ar)	Conglomerates, breccias, sandstones, siltstones and mudstones	Gravity flows, turbidity current, sheet floods of fandeltas	*Beltanelliformis* sp.	*Gordia* isp., *Planolites* isp., *Skolithos* isp.	Ciguel et al. (1992); Drefahl and Silva (2007); Netto (2012)
São Francisco Basin, Brazil	Bambuí Gr., Sete Lagoas Fm.	710 Ma (Pb–Pb) 557 Ma (U–Pb) 550-542 Ma (*Cloudina* biozone)	Thrombolites	Marine shallow-water	*Bambuilithos teixeranus*, *Bambuites erichseni*	*Cloudina* sp., *Corumbella* sp.	Paula-Santos et al. (2014); Sommer (1971, 1981, 1982); Vieira et al. (2007); Warren et al. (2014)
Jaibaras Basin, Brazil	Contra Fogo Sandstone (Pacujá Fm.?/Ipu Fm.	562 + 19 Ma Rb/Sr (introded dyke at Ubajara Gr.)	Coarse, strongly silicified and immature sandstone	Fluvio-marine system	*Charniodiscus arboreus*, ?*Charniodiscus concentricus*, *Cyclomedusa davidi*, *Ediacaria flindersi*, *Medusinites asteroides*	*Kimberella* sp., *Bavlinella* sp., *Leiospheridia* sp.	Barroso et al. (2014); Chiglino et al. (2015)

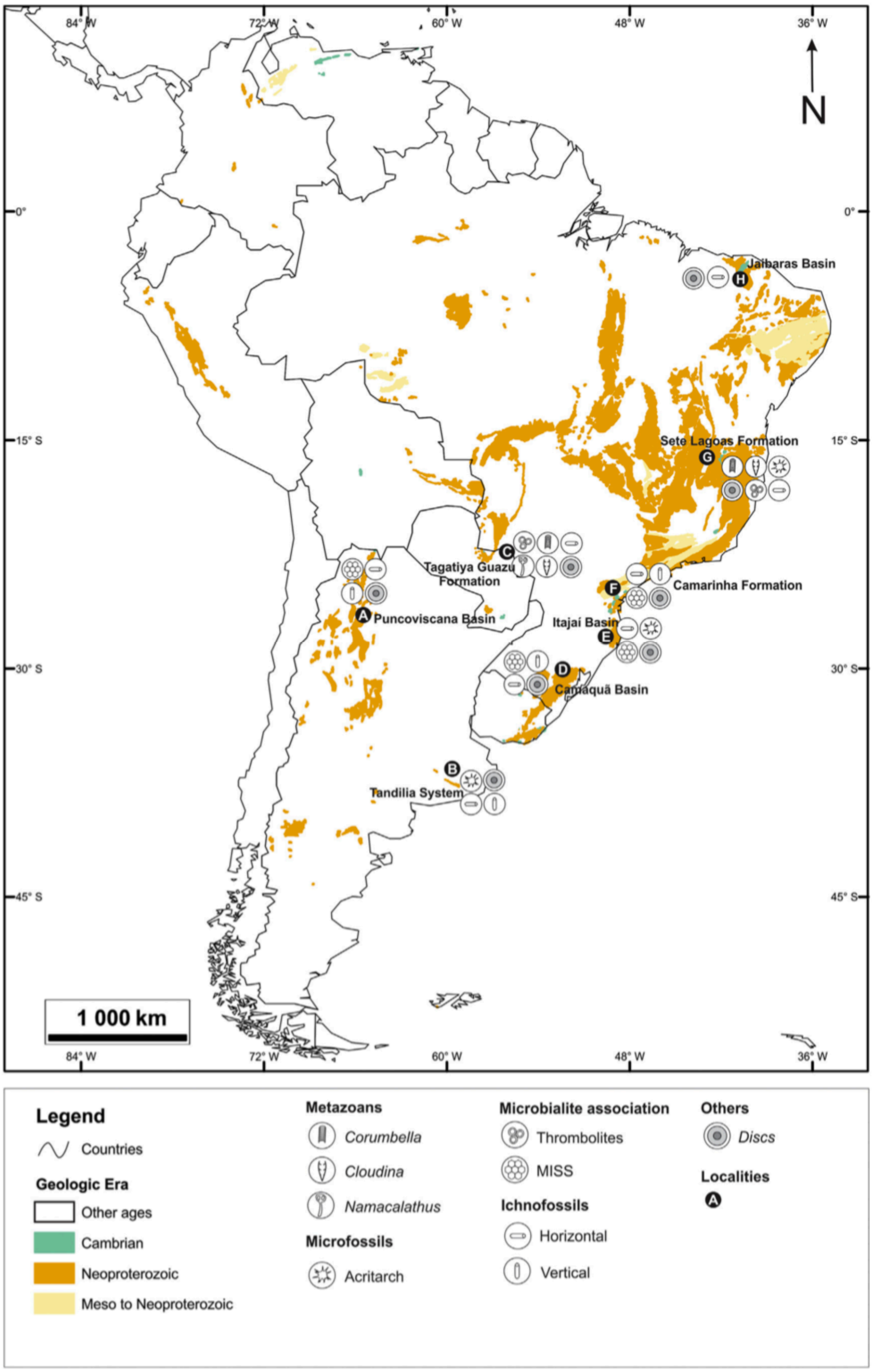

(caption on next page)

Fig. 1. Map of Proterozoic to Cambrian geologic units of South America highlighting the occurrence of discoidal structures, metazoans, microfossils and other main paleontological components. 1 – Tandilla System, La Providencia Group (AR), 2 – Puncoviscana Basin (AR), 3 – Itapucumi Group (PY), 4 – Arroyo del Soldado Group (UY), 5 – Camaquã Basin, Santa Barbara and Bom Jardim groups (BR), 6 – Camarinha Basin (BR), 7 – Itajaí Basin (BR), 8 – Corumbá Group (BR), 9 – Murciélago Group (BO), 10 – Araras Group (BR), 11 – Bambuí Group (BR), 12 – Jaibaras Basin (BR). Based in Sommer (1971), Ciguel et al. (1992), Netto et al. (1992), Paim et al. (1997), Aceñolaza (2004), Zucatti da Rosa (2005), Drefahl and Silva (2007), Netto (2012), Warren et al. (2011, 2014), Barroso et al. (2014), Sanchez (2014), Arrouy et al. (2016), Inglez et al. (2016).

3.1. Puncoviscana Basin – Puncoviscana Formation (northwestern Argentina) (A)

In the central Andean region of South America, the Neoproterozoic to Early Cambrian sequence correspond to siliciclastic succession of the Puncoviscana Formation, which is best exposed in northwestern Argentina (Figs. 1 and 2). It consists of an up to 2000-m-thick, intensely folded, slightly metamorphosed succession of slates and schists deposited in diverse sedimentary environments (Aceñolaza and Durand, 1986; Jezek, 1990; Aceñolaza et al., 1999). Due to the structural particularities of the Puncoviscana Formation, is difficult to determine its precise depositional age and establish the correlation with other coeval units, and a major effort is necessary to integrate stratigraphic, geochronological and paleontological data in order to envisage the precise timing of deposition of this unit (Acenolaza and Acenolaza, 2007). Based on detrital zircon grains, Lork et al. (1990) suggested a maximum age of 530 Ma, whereas other authors dated intrusive plutonic bodies between 536 ± 7 Ma and 534 ± 9 Ma and metamorphic events around 530 and 540 Ma (Bachmann et al., 1987; Adams et al., 1990) (Table 2). The Puncoviscana Formation (Figs. 1 and 2) records a diverse ichnofauna, with different trace fossils typical of locomotion (trails and tracks), as well as feeding and grazing furrows (Acenolaza and Acenolaza, 2007). This association, marked by the ichnogenera *Archaeonassa* isp, *Nereites* isp., *Oldhamia* isp., *Thalassinoides* isp., *Paleophycus* isp. and *Treptichnus* isp. (see Table 1, for a complete list of ichnogenera), suggest an early Cambrian age for the unit and denotes a significant biological activity in the shallow substrate (Durand and Aceñolaza, 1990; Aceñolaza and Tortello, 2003; Buatois and Mángano, 2003; Acenõlaza, 2004; Seilacher et al., 2005).

The record of body fossil impressions is limited to few occurrences associated to deposits of shallower facies (within the *Nereites* association) and are represented by enigmatic forms belonging to *Selkirkia* sp. and *Beltanelloides* sp. (Acenõlaza and Durand, 1973; Acenolaza and Acenolaza, 2007). *Selkirkia* sp. (reinterpreted as such by Acenolaza and Acenolaza, 2007, previously considered *Sphenothallus*? sp., in Acenõlaza, 2004) is a tube-like fossil, preserved as a flattened impression preserved in fine-to medium-grained sandstones and interpreted as an annelid-related organism (Acenõlaza, 2004). *Beltanelloides* sp. (Acenolaza and Acenolaza, 2007 but previously considered as an ichnofossil and identified to the taxon *Beltanelliformis* isp. by Acenõlaza and Durand, 1973) occurs in the same succession. It is characterized as an isolated discoidal protrusion of 10–50 mm in diameter with a well-developed central depression (Acenolaza and Acenolaza, 2007) (Fig. 3A). The fossil would represent molds and impressions of a soft-bodied spherical organism, filled with sediment after obrution by fine-grained sediments (Leonov, 2007, but see the discussion presented by Ivantsov et al., 2014; Bobrovskiy et al., 2018). This taphonomic model is typical of that observed in the context of preservation of Ediacaran macroorganisms (Waggoner, 2003; Clapham et al., 2003; McCall, 2006; MacGabhann, 2007). Thus, its presence in association with an ichnological assemblage typical of lower Paleozoic settings is worthy to be further investigated.

3.2. Rio de La Plata Craton – La Providencia group, Cerro Negro formation (Argentina) (B)

The La Providencia Group occurs at the south of Buenos Aires Province, Argentina (Figs. 1 and 2), comprising the youngest Neoproterozoic unit exposed in the tectonic province of the Tandilia System (Pankhurst et al., 2003; Cingolani, 2011; Poiré, 2002). This unit is composed of a ~40 m thick carbonate package of greenish laminated mudstones, with occasional ripple cross-lamination in the first 8 m, and black thinly laminated mudstones in its upper portion (Gómez-peral et al., 2017,2018). The ages of this unit has been inferred based on the presence of fragments of what seems to be bioclastic material, suggested by Gaucher et al. (2005) to be skeletal remains of cf. *Cloudina riemkeae,* implying ages between 550 and 542 Ma (Fig. 2). Also, chemostratigraphical trends of $\delta^{13}C$ values correlate this unit to a global pattern observed in Ediacaran successions, suggesting ages between 590 and 580 Ma (Gómez-Peral et al., 2007). More recently, the unit was considered to be Late Ediacaran due to its microfossil assemblage, which includes sphaeromorphous acritarchs, such as *Synsphaeridium* sp., *Trachysphaeridium* sp. and *Leiosphaeridia* sp. (Gaucher et al., 2005; Arrouy, 2015). In addition, the presence of abundant discoidal structures interpreted as taphonomic variants of holdfasts within the *Aspidella* plexus (Arrouy et al., 2016) was also used to infer an Ediacaran age for the upper part of this unit. In turn, the La Providencia Group lies over an erosive unconformity developed at the top of the Loma Negra Formation, Sierras Bayas Group (Fig. 2) (Arrouy et al., 2015).

The La Providencia Group was recently subdivided in three lithostratigraphic units including, in ascending order, the Avellaneda, Alicia and Cerro Negro Formations (Arrouy et al., 2015). The Avellaneda Formation is composed of argillites with significant carbonate contributions, with increasingly siliciclastic content upwards, which is interpreted as deposited in a low energy environment (Arrouy et al., 2015). This unit is succeeded by dark colored, organic-rich shales and mudstones of the Alicia Formation that were deposited in distal, low energy subtidal settings, under transgressive conditions (Arrouy, 2015).

The Cerro Negro Formation lies above an erosive unconformity over Alicia Formation and comprises a 75 m-thick package of sandstones with cross stratification, tidal bundles, wavy cross lamination, heterolithic beds and massive, reddished mudstones. The close association of sedimentary facies deposited by tractive currents and suspension, as well as evidences of occasional subaerial exposure, led Arrouy et al. (2015) to interpret this unit as deposited in inter-to subtidal settings. Notably, the Cerro Negro Formation has abundant and diverse MISS (Microbially Induced Sedimentary Structure, *sensu* Noffke, 2001 structures associated with fine micaceous sandstone facies. MISS include 'Kinneyia', which are characterized by well-developed parallel millimetric ridges and 'Honeycomb-structures', with typical round to slightly elongated pits between discrete crests (Porada and Bouougri, 2007; Porada et al., 2008). In addition, the 'Arumberia-structure' is another common feature recorded in this unit, which is indicative of a complex microbial community (Kolesnikov et al., 2012).

The Cerro Negro Formation is also rich in discoidal structures that are densely distributed in the upper part of very fine massive sandstone beds rich in synsedimentary deformation structures (Fig. 3B–D). However, a great portion of discs cannot be securely oriented due to the remobilized nature of the rock slabs containing the discs that are available in the quarries (Arrouy et al., 2016). Arrouy et al. (2016) described part of these discoidal forms and assigned them to the *Aspidella*-plexus type-morph, mainly based on morphological similarities and size-class distribution patterns observed in the field. The discs are characterized as positive epirelief structures that vary between 6 mm and 140 mm in diameter. They are tridimensionally preserved and are marked by a smooth oxidized upper surface (Fig. 3B), commonly with a

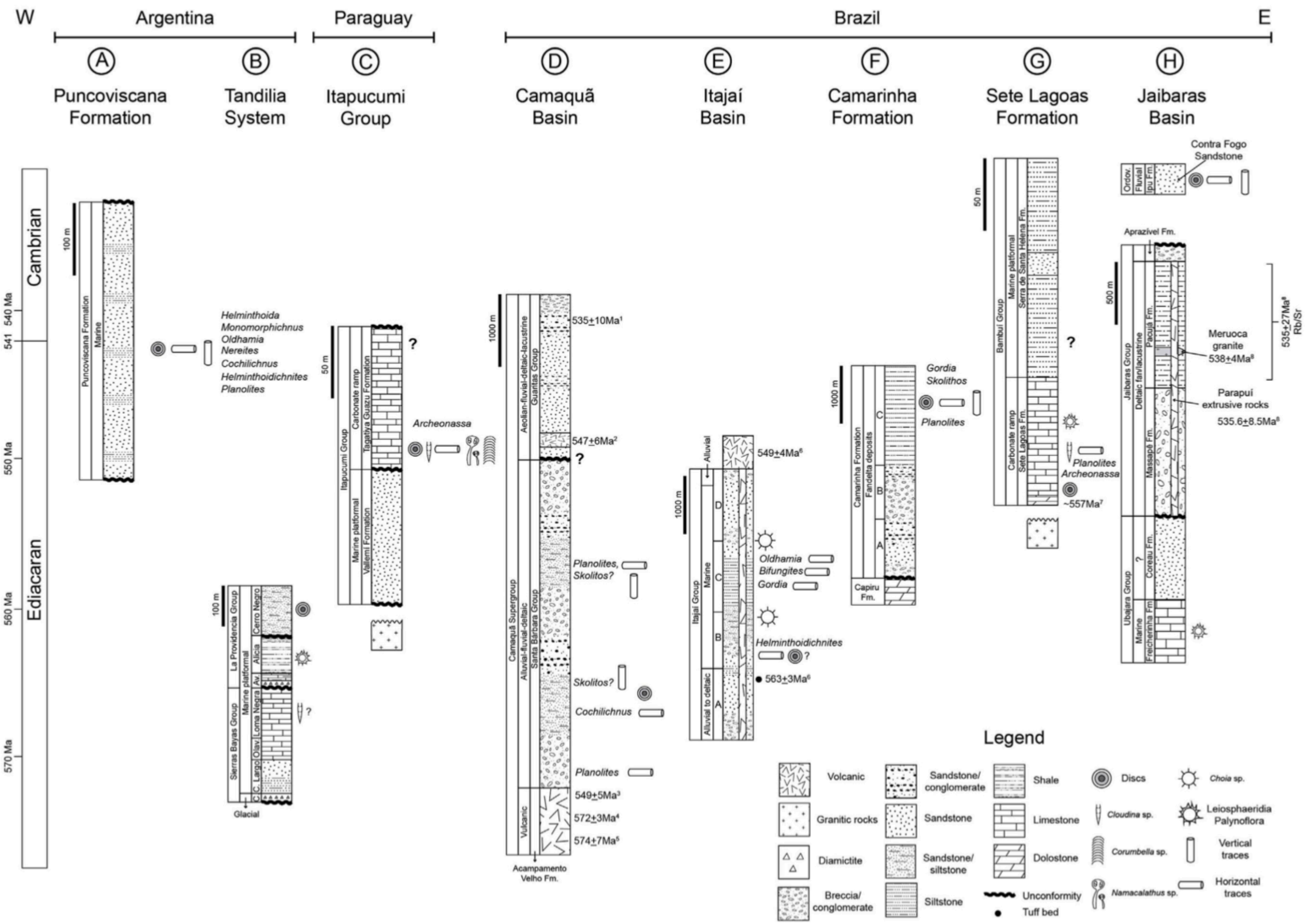

Fig. 2. Generalized stratigraphic columns showing ages, paleoenvironment and fossil record of Ediacaran-Cambrian units of South America (see Fig. 1). The sections do not have the same vertical scale. Data were compiled from the following: (A) Puncoviscana Formation: Aceñolaza (2004); (B) Tandilia System: Arrouy et al. (2016), Arrouy (2015); (C) Itapucumi Group: Warren et al. (2011); (D) Camaquã Basin: Netto et al. (1992), Paim et al. (2000); (E) Itajaí Basin: Zucatti da Rosa (2005); (F) Camarinha Formation: Drefahl and Silva (2007), Ciguel et al. (1992); (G) Sete Lagoas Formation: Warren et al. (2014), Paula-Santos et al. (2014); (H) Jaibaras Basin: Barroso et al. (2014), Chiglino et al. (2015).

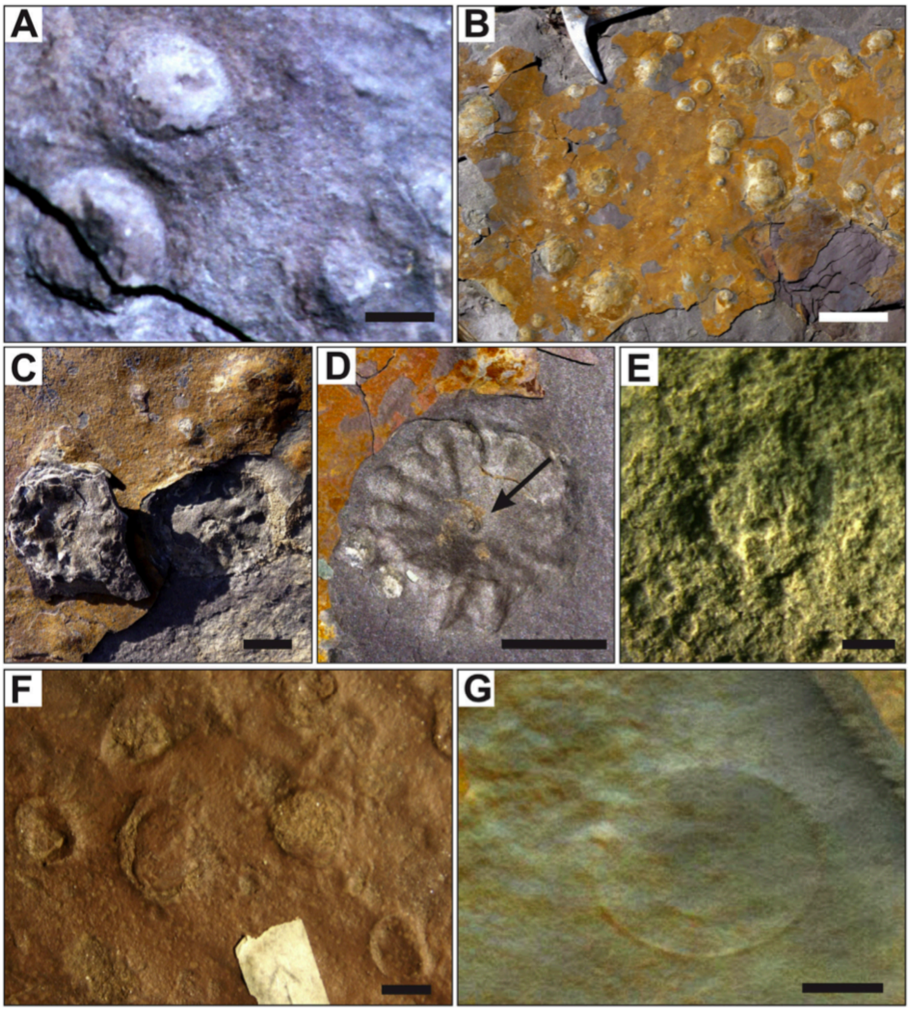

Fig. 3. - Discoidal structures from South America. A. Centimeter-size discs preserved in positive epirelief, showing central depression, Puncoviscana Formation, Puncoviscana Basin, Argentina (credited to Aceñolaza). B. Tens of discoidal structures with different sizes preserved in positive epirelief in fine sandstones, Cerro Negro Formation, La Providencia Group, Argentina. C and D. Detail of discs from Cerro Negro Formation. C. Fragmented specimen with detached upper positive feature, showing the tridimensional character of these structures and its internal wrinkled aspect. D. Radial wrinkles observed in lower surface of discs (negative epirelief) with a well marked central structure (black arrow). E. Discoidal structure exhibiting a small ellipsoidal central boss, Tagatiya Guazu Formation, Itapucumi Group, Paraguay F. Several discoidal imprints preserved as positive hyporelief in fine sandstones from the Santa Bárbara Group, Camaquã Basin. Brazil. G. Detail of a single specimen of a disc characterized by two concentric ridges separated by shallow groves, Depositional Sequence II, Itajaí Basin, Brazil (picture from Zucatti da Rosa, 2005) Scale bars of 10 mm in A and F, 150 mm in B, 20 mm in C, D and E and 5 mm in G; 2 mm in C, D.

central discrete depression. Internally to the smooth surface of the discs (Fig. 3C), well-marked radial wrinkles (Fig. 3C and D) irradiate from its central portion (Fig. 3-D) (Arrouy et al., 2016; Inglez, 2018). Some other features with an elongated or irregular geometry and a positive relief occur in the same beds where discs are observed and two of them seem to terminate in a discoidal structure. Due to its rough "leaf-like geometry", these features were interpreted by Arrouy et al. (2016) as a poorly preserved impression of a frond. However, the preservation is poor, and it is not clear if such structures are indeed partially preserved fronds or even possible surficial weathering-derived structures.

Additionally, these discoidal structures have a series of internal laminations and textures that resembles that developed through processes of microbial grain binding and trapping, suggesting that at least part of this material may have originated through these processes (Menon et al., 2016; Inglez, 2018).

3.3. *Rio Apa Craton – Itapucumi Group, Tagatiya Guazu Formation (Northeastern Paraguay) (C)*

The Itapucumi Group (Figs. 1 and 2) occurs in northeastern Paraguay, as a narrow trust-and-fold belt close to the Paraguay River ("Vallemí Mobile Belt" after Campanha et al., 2010) and as an unmetamorphosed and undeformed extensive sedimentary cover above the Paleoproterozoic basement of the Apa Complex.

The Itapucumi Group is a ~400-m-thick succession, comprising siliciclastic/volcanic rocks of the Vallemí Formation at the base, followed by limestones and dolostones of the Camba Jhopo and Tagatiya Guazu formations, which are capped by marls, limestones and pelites of the Cerro Curuzu Formation. The Tagatiya Guazu is essentially carbonatic and is composed of grainstones with wave ripples and tidal bundles, ooid grainstones, oncolites and heterolithic facies (Warren et al., 2011). Thrombolites with teepees, mudcracks and salt pseudomorphs are also found (Warren et al., 2011), suggesting deposition under evaporitic conditions in inter-to supratidal setting with strong microbial/organic contribution.

The Tagatiya Guazu Formation has an emblematic fossil content characterized by typical species of the classic Ediacaran Nama Type assemblage (*sensu* Waggoner, 2003), including *Cloudina* sp., *Corumbella* sp., *Namacalathus* sp., as well as putative trace fossils, and occasional discoidal structures (Table 2; Warren et al., 2011; Warren et al., 2017). *Cloudina* sp., and *Corumbella* sp. occur abundantly as laterally discontinuous, shelly concentrations around thrombolitic domes. These concentrations are made of tinny, transported and reworked bioclastic remains, commonly representing parautochthonous elements, as well as loosely packed shell concentrations containing *in situ* (autochthonous) individuals (Warren et al., 2012).

Discoidal features are restricted to three specimens (see Fig. 3E) and are characterized by elliptical structures preserved in positive hyporelief, exclusively in fine grainstone facies, associated with fragments of *Cloudina* shells. The discs range from 6.6 to 8.6 mm, with slightly elevated borders, 1.7 mm wide and an elevated central elliptical structure (Warren et al., 2011). The simple specimens described are poorly preserved and the absence of diagnostic features precludes a more accurate classification. Thus, although the discs from the Itapucumi Group resemble molds of soft-bodied organisms, the origin of these structures are tentatively interpreted as microbially-influenced (Warren et al., 2011). The presence of very thin and crinkled lamination associated with MISS structures in the samples analyzed, reinforces the hypothesis that the Paraguayan discs are probably related to the microbial dynamics, representing either gas domes, Intrites-like structures (ILS, *sensu* Menon et al., 2016) or even microbial colonial aggregates.

3.4. *Camaquã Basin – Bom Jardim and Santa Bárbara Groups (Southern Brazil) (D)*

The Camaquã Basin (Figs. 1 and 2), South Brazil, is a rift basin developed during the upper Neoproterozoic to lower Paleozoic (600–530 Ma, Almeida et al., 2012) as a result of post-orogenic extensional tectonics related to the end of the Brasiliano cycle (Fragoso-César et al., 2000; Almeida et al., 2012). The basin boundaries are marked by well-developed fault zones and accommodates a ~10.000 m-th[illegible] package of sedimentary and volcanic rocks of the Camaquã Supergroup (Fragoso César et al., 2000; Almeida et al., 2012). From the base to the top, the unit is divided into four distinct groups, separated from each other by major regional unconformities (commonly referred to as 'Allogroups', Paim et al., 2000), as follows: the Maricá, Bom Jardim (with a significant volcanic contribution), Santa Bárbara, and Guaritas groups (Paim et al., 2014; Almeida et al., 2012).

Regarding the paleoenvironmental context, the main discussion is focused on the continental or marine influence for the Maricá, Bom Jardim, and Santa Bárbara groups (Fragoso-César et al., 2000; Netto, 2012; Marconato et al., 2014; Paim et al., 2014). In this context, the authors interpreted the diverse ichnological assemblage altogether with the putative body fossils in the Bom Jardim and Santa Bárbara groups as suggestive of Edicaran to lower Cambrian in age as well as with marine influence (Netto et al., 1992; Netto, 2012).

The Bom Jardim Group is marked by two main sequences: (a) a progradational deltaic succession, with pro-deltaic deposits at the base that grades upwards to delta front deposits, and (b) a fluvio-lacustrine sequence, with fluvial conglomerates at the base that grades to intercalated fluvial sandstones and muddy lacustrine deposits (Janikian, 2004). The paleontological record comprises a trace fossil assemblage characterized by simple horizontal traces typical of *Planolites* isp., as well as rare short bilobed traces. They are preserved at the soles of fine sandstones, commonly associated to MISS, such as wrinkle structures, 'elephant skin', and 'Kinneyia-type' structures (Netto et al., 1992; Netto, 2012). Discoidal features were also described by Netto et al. (1992) and Netto (2012) as *Beltanelliformis* isp., which was interpreted as cnidarian resting traces and putative body fossil *Intrites* sp.

The Santa Bárbara Group is a thick sedimentary succession, marked by facies associations such as conglomerates and conglomeratic sandstones, interpreted as deposits of alluvial fans; trough cross-stratified sandstones and pebbly sandstones interpreted as fluvial channel belts and heterolithic facies with intercalations of fine-grained sandstones and mudstones deposited as fluvial floodplains (Marconato et al., 2014; Paim et al., 2014). However, its paleontological record suggests a marine influence for at least part of the succession (see Netto et al., 1992; Netto, 2012). The authors described the presence of ichnofossils such as the dumb-bell shaped *Arthraria antiquata*, simple horizontal traces like *Cochlichnus* isp., *Paleophycus* isp., probing burrows assigned to *Treptichnus* isp. and discoidal cnidarian resting traces such as *Bergaueria hemispherica.* As possible body fossils, basal discoidal imprints (holdfasts) were interpreted as *Aspidella* sp., *Intrites* sp., and *Sekwia* sp. (Fig. 3F). All these occurrences are in close association with MISS and mostly preserved as hyporelief structures which, in association with a an ichnofossil assemblage marked by the presence of *Cochlichnus* isp., *Paleophycus* isp and *Treptichnus* isp., suggests a paleopbiological context coherent to that expected in the Ediacaran-Cambrian boundary. In this sense, the diversity of discoidal forms could potentially represent imprints of macroorganisms on a microbially-bounded substrate, deserving a more detailed investigation.

3.5. *Itajaí Basin – depositional Sequence II (Southern Brazil) (E)*

The Itajaí Basin (Figs. 1 and 2) is a Neoproterozoic-early Paleozoic foreland basin located in the State of Santa Catarina, southern Brazil (Rostirolla and Figueira, 1995). This unit corresponds to a volcano-sedimentary succession deposited in a marine and deltaic setting in a continental platform (Silva, 1991). The Itajaí Basin is subdivided in four depositional sequences (Paim and Fonseca, 2004) marked by fluvial and fan delta deposits at the base, which grade to a shelf marine sequence to the top. This succession is covered by deep marine deposits, represented by a turbidity complex, and culminates in a new progradational cycle with shallow marine and deltaic deposits. Most of the fossils described for the Itajaí Basin were found in deposits generated in a transgressive system tract (TST) of the Sequence 2 (Paim and Fonseca, [illegible]fically in a slightly deformed prodeltaic succession characterized by fine-grained sandstones, siltstones and mudstones (Zucatti da Rosa, 2005). In these deposits MISS structures, such as elephant, skin are relatively common. On the other hand, poorly preserved impressions assigned to soft-bodied organisms, as *Parvancorina* sp., *Charniodiscus?* sp., *Cyclomedusa* sp. and *Aspidella* sp. are very rare (see Table 2). Doubtful specimens of Cambrian affinity, such as the sponges *Choia* sp.. are also described, as well as putative sclerites of *Chancelloria* sp., the ichnofossil *Helminthodichnites* isp., acritarchs and other organisms with uncertain affinity (Paim et al., 1997; Zucatti da Rosa, 2005).

The discoidal fossils described in the Itajaí Basin occur in mudstones and laminated siltstones associated with MISS and putative *Chancelloria* (Zucatti da Rosa, 2005). The few (only two) samples consist of poorly preserved impressions in positive hyporelief composed of two concentric circles varying from 15 to 40 mm in diameter. The simple discoidal forms were described as a *Cyclomedusa* impression (Fig. 3G), whereas the other specimen was classified as *Charniodiscus?*, due to the inconclusive presence of six delicate protrusions distributed along the area of the disc, and the putative elongated structure that seems to be connected to the central part of the disc (however, none of these features are clearly recognizable in the pictures provided in Zucatti da Rosa, 2005). The *Charniodiscus?* specimen is slightly bended, suggesting that this were folded during deposition, according to the author, but no further discussion in terms of taphonomy or preservation pathways was provided by Zucatti da Rosa (2005). The specimens of *Aspidella* sp. occur in fine sandstone beds and are characterized by simple impressions and molds slightly conical in shape and present raised borders and a small boss (or protrusion) at its central portion. The diameter varies between 2 mm and 6 mm (Zucatti da Rosa, 2005).

3.6. "Camarinha Basin" – Camarinha Formation (Southern Brazil) (F)

The Camarinha Formation is a Neoproterozoic-Early Cambrian volcanic-sedimentary succession located at the central-east of the Paraná State, southern Brazil (Figs. 1 and 2). Soares (1987) formerly described the Camarinha Formation as characterized by conglomerates, breccias, immature and moderately-to poorly-sorted sandstones, siltstones, mudstones and rhythmites. The unit was divided into three distinct successions, informally named as A, B and C (Soares, 1987). The units A and C are predominantly psamo-pelitic and the unit B is composed of conglomerates deposited in progradational fan systems, and retrogradational coastal environments (fan deltas). Trace fossils such as *Gordia arcuata*, *Planolites montanus*, *Skolithos* and *Cubichnia* (supposedly cnidarian resting traces, Table 2) in succession C, characterizes the Camarinha Formation as a marine succession deposited at the end of the Neoproterozoic (Ciguel et al., 1992).

Possible discoidal fossils were also found in succession C associated with sandstone layers with clay-silty lenses of rhythmically undulating surfaces, commonly associated with MISS. The discoidal structures (Fig. 4A) have domal forms preserved in positive epirelief, lying on the crests and troughs of a corrugated surface possibly related to the influence of microbial mats. Some of the discs are ovoid in shape and aligned, suggesting an apparent orientation. The forms are submillimetric in thickness, with diameters varying between 4 and 9 mm. Their central portion is commonly depressed and radial markings are ascribed as rare morphologies. Such structures were interpreted by Ciguel et al. (1992) as resting traces of medusoid organisms, and subsequently reinterpreted by Drefahl and Silva (2007), who assigned them to the genus *Beltanelliformis* sp., interpreted as epibenthic bodies preserved tridimensionally. A distinct interpretation was considered by Netto 2012, though (see section 3, item D).

3.7. São Francisco Craton – Bambuí Group, Sete Lagoas formation (Central Brazil) (G)

The Bambuí Group is located at the central-eastern Brazil and comprises an extensive cratonic cover lying in erosional contact over the Paleoproterozoic and Archean basement of the São Francisco Craton (SFC) (Fig. 1). Locally, the Bambuí Group overlies rocks of the Macaúbas/Jequitaí formations and the Carrancas conglomerate, units composed of glaciogenic rocks supposedly deposited during the Sturtian glaciation (Martins-Neto and Alkmim, 2001; Figueiredo et al., 2009).

The Bambuí Group, a ~700- to 1000 m-thick mixed carbonate-siliciclastic succession, is subdivided into five units, namely from base to top: the Sete Lagoas, Serra de Santa Helena, Lagoa do Jacaré, Serra da Saudade, and Três Marias formations. The Sete Lagoas Formation is mainly composed of mudstones, ooid grainstones, peloidal packstones,

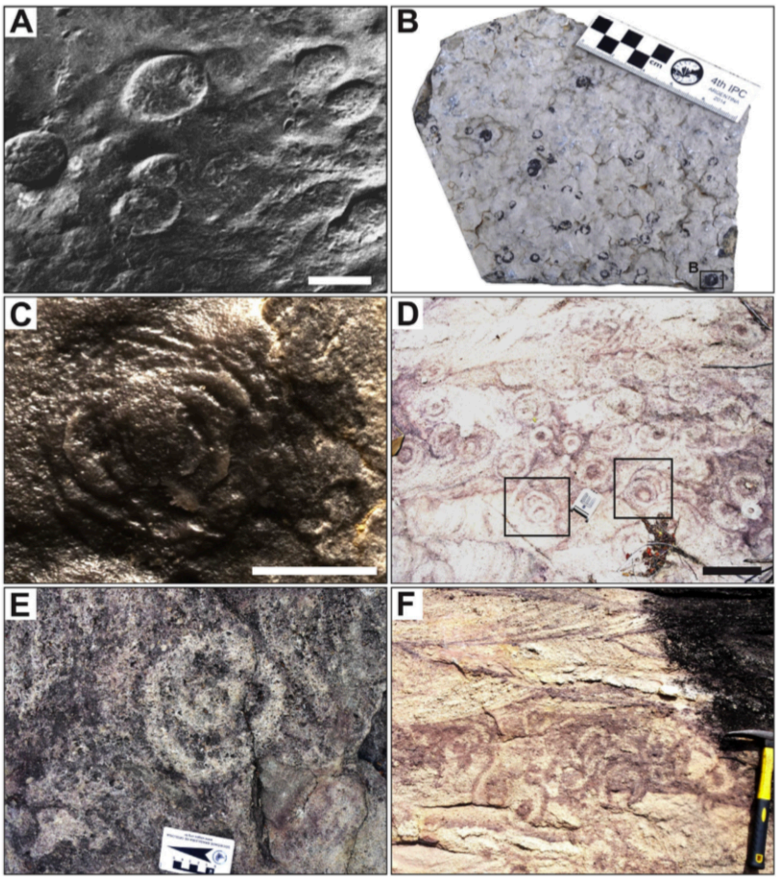

Fig. 4. – Discoidal structures from South America (cont.). A. Elongated unornamented discoidal structures preserved in positive epirelief. Note that the central portion of the discs is slightly depressed, Camarinha Formation, Camarinha Basin, Brazil (picture from Drefahl and Silva, 2007). B. Several small black-colored discs over thrombolites, Sete Lagoas Formation, Bambuí Group, Brazil. C. Detail of figure B showing a disc with well marked concentric radial ridges and groves. D. Several decimeter size discoidal features densely distributed in the bedding planes of coarse sandstones of the Ipu Formation. Note the concentric internal pattern, commonly marked by two main rings of darker colour. Discs sometimes over cross each other (black squares). E. Detail of concentric discoidal structure of the Ipu Formation, preserved in a weathered surface. F. Similar discoidal features seen in cross section in the same outcrop illustrated in Fig. D and E The Scale bar is 5 mm in A and C; 150 mm in D; Hammer length: 300 mm. (For interpretation of the references to color in this figure legend, the reader is referred to the Web version of this article.)

dolomudstones, microbialites facies and rare intraformational breccias (Vieira et al., 2007). Recent U–Pb ages obtained by detrital zircons from the upper part of the this unit indicate a maximum depositional age of 557 Ma (Paula-santos et al., 2014), consistent with the interval defined by the *Cloudina* index fossil described in thrombolytic facies at the lower to middle part of the unit (Warren et al., 2014).

At the southern exposures of the Bambuí Group, Sommer (1971) described the occurrence of dark (carbonaceous?), small spherical structures, with sizes ranging from 70 to 200 μm, preliminary named as *Bambuites erichsenii*. Sanchez (2014) reinterpreted this occurrence as a synonym of the Ediacaran acritarch *Leiosphaeridia jacutica*. This species is considered part of the Edicaran *Leiosphere* Palynoflora (ELP) biozone, which corresponds to the lower Ediacaran Period (Grey, 2005).

As pointed out by Sanchez (2014), a considerable number of problematic structures, putative macrofossils and dubious fossils are associated with microbial facies in the Sete Lagoas Formation. Sommer (1981, 1982) described nodular structures similar to oncoids as the species *Bambuilithos teixeranus* and *Bambuilithos hectoris*. Later, Sanchez (2014) reinterpreted these forms as pseudofossils or dubiofossils of uncertain affinity, suggesting that *Bambuilithos teixeranus* could possibly represent a synonym of *Nemiana simplex*, commonly preserved in fine sandstone facies as circular impressions in positive epirelief (Leonov, 2007; Sanchez, 2014). At the northern portion of the SFC, the Sete Lagoas Formation contains a more diverse fossil assemblage associated with the ichnogenera *Paleophycus* and *Archaeonassa* (Table 2, Warren et al., 2014). Recently, Inglez et al. (2016) presented a brief report of few discoidal structures (50 specimens) in close association with thrombolitic and microbial facies, which is deposited under shallow-water conditions. At least 10 specimens were reported occurring as low relief structures at the upper surface of thrombolytic beds. They are dark-colored with variable diameters (20–40 mm), and well-marked concentric ornamentation (Fig. 4B and C). Despite showing apparent organic appearance, sectioning of this material did not reveal any clear character in terms of internal texture or structure that could indicate its putative biological affinity (Inglez et al., 2016). However, based on morphological parameters, these small concentric discs, as well as the putative *Nemiana*-like discs described in this unit could represent discoidal or spherical colonial forms of cyanobacteria (Grazhdankin and Gerdes, 2007; Bobrovskiy et al., 2018).

3.8. Jaibaras Basin - Jaibaras Group, Pacujá Formation (?) (Northeastern Brazil) (H)

The Jaibaras Group, located at the State of Ceará, northeastern Brazil (Figs. 1 and 2), comprises an immature terrigenous succession filling the Jaibaras rift basin, which was generated during extensive events occurred in the Ediacaran-Cambrian transition (Oliveira, 2000). The Ediacaran-Cambrian age of the succession was inferred mainly based on data from the Coreaú Dyke Swarm, whose intrusion indicates the first stages of rift development nearly 562 ± 10 Ma ago (Tavares Jr. et al., 1990), and the ages of the metamorphic event over the Pacujá Formation of 535 ± 27 Ma (Barroso et al., 2014).

The putative fossils and biological structures described were compared with those from the White Sea assemblage (Australia and Russia, Barroso et al., 2014). Based on data from these authors, the fossil assemblage includes impressions and trace fossils represented by thousands of specimens, most of them discoidal structures (Fig. 4D–F). Yet, the assemblage also comprises doubtful bilaterian forms with possible Ediacaran affinity. At least eight genera of soft-bodied organisms were recorded in the Pacujá Formation, including *Charniodiscus*, *Cyclomedusa*, *Ediacaria*, *Kimberella*, *Medusinites*, *Palaeophragmodictya*, *Parvancorina* and *Pectinifrons*. Besides, simple trace fossils, such as *Arenicolites*, *Palaeophycus* and *Planolites* were also identified, which does not contribute to determine the age of deposition of this unit (Barroso et al., 2014, Table 2). The discoidal forms are represented by the following taxa: *Charniodiscus arboreus*, ?*Charniodiscus concentricus*, *Cyclomedusa davidi*, *Ediacaria flindersi*, and *Medusinites asteroides*. *Charniodiscus arboreus* occur as a single specimen identified as a frond-shaped impression, with a 330 mm long and 25 mm wide central stem, and 90 mm long, obliquely diverging branches. No attachment structure (discoidal holdfast) was described for this specimen. However, the original publication (see Barroso et al., 2014, Fig. 4-A) lacks appropriate description and illustrations of the specimens, as well as their comparision with paratypes from other localities (e.g. Glaessner and Daily, 1959; Laflamme et al., 2004). The structures are preserved in positive epirelief, with doubtful anatomical elements preserved both as positive or negative relief (Barroso et al., 2014). The form referred with doubts to *Charniodiscus concentricus* comprises a single impression preserved in positive epirelief and is characterized by two concentric rings separated from each other by a depression. The outer and inner discs have diameters of 130 and 60 mm, respectively. The specimen assigned to *Cyclomedusa davidi* is represented by a circular impression in positive epirelief with two concentric rings of 120 and 70 mm (outer and inner rings, respectively) with a small depression in the center with 15 mm in diameter. All rings are separated from each other by slightly raised edges (Barroso et al., 2014). The single specimen assigned to *Ediacaria flindersi* consists of a fragment characterized as a discoidal impression in positive epirelief composed of two superimposed discs (the inner disc raised above the outer disc) with diameters varying between 145 mm (outer disc) and 100 mm. No radial grooves or other ornamentations were observed. The *Medusinites asteroides* specimen is a set of concentric discs separated from each other by a surrounding depression forming a circular impression in positive epirelief with a diameter of 100 mm. Subordinately, some disc occur as circular forms apparently presenting invagination structures or radial grooves.

The Pacujá Formation is a middle to intermediate lithostratigraphic unit of the Jaibaras Group and is mainly composed of siltstones and micaceous sandstones, interpreted as fluvio-estuarine deposits (Barroso et al., 2014). The fossil assemblage occurs in a 100 m-thick succession of coarse and immature sandstones with planar lamination, trough cross bedding and symmetrical ripple marks. It is important to note that this facies association, as described by Barroso et al. (2014) in this locality is very similar to the Silurian Ipu Formation, located at the base of the Parnaíba Basin, that regionally overlies the Jaibaras Basin (Goés and Feijó, 1994). So, the fossil-bearing beds were assigned to the Pacujá Formation based on regional correlation, although no detailed geological map is available to discriminate the supposed Neoproterozoic succession from the well-constrained Silurian unit of the base of the Parnaíba Basin (Barroso et al., 2014).

. We analyzed hundreds of discoidal forms during a field work to the original locality where Barroso et al. (2014) described the supposed fossil material. Specimens are easily recognizable in the bedding planes of massive, very coarse, immature sandstones, where they are associated to sinuous horizontal traces. Discs range in size from 50 to 150 mm and are commonly characterized by two concentric circles, with similar grain size and mineralogy of the rock matrix (Fig. 4D). However, in weathered surfaces, the concentric discs are seen as alternating ridges and grooves (positive and negative relief features, respectively, Fig. 4E). Such structures could result from distinct patterns of alteration due to diagenetic differential cementation. In some cases, overlapping is observed, and two or more discs seem to superimpose each other (Fig. 4D).

In addition, cross-section expositions in the outcrops revealed that these discoidal marks also represent circular features in vertical section, sometimes cutting sedimentary structures (Fig. 4F). This circular geometry observed either in the bedding planes and in cross section strongly indicates a tridimensional, spherical-like morphology of these structures. Nonetheless, Braga de Souza et al. (2015) presented in this same succession the occurrence of *Circulichnis* isp., whose description is coherent with our observations regarding these circular structures as seen in the bedding planes.

This new field data, altogether with regional geological mapping

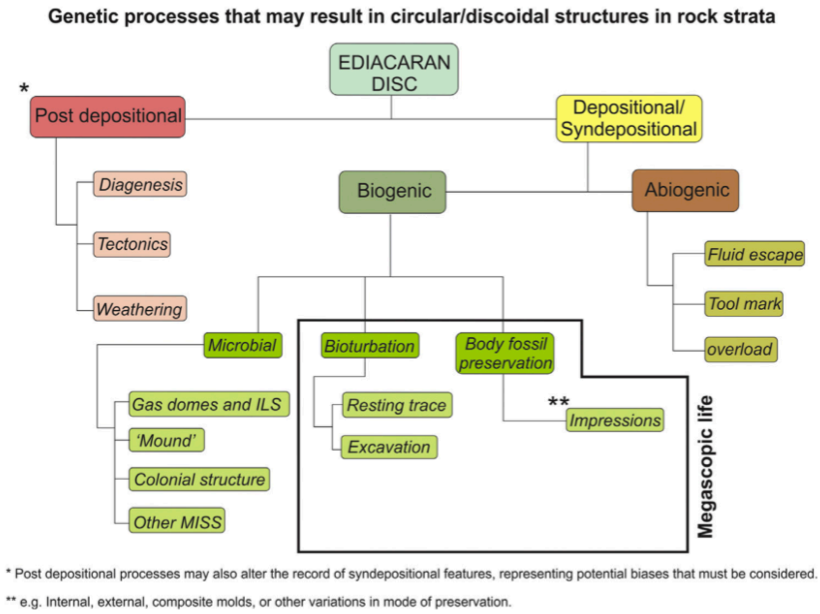

Fig. 5. – Organization chart systematizing the main and possible interpretational pathways regarding problematic Ediacaran discoidal structures.

(Cavalcante et al., 2003) and faciologic association observed in this locality, allowed us to constrain this occurrence as belonging to fluvial deposits of the much younger Ipu Formation, which is Silurian in age (Góes and Feijó, 1994). In addition, the spherical morphology of the discoidal structures that cross cut sedimentary structures and are marked by regions of differential cementation, suggest that they may originate from post-depositional, probably diagenetic processes. A revision of its potential ichnological significance however, is not in the scope of this contribution. Nevertheless, the presence of these structures in Silurian strata (Góes and Feijó, 1994) allow us to securely discard them as truly discoidal fossils of the Ediacaran Period.

4. Ediacaran discords: biological or abiological nature of South American discoidal structures

The literature encompassing the paleontological record of Ediacaran soft-bodied macrofossils in South America can be considered in many cases preliminary. Among the eight occurrences considered in this contribution, two are restricted to conference abstract and extended abstract (Drefahl and Silva, 2007; Inglez et al., 2016), one is presented exclusively on an unpublished masters' thesis (Zucatti da Rosa, 2005) and two peer reviewed publications only mention the presence of discs, without presenting further precise analysis focused on the discoidal structures (Acenolaza and Acenolaza, 2007; Warren et al., 2011). This scenario illustrates the potential for more detailed studies in Ediacaran terrains in South America. Thus, in the next sections, we advocate for the importance of a multi-proxy approach in the study of candidate Ediacaran fossils, therefore avoiding paleobiological and taxonomic interpretations without a clear indication of their biogenic nature and affinities. In the especific case of the discoidal fossils their taxonomic classification presents a series of issues, most of them arose from their simple morphology. Consequently, a highly consistent phylogenetic relationship or even taxonomical identification are hampered. Furthermore, the taxonomical uniformitarianism is difficult to be properly applied, as those simple forms might have evolved independently in distinct multiple lineages. A final issue is taphonomically-related, as many of their morphological patterns might have derived from distinct taphonomic conditions, rather than anatomical and interspecific characters (MacGabhann, 2007). In South American disc assemblages, there are mentions of possible stem-like structures made by Zucatti da Rosa (2005) and Arrouy et al. (2016). Nevertheless, although the evidences presented are certainly suggestive, the material deserves better sampling and more detailed investigation in order to confirm their interpretation. In this sense, the lack of clear stem-like structures showing attached fronds, as well as the absence of other clear representatives of Ediacaran soft-bodied organisms contribute for the problematic character of the specimens in those assemblages.

Concerning the biotic or abiotic origin of the problematic structures, this discussion has become a commonplace in studies regarding the earliest records of Archean life, as revisited by Awramik and Grey (2005). The implications for questions related to the origin of life on Earth, the nature of a hypothesized *Last Universal Common Ancestor*, and even the possibility of existence of extraterrestrial life certainly justify the high levels of scrutiny in the identification of putative biological structures in Archean strata (Brasier et al., 2002, 2005; 2015; Awramik and Grey, 2005; Wacey et al., 2010).

When discussing the Ediacaran fossil record, the questions erected are related to the diversification of early multicellular organisms, including animals, as well as their ecosystem structuring (Waggoner, 2003; Droser et al., 2006; Darroch et al., 2013). Even before discussing these subjects, it is essential to establish clear criteria of biogenicity, in order to systematically describe and interpret problematic structures identified in Ediacaran strata, similarly to what is being done with the record of Archean life (Brasier et al., 2002, 2005; Awramik and Grey, 2005; Wacey et al., 2010).

When analyzing Ediacaran strata in search for evidence of complex life, especially when dealing with morphologically simple structures, such as discoidal markings, some questions must be considered: (a) can these structures be compared to or identified as sedimentary/synsedimentary features? Alternatively, could they represent a post depositional structure, related to diagenesis, tectonics or weathering? (b) If evidence suggests that the structures have a depositional or syndepositional origin, can we explain their genesis by means of inorganic processes? (c) if not, couldpaleoenvironmental and paleobiological context indicate features related to their biological origin and genesis (Fig. 5)?

In this sense, these questions would represent consecutive null hypothesis to be tested and falsified employing the combination of various sorts of analytical techniques, in order to link a more generalized (e.g., stratigraphical and sedimentological data collected in the field) to a more specific perspective (e.g., petrography, geochemistry and taxonomy).

Regarding the South American occurrences reviewed in this contribution their issues are mostly related to the lack of clear criteria to distinguish biotic structures and probable macrofossils from other structures that could be generated from abiotic processes. Nevertheless, we consider few other issues that are worthy to be further discussed and investigated in detail, concerning the study of discoidal structures in South America: (a) the analytical techniques used to define shape, composition, relationship between the matrix and the fossils, as well as the preservational parameters inferred; (b) the ages of the deposits that contain them; (c) the sedimentary settings in which they occur and d) the taxonomic, taphonomic and general paleobiological interpretations considered in some cases.

4.1. Analytical assessment and preservational pathways

A more systematic approach using biogenicity criteria and preservational pathways would greatly contribute for the study of discoidal fossils in the South American Ediacaran fossil-bearing strata. For wordwide occurrences, recent works have shown that a multi-analytical approach is recommended in order to better understand the genesis, preservational pathways and classification of enigmatic structures and putative fossils (Gehling et al., 2000; Tarhan et al., 2010, 2015; Retallack, 2012a,b; Bykova et al., 2017; Burzynski et al., 2017; Bobrovskiy et al., 2018). Discoidal structures can be originated under a great variety of paleoenvironmental conditions, and many previously described taxa were reinterpreted in the past decade as inorganic or microbial structures (Van Loon, 2008; Hagadorn and Miller, 2011; Ivantsov et al., 2014; Menon et al., 2015, 2016). As such, the analysis of the depositional context in which they occur, their relationship with MISS (see Gehling and Droser, 2009 for a discussion concerning sedimentary microbial textures developed due to this interaction), as well as their modes of occurrence (epirelief, hyporelief or even endorelief) and internal structures (through detailed petrographic analysis) is crucial to precisely determine their origin. Through these distinct parameters, the sedimentary and/or paleobiological significance of those discoidal structures can be more accurately accessed (Tarhan et al., 2010, 2015; Menon et al., 2015, 2016; Burzynski et al., 2017).

In a standard procedure, fossils are examined, measured and photographed under a reflected light stereomicroscope. Serial sections provide a cross-sectional view of the fossils, and help to imaging their internal structure. Also, when there is enough contrast between fossil and matrix, X-ray computed tomography (CT) and microcomputed tomography (microCT) has been used as powerful non-destructive tools for a three-dimensional visualization. However, because discoidal structures are morphologically simple, caution must be taken when using techniques that rely very much on the subjective grouping and the interpretation of the few simple characters (e.g., Burzynski et al., 2017).

Energy dispersive spectroscopy (EDS) elemental maps and Raman spectroscopy analysis can be very helpful to identify microstructure and different mineral coatings within or on top of the discoidal structures, providing information about their taphonomic preservational pathways (e.g., Wan et al., 2014; Luo et al., 2016). For fossils preserved as carbon compressions, variable-voltage backscattered-electron scanning microscopy (BSE-SEM) has been used to elucidate cellular structures (Tang et al., 2016). However, caution should be taken if the detected geochemical signal corresponds to the discoidal structure or the external microbial mat in which it was embedded. Moreover, the focused ion beam electron microscopy (FIB-EM) analysis complements the SEM studies and provides an ultra-high resolution for investigating those fossils, also improving the magnification of the images acquired (Schiffbauer and Xiao, 2009; Laflamme et al., 2011).

Discoidal fossils preserved as molds or casts can sometimes resemble nodules, concretions or other sedimentary structures. For these cases, a geochemical investigation would complement the morphological analysis of discs and provide insights about the redox conditions of the environment in which they lived and how they were fossilized (e.g., Bykova et al., 2017).

Recently, biomarkers have been used to understand the phylogenetic affinity of discoidal fossils, such as *Nemiana* (Bobrovskiy et al., 2018). However, the preservation of biomarker features occurs only when the strata have undergone a mild burial temperature history (Goryl et al., 2018).

4.2. Uncertain ages of the disc-bearing units

The ages of some disc-bearing units in South America are not well constrained yet, since precise radiometric ages, and stratigraphical/biostratigraphical correlations are still missing. This is specially the case, when considering the ages of the Pacujá, Puncoviscana, Camarinha and Cerro Negro Formations, the Bom Jardim and Santa Bárbara Groups, and the Itajaí Basin disc-bearing strata. For example, in some of these units, such as in the Pacujá, Puncoviscana and Cerro Negro formations, the ages of the deposits were at least in part, inferred based on the macrofossils and ichnofossils as well as regional correlations (Barroso et al., 2014; Acenolaza and Acenolaza, 2007; Arrouy et al., 2016). Moreover, precise detrital zircon ages, which could refine chronostratigraphic hypotheses, are still missing for those localities.

The depositional age of the Pacujá Formation, was constrained between 562 and 535 Ma, suggesting that the deposition lasted between the Ediacaran to lower Cambrian. However, as discussed in section 3-H, the fossil-bearing strata described by Barroso et al. (2014) was confirmed in this work as correlated to the Ipu Formation, considered the base of the Paleozoic Parnaíba Basin (Cavalcante et al., 2003).

Other issues can also be assigned to the deposits of the Itajaí and Puncoviscana basins, in which the ages were inferred based on regional geochronological data and where stratigraphical correlations are precluded due to the intense deformation of the rock package (Paim and Fonseca, 2004; Zucatti da Rosa, 2005; Acenolaza and Acenolaza, 2007). Furthermore, in the case of the Puncoviscana Formation, the ichnofossil assemblage is strongly indicative of a lower Cambrian age (Acenolaza and Acenolaza, 2007), despite the regional geochronological data suggesting an initial sedimentation during the Ediacaran.

Carbon and strontium chemostratigraphy have been widely used as proxies for Ediacaran carbonate rocks and are very useful in the correlation of Ediacaran strata (i.e., comparison with other well-established Ediacaran profiles in other basins). Renium-Osmium radioactive isotope system can potentially provide precise and accurate depositional ages for black shales (Kendall et al., 2009). Thus, this geochemical analytical approach can be viewed as prospects of interest at least for units with carbonatic contributions, such as the Sete Lagoas Formation in Brazil and Tagatiya Guazu Formation in Paraguay.

4.3. Sedimentary environment of the fossil-bearing strata: continental vs. marine settings

The interpretation of the depositional sequences is also particularly important when dealing with the nature of those enigmatic structures and putative Ediacaran fossils in South American sedimentary units. Members of the Ediacara biota are worldwidely recorded in a variety of sedimentary facies, which include both shallow (Gehling et al., 2000; Gehling and Droser, 2013) and deep marine environments (Narbonne, 2005; Narbonne et al., 2014). This marine nature suggested by faciological associations is reinforced by compelling evidence based on morphological parameters that indicates that some Ediacaran taxa could be related to known Phanerozoic marine phyla (Fedonkin et al., 2007; Xiao and Laflamme, 2008; Gehling and Droser, 2013).

On the other hand, interpretations on Ediacara Member deposits of the Flinders Ranges, South Australia, suggested the development of paleosols associated to fossiliferous beds (Retallack, 2012a,b). According to those interpretations, in fossil-rich intervals, light carbon and oxygen isotopic values and carbonate nodules associated to loess size particles, deformational structures and weathering features represent typical paleosol characters. This led the same author to formalize the idea that these fossils could represent large terrestrial sessile organisms, dwelling in organic soils (Retallack, 2012a,b). Although these evidences bring new elements into the discussion of the paleobiology of some still enigmatic forms of the Ediacaran biota, they can be falsified (Xiao, 2013). By using a distinct interpretation, geochemical trends could be related to telodiagenetic alteration, whereas deformational structures could develop through fluid escape processes, and carbonate nodules are commonly associated to marine settings.

As in other Ediacaran units with similar fossil assemblages (Narbonne, 2005; Narbonne et al., 2014), sedimentological and stratigraphical data points to a marine-influenced deposition, and no paleosol evidence seems to be definitive. Hence, the presence of putative Ediacaran macrofossils in true continental deposits should be considered with caution.

In our case study, units such as the Bom Jardim and Santa Bárbara groups of the Camaquã Basin, the ichnofossil association marked by the presence of *Bergaueria* isp. and *Treptichnus* isp., for example could indicate at least a brief marine influence during the deposition of the fossil-bearing strata (Netto, 2012). Nevertheless, detailed sedimentologic and stratigraphic studies focused on the facies analyses and architectural elements of these units are still missing. Furthermore, the solely presence of discoidal structures, for which the origin is usually unclear, should not be taken as any paleoenvironmental indicator.

4.4. Taxonomic assignment, taphonomic protocol and paleobiological implications

The taxonomic treatment given to the discussed South American Ediacaran discoidal structures is one of the main issues to be solved in future researches. At this moment, the taxonomic assignment given to various structures and putative fossils must be viewed with caution. Yet, it is noteworthy that most of the available descriptions were made based on few specimens, or even just one individual. This observation is especially valid for those structures studied in the Tagatiya Guazú Formation, Itajaí Basin, and Sete Lagoas Formation (see Section 3C, E and G, respectively) (Ciguel et al., 1992; Zucatti da Rosa, 2005; Warren et al., 2011; Inglez et al., 2016). Additionally, in almost all cases, the material is usually poorly preserved, and the morphological variations (taphonomic variants) of a given structure were fully considered by previous authors. Hence, the proper description and classification of the Ediacaran discoidal structures and other associated putative soft-bodied fossils is not an easy task. Even though, in some contributions those structures were referred to well-stablished Ediacaran genera, such as *Cyclomedusa* sp., *Ediacaria* sp. and *Aspidella* sp. (see Zucatti da Rosa, 2005; Netto, 2012; Barroso et al., 2014). As comented by Gehling et al. (2000), this may add noise and confusion to the study of discoidal fossils and interpretations must consider taphonomic analysis and sampling enough for statistical analyses. Although hundreds of specimens from the Cerro Negro Formation, Argentina, were analyzed (Arrouy et al., 2016), the taxonomic assignment of discs from the Cerro Negro Formation to the *Aspidella*-plexus should also include its internal morphology.

Finally, according to recent revisions on the paleobiological significance of the genera *Beltanelloides*, *Beltanelliformis,* and *Nemiana*, these discoidal structures would represent neither body fossils, nor trace fossils, but rather colonial cyanobacteria, similar to the modern freshwater genera *Nostoc* (Ivantsov et al., 2014; Bobrovskiy et al., 2018). Consequently, the record of *Beltanelloides* sp., Puncoviscana Formation, Puncoviscana Basin (Acenolaza and Acenolaza, 2007), *Beltanelliformis* isp., Bom Jardim Group, Camaquã Basin (Netto, 2012), and *Nemiana* sp., Sete Lagoas Formation, São Francisco Craton (Sanchez, 2014) must be viewed with caution. If the identification of these South American structures is accurate, and that the interpretations by Ivantsov et al. (2014) and Bobrovskiy et al. (2018) are correct, the presence of these spherical microbial colonies would be coherent with a depositional environment characterized by a high microbiological (mainly bacterial) activity. Furthermore, the presence of *Beltanelloides* in association with possible lower Cambrian traces in the Puncoviscana Formation suggests that the stratigraphic range of these colonial forms extended into the lower Paleozoic. Hence, caution must be taken when using the *Beltanelloides-Nemiana-Beltanelliformis* association as an indicator of Ediacaran age for any depositional unit.

5. Summary

In this contribution, the occurrence of putative Ediacaran soft-bodied fossils and other associated structures were reviewed, and critical questions concerning their interpretation were raised. Based on our database a considerable number of occurrences were already reported for Ediacaran-Cambrian terrains from Brazil, Argentina and Paraguay. Notably, the scope of the vast majority of those studies can be considered preliminary, either due to the own format of the original publication or to the methods and techniques available at the time of the study. The origins, modes of preservation, age, and depositional settings of many findings are still controversial. Good examples are the occurrences in the Itajaí Basin, where a reassessment of the material is recommended in order to establish reliable criteria to interpret the discs either as biotic or abiotic structures. Only few studies focused in the nature and paleontology of the discoidal structures, which resembles those of the *Aspdiella*-plexus, as well as in the description of other fossil metazoans (Warren et al., 2011, 2012, 2014; Pacheco et al., 2015; Parry et al., 2017). In general, the description of putative fossils of discoidal organisms do not take into consideration a broad set of analysis to investigate the taxonomy and preservational parameters required for determining the nature of these enigmatic forms (Gehling et al., 2000; MacGabhann, 2007; Menon et al., 2015, 2016).

Recent studies demonstrate that the integration of various analytical techniques, including the sectioning of samples, geochemical and petrographic analysis (through optical and scanning electric microscope), as well as 3D microtomography are crucial in the study of those enigmatic structures. These techniques can reveal much of the internal morphologies of the discs, helping us to improve our understanding on their nature (Gehling et al., 2000; Tarhan et al., 2010, 2015; Arrouy et al., 2016; Bobrovskiy et al., 2018; Inglez, 2018). In this context, future studies on South American Ediacaran discoidal structures must be conducted by means of these techniques. Until then, part of the South American material reviewed in this contribution can be considered dubiofossils. Thus, they deserve further analysis and should be viewed with caution when utilized as paleoenvironmental, paleobiological or bioestratigraphical indicators. This is certainly the case of occurrences described in the Itajaí Basin (Zucatti da Rosa, 2005) and the Camarinha Formation (Drefahl and Silva, 2007) where better sampling and a more detailed investigation would contribute to the understanding of enigmatic structures mentioned in the literature.

For those occurrences associated with carbonate settings (Sete Lagoas, Taguatiya Guazu) or even with internal structure with laminations, we suggest that discs could be resulted from the interaction between microbial communities and the substrate. In all cases, a multiproxy analysis altogether with systematic sampling would avoid taphonomic bias.

Finally, our revision and new field data, allowed us to correctly position the structures described by Barroso et al. (2014) in the Silurian

Ipu Formation, of the Parnaíba Basin. Our data also suggests that the circular markings probably represent diagenetic features, although the combination of new set of analysis such as serial grinding and petrography could help in elucidate this issue and possibly falsify other biogenetic interpretations presented for this material (Braga de Souza, 2015).

Acknowledgments

The authors thank the Cementos Avellaneda S.A for logistic support in the field works in Olavarría, Argentina. The authors also thank M. Drefahl, G. Aceñolaza, A. Zucatti da Rosa for the access to the photographic material and Milena B. Rosa for the help with designing Fig. 1. We also thank the reviewers Dr. Latha Menon and Dr. Mirian Liza Alves Forancelli Pacheco for their corrections and suggestions that improved the final version of this contribution. Financial support was provided by CNPq (grant 444070/2014-1) and FAPESP (grant 2015/24608-3). L.V. Warren and M.G. Simões are fellows of the CNPq.

Appendix A. Supplementary data

Supplementary data to this article can be found online at https://doi.org/10.1016/j.jsames.2018.11.023.

References

Acenõlaza, F.G., Durand, F.R., 1973. Trazas fósiles del basamento cristalino del noroeste argentino. Bol. Asoc. Geol. Cordoba 1, 45–52.
Aceñolaza, F.G., Durand, F.R., 1986. Upper Precambrian–Lower Cambrian biota from the northwest of Argentina. Geol. Mag 123, 367–375.
Aceñolaza, G.F., Tortello, M.F., 2003. El Alisal: a new locality with trace fossils of the Puncoviscana Formation (late Precambrian–early Cambrian) in Salta province, Argentina. Geol. Acta 1, 95–102.
Acenõlaza, G.F., 2004. Precambrian–Cambrian ichnofossils, an enigmatic 'annelid tube' and microbial activity in the Puncoviscana Formation (La higuera; tucumán province, NW Argentina). Geobios 37, 127–133.
Aceñolaza, F.G., Aceñolaza, G.F., Esteban, S., 1999. Bioestratigrafía de la Formación Puncoviscana y unidades equivalentes en el NOA. In: Relatorio XIV Congreso Geológico Argentino. Geología Del Noroeste Argentino, pp. 91–114.
Acenolaza, G., Acenolaza, F., 2007. Insights in the Neoproterozoic Early Cambrian transition of NW Argentina: facies, environments and fossils in the proto-margin of western Gondwana. Geol. Soc. London, Spec. Publ. 286, 1–13. https://doi.org/10.1144/SP286.1.
Adams, C., MIller, H., Toselli, A.J., 1990. Nuevas edades de metamorfismo por el método K-Ar de la Formación Puncoviscana y equivalentes, NW de Argentina. In: Aceñolaza, F.G., Miller, H., Tosell, A.J. (Eds.), El Ciclo Pampeano En El Noroeste Argentino. INSUGEO - Serie de Correlación Geológica, pp. 199–208.
Almeida, R.P., Santos, M.G.M., Fragoso-Cesar, A.R.S., Janikian, L., Fambrini, G.L., 2012. Recurring extensional and strike-slip tectonics after the Neoproterozoic collisional events in the southern Mantiqueira province. An. Acad. Bras. Cienc. 84, 347–376. https://doi.org/10.1590/S0001-37652012005000034.
Alpert, S.P., 1973. Bergaueria prantl (cambrian and ordovician), a probable actinian trace fossil. J. Paleontol. 47, 919–924.
Anderson, R.P., Tarhan, L.G., Cummings, K.E., Planavslky, N.J., Bjørnerud, M., 2016. Macroscopic structures in the 1.1. Ga continental copper Harbor Formation: concretions or fossils? Palaios 31, 327–338. https://doi.org/10.2110/palo.2016.013.
Arrouy, M.J., 2015. Sedimentología y estratigrafía de los depósitos ediacaranos-paleozoicos, suprayacentes a las calizas del precámbrico del Sistema de Tandilia, Provincia de Buenos Aires, Argentina. Universidad Nacional de La Plata.
Arrouy, M.J., Poiré, D.G., Peral, L.E.G., Canalicchio, J.M., 2015. Sedimentología y estratigrafía del Grupo La Providencia (NOm. Nov.): cubierta Superior Neoproterozoica, Sistema de Tandilia, Argentina. Lat. Am. J. Sedimentol. Basin Anal. 22, 171–189.
Arrouy, M.J., Warren, L.V., Quaglio, F., Poiré, D.G., Simões, M.G., Rosa, M.B., Peral, L.E.G., 2016. Ediacaran discs from South America: probable soft-bodied macrofossils unlock the paleogeography of the Clymene Ocean. Sci. Rep. 6, 30590. https://doi.org/10.1038/srep30590.
Awramik, S.M., Grey, K., 2005. Stromatolires: biogenicity, biosignatures, and bioconfusion. In: Hoover, R.B., Levin, G.V., Rozanov, A.Y., Gladstone, G.R. (Eds.), Astrobiology and Planetary Misisons. Proceedings of SPIE. California, San Diego. https://doi.org/10.1117/12.625556.
Bachmann, G., Grauert, B., Lork, A., Miller, H., 1987. El magmatismo Cámbrico Medio-Cámbrico Superior en el basamento del noroeste Argentino: investigaciones isotópicas y geocronológicas sobre los granitoides de los complejos intrusivos Santa Rosa de Tastil y Cañaní. In: 10o Congresso Geologico Argentino. Tu-cumã, pp. 125–127.
Barroso, F.R.G., Viana, M.S.S., de Lima Filho, M.F., Agostinho, S.M.O., 2014. First ediacaran fauna occurrence in northeastern Brazil (Jaibaras Basin, ?Ediacaran-Cambrian): preliminary results and regional correlation. An. Acad. Bras. Cienc. 86, 1029–1042. https://doi.org/10.1590/0001-3765201420130162.
Becker-Kerber, B.B., Da Rosa, A.L.Z., Gabas, S.G., De Moraes Leme, J., Pacheco, M.L.A.F., 2013. O registro fossilífero de metazoários ediacaranos na América do Sul e suas implicações nos estudos sobre origem e complexificação da vida animal. Geol. USP - Ser. Cient 13, 51–64. https://doi.org/10.5327/Z1519-874X201300030006.
Billings, E., 1872. On some fossils from the Primordial rocks of Newfoundland. Can. Nat. Geol. 465–479.
Bobrovskiy, I., Hope, J.M., Krasnova, A., Ivantsov, A., Brocks, J.J., 2018. Molecular fossils from organically preserved Ediacara biota reveal cyanobacterial origin for Beltanelliformis. Nat. Ecol. Evol. 3–8. https://doi.org/10.1038/s41559-017-0438-6.
Braga de Souza, A., Sousa, M.J.G., Silva Filho, W., Viana, A.O.B., Santos, F., 2015. Significado Paleoambiental de Icnofósseis em Arenitos Silurianos da Região de Santana do Acaraú – Ceará. Estudos Geológicos. https://doi.org/10.18190/1980-8208/estudosgeologicos.v25n2p39-52.
Brasier, M., Antcliffe, J., Saunders, M., Wacey, D., 2015. Changing the picture of Earth's earliest fossils (3.5–1.9 Ga) with new approaches and new discoveries. Proc. Natl. Acad. Sci. U. S. A 112, 4859–4864. https://doi.org/10.1073/pnas.1405338111.
Brasier, M.D., Green, O.R., Jephcoat, A.P., Kleppe, A.K., Van Kranendonk, M.J., Lindsay, J.F., Steele, A., Grassineau, N.V., 2002. Questioning the evidence for Earth's oldest fossils. Nature 416, 76.
Brasier, M.D., Green, O.R., Lindsay, J.F., Mcloughlin, N., Steele, A., Stoakes, C., 2005. Critical testing of Earth ' s oldest putative fossil assemblage from the ∼ 3 . 5 Ga Apex chert , Chinaman Creek , Western Australia. Precambrian Res. 140, 55–102. https://doi.org/10.1016/j.precamres.2005.06.008.
Buatois, L.A., Mángano, M.G., 2003. Early colonization of the deep sea : Ichnologic evidence of deep- marine benthic ecology from the Early Cambrian of Northwest. Palaios 18, 572–581.
Burzynski, G., Narbonne, G.M., 2015. The discs of Avalon: Relating discoid fossils to frondose organisms in the Ediacaran of Newfoundland, Canada. Palaeogeogr. Palaeoclimatol. Palaeoecol. 434, 34–45. https://doi.org/10.1016/j.palaeo.2015.01.014.
Burzynski, G., Narbonne, G.M., Dececchi, T.A., Dalrymple, R.W., 2017. The ins and outs of Ediacaran discs. Precambrian Res. 300, 246–260. https://doi.org/10.1016/j.precamres.2017.08.012.
Buss, L.W., Seilacher, A., 1994. The phylum vendobionta - a sister group of the Eumetazoa. Paleobiology 20, 1–4. https://doi.org/10.2307/2401145.
Bykova, N., Grazhdankin, B.C.G.D., Xiao, V.R.S., 2017. A geochemical study of the Ediacaran discoidal fossil Aspidella preserved in limestones : implications for its taphonomy and ... A geochemical study of the ediacaran discoidal fossil aspidella preserved in limestones : implications for its taphonomy and P. https://doi.org/10.1111/gbi.12240.
Callow, R.H.T., Battison, L., Brasier, M.D., 2011. Diverse microbially induced sedimentary structures from 1Ga lakes of the Diabaig Formation, Torridon Group, northwest Scotland. Sediment. Geol. 239, 117–128. https://doi.org/10.1016/j.sedgeo.2011.06.002.
Cavalcante, J.C., Vasconcelos, A.M., Gomes, F.E.M., 2003. Atlas de geologia e recursos minerais do Ceará. Sist. informações Geográficas SIG, Secr. dos Recur. Hídricos do Estado do Ceará. CPRM/Serviço Geológico do Bras. Fortaleza, CD-Rom.
Chiglino, L., Gaucher, C., Sial, A.N., Ferreira, V.P., 2015. Acritarchs of the ediacaran frecheirinha formation, Ubajara group, Northeastern Brazil. An. Acad. Bras. Cienc 87, 635–649. https://doi.org/10.1590/0001-3765201520140430.
Ciguel, J.H.G., Góis, J.R., Aceñolaza, F.G., 1992. Ocorrência de icnofosseis em depd-sitos molássicos da Formação Camarinha (Neoproterozóico III - cambriano Inferior), no Estado do Paraná Brasil. Série Correlação Geológica 9, 157–158.
Cingolani, C.A., 2011. The Tandilia system of Argentina as a southern extension of the Río de la Plata craton: an overview. Int. J. Earth Sci. 100, 221–242. https://doi.org/10.1007/s00531-010-0611-5.
Clapham, M.E., Narbonne, G.M., Gehling, J.G., Clapham, M.E., Narbonne, G.M., Gehling, J.G., 2003. Paleoecology of the Oldest Known Animal Communities : Ediacaran Assemblages at Mistaken Point , Newfoundland Paleoecology of the Oldest Known Animal Communities : Ediacaran Assemblages at Mistaken Point , Newfoundland, vol. 29. pp. 527–544.
Darroch, S.A.F., Laflamme, M., Clapham, M.E., Darroch, S.A.F., Laflamme, M., Clapham, M.E., 2013. Population structure of the oldest known macroscopic communities from Mistaken Point , Newfoundland. Paleobiology 39, 591–608. https://doi.org/10.1666/12051.
Davies, N.S., Liu, A.G., Gibling, M.R., Miller, R.F., 2016. Resolving MISS conceptions and misconceptions: a geological approach to sedimentary surface textures generated by microbial and abiotic processes. Earth Sci. Rev. 154, 210–246. https://doi.org/10.1016/j.earscirev.2016.01.005.
Drefahl, M., da Silva, R.C., 2007. Ediacaran fossils occurrence in Camarinha Formation (upper neoproterozoic), Paraná state southeast. In: XX Congresso Brasileiro de Paleontologiapp. 1–10.
Droser, M.L., Gehling, J.G., 2015. The advent of animals : the view from the. Ediacaran 112, 4865–4870. https://doi.org/10.1073/pnas.1403669112.
Droser, M.L., Gehling, J.G., Jensen, S.R., 2006. Assemblage palaeoecology of the Ediacara biota : the unabridged edition ? Palaeogeogr. Palaeoclimatol. Palaeoecol. 232, 131–147. https://doi.org/10.1016/j.palaeo.2005.12.015.
Durand, F.R., Aceñolaza, F.G., 1990. Caracteres biofaunísticos, paleoecológicos y paleogeográficos de la Formación Puncoviscana (Precámbrico superior-Cámbrico inferior) del Noroeste Argentino. El Ciclo Pampeano en el Noroeste Argentino. Ser.. Correlación Geológica 4, 71–112.
Dzik, J., Martyshyn, A., 2017. Hydraulic sediment penetration and seasonal growth of petalonamean basal discs from the Vendian of Ukraine. Precambrian Res. 302, 140–149. https://doi.org/10.1016/j.precamres.2017.09.024.

El Albani, A., Bengtson, S., Canfield, D.E., Riboulleau, A., Bard, C.R., Macchiarelli, R., Pemba, L.N., Hammarlund, E., Meunier, A., Mouele, I.M., Benzerara, K., Bernard, S., Boulvais, P., Chaussidon, M., Cesari, C., Fontaine, C., Chi-Fru, E., Ruiz, J.M.G., Gauthier-Lafaye, F., Mazurier, A., Pierson-Wickmann, A.C., Rouxel, O., Trentesaux, A., Vecoli, M., Versteegh, G.J.M., White, L., Whitehouse, M., Bekker, A., 2014. The 2.1 Ga old Francevillian biota: biogenicity, taphonomy and biodiversity. PloS One 9. https://doi.org/10.1371/journal.pone.0099438.

Eskrigge, R.A., 1868. Geological notes made during a tour in Leicestershire. Trans. Manchester Geol. Soc. 7, 51–57.

Fairchild, T.R., Sanchez, E.A.M., Pacheco, M.L.A.F., De Moraes Leme, J., 2012. Evolution of Precambrian life in the Brazilian geological record. Int. J. Astrobiol. 11, 309–323. https://doi.org/10.1017/S1473550412000183.

Fedonkin, M.A., 1980. New representantives of precambrian coelenterata north of the Russian platform. Paleontology 2, 7–15.

Fedonkin, M.A., 1978. A new find of non-skeletal soft-bodied metazoa in Vendian deposits of the Zimniy Bereg area on the White Sea. Dokl. Akad. Nauk. 239, 95–98.

Fedonkin, M.A., Simonetta, A., Ivantsov, A.Y., Animale, B., Pardi, L., 2007. New data on Kimberella, the Vendian mollusc-like organism (White Sea region, Russia): Palaeoecological and Evolutionary Implications. pp. 157–179.

Figueiredo, F.T., Almeida, R.P., Tohver, E., Babinski, M., Liu, D., Fanning, C., 2009. Neoproterozoic glacial dynamics revealed by provenance of diamictites of the bebedouro Formation, São Francisco Craton, central eastern Brazil. Terra. Nova 21, 375–385. https://doi.org/10.1111/j.1365-3121.2009.00893.x.

Ford, T.D.B.Y., 1958. Pre-Cambrian fossils from Charnwood forest. Proc. Yorks. Geol. Soc. 31, 211–217. https://doi.org/10.1144/pygs.31.3.211.

Fragoso-César, A.R.S., Fambrini, G.L., Almeida, R.P., Pelosi, A.P.M.R., Janikian, L., Riccomini, C., Machado, R., Nogueira, A.C.R., Saes, G.S., 2000. The Camaquã extensional basin: neoproterozoic to early cambrian sequences in southernmost Brazil. Rev. Bras. Geociencias 30, 442–445.

Gaucher, C., Poire, D.G., Gomez Peral, L., Chiglino, L., 2005. Litoestratigrafia, bioestratigrafia y correlaciones de las sucesiones sedimentarias del neoproterozoico-cambrico del craton del rio de La plata (Uruguay y Argentina). Lat. Am. J. Sedimentol. Basin Anal. 12, 145–160.

Gehling, J.G., Droser, M.L., 2009. Textured organic surfaces associated with the Ediacara biota in South Australia. Earth Sci. Rev. 96, 196–206. https://doi.org/10.1016/j.earscirev.2009.03.002.

Gehling, J.G., Droser, M.L., 2013. How well do fossil assemblages of the Ediacara Biota tell time ? https://doi.org/10.1130/G33881.1.

Gehling, J.G., Narbonne, G.M., Anderson, M.M., 2000. The first named Ediacaran body fossil, Aspidella terranovica. Palaeontology 43, 427–456. https://doi.org/10.1111/j.0031-0239.2000.00134.x.

Glaessner, M.F., 1959. Precambrian coelenterata from Australia, Africa and England. Nature 183, 1472–1473.

Glaessner, M.F., Daily, B., 1959. The geology and Late Precambrian fauna of the Ediacara fossil reserve. Record S. Aust. Mus. 13, 369–401.

Glaessner, M.F., Wade, M., 1966. The late precambrian fossils from Ediacara, South Australia. Paleontology 9, 599–628.

Glaessner, M.F., Walter, M.R., 1975. Alcheringa : an Australasian Journal of Palaeontology New Precambrian Fossils from the Arumbera Sandstone , Northern Territory. pp. 37–41. Australia. https://doi.org/10.1080/03115517508619480.

Góes, A.M.O., Feijó, F.J., 1994. Bacia do Parnaíba. Bol. Geoci. PETROBRAS 8, 57–67.

Gómez-peral, L.E., Kaufman, A.J., Arrouy, M.J., Richiano, S., Sial, A.N., Póiré, D.G., Ferreira, V.P., 2018. Preglacial palaeoenvironmental evolution of the ediacaran loma Negra Formation , far southwestern gondwana , Argentina. Precambrian Res. 315, 120–137. https://doi.org/10.1016/j.precamres.2018.07.005.

Gómez-Peral, L.E., Poiré, D.G., Strauss, H., Zimmermann, U., 2007. Chemostratigraphy and diagenetic constraints on neoproterozoic carbonate successions from the Sierras Bayas group , Tandilia system , Argentina. Chem. Geol. 237, 109–128. https://doi.org/10.1016/j.chemgeo.2006.06.022.

Gómez-peral, L.E., Sial, A.N., Arrouy, M.J., Richiano, S., Ferreira, V.P., 2017. Paleo-climatic and paleo-environmental evolution of the Neoproterozoic basal sedimentary cover on the Río de La Plata Craton , Argentina : insights from the δ13C chemostratigraphy. Sediment. Geol. 353, 139–157. https://doi.org/10.1016/j.sedgeo.2017.03.007.

Goryl, M., Marynowski, L., Brocks, J.J., Bobrovskiy, I., Arkadiusz, D., 2018. Exceptional preservation of hopanoid and steroid biomarkers in Ediacaran sedimentary rocks of the East European Craton. Precambrian Res. 316, 38–47. https://doi.org/10.1016/j.precamres.2018.07.026.

Grazhdankin, D., Gerdes, G., 2007. Ediacaran microbial colonies. Lethaia 40, 201–210. https://doi.org/10.1111/j.1502-3931.2007.00025.x.

Grey, K., 2005. Ediacaran palynology of Australia. Mem. Assoc. Australas. Palaeontol. 31, 1–439.

Hagadorn, J.W., Bottjer, D.J., 1997. Wrinkle stru ctures : microbially mediated sedimentary stru ctures common in subtidal sili cicl astic settings at the Proterozoic-Phanerozoic transition. Geology 25, 1047–1050. https://doi.org/10.1130/0091-7613(1997)025 < 1047:WSMMSS > 2.3.CO;2.

Hagadorn, J.W., Miller, R.F., 2011. Hypothesized cambrian medusae from saint John, new brunswick, reinterpreted as sedimentary structures. Atl. Geol. 47, 66–80. https://doi.org/10.4138/atlgeol.2011.002.

Hill, E., Bonney, T.G., 1877. The pre-Carboniferous rocks of Charnwood Forest. Q. J. Geol. Soc. Lond. 33, 754–789.

Hofmann, H.J., Fritz, W.H., Narbonne, G.M., 1983. Ediacaran (precambrian) fossils from werneck Mountains, northwestern Canada. Science 221, 455–457 (80-.).

Hofmann, H.J., 1981. First record of a late Proterozoic faunal assemblage in the North American Cordillera. Lethaia 14, 303–310.

Hofmann, H.J., 1971. Precambrian fossils, pseudofossils and problematica in Canada: Geological Survey of Canada. Geol. Surv. Canada Bull. 189, 1–146.

Hofmann, H.J., Mountjoy, E.W., Teitz, M.W., 1985. Ediacaran fossils from the miette group, rocky Mountains, british columbia, Canada. Geology 13, 819–821.

Howe, M.P.A., Evans, M., Carney, J.N., Wilby, P., 2012. New perspectives on the globally important Ediacaran fossil discoveries in Charnwood Forest , UK : harley ' s 1848 prequel to Ford (1958). Proc. Yorks. Geol. Soc. 59, 137–144. https://doi.org/10.1144/pygs2012-321.

Hoyal Cuthill, J.F., Han, J., 2018. Cambrian petalonamid Stromatoveris phylogenetically links Ediacaran Biota to later animals. Paleontology 61, 813–823. https://doi.org/10.1111/pala.12393.

Inglez, L., 2018. Estruturas discoides na Formação Cerro Negro (Grupo La Providencia), Argentina e suas implicações para a paleontologia de macrorganismos Pré-Cambrianos. São Paulo State University.

Inglez, L., Okubo, J., Uhlein, G.J., Quaglio, F., Arrouy, M.J., Poiré, D.G., Simões, M.G., Warren, L.V., 2016. New Ediacaran discoidal structures from South America and the implications for their biogenic origin. In: Congresso Brasileiro de Geologia, vol. 48. pp. 1 Porto Alegre.

Ivantsov, A.Y., Gritsenko, V.P., Konstantinenko, L.I., Zakrevskaya, M.A., 2014. Revision of the problematic vendian macrofossil Beltanelliformis (= Beltanelloides, nemiana). Paleontol. J. 48, 1415–1440. https://doi.org/10.1134/S0031030114130036.

Janikian, L., 2004. Seqüências deposicionais e evolução paleoambiental do Grupo Bom Jardim e da Formação Acampamento Velho, Supergrupo Camaquã, Rio Grande do Sul.

Jenkins, R.J.F., Gehling, J.G., 1978. A review of frond-like fossils of the Ediacara assemblage. Record S. Aust. Mus. 17, 347–359.

Jezek, P., 1990. Análisis sedimentológico de la Formación Puncoviscana entre Tucumán y Salta. El Ciclo Pampeano en el Noroeste Argentino. Ser. Correlación Geológica 4, 9–36.

Kahle, C.F.J., 2009. Subaerial gutter marks. raindrop impressions, scour marks and other sedimentary structures, silurian tymochtee dolomite, waterville, Ohio. Carbonates Evaporites 24, 33–44.

Kendall, B., Creaser, R.A., Gordon, G.W., Anbar, A.D., 2009. Re–Os and Mo isotope systematics of black shales from the middle proterozoic velkerri and wollogorang formations, McArthur basin, northern Australia. Geochem. Cosmochim. Acta 73, 2534–2558.

Kerber, B.B., Da Rosa, A.L.Z., Gabas, S.G., De Moraes Leme, J., Pacheco, M.L.A.F., 2013. O registro fossilífero de metazoários ediacaranos na América do Sul e suas implicações nos estudos sobre origem e complexificação da vida animal. Geol. Usp. Série Científica 13, 51–64. https://doi.org/10.5327/Z1519-874X201300030006.

Kolesnikov, A.V., Grazhdankin, D.V., Maslov, A.V., 2012. Arumberia-type structures in the upper vendian of the urals. Dokl. Earth Sci. 447, 1233–1239. https://doi.org/Doi 10.1134/S1028334x12110013.

Laflamme, M., Narbonne, G.U.Y.M., Anderson, M.M., 2004. Morphometric Analysis of the Ediacaran Frond Charniodiscus from the Mistaken Point Formation, Newfoundland. J. Paleontol 78, 827–837.

Laflamme, M., Schiffbauer, J., Dornbos, S., 2011. Quantifying the Early Evolution of Life: Numerical Approaches to the Evaluation of Fossils and Ancient Ecosystems, first ed. vol. 36 Springer Netherlands, Netherlands Topics in Geobiology. https://doi.org/10.1007/978-94-007-0680-4.

Leonov, M.V., 2007. Comparative taphonomy of Vendian genera Beltanelloides and nemiana: taxonomy and lifestyle. In: Vickers-rich, P., Komarower, P. (Eds.), The Rise and Fall of the Ediacaran Biota. Geological Society, London, Specal Publications, pp. 259–267.

Liu, A.G., 2016. Framboidal pyrite shroud confirms the "death mask " model for moldic preservation of Ediacaran soft-bodied organisms. Palaios 31, 259–274. https://doi.org/10.2110/palo.2015.095.

Lork, A., Miller, H., Kramm, U., Grauert, B., 1990. Sistemática U-Pb de circones detríticos de la Formación Puncoviscana y su significado para la edad máxima de sedimentación en la Sierra de Cachi (prov. De Salta, Argentina). Aceñolaza, F.G., Miller, H., Toselli, A.J. (Eds.), El Ciclo Pampeano En El Noreste Argentino. Serie Correlación Geológica 199–208.

Lucas, S.G., 2001. Taphotaxon. Lethaia 34, 30.

Luo, C., Zhu, M., Reitner, J., 2016. The Jinxian Biota revisited: taphonomy and body plan of the Neoproterozoic discoid fossils from the southern Liaodong Peninsula, North China. Paläontol. Z. 90, 205–224. https://doi.org/10.1007/s12542-016-0289-5.

MacGabhann, B.A., 2014. There is no such thing as the "Ediacara Biota. Geosci. Front. 5, 53–62. https://doi.org/10.1016/j.gsf.2013.08.001.

MacGabhann, B.A., 2007. Discoidal fossils of the Ediacaran biota: a review of current understanding. Geol. Soc. London, Spec. Publ. 286, 297–313. https://doi.org/10.1144/SP286.21.

Mapstone, N.B., McIlroy, D., 2006. Ediacaran fossil preservation : taphonomy and diagenesis of a discoid biota from the Amadeus Basin , central Australia. Precambrian Res. 149, 126–148. https://doi.org/10.1016/j.precamres.2006.05.007.

Marconato, A., Paes, R., Almeida, D., 2014. Pre-vegetation fluvial floodplains and channel-belts in the late neoproterozoic – cambrian Santa Bárbara group (southern Brazil). Sediment. Geol. 300, 49–61.

Martins-Neto, M.A., Alkmim, F.F., 2001. Estratigrafia e evolução tectônica das bacias neoproterozoicas do paleocontinente São Francisco e suas margens: registro da quebra de Rodínia e colagem de Gondwana. In: Pinto, C.P., Martins-Neto, M.A. (Eds.), Bacia Do São Francisco: Geologia E Recursos Naturais. Belo Horizonte, pp. 31–54.

McCall, G.J.H., 2006. The Vendian (Ediacaran) in the geological record: enigmas in geology's prelude to the Cambrian explosion. Earth Sci. Rev. 77, 1–229. https://doi.org/10.1016/j.earscirev.2005.08.004.

McMenamin, M.A.S., 1986. The garden of ediacara. Palaios 178–182. https://doi.org/10.2307/3514512.

Menner, V.V., 1963. Paleontological foundation of Upper Pre cambrian stratigraphy:

other problematic fossils. Strat. Graf. SSSR. Verkhnii dokembrii 504–506.
Menon, L.R., Mcilro, D., Brasier, M.D., 2013. Evidence for Cnidaria-like behavior in ca. 560 Ma ediacaran Aspidella. Geology 41, 895–898. https://doi.org/10.1130/G34424.1.
Menon, L.R., Mcilroy, D., Brasier, M.D., 2016.). " Intrites " from the Ediacaran Longmyndian Supergroup , UK : a New Form of Microbially-induced Sedimentary Structure (MISS. Geol. Soc. London, Spec. Publ. https://doi.org/10.1144/SP448.12.
Menon, L.R., McIlroy, D., Liu, A.G., Brasier, M.D., 2015. The dynamic influence of microbial mats on sediments: fluid escape and pseudofossil formation in the Ediacaran Longmyndian Supergroup, UK. J. Geol. Soc. London. 173, 177–185. https://doi.org/10.1144/jgs2015-036.
Metz, R., 1981. Why not raindrop impressions? J. Sediment. Petrol. 51, 265–267.
Moussa, M.T., 1974. Rain-drop impressions? J. Sediment. Petrol. 44, 1118–1121.
Narbonne, G.M., 2005. The ediacara biota: neoproterozoic origin of animals and their ecosystems. Annu. Rev. Earth Planet Sci. 33, 421–442. https://doi.org/10.1146/annurev.earth.33.092203.122519.
Narbonne, G.M., Hofman, H.J., 1987. Ediacaran biota of the wernecke Mountains, yukon, Canada. Palaeontology 30, 647–676.
Narbonne, G.M., Laflamme, M., Trusler, P.W., Dalrymple, R.W., Greentree, C., 2014. Deep-water Ediacaran fossils from northwestern Canada: taphonomy, ecology, and evolution deep-water Ediacaran fossils from NW Canada. J. Paleontol. 88, 207–223.
Netto, R.G., 2012. Evidences of life in terminal proterozoic deposits of southern Brazil. Synthesis 15–26.
Netto, R.G., Paim, P.S.G., Martini da Rosa, C.L., 1992. Informe preliminar sobre a ocorrência de traços fósseis nos sedimentitos das Bacias do Camaquã e Santa Bárbara, in: 1st Workshop Sobre as Bacias Molássicas Brasilianas. Anais 90–96 São Leopoldo.
Noffke, N., 2009. The criteria for the biogeneicity of microbially induced sedimentary structures (MISS) in Archean and younger, sandy deposits. Earth Sci. Rev. 96, 173–180. https://doi.org/10.1016/j.earscirev.2008.08.002.
Noffke, N., Gerdes, G., Klenke, T., 2003. Benthic cyanobacteria and their influence on the sedimentary dynamics of peritidal depositional systems (siliciclastic, evaporitic salty, and evaporitic carbonatic). Earth Sci. Rev. 62, 163–176. https://doi.org/10.1016/S0012-8252(02)00158-7.
Noffke, N., Gerdes, G., Klenke, T., Krumbein, W.E., 2001. Microbially induced sedimentary structures indicating climatological, Hydrological and depositional conditions within recent and pleistocene coastal facies zones (Southern Tunisia). Facies 44, 23–30. https://doi.org/10.1007/BF02668164.
Noffke, N., Gerdes, G., Klenke, T., Krumbein, W.E., 1996. Microbially induced sedimentary structures - examples from modern sediments of siliciclastic tidal flats. Zbl. Geol. Paläont. I, 307–316.
Noffke, N., Krumbein, W.E., 1999. A quantitative approach to sedimentary surface structures contoured by the interplay of microbial colonization and physical dynamics. Sedimentology 46, 417–426. https://doi.org/10.1046/j.1365-3091.1999.00218.x.
Oliveira, D.C., 2000. Stratigraphic interplays between igneous and sedimentary events in the early palaeozoic Jaibaras Trough (Northeast Brazil). Revista Brasileira de Geologia 30, 427–431.
Pacheco, M.L.A.F., Galante, D., Rodrigues, F., De, J., 2015. Insights into the skeletonization , lifestyle , and affinity of the unusual ediacaran fossil Corumbella. PloS One 10, 1–19. https://doi.org/10.1371/journal.pone.0114219.
Paim, P.S.G., Chemale Junior, F., Lopes, R. da C., 2000. A bacia do Camaquã. In: Holz, M., De Ros, L.F. (Eds.), Geologia Do Rio Grande Do Sul. CIGO/UFRGS, pp. 231–274.
Paim, P.S.G., Chemale Junior, F., Wildner, W., 2014. Estágios evolutivos da bacia do Camaquã (rs). Cienc. Nat. 36, 183–193. https://doi.org/10.5902/2179460X13748.
Paim, P.S.G., Fonseca, M.M., 2004. Bacias do estágio da transição da plataforma Sulamericana. In: Mantesso-Neto, Bartorelli, Carneiro, Brito-Neves (Eds.), Geologia Do Continente Sul-Americano: Evolução Da Obra de Fernando Flávio Marques de Almeida. Beca, São Paulo.
Paim, P.S.G., Leipnitz, I., da Rosa, A.L.Z., da Rosa, Á.A.S., 1997. Preliminary report on the occurrence of Chancelloria sp. in the Itajaí basin, southern Brazil. Rev. Bras. Geociencias 27, 303–308.
Palij, V.M., 1976. Remains of a skeletonless fauna and traces of life ability from deposits of the Upper Precambrian and Lower Cambrian of Podolia. In: Paleontologiya I Stratigrafiya Verkhnego Dokembriya I Nizhnego Paleozoya Yugozapada VostochnoEvropeiskoi Platformy (Paleontology and Stratig Raphy of the Upper Precambrian and Lower Paleozoic of the Southwestern East European Platform). Naukova Dumka, Kiev, pp. 63–77.
Pankhurst, R.J., Ramos, A., Linares, E., 2003. Antiquity of the río de la Plata craton in Tandilia, southern Buenos Aires province, Argentina. J. South Am. Earth Sci. 16, 5–13. https://doi.org/10.1016/S0895-9811(03)00015-4.
Parry, L.A., Boggiani, P.C., Condon, D.J., Garwood, R.J., Leme, J., de, M., McIlroy, D., Brasier, M.D., Trindade, R., Campanha, G.A.C., Pacheco, M.L.A.F., 2017. Ichnological evidence for meiofaunal bilaterians from the terminal Ediacaran and earliest Cambrian of Brazil. Nat. Ecol. Evol. 1, 1455.
Paula-santos, G.M., Babinski, M., Kuchenbecker, M., Caetano-filho, S., Ivan, R., Pedrosa-soares, A.C., 2014. New evidence of an Ediacaran age for the Bambuí Group in southern São Francisco craton (eastern Brazil) from zircon U – Pb data and isotope chemostratigraphy. Gondwana Res. 28 (2), 702–720. https://doi.org/10.1016/j.gr.2014.07.012.
Poiré, D.G., 2002. Neoproterozoic/lower paleozoic sedimentary successions of the Tandilia system, Argentina. IGCP 478, 1–57.
Põldsaar, K., Ainsaar, L., 2014. Extensive soft-sediment deformation structures in the early Darriwilian (Middle Ordovician) shallow marine siliciclastic sediments formed on the Baltoscandian carbonate ramp , northwestern Estonia. Mar. Geol. 356, 111–127. https://doi.org/10.1016/j.margeo.2013.08.012.
Porada, H., Bouougri, E.H., 2007. Wrinkle structures-a critical review. Earth Sci. Rev. 81, 199–215. https://doi.org/10.1016/j.earscirev.2006.12.001.
Porada, H., Ghergut, J., Bouougri, E.H., 2008. Kinneyia-type wrinkle structures–critical review and model of formation. Palaios 23, 65–77. https://doi.org/10.2110/palo.2006.p06-095r.
Pringle, J.K., Westerman, a R., Stanbrook, D. a, Tatum, D.I., Gardiner, a R., 2007. Sand volcanoes of the carboniferous ross formation, county clare, western Ireland: 3-D internal sedimentary structure and formation. In: Hurst, A., Cartwright, J. (Eds.), Sand Injectites: Implications for Hydrocarbon Exploration and Production, pp. 227–231. https://doi.org/-.
Retallack, G.J., 2016. Ediacaran Fossils in Thin-section Ediacaran Fossils in Thin-section 5518. https://doi.org/10.1080/03115518.2016.1159412.
Retallack, G.J., 2012a. Ediacaran life on land. Nature 1–4. https://doi.org/10.1038/nature11777.
Retallack, G.J., 2012b. Were Ediacaran siliciclastics of South Australia coastal or deep marine ? Sedimentology 59, 1208–1236. https://doi.org/10.1111/j.1365-3091.2011.01302.x.
Rostirolla, S.P., Figueira, E.G., 1995. Associações de fácies turbidíticas do Grupo Itajaí, SC:sedimentação de água profunda em uma bacia de antepaís. Bol. Parana. Geociencias 43, 79–94.
Salter, J.W., 1856. On fossil remains in the cambrian rocks of the longmynd and north wales. Proc. Geol. Soc. 246–251. https://doi.org/10.1144/GSL.JGS.1856.012.01-02.31.
Sanchez, E.A.M., 2014. O registro paleontológico da Formação Sete Lagoas como documento da história geológica do Neoproterozoico brasileiro. São Paulo University.
Schiffbauer, J.D., Xiao, S., 2009. Novel application of focused ion beam electron microscopy (FIB-EM) in preparation and analysis of microfossil ultrastructures : a new view of complexity in early eukaryotic organisms. Palaios 24, 616–626. https://doi.org/10.2110/palo.2009.p09-003r.
Seilacher, A., 1992. Vendobionta and Psammocorallia - lost constructions of Precambrian evolution. J. Geol. Soc. London 607–613.
Seilacher, A., 1984. Late precambrian and early cambrian metazoa: preservational or real extinctions? In: Holland, A.F., Trendall, A.F. (Eds.), Patterns of Change in Earth Evolution. Springer-Verlag, Berlin, Heidelberg, New York, Tokyo, pp. 159–168.
Seilacher, A., Buatois, L.A., Mángano, M.G., 2005. Trace fossils in the Ediacaran – cambrian transition : behavioral diversification , ecological turnover and environmental shift. Palaeogeogr. Palaeoclimatol. Palaeoecol. 227, 323–356. https://doi.org/10.1016/j.palaeo.2005.06.003.
Shen, Y., Zhang, T., Hoffman, P.F., 2008. On the Coevolution of Ediacaran Oceans and Animals.
Silva, L.C., 1991. O Cinturão Metavulcanossedimentar Brusque e a evolução policíclica das faixas dobradas Proterozóicas no sul do Brasil: uma revisão. Rev. Bras. Geociências 21, 60–73.
Soares, P.C., 1987. Seqüências tecto-sedimentares e tectônica deformadora no centro-oeste do Escudo Paranaense. In: In: Geologia, S.B. de (Ed.), III Simpósio Sul-Brasileiro de Geologia, vol. 2. Atas, Curitiba, pp. 743–771.
Sommer, F.W., 1982. Mais oncólitos do calcário Bambuí de Minas Gerais.pdf. An. Acad. Bras. Cienc. 54, 343–349.
Sommer, F.W., 1981. Oncólitos do calcário Bambuí de Minas gerais. An. Acad. Bras. Cienc. 53, 785–791.
Sommer, F.W., 1971. Microfósseis do calcário Bambuí, de Pedro leopoldo, estado de Minas gerais. An. Acad. Bras. Cienc. 43, 135–139.
Sprigg, R.G., 1949. Early cambrian "jellyfishes" of ediacaran, south Australia, and Mount John, kimberley district, western Australia. Trans. Roy. Soc. S. Aust. 73, 72–99.
Sprigg, R.G., 1947. Early cambrian (?) jellyfishes from Flinders ranges, south Australia. Trans. Roy. Soc. S. Aust. 71, 212–224.
Strzebonski, P., Uchman, A., 2015. The trace fossil Gyrophyllites in deep-sea siliciclastic deposits of the Istebna Formation (Upper Cretaceous – palaeocene) of the Carpathians : an example of biologically controlled distribution. Palaeogeogr. Palaeoclimatol. Palaeoecol. 426, 260–274. https://doi.org/10.1016/j.palaeo.2015.03.004.
Sun, Weiguo, 1986. Precambrian medusoids: the Cyclomedusa plexus and Cyclomedusa-like pseudofossils. Precambrian Res. 31, 325–360. https://doi.org/10.1016/0301-9268(86)90039-2.
Taj, R.J., Aref, M.A.M., Schreiber, B.C., 2014. The influence of microbial mats on the formation of sand volcanoes and mounds in the red sea coastal plain, south Jeddah, Saudi Arabia. Sediment. Geol. 311, 60–74. https://doi.org/10.1016/j.sedgeo.2014.06.006.
Tang, Q., Pang, K., Yuan, X., Xiao, S., 2016. Electron microscopy reveals evidence for simple multicellularity in the Proterozoic fossil Chuaria Electron microscopy reveals evidence for simple multicellularity in the Proterozoic fossil Chuaria. Geology. https://doi.org/10.1130/G38680.1.
Tarhan, L.G., Droser, M.L., Gehling, J.G., 2010. Taphonomic controls on ediacaran diversity: uncovering the holdfast origin of morphologically variable enigmatic structures. Palaios 25, 823–830. https://doi.org/10.2110/palo.2010.p10-074r.
Tarhan, L.G., Droser, M.L., Gehling, J.G., Dzaugis, M.P., 2015. Taphonomy and morphology of the Ediacara form genus Aspidella. Precambrian Res. 257, 124–136. https://doi.org/10.1016/j.precamres.2014.11.026.
Tu, C., Chen, Z.Q., Retallack, G.J., Huang, Y., Fang, Y., 2016. Proliferation of MISS-related microbial mats following the end-Permian mass extinction in terrestrial ecosystems: evidence from the Lower Triassic of the Yiyang area, Henan Province, North China. Sediment. Geol. 333, 50–69. https://doi.org/10.1016/j.sedgeo.2015.12.006.
Van Loon, A.J., 2008. The nature of Mawsonites (Ediacara fauna). Gondwana Res. 14, 175–182. https://doi.org/10.1016/j.gr.2007.08.009.
Van Loon, A.J., Maulik, P., 2011. Abraded sand volcanoes as a tool for recognizing paleo-earthquakes, with examples from the Cisuralian Talchir Formation near Angul (Orissa, eastern India). Sediment. Geol. 238, 145–155. https://doi.org/10.1016/j.

sedgeo.2011.04.009.
Vieira, L.C., Nogueira, A.C.R., Ader, M., 2007. Identification if a sturtian cap carbonate in the neoproterozoic Sete Lagoas carbonate platform, Bambuí group. Brazil. C.R. Geosci. 339, 240–258.
Wacey, D., Gleeson, D., Kilburn, M.R., 2010. Microbialite taphonomy and biogenicity : new insights from NanoSIMS. Geobiology 403–416. https://doi.org/10.1111/j.1472-4669.2010.00251.x.
Wade, M., 1972. Hydrozoa and scyphozoa and other medusoids from the precambrian ediacara fauna, south Australia. Palaeontology 15, 197–225.
Wade, M., 1969. Medusae from uppermost precambrian or cambrian sandstones, Central Australia. Palaeontology 12 (3), 351–365.
Waggoner, B., 2003. The ediacaran biotas in space and time. Integr. Comp. Biol. 113, 104–113.
Wan, B., Xiao, S., Yuan, X., Chen, Z., Pang, K., Tang, Q., Guan, C., Maisano, J.A., 2014. Orbisiana linearis from the early Ediacaran Lantian Formation of South China and its taphonomic and ecological implications. Precambrian Res. 255, 266–275. https://doi.org/10.1016/j.precamres.2014.09.028.
Warren, L.V., Fairchild, T.R., Gaucher, C., Boggiani, P.C., Poiré, D.G., Anelli, L.E., Inchausti, J.C.G., 2011. Corumbella and in situ Cloudina in association with thrombolites in the ediacaran Itapucumi group, Paraguay. Terra. Nova 23, 382–389. https://doi.org/10.1111/j.1365-3121.2011.01023.x.
Warren, L.V., Quaglio, F., Simões, M.G., Gaucher, C., Riccomini, C., Poiré, D.G., Freitas, B.T., Boggiani, P.C., Sial, A.N., 2017. Cloudina - Corumbella - Namacalathus association from the Itapucumi group , Paraguay : increasing ecosystem complexity. Precambrian Res. 298, 79–87. https://doi.org/10.1016/j.precamres.2017.05.003.
Warren, L.V., Pacheco, M.L.A.F., Fairchild, T.R., Simões, M.G., Riccomini, C., Boggiani, P.C., Cáceres, A.A., 2012. The dawn of animal skeletogenesis : ultrastructural analysis of the Ediacaran metazoan Corumbella werneri. Geology 1–4. https://doi.org/10.1130/G33005.1.
Warren, L.V., Quaglio, F., Riccomini, C., Simões, M.G., Poiré, D.G., Strikis, N.M., Anelli, L.E., Strikis, P.C., 2014. The Puzzle Assembled : Ediacaran Guide Fossil Cloudina Reveals an Old Proto-Gondwana Seaway 1–4. https://doi.org/10.1130/G35304.1.
Watts, W.W., 1947. Geology of the ancient rocks of Charnwood forest, leicestershire. Leicester lit. Philos. Soc. Leicester.
Weston, T.C., 1892. Notes on concretionary structures. Trans. Nov. Scotian Inst. Sci 137–142.
Xiao, S., 2013. Fossils come in to land. Nature 493, 28–29. https://doi.org/10.1038/nature11765.
Xiao, S., Laflamme, M., 2008. On the Eve of Animal Radiation : Phylogeny , Ecology and Evolution of the Ediacara Biota. https://doi.org/10.1016/j.tree.2008.07.015.
Zucatti da Rosa, A.L., 2005. Evidências de vida no Ediacarano inferior da Bacia do Itajaí, SC. Universidade do Vale do Rio dos Sinos.

Apêndice C: Co-autoria em artigos científicos relacionados ao tópico da tese: Uhlein et al. (2019). Ediacaran paleoenvironmental changes recorded in the mixed carbonatesiliciclastic Bambuí Basin, Brazil", *Palaeogeography, Palaeoclimatology, Palaeoecolog*y, *517: 39-51*.

Palaeogeography, Palaeoclimatology, Palaeoecology 517 (2019) 39–51

Contents lists available at ScienceDirect

Palaeogeography, Palaeoclimatology, Palaeoecology

journal homepage: www.elsevier.com/locate/palaeo

Ediacaran paleoenvironmental changes recorded in the mixed carbonate-siliciclastic Bambuí Basin, Brazil

Gabriel J. Uhlein[a,*], Alexandre Uhlein[a,1], Egberto Pereira[b,1], Fabrício A. Caxito[a,1], Juliana Okubo[c], Lucas V. Warren[c,1], Alcides N. Sial[d,1]

[a] Centro de Pesquisas Manoel Teixeira da Costa, Instituto de Geociências, Universidade Federal de Minas Gerais, Campus Pampulha, Av. Antônio Carlos 6627, 31270-901 Belo Horizonte, MG, Brazil
[b] Departamento de Paleontologia e Estratigrafia, Faculdade de Geologia, Universidade do Estado do Rio de Janeiro – UERJ, Av. São Francisco Xavier, 524, Maracanã, 20550-013 Rio de Janeiro, RJ, Brazil
[c] Departamento de Geologia Aplicada, Instituto de Geociências e Ciências Exatas, Universidade Estadual Paulista, Avenida 24A, 1515, 13506-900 Rio Claro, SP, Brazil
[d] NEG-LABISE, Departamento de Geologia, Universidade Federal de Pernambuco, Av. da Arquitetura, s/n, 50670-901 Recife, PE, Brazil

ARTICLE INFO

Keywords:
West Gondwana
Paleogeography
Depositional settings
Chemostratigraphy
Carbon isotope excursion
Carbon burial

ABSTRACT

Significant Ediacaran paleoenvironmental changes recorded in the mixed carbonate-siliciclastic Bambuí Basin, east-central Brazil, outcrop in one of the best-preserved sites, the Januária paleo-high. From a detailed stratigraphic and chemostratigraphic approach (carbon and oxygen isotopes, total organic carbon, total sulfur and selected elements abundances), we identified transgressive-regressive intervals and depositional settings within the Bambuí Group stratigraphy and developed a new model for the origin of the extremely positive Middle Bambuí Excursion (MIBE) present in the middle section of the basin. A post-Marinoan cap carbonate interval is recorded in the first ~10 m, preserving aragonite pseudomorph fans, barite-rich layers and negative $\delta^{13}C$ anomaly. A hiatus separates the cap carbonate from the late Ediacaran succession that makes up the remaining Bambuí Group. The younger intervals preserve both siliciclastic (middle Serra de Santa Helena Formation) and carbonate (middle/upper Sete Lagoas and Lagoa do Jacaré formations) shallow-water depositional settings, requiring tectonic influence or climatic changes in source areas. The MIBE yields $\delta^{13}C$ values as high as +14‰ and extends for about 350 m, from the upper Sete Lagoas Formation to the lower Serra da Saudade Formation. We suggest a model of a restricted basin setting that favored local carbon isotopic signals in the $\delta^{13}C$ record of sedimentary carbonates through preferential weathering of ancient carbonate platforms on the continent and higher burial rate of authigenic carbonate. This scenario caused the global $\delta^{13}C$ budget to be affected by an offset of, at least, +4‰ in sedimentary carbonates deposited on the São Francisco craton and along its margin during the terminal Ediacaran. Many previous studies suggested a restricted nature for the middle Bambuí Basin, which probably resulted from the central position of the São Francisco paleocontinent within the mosaic of collisional blocks during the SW Gondwana amalgamation.

1. Introduction

The Ediacaran Period (635–541 Ma) was marked by the most significative biological and geochemical changes in Earth's geologic record. This interval comprises at least three extremely negative carbon isotope excursions related to three putative global glacial events, steeply rising seawater $^{87}Sr/^{86}Sr$, geochemical evidences for increasing oxygenation of the deep ocean and the emergence of the first metazoans (e.g. Narbonne, 2005; Fike et al., 2006; Narbonne et al., 2012; Sahoo et al., 2016; Xiao et al., 2016). Many of these global events are well recorded in distinct Ediacaran basins, such as in Northwest Canada (Macdonald et al., 2013), South China (Tahata et al., 2013), Namibia (Kaufman et al., 1991; Halverson et al., 2005; Penny et al., 2014), Oman (Fike et al., 2006), Australia (Calver, 2000) and Paraguay (Warren et al., 2011, 2012). In Brazil, the most well-known Ediacaran basins from the stratigraphic, paleontological and geochemical approach, are the early Ediacaran Araras Group in the Amazon craton (e.g. Nogueira et al., 2007; Sansjofre et al., 2011, 2014) and the late Ediacaran Corumbá Group in the South Paraguay Belt (e.g. Gaucher et al., 2003; Boggiani et al., 2010).

* Corresponding author.
E-mail address: guhlein@ufmg.br (G.J. Uhlein).
[1] Fellow of the Brazilian Research Council (CNPq).

https://doi.org/10.1016/j.palaeo.2018.12.022
Received 11 July 2018; Received in revised form 24 December 2018; Accepted 30 December 2018
Available online 03 January 2019
0031-0182/

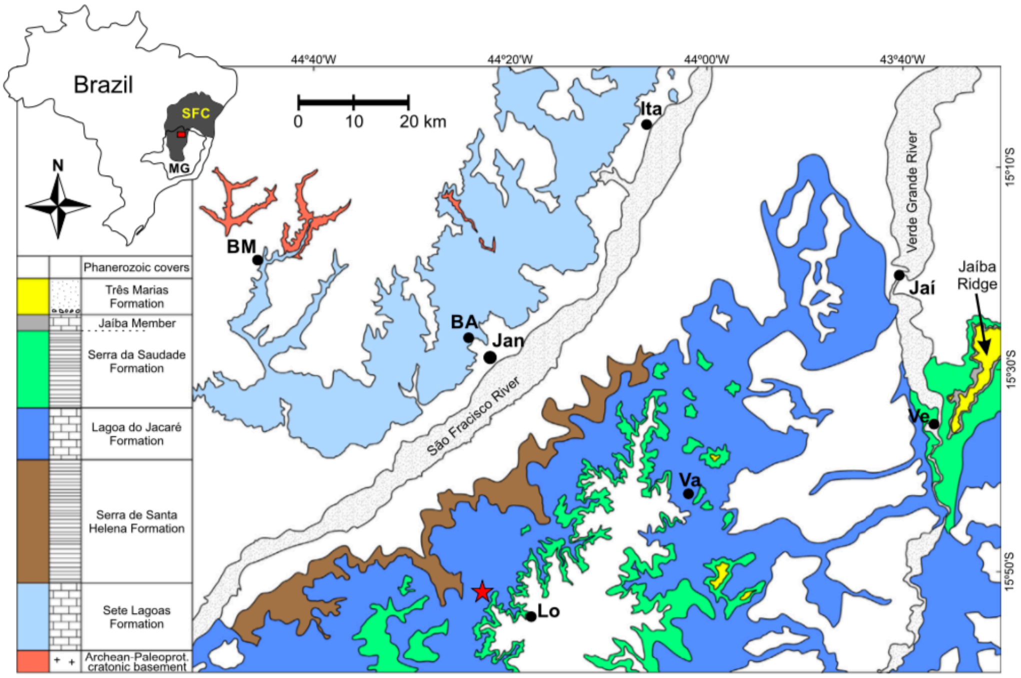

Fig. 1. Geologic map of the northern Minas Gerais state in the region of the São Francisco and Verde Grande Rivers valleys (Januária paleo-high). SFC and MG in the inset mean São Francisco craton and Minas Gerais state, respectively. Cities and villages: Bonito de Minas (BM); Brejo do Amparo (BA); Januária (Jan); Itacarambi (Ita); Lontra (Lo); Varzelândia (Va); Verdelândia (Ve); Jaíba (Jaí). The red star in the map indicates the 1-PSB-14-MG drillcore. Compiled from 1:100.000 geologic maps of Kuchenbecker et al. (2013), Romano et al. (2014, 2015), A. Uhlein et al. (2014), G.J. Uhlein et al. (2014) and Caxito et al. (2014). (For interpretation of the references to colour in this figure legend, the reader is referred to the web version of this article.)

An Ediacaran age was recently assigned to the Bambuí Group after three pivotal evidence: (1) recognition of early Ediacaran post-glacial cap carbonate interval at its base (Caxito et al., 2012a; Okubo et al., 2018), (2) identification of *Cloudina*-rich levels together with sparse *Corumbella* fragments and ichnofossils in the middle Sete Lagoas Formation (Warren et al., 2014) and (3) dating of detrital zircons of Ediacaran age (Paula-Santos et al., 2015). The Sete Lagoas Formation, and especially its early Ediacaran cap carbonate interval, is undoubtedly the best studied interval in the Bambuí Basin (e.g. Vieira et al., 2007a, 2007b, 2015; Caxito et al., 2012a, 2018; Alvarenga et al., 2014; Drummond et al., 2015; Paula-Santos et al., 2015, 2017; Kuchenbecker et al., 2016a; Perrella et al., 2017; Crockford et al., 2017; Okubo et al., 2018). However, integrate studies covering all units of the Bambuí Basin regarding its stratigraphy, chemostratigraphy and basin evolution are yet to be conducted. The newly established Ediacaran age for the Bambuí Basin opens new research frontiers, especially regarding the possibility of bio-, chemo-, chrono- and lithostratigraphic correlations with many other coeval basins around the world. In this paper, we present new data acquired from the Bambuí Basin in one of the best-exposed and less known sites, the Januária paleo-high (Figs. 1 and 2). In this area, a whole succession allows us to access the entire basin stratigraphy as non-deformed and unmetamorphosed rocks that enable the acquisition of reliable stratigraphic and chemostratigraphic data. Therefore, the data presented in this paper constitute the most complete and integrate stratigraphic archive of the Bambuí Group in a single study area, including 105 new carbon and oxygen isotope analysis and 147 total organic carbon and total sulfur data. We also present a complete stratigraphic framework for the Bambuí Group and discuss the origin of the highly positive carbon isotope anomaly in its middle portion (the MIddle Bambuí carbon isotope Excursion, or MIBE). As deposition of the Bambuí Group probably spanned the entire Ediacaran (and perhaps up to the Cambrian), the data presented here are fundamental to understand the evolution of an Ediacaran mixed carbonate-siliciclastic succession strongly influenced by unprecedented geochemical and biological changes in this key interval of Earth's history.

2. Geologic setting

The Bambuí Group is a north-south trending basin that covers hundreds of thousands of square kilometers in the states of Minas Gerais, Bahia, Goiás and Tocantins in east-central Brazil. It comprises a mixed carbonate-siliciclastic succession (Dardenne, 1978) composed of, from base to top: Jequitaí Formation (siliciclastic, glacial); Sete Lagoas Formation (carbonate ramp, marine), Serra de Santa Helena Formation (siliciclastic/carbonate, shallow-marine) Lagoa do Jacaré Formation (carbonate, marine), Serra da Saudade Formation (siliciclastic, marine) and Três Marias Formation (siliciclastic, continental to marine). This putative foreland basin was entirely deposited in the upper Neoproterozoic (late Cryogenian to Ediacaran) and probably developed on the western margin of the São Francisco craton in response to orogenic loading due to the advance of Brasiliano/Pan-African thrust fronts (Dardenne, 1978; Chang et al., 1988; Martins-Neto, 2009; Sial et al., 2009; Reis and Suss, 2016; Uhlein et al., 2017). Locally, the Bambuí succession overlies Mesoproterozoic to early Neoproterozoic metasedimentary rocks such as the Paranoá, Conselheiro Mata and Macaúbas Groups (Santos et al., 2004; Alvarenga et al., 2007, 2012, 2014). On the Sete Lagoas and Januária paleo-highs, the Bambuí Group overlies the Archean and Paleoproterozoic cratonic basement (Vieira et al., 2007a; Uhlein et al., 2016; Perrella et al., 2017; Fig. 1).

The Jequitaí Formation comprises a ca. 100 m-thick package of glacial diamictites, siltstones and sandstones locally covering glacial striated pavements (Isotta et al., 1969; Uhlein et al., 2011a). Above this

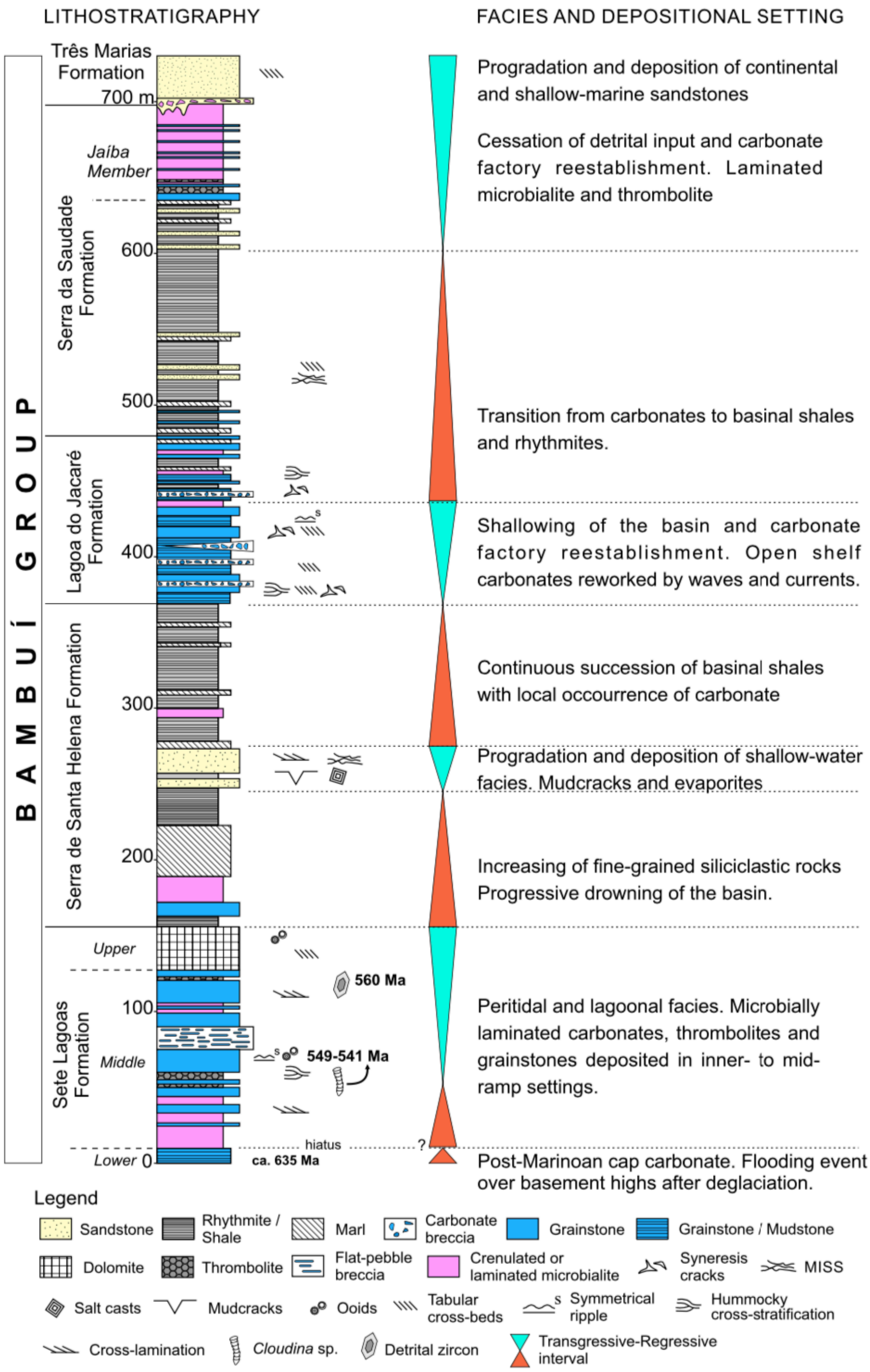

Fig. 2. Lithostratigraphy of the Bambuí Group outcropping on the Januária paleo-high. *Cloudina* biostratigraphic range based on Grotzinger et al. (1995) and Amthor et al. (2003). U-Pb detrital zircon data from Paula-Santos et al. (2015).

succession, the lower Sete Lagoas Formation represents the beginning of deposition of the carbonate succession of the Bambuí Group. It comprises the post-glacial early Ediacaran deposits characterized by pink dolostones and limestones that bear many characteristics of a post-Marinoan cap carbonate interval such as: (1) a basal pink cap dolostone with negative $\delta^{13}C$ and $\delta^{18}O$ values that decrease up section; (2) an overlying transgressive carbonate interval with aragonite pseudomorphs and locally barite fans. In these layers, negative $\delta^{13}C$ gradually increase upwards to around 0‰ (Caxito et al., 2012a; Alvarenga et al., 2014; Okubo et al., 2018). Recently, Crockford et al. (2017) analyzed the cm-thick barite layers for triple oxygen and sulfur isotopes and identified a strong negative $\Delta^{17}O$ anomaly down to −1.05‰. The authors suggest a global character for this geochemical signal used to cross-correlate Marinoan post-glacial cap carbonates around the world (with examples in China, Mauritania, Canada, Australia and now, Norway and Brazil). $^{87}Sr/^{86}Sr$ data show constant values around 0.7075 rarely reaching up to 0.7083 (Caxito et al., 2012a, 2018; Alvarenga et al., 2014; Paula-Santos et al., 2017). Deposition of the middle Sete Lagoas Formation carbonate interval, sitting above the cap carbonate interval, is constrained to the late Ediacaran due to *Cloudina*-bearing levels identified on the Januária paleo-high and detrital zircons as young as ca. 560 Ma (Warren et al., 2014; Paula-Santos et al., 2015). This suggests a cryptic discordance between the post-Marinoan cap carbonate and the upper sequence containing Ediacaran detrital zircons and *Cloudina* remnants, which is also supported by different detrital zircon provenance patterns from western conglomeratic wedges below (younger zircons at ca. 630 Ma) and above (younger zircons at ca. 560 Ma; Uhlein et al., 2017).

Detrital zircons recovered from other Bambuí Group units (Sete Lagoas Formation and above) also yield Ediacaran youngest U-Pb age peaks. Differences in Ediacaran age spectras between units are related to changes in provenance within the Bambuí Basin and position of the sample collection site, if it is close to the westward early Ediacaran Brasília Belt (Rodrigues, 2008; Uhlein et al., 2017) or to the eastward middle/late Ediacaran Araçuaí Belt (Paula-Santos et al., 2015; Kuchenbecker et al., 2015).

The Serra de Santa Helena, Lagoa do Jacaré and Serra da Saudade formations (all presumably terminal Ediacaran in age), make up a carbonate interval (Lagoa do Jacaré) between two fine-grained mainly siliciclastic units (Serra de Santa Helena and Serra da Saudade). Carbonates from the Serra de Santa Helena and Lagoa do Jacaré formations yield very positive $\delta^{13}C$ values (locally up to +16‰) and almost invariant $^{87}Sr/^{86}Sr$ ratios around 0.7075, something unusual for late Ediacaran carbonates (Iyer et al., 1995; Santos et al., 2004; Misi et al., 2007; Paula-Santos et al., 2017). Finally, the succession culminates with cross-bedded sandstones and shales of the Três Marias Formation that represent a progradation of fluvial to shallow-marine deposits over the marine succession.

In the southern Bambuí Basin, the Carrancas Formation outcrops above the cratonic basement and below the Sete Lagoas Formation, recording graben filling sedimentation before the onset of the Marinoan glaciation (Cryogenian interglacial) over the São Francisco craton (Uhlein et al., 2013, 2016). This classic stratigraphic framework is, however, not valid for the whole Bambuí Group, as in the southwestern part of the basin, where foreland-related conglomerate wedges (the Samburá and Lagoa Formosa formations) are interbedded with the base and upper parts of the Bambuí Group (Uhlein et al., 2011b, 2017).

3. Methods

Sedimentological and stratigraphic interpretations are based on high detail field descriptions. Almost all samples were collected in the course of measuring stratigraphic sections in the field. The exception is samples from the Serra de Santa Helena Formation provided by the Brazilian Geological Service (Brandalise, 1980), which were collected from a drillcore located near the town of Lontra (see the red star in Fig. 1 for location). Emphasis was placed on recognizing stacking patterns, stratigraphic surfaces, understanding paleoenvironmental settings, regional stratigraphic trends and collection of samples for chemostratigraphic analysis. Strata are generally flat-lying or gently folded; however, deformation with the development of an incipient east-dipping cleavage and open folds with N-S trending axis become more prominent to the east near the Araçuaí Fold Belt west-verging thrust fronts.

Non-weathered dolostones, limestones and shales free of veining or intense recrystallization features were preferably selected for sampling. The rock samples were sectioned in slabs, powdered in agate mortar and sieved through an 80 µm sieve in the facilities of the Centro de Pesquisa Manoel Teixeira da Costa (CPMTC), Instituto de Geociências, UFMG, for total organic carbon (TOC) and total sulfur analyses. For isotopes, about 20 mg of powder was obtained via microdrilling of the rock slabs.

For total organic carbon and total sulfur analyses, about 250 mg of sample was fumed with HCl (50%) to remove inorganic carbon for 18 h. The decarbonated sample was six times rinsed with distilled water, taken to complete dryness and analyzed for carbon and sulfur content via combustion at 1350 °C with a LECO SC-632 analyzer hosted in the Chemostratigraphic and Organic Geochemistry Laboratory of the Universidade do Estado do Rio de Janeiro (UERJ). The accuracy of the analysis was based on the standard LECO-TOC 502-308-L1017 (TOC = 2.30%; TS = 0.031%). The weight difference after decarbonation process measured the carbonate content of each sample.

Carbonate samples (carbonate content > 50%) from the Sete Lagoas, Serra de Santa Helena, Lagoa do Jacaré and Serra da Saudade formations had their carbon and oxygen isotope ratios measured on a Kiel IV Carbonate Devise coupled to a Delta V Plus - IRMS (Thermo Scientific) system in the Chemostratigraphic and Organic Geochemistry Laboratory of the Universidade do Estado do Rio de Janeiro, Brazil. Approximately 100 µg of sample powder were weighed into glass vials and reacted individually with H_3PO_4. The released CO_2 was collected cryogenically, and isotope ratios were measured against an in-house reference gas in dual inlet mode. Samples were calibrated to VPDB (Vienna Pee Dee Belemnite) using the IAEA-CO-1-Marble standard reference ($\delta^{13}C = +2.492‰_{VPDB}$; $\delta^{18}O = -2.4‰_{VPDB}$). Errors for $\delta^{13}C$ and $\delta^{18}O$ were better than 0.04‰ and 0.08‰ (1σ), respectively, based on repeated analyses of standards.

The Jaíba Member carbonates had their CO_2 extracted on a high vacuum line after reaction with phosphoric acid at 25 °C, and cryogenically cleaned at the Stable Isotope Laboratory (LABISE) of the Department of Geology, Universidade Federal de Pernambuco, Brazil. Released CO_2 gas was analyzed for O and C isotopes in a double inlet, triple collector mass spectrometer (VG-Isotech SIRA II), using the BSC reference (Borborema Skarn Calcite) that was calibrated against NBS-20 ($\delta^{13}C = -1.05‰_{VPDB}$; $\delta^{18}O = -4.22‰_{VPDB}$). The external precision, based on multiple standard measurements of NBS-19, was better than 0.1‰ for carbon and oxygen.

Mn, Mg, Sr and Ca abundances were analyzed by SGS Geosol (Vespasiano town, Brazil). Concentrations were measured via ICP-OES after fusion with lithium metaborate/tetraborate and digestion with diluted nitric acid. Analytical errors are within 5% for major elements.

4. The Bambuí Basin on the Januária paleo-high

4.1. Facies and depositional settings

4.1.1. Sete Lagoas Formation

The basal part of the Sete Lagoas Formation in the Januária paleo-high is characterized by the presence of typical features found in post-Marinoan cap carbonates around the world (Hoffman and Schrag, 2002; Hoffman, 2011). This interval starts with a 1–2 m-thick laminated and micropeloidal beige cap dolostone deposited directly above gneisses of the Paleoproterozoic basement (Fig. 3A). The cap dolostone succession

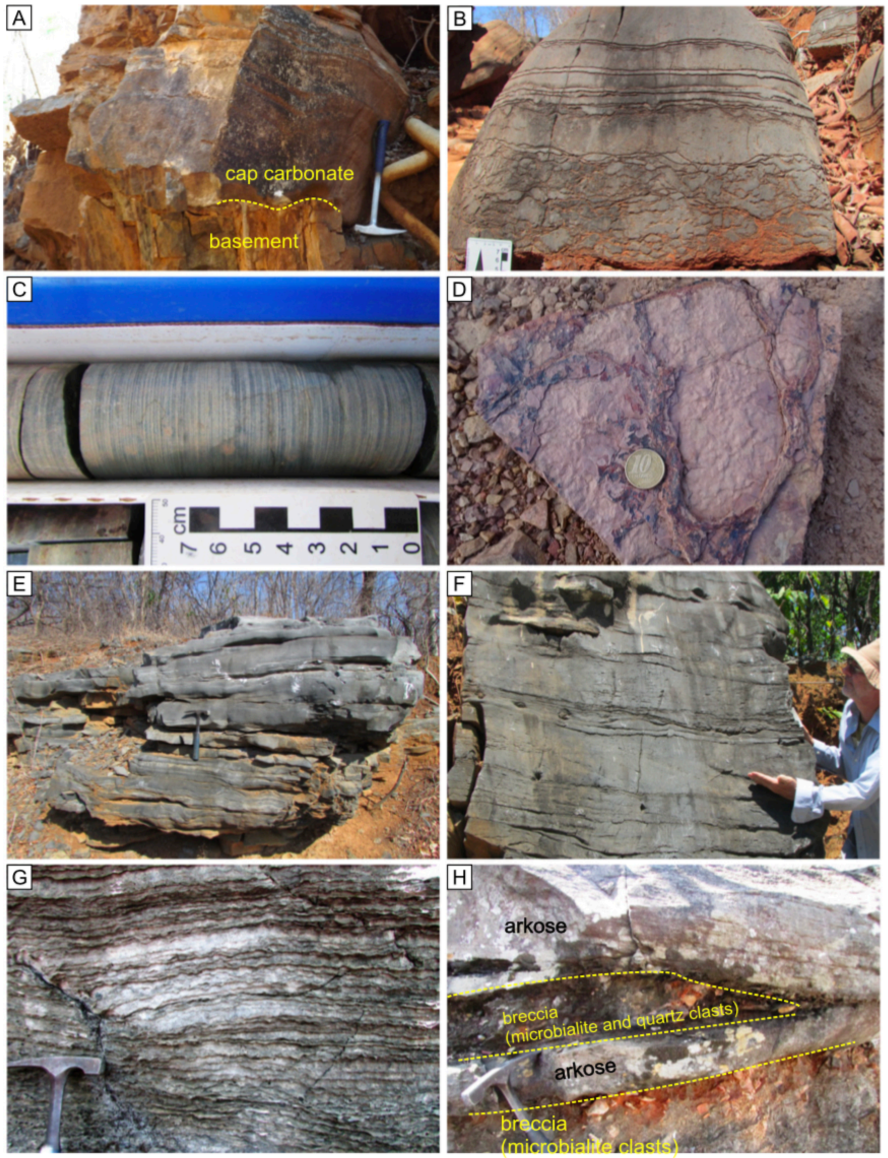

Fig. 3. Lithofacies of the Bambuí Group. A) Sharp and irregular contact (yellow line) of the lower Sete Lagoas cap carbonate with the basement gneiss; B) Thrombolites-grainstones facies association in the middle part of the unit; C) Detail of mud-silt rhythmite facies of the lower Serra de Santa Helena Formation; D) Shale with polygonal mudcracks of the middle Serra de Santa Helena Formation; E) Black to gray laminated carbonates of the Lagoa do Jacaré Formation; F) Grainstones with tabular cross-stratifications intercalated by microbialite beds; G) Microbial lamination in carbonates of the Jaíba Member (upper Serra da Saudade Formation); H) Arkose and breccia intercalation in the lower Três Marias Formation. (For interpretation of the references to colour in this figure legend, the reader is referred to the web version of this article.)

is overlain by ~10 m of laminated mudstone, and when basal dolostone is absent, mudstone covers the basement rocks (as in our sampling site). The thinly laminated mudstones are light-gray and contain centimetric to decimetric fans of aragonite pseudomorphs and barite-rich layers. Aragonite pseudomorph fans at this same stratigraphic interval were already described in other locations throughout the basin (Vieira et al., 2015; Kuchenbecker et al., 2016a). In contrast, layers of barite were only recently described in the lower part of the Bambuí Group succession, discovered during mapping of the Januária area (A. Uhlein et al., 2014, G.J. Uhlein et al., 2014) and studied after that by different authors (Crockford et al., 2017; Okubo et al., 2018). The barite fans are thin (1–5 cm) and preserved in irregular layers within laminated mudstones as authigenic and diagenetic microcrystalline minerals (see Okubo et al., 2018 for a more detailed description of seafloor precipitates and authigenic minerals in the lower Sete Lagoas Formation).

During the end-Cryogenian glaciation, the central part of the basin (the Januária paleo-high) was probably emerged as attested by the absence of glaciogenic deposits and the direct contact of the Sete Lagoas cap carbonate with the cratonic basement. To the south of the Januária paleo-high area, the 1-PSB-14-MG drillcore of the Brazilian Geological Survey intercepted a 3 m-thick diamictite below the Sete Lagoas cap carbonate indicating post-glacial drowning from south to north. Thus, the cap carbonate records flooding (transgressive) event over basement highs after deglaciation. This interval is limited to ~10 m in thickness and is much thinner than other coeval succession described in other parts of the Bambuí Basin, where it can reach up to 80 m in thickness (e.g. Caxito et al., 2012a, 2018; Alvarenga et al., 2014). This reduced thickness is probably due to the higher basement elevation and landward thinning and tapering of the cap carbonate succession.

The Sete Lagoas Formation bears evidence to suggest a hiatus separating its lower and middle/upper parts (Fig. 2). The many aspects suggesting a record of post-Marinoan cap carbonate deposition in the lower Sete Lagoas Formation (ca. 635 Ma; Caxito et al., 2012a; Crockford et al., 2017; Okubo et al., 2018) contrast with the occurrence of *Cloudina* sp. and detrital zircons as young as ca. 560 Ma in the middle and upper Sete Lagoas Formation (Warren et al., 2014; Paula-Santos et al., 2015).

The middle Sete Lagoas Formation is composed of crenulated and laminated microbialite, grainstone, thrombolite and carbonate flat-pebble breccia (Figs. 2 and 3B). This interval is the most extensively developed in the Sete Lagoas Formation on the Januária paleo-high. The succession begins as an interval of 20 to 30 m of crenulated and occasionally laminated microbialites until wave, cross-laminated grainstone facies gradually prevail over the microbialites. Above the 50 m mark, the succession is composed of thrombolites and thin microbialites interbedded with grainstones facies. There is a progressive increase in the abundance of grainstone with wave ripples or hummocky cross-stratification and massive oolitic beds toward the top. This facies succession is representative of an inner-ramp (lagoonal-barrier island) and mid-ramp depositional settings. The skeletal fossils of the Nama Assemblage found in the Sete Lagoas Formation (including the guide fossil *Cloudina* and rare *Corumbella* specimens; Warren et al., 2014) are restricted to the thrombolite-laminated microbialite-grainstone facies association. *Cloudina* shells are preserved as fragments in bedding parallel, perpendicular or oblique position and commonly disperse bioclastic lenses. Loosely to closely packed shells are often disarticulated and can reach up to 1.5 cm in length.

Flat-pebble breccias characterize the uppermost part of the middle Sete Lagoas Formation and consist of at least 15 m of brecciated rudstone intercalated with thin beds of thrombolites, crenulated microbialites and rare grainstones. Usually, the rudstone beds consist of sub-horizontal (locally imbricated) tabular intraclasts of microbialite and form predominantly tabular beds with thickness up to 2 m. Grainstone beds with cross-stratification and ooids associated with microbialites from a likely lagoonal-barrier island setting outcrop above the rudstones. Dolomitized oolitic beds constitute the last 10s of meters of the Sete Lagoas Formation with abundant small-scale trough cross-stratification. This interval consists of altered carbonate rocks with variable degrees of fluid-rock interaction. The dolomitization resulted in intensely brecciated dolostones sectioned by silica veins, especially in outcrops near the town of Itacarambi (Fig. 1). Toward the top of the succession, dolomitized brecciated beds and karstified stromatolites are common.

4.1.2. *Serra de Santa Helena Formation*

The first appearance of fine-grained siliciclastic deposits is here considered to be the stratigraphic datum for the base of the Serra de Santa Helena Formation. The contact between the Sete Lagoas carbonates and the Serra de Santa Helena siltstones and shales characterizes the beginning of a transgressive interval that resulted in the first basin-wide drowning. The first 65 m of the unit are composed of rhythmites, microbial carbonates and marls until the occurrence of gray rhythmites locally with 1–2 mm in size euhedral pyrites (Fig. 3C). Above it, sandstones found in the middle Serra de Santa Helena Formation are matrix-rich and feldspathic, commonly preserving heterolithic bedding (flaser and wavy). Fine-grained sandstones with microbially induced sedimentary structures (MISS; sensu Noffke et al., 1996), shales with mudcracks (Fig. 3D) and rare levels containing salt casts are typical in this interval, suggesting deposition in inter- to supratidal settings under arid to evaporitic conditions. Also, small (< 1 cm) and simple horizontal burrows are found on shallow-water sandstones in the middle Serra de Santa Helena Formation. The last meters of the Serra de Santa Helena Formation are marked by a new transgressive interval and deposition of black to gray rhythmites with rare intercalations of marls and microbialites.

4.1.3. *Lagoa do Jacaré Formation*

The Lagoa do Jacaré Formation comprises two distinct sedimentary intervals: one succession of essentially carbonates and another constituted of mixed carbonate-siliciclastic deposits. The first ~70 m are dominantly composed of dark to dark-gray grainstone, mudstone and rudstone facies (Fig. 3E). The grainstone beds commonly show tabular geometry and trough or hummocky cross-bedding, with rare occurrences of normally graded beds. High-frequency intercalations of grainstones and mudstones often contain levels with synaeresis cracks associated with thin rudstone beds with rip up clasts. The presence of crenulated microbialite between cross-beds and grainstones with wave ripples in the uppermost meters of the first ~70 m-thick succession suggests deposition under shallow-water conditions during a facies regression interval (Figs. 2 and 3F). The Lagoa do Jacaré carbonates, in contrast to the Sete Lagoas carbonates, show evidence for open marine deposition due to the frequent presence of fair-weather and storm-wave influenced deposits and the absence of vertically and laterally continuous microbialite facies. The upper Lagoa do Jacaré Formation yield recurrent intercalations of shales and rhythmites with carbonates deposited during a marine transgression.

The occurrence of both siliciclastic (middle Serra de Santa Helena Formation) and carbonate (Sete Lagoas and Lagoa do Jacaré formations) shallow-water deposits in the Bambuí Group succession suggests that sea-level changes are not the only controlling factor for clastic or carbonate sedimentation in the basin. Other factors, such as enhanced detrital input probably induced by tectonic events occurring in the surrounding high topographic areas must have played an essential role in the sedimentation style. Reactivation of basement uplifts, cannibalization of uplifted basin areas and rapid erosion of mountain belts may explain enhanced detrital input (Sinclair and Allen, 1992; Allen and Allen, 2005), which hampered carbonate production and promoted deposition of siliciclastic sediments in the middle Serra de Santa Helena Formation.

4.1.4. *Serra da Saudade Formation*

The Serra da Saudade Formation in the Januária paleo-high is commonly eroded before deposition of the Cretaceous sandstones from the Urucuia Group or partially covered by recent alluvial sediments of the Verde Grande River (Fig. 1). This unit comprises about 200 m of fine-grained siliciclastic sediments mainly constituted by greenish rhythmites and shales with intercalations of fine-sandstone, grainstone and marl deposited during a new basin-wide drowning. Two levels with well-preserved MISS (*Kinneyia*-type; Porada et al., 2008) occur near the base and are similar to small-scale ripples (millimetric), locally showing a typical honeycomb arrangement and linear features interpreted as a product of the interaction of microbial substrate and bottom currents. In the upper Serra da Saudade Formation, the increase in the sand/mud ratio given by the frequent intercalations of fine-grained sandstones characterizes the initiation of a regressive interval that culminates with the deposition of biogenic carbonates of the Jaíba Member. This unit shows crenulated microbialites and rare thrombolites often displaying wavy and chaotic biogenic lamination (Fig. 3G). Cross-laminated grainstone and grainstone-mudstone intercalations occur in the few meters below the level where microbialites are dominant toward the top of the succession.

4.1.5. *Três Marias Formation*

The uppermost unit of the Bambuí Group in the Januária paleo-high area is mainly well preserved at the top of the Jaíba Ridge (Fig. 1). The contact between the Jaíba Member and Três Marias Formation is sharp and constitute a regional unconformity (see Kuchenbecker et al., 2016b for an extended discussion about the eastern Três Marias Formation). At the Jaíba Ridge, the Três Marias Formation starts with a 1 to 2 m-thick bedded breccia made of microbialite clasts (up to cobble in size). Above it, massive to cross-bedded arkoses prevail often showing tabular and trough cross-beds and rarely current ripple lamination. Thin lens-

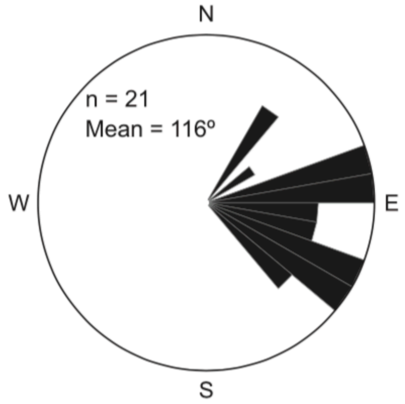

Fig. 4. Rose diagram for tabular and trough cross-bedding paleocurrent data from sandstones of the Três Marias Formation outcropping at the Jaíba Ridge. (For interpretation of the references to colour in this figure legend, the reader is referred to the web version of this article.)

shaped breccia with clasts of microbialite and quartz may occur between basal arkose beds (Fig. 3H). Paleocurrent data obtained from tabular and trough cross-bedded sandstones indicate a sedimentary dispersion from west to east of the basin (Fig. 4), following the general northwest sedimentary provenance attributed to the Três Marias Formation in the central Bambuí Basin.

4.2. New chemostratigraphic data

The chemostratigraphic information presented here comprises several carbon and oxygen isotopes data from carbonates ($\delta^{13}C$, $\delta^{18}O$) coupled with total organic carbon content and total sulfur (TOC, TS) from carbonates and shales and Mn/Sr, Mg/Ca ratios from carbonates. Their stratigraphic trends are shown in Fig. 5, and the detailed descriptions of the data follow the same stratigraphic arrangement presented in the last section.

4.2.1. Sete Lagoas Formation

Carbonate rocks of the Sete Lagoas Formation show $\delta^{13}C$ values from −4 to +4.5‰ and $\delta^{18}O$ from −11.7 to −1.6‰. Negative $\delta^{13}C$ are limited to the lower interval (cap carbonate), and a progressive enrichment in the heavy isotope is observed toward dolomites of the upper Sete Lagoas Formation. The thrombolite-grainstone association (with local *Cloudina*-rich levels) in the middle interval is marked by slightly positive $\delta^{13}C$ values (+0.1 to +0.6‰) and $\delta^{18}O$ about −6‰. TOC contents are low with a slight increase to 0.11% in the same thrombolite-grainstone association, probably due to the regular intercalation of black to dark-gray grainstones. Total sulfur contents are also meager and invariant. Mn/Sr ratios are below 1.0, with some exceptions at the base and in the upper unit where it reaches higher values (4.0). Mg/Ca are generally low (< 0.13) and only the upper dolostones reach higher ratios (0.5) and heavier $\delta^{18}O$, probably due to dolomitization process. There is a lack of covariation between TOC and carbonate content with $\delta^{13}C$ (Fig. 5).

4.2.2. Serra de Santa Helena Formation

Carbonates and marls from the Serra de Santa Helena Formation show heavy $\delta^{13}C$ values from 3.0 to anomalous +12.5‰, while $\delta^{18}O$ varies from −12.8 to −4.4‰ (Fig. 5). TOC and TS contents are equally low, with enrichments not well correlated (r = +0.37, p(a) < 0.05, n = 41; not shown). Mn/Sr and Mg/Ca ratios are below 0.9 and 0.17, respectively. One grainstone sample with carbonate content of 80% yielded the highest Mn/Sr ratio (13.8).

4.2.3. Lagoa do Jacaré Formation

The whole Lagoa do Jacaré Formation is highly enriched isotopically, with $\delta^{13}C$ values reaching up to +14.5‰ at the base and grading to lighter values (+6.7‰) upsection (Fig. 5). $\delta^{18}O$ varies between −12.3 and −4.1‰ with most values around −6.0‰. Although low (< 0.2%), TOC is higher at the lower part and show weak covariation with $\delta^{13}C$ (Fig. 5) and moderate with TS (r = +0.73, p(a) < 0.01, n = 41; not shown). The highest Mn/Sr ratio is 0.5 and the Mg/Ca ratios are all below 0.02.

4.2.4. Serra da Saudade Formation

Carbonates and marlstones at the base of the Serra da Saudade Formation show lighter $\delta^{13}C$ values compared to the previous unit (+2.9 to +6.6‰), although still enriched in the heavy ^{13}C isotope. $\delta^{18}O$ varies between −10.6 and −6.6‰. While total sulfur content is very low and invariant, TOC reaches its maximum values in all Bambuí stratigraphy in the upper Serra da Saudade Formation (0.22%).

Jaíba Member – Microbialites and grainstones of the upper Serra da Saudade Formation show $\delta^{13}C$ of +0.9 to +3.3‰ and $\delta^{18}O$ between −12.7 and −7.4‰, with lighter oxygen isotopes at the lower interval. Mn/Sr ratios are as high as 1.2 and down to 0.09. Mg/Ca ratios below 0.006 imply a strong calcitic nature for the Jaíba carbonates.

5. Discussions

5.1. Influence of diagenesis in carbon isotopes

Usually, $\delta^{18}O$ values are more prone to diagenetic alteration than $\delta^{13}C$ due to different alteration thresholds during fluid-rock interaction (e.g. Jacobsen and Kaufman, 1999) and the cross-plot of $\delta^{13}C$ vs. $\delta^{18}O$ is commonly used as a proxy to evaluate the influence of meteoric fluids and burial diagenesis (e.g. Derry, 2010; Bishop et al., 2014). For the Bambuí Basin carbonates at the Januária paleo-high, $\delta^{13}C$ vs. $\delta^{18}O$ cross-plot shows scattered data points, suggesting little to no impact of diagenesis (Fig. 5). The only exception suggesting some degree of diagenetic overprint are carbonates from the middle Sete Lagoas Formation that show positive covariation between samples with $\delta^{13}C$ and $\delta^{18}O$ of −1 to +1‰ and −12 to −6‰, respectively (r = 0.82, p(a) < 0.01, n = 44).

Mn/Sr ratios are commonly used as a screening test for possible diagenetic influence on isotopes, since during marine and meteoric diagenesis of limestone Mn content increases and Sr abundance decreases (Brand and Veizer, 1980; Jacobsen and Kaufman, 1999). Limestones from the Bambuí Group appears to be well preserved. Apart from one sample with Mn/Sr > 10, all others have very low ratios (mean Mn/Sr = 0.17), and there is a lack of covariance between Mn/Sr and $\delta^{13}C$ (Fig. 6). Both samples with the most negative and positive $\delta^{13}C$ values (−4.0 and +14‰) show virtually equal low Mn/Sr values of 0.04 and 0.05, respectively. Mn/Sr vs. $\delta^{18}O$ cross-plot show a weak exponential correlation of ^{18}O depletion and Mn/Sr increase typical of meteoric diagenesis (Fig. 6). Curiously, two samples of dolostone from the upper Sete Lagoas Formation with heavier $\delta^{18}O$ are outsiders, probably due to oxygen isotope alteration by dolomitization process rather than meteoric diagenesis, as seen by the higher Mg/Ca ratio among other samples. However, dolomitization is not an important process in the remaining Bambuí Group since all other samples are calcitic carbonates with very low and invariant Mg/Ca ratios and show a lack of correlation with $\delta^{13}C$ or $\delta^{18}O$ (Fig. 6). Dolomitization processes (limited to the uppermost Sete Lagoas Formation) altered only the $\delta^{18}O$ values toward ^{18}O depletion. Thus, we exclude the possibility that post-depositional processes caused the chemostratigraphic fluctuations in the carbon and oxygen isotopes recorded in the Bambuí Basin, rather inferring that they resulted from primary perturbations of the marine dissolved inorganic carbon pool.

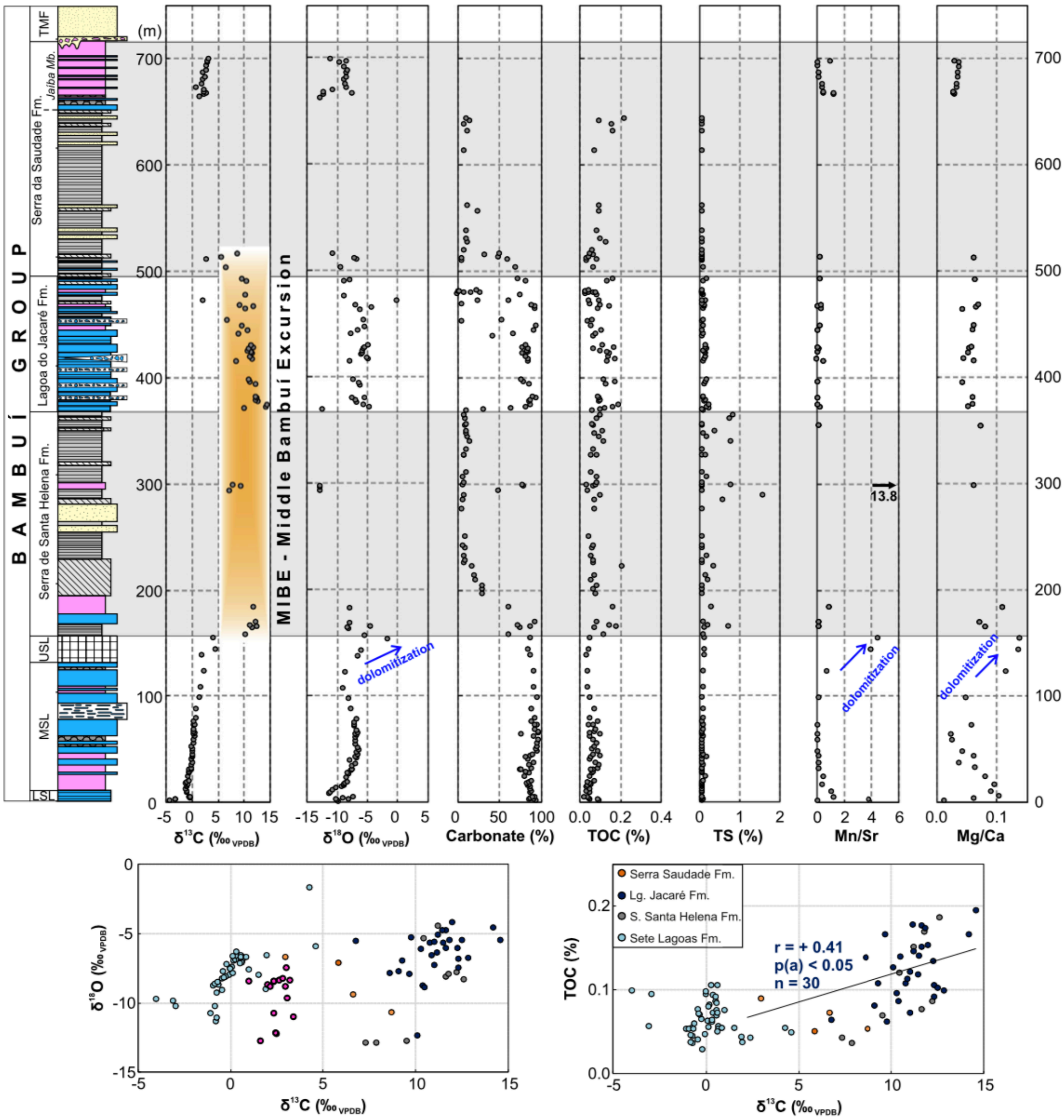

Fig. 5. Chemostratigraphic data of the Bambuí Basin. Measured geochemical data include carbon and oxygen isotopes ($\delta^{13}C$, $\delta^{18}O$), carbonate content percentage (Carbonate %), total organic carbon content (TOC %), total sulfur content (TS %) and Mn/Sr and Mg/Ca ratios. $\delta^{13}C$ and $\delta^{18}O$ were measured only for samples with carbonate content > 50%. The linear regression line in the $\delta^{13}C$ vs. TOC diagram was calculated for the Lagoa do Jacaré samples. See Fig. 2 for the legend of the lithotypes. LSL, MSL and USL mean lower, middle and upper Sete Lagoas Formation, respectively. Gray and white rectangles along the data were used to emphasize the lithostratigraphic limits. All the data can be found in the online Supplementary Material.

5.2. The chemostratigraphic record of the Bambuí Basin in the Januária paleo-high and the Middle Bambuí Excursion (MIBE)

All samples yielded surprisingly low TOC values ranging from 0.03 to 0.22% (mean = 0.08 ± 0.04; n = 147), regardless if deep- or shallow-water facies lithotypes, suggesting a low flux of organic carbon to seafloor environment (export productivity). Many depositional and post-depositional factors influence the TOC values, including sedimentation rate, seawater redox state (Canfield, 1994), loss of organic carbon during thermal maturation (Raiswell and Berner, 1987) and oxidative weathering in outcrop (Petsch et al., 2000). From our data, sedimentation rate and oxidative weathering in outcrop can both be excluded as possible factors due to the non-dependence between TOC and lithotypes or depositional settings (different sedimentation rates), and the equal low TOC values acquired from both 1-PSB-14-MG drillcore and outcrops (Fig. 5). Thus, high bottom-water O_2 content or

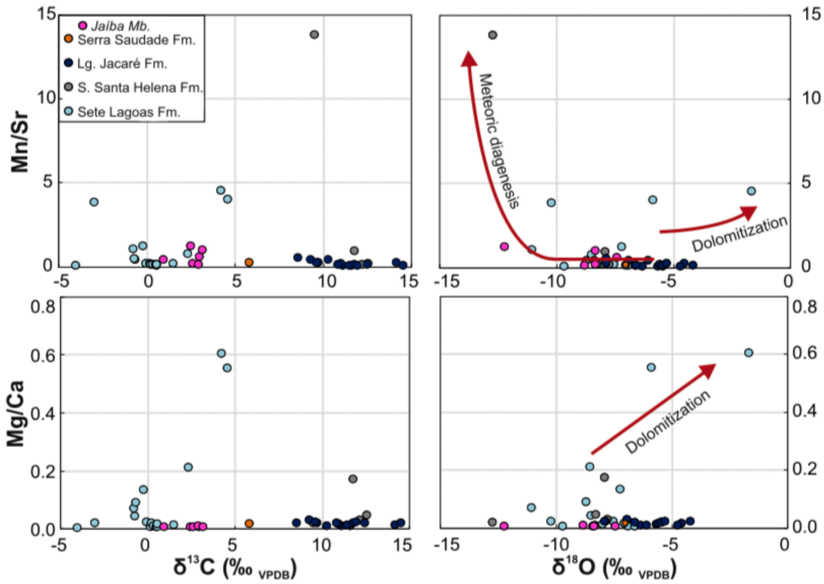

Fig. 6. Binary plots of $\delta^{13}C$, $\delta^{18}O$, Mn/Sr and Mg/Ca of the Bambuí Basin carbonates outcropping at the Januária paleo-high.

thermal maturation (and eventually, low-grade metamorphism) may be responsible for such uniform low TOC values in the Bambuí Group carbonates. Caxito et al. (2018) presented chromium isotope and geochemical evidence that oxygenated conditions prevailed in the upper Sete Lagoas Formation and may explain the low TOC values during this interval. However, this may not be true for the black, pyrite-rich carbonates of the Lagoa do Jacaré Formation, but this hypothesis remains to be tested by ongoing chemostratigraphic studies by the same authors.

Carbon isotope data of the Bambuí Group occurring over the Januária paleo-high are characterized by negative $\delta^{13}C$ values in the lower Sete Lagoas Formation that record the post-Marinoan cap carbonate interval. These are readily superimposed by slightly positive values in turn capped by very high $\delta^{13}C$ carbonates that dominate the entire succession throughout the Serra de Santa Helena, Lagoa do Jacaré and lower Serra da Saudade formations (about 350 m-thick of heavy $\delta^{13}C$ carbonates). The return to moderately positive carbon isotopes values in the microbialites and grainstones of the Jaíba Member makes up the upper Bambuí Group (Figs. 2 and 5). The MIBE at the Januária paleo-high is consistent with values found in other parts of the basin at the same stratigraphic position (Iyer et al., 1995; Santos et al., 2000; Martins and Lemos, 2007; Alvarenga et al., 2014; Paula-Santos et al., 2017).

The carbon isotope value of sedimentary carbonates ($\delta^{13}C_{carb}$) bears directly on the global redox balance and can be calculated based on the rearranged carbon isotope mass balance equation (Hayes et al., 1999): $\delta^{13}C_{carb} = (f_{org} * \Delta^{13}C) + \delta^{13}C_i$, where f_{org} is the fraction of carbon buried as organic matter, $\delta^{13}C_i$ is the total carbon input to the surface environment (−5‰ at present) and $\Delta^{13}C$ is carbon isotope discrimination between carbonate and organic matter (earlier in the Phanerozoic Eon, $\Delta^{13}C$ mostly remained between 28 and 32‰; Hayes et al., 1999).

From the carbon isotope mass balance equation, it is conclusive that to maintain a $\delta^{13}C_{carb}$ at +10‰ (main $\delta^{13}C_{carb}$ during the MIBE), one must increase f_{org}, $\delta^{13}C_i$ and/or $\Delta^{13}C$. Due to the linear relationship between the variables, independent changes in one of them must result in very high values to sustain a $\delta^{13}C_{carb}$ of +10‰ during much of the middle Bambuí Basin deposition. As an example, an estimate for f_{org} is calculated around 0.50, which is anomalously high and implies unusually elevated organic carbon burial rates (f_{org} is about 0.25 during most of the Phanerozoic). $\Delta^{13}C$ varies in response to evolutionary and environmental changes. Larger $\Delta^{13}C$ values are commonly a result of microbial reworking by non-photosynthetic chemoautotrophic bacteria causing further enrichment of ^{12}C in organic matter (Hayes et al., 1999; Samuelsson and Strauss, 1999; Shields et al., 2002), or due to high concentration of dissolved CO_2 in the ocean (Hayes et al., 1999; Kaufman and Xiao, 2003; Sansjofre et al., 2011). In order to precipitate a sedimentary carbonate with $\delta^{13}C$ of +10‰, a very unlikely growth of $\Delta^{13}C$ to 60‰ would be required (neglecting imbalances in other inputs). However, data from Iyer et al. (1995) suggest little variation in $\Delta^{13}C$ between the lower and middle Bambuí carbonates (25–30‰), which would primarily suggest that larger $\Delta^{13}C$ cannot be responsible alone for such positive $\delta^{13}C$.

Total carbon input ($\delta^{13}C_i$) to the surface environment usually corresponds to a bulk crustal and mantle $\delta^{13}C$, although it does not have to be the case on time-scales shorter than 100 million years (Des Marais, 1997). Since surface weathering is the most variable source of ocean carbon, the isotopic composition of $\delta^{13}C_i$ depends on the proportion of carbonate versus organic matter weathered on the continent and delivered to the basin. Thus, changing in the source of weathered carbon may affect $\delta^{13}C_i$. During regressions of the shoreline and exposure of vast areas of low-lying platform carbonates to chemical weathering, the $\delta^{13}C_i$ may be increased by the preferential dissolution of sedimentary carbonates on the continent ($\delta^{13}C$ mean global C reservoir of −1 to +4‰; Des Marais, 1997) causing $\delta^{13}C$ increase in the surface seawater (Shields et al., 1997; Kump et al., 1999; Saltzmann et al., 2000). This might be notably true for basins with low connectivity with the global ocean.

Development of estimates of ancient isotopic values of carbon input and its influence extent on surface waters are a fundamental problem and of primary necessity. A $\delta^{13}C_i$ of +2.5‰ would be necessary to maintain $\delta^{13}C_{carb}$ at +10‰ during the MIBE, requiring an enormous volume of ^{13}C-enriched carbonates to be weathered from the exposed continents. The constant low $^{87}Sr/^{86}Sr$ ratios recorded in the Bambuí Basin carbonates (mainly the late Ediacaran upper Sete Lagoas Formation and overlying units; Paula-Santos et al., 2017) may support an imbalance toward greater weathering of ancient platform carbonate (and maybe reworking of intrabasinal carbonate) that buffered the Sr isotope signal. However, both local $^{87}Sr/^{86}Sr$ and $\delta^{13}C_i$ signals can only be significant on a basin scale with a high degree of basin restriction. Again, it is unlikely that a substantial change in total carbon input to the basin may be the single responsible for such 350 m-thick ^{13}C-enriched carbonates.

Besides these variables, the fraction of carbon buried as authigenic carbonate (f_{ac}) may represent a substantial global carbon sink and can be further added to the carbon isotope mass balance equation (Schrag et al., 2013). In basins with anoxic bottom waters along the shelf and slope, the increase in abundance of other electron acceptors (such as SO_4^{2-} or Fe^{3+}) would be expected to increase f_{ac} and the average isotopic offset between authigenic carbonate and dissolved inorganic carbon pool (DIC; Higgins et al., 2009). The sulfate or iron reduction commonly occurs through oxidation of methane (anaerobic methane oxidation, AOM) or organic carbon, respectively, and imply precipitation of isotopically light authigenic carbonates. Thus, higher values of f_{ac} (and the increase of in situ inorganic carbonate precipitation, within sediment pore waters), enable higher $\delta^{13}C$ of sedimentary carbonate without a shift from modern f_{org} values (Schrag et al., 2013). The carbonates of the Lagoa do Jacaré Formation are commonly enriched in euhedral and framboidal pyrites, and pyrite burial can be an important source of alkalinity that enhances the precipitation of authigenic carbonate phases (production of hydrogen sulfide and carbonate alkalinity during bacterial sulfate reduction; Berner et al., 1970; Sternbeck and Sohlenius, 1997). However, to maintain $\delta^{13}C_{carb}$ at +10‰ and $f_{org} = 0.25$, require that authigenic carbonate make up anomalously 60% of the global carbon sink, which is virtually impracticable. Furthermore, we did not find significant negative carbon isotope values to sustain such high f_{ac}. Particularly noteworthy is the fact that this is the first work to present a complete $\delta^{13}C$ data of the whole Bambuí Basin and future new data from deep water sections may be fruitful in understanding the real importance of authigenic carbonate burial to the MIBE.

Thus, we suggest that the ^{13}C-enriched carbonates of the middle Bambuí Basin cannot be explained solely by very high rates of organic burial or broad methanogenesis. The MIBE is instead explained concerning a complex interplay of different causes but linked to one fundamental parameter: a restricted basin. Poor ocean ventilation would be necessary to amplify and to record, along the stratigraphy, the local signals that affect the carbon cycle. A change in total carbon input to the basin due to preferential weathering of ancient sedimentary carbonates on the continents and higher burial rates of authigenic carbonate due to methane or organic matter oxidation (via sulfate or iron reduction), seem to be the most significant causes for the ^{13}C-enrichment in sedimentary carbonates during the MIBE.

Circa 150 m above the end of the MIBE, the Jaíba Member carbonates present almost constant less fractionated $\delta^{13}C$ values (+2 to +3‰). Comparing to the carbonates within the MIBE, the Jaíba microbialites probably reflect a different biogeochemical scenario of deposition and suggest a short-lived influence of local isotopic signals in the Bambuí Basin.

5.3. Age constraints and paleogeographic extent of the MIBE

Kaufman et al. (2009) argued that the carbon isotope positive excursion and the $^{87}Sr/^{86}Sr$ ratios around 0.7075 recorded in the middle Bambuí Group in east-central Brazil are correlated to the Cryogenian, pre-Marinoan interval (the so-called "Keele peak"; Kaufman et al., 1997; Halverson et al., 2005). However, the MIBE commonly reaches values beyond +10‰ and locally up to +16‰, much higher than what is usually found in successions preceding the Marinoan glaciation (Kaufman et al., 1997; McKirdy et al., 2001; Halverson et al., 2005; Johnston et al., 2012; Uhlein et al., 2016). More importantly, due to the ca. 560 Ma, late Ediacaran detrital zircons (Paula-Santos et al., 2015) and *Cloudina*-bearing levels (Warren et al., 2014) found in the middle/upper Sete Lagoas Formation (at least 100 m *below* the MIBE), such positive anomaly recorded in the carbonates of the middle Bambuí Group cannot be correlated to a late Cryogenian age and should correspond to a carbon isotope excursion younger than 560 Ma (considering the maximum depositional age from detrital zircons and the presence of putative trace fossils) or 549 Ma (considering the lower limit of the *Cloudina* biozone). A positive $\delta^{13}C$ excursion with such magnitude is unknown in any basin younger than 560 Ma (e.g. Prokoph et al., 2008; Krissansen-Totton et al., 2015). However, Uhlein et al. (2017) suggested that the MIBE may be correlated to the very stable values of the late Ediacaran positive carbon isotope plateau (EPIP; e.g. Zhu et al., 2017), recorded after the end of the Shuram excursion and the first *Cloudina* occurrences, and before the negative excursion (BACE) typical of the Ediacaran-Cambrian boundary (e.g. Zhu et al., 2005; Macdonald et al., 2013; Li et al., 2016).

Here, we suggest that during the terminal Ediacaran, probably due to basin restriction and a reservoir effect, the global carbon cycle was locally altered, amplifying the $\delta^{13}C$ signal recorded in the middle Bambuí carbonates by an offset of at least +4‰ compared to the global $\delta^{13}C$ curve (EPIP). Thus, rather than an outsider $\delta^{13}C$ record, the MIBE is here interpreted as correlated to post-Shuram excursion carbonates of the terminal Ediacaran Period, such as the Dengying Formation of South China (Cui et al., 2016), upper Kuibis and Schwarzrand subgroups of Namibia (Kaufman et al., 1991) and upper Buah Formation (Nafun Group) and lower Ara Group of Oman (Amthor et al., 2003; Fike et al., 2006). The MIBE might reflect a spatial heterogeneity of the terminal Ediacaran carbon cycling caused by the paleogeography of continental blocks during West Gondwana amalgamation (see below).

In a recent compilation, Sial et al. (2016) presented chemostratigraphic data from several Neoproterozoic basins in South America. From that data, we suggest that the positive $\delta^{13}C$ excursion recorded in the middle Bambuí Basin may be more widespread than previously thought. Several small Ediacaran basins in the eastern São Francisco craton and the northern belts preserve a positive $\delta^{13}C$ excursion commonly reaching above +10‰. The Salitre Formation (Una Group), Serra do Paraíso and Água Preta formations (Rio Pardo Basin), São Desidério Formation (Rio Preto Belt), Olhos D'água Formation (Sergipano Belt), and Barra Bonita Formation (Riacho do Pontal Belt), although lacking physical connection with the Bambuí Basin, have been tentatively correlated mainly due to their similar lithostratigraphy, carbon and strontium isotopes data and late Neoproterozoic age (Egydio-Silva et al., 1989; Pedreira, 1999; Misi et al., 2007, 2011; Sial et al., 2009, 2016; Cezario, 2011; Caxito et al., 2012a, 2012b, 2016; Fig. 7). If these positive carbon isotope excursions are correctly correlated and primary in origin (an interpretation supported by the geochemical parameters in the papers mentioned above), then the MIBE seems to be a landmark of terminal Ediacaran $\delta^{13}C$ record preserved over the São Francisco paleocontinent.

During West Gondwana amalgamation in the late Ediacaran, the São Francisco paleocontinent may have had a central configuration in the mosaic of collisional blocks (Fig. 7), being the locus of convergence between the Amazon, West Africa, Sahara, Congo and Paranapanema blocks (e.g. Tohver et al., 2006, 2010; Meert and Lieberman, 2008; Merdith et al., 2017). The enclosure of intracratonic and marginal basins by several colliding continental masses and the progressive narrowing of the ocean connections were probably responsible for periods of basin restriction. Several authors already proposed the restricted nature of the Bambuí Basin (Iyer et al., 1995; Santos et al., 2000; Martins and Lemos, 2007; Alvarenga et al., 2014; Drummond et al., 2015) and recently corroborated by chemostratigraphic data by Paula-Santos et al. (2017, 2018) and Hippertt (2018), which suggest a restricted stage from the upper Sete Lagoas Formation and overlying units. Thus, environmental and basinal context favored basin restriction, which enabled the $\delta^{13}C$ of surface seawater to be significantly influenced by a local increase in the weathering of ancient carbonate rocks on the continent. Also, the restricted nature of the middle Bambuí Basin may have favored anoxic bottom waters and higher burial rates of authigenic carbonate. The return to less fractionated values at the Jaíba

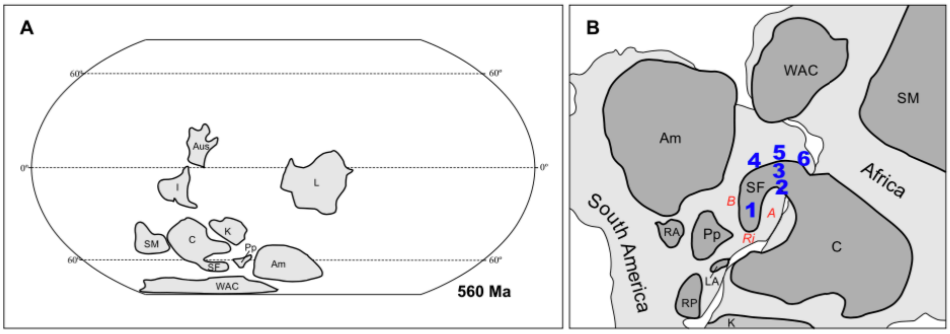

Fig. 7. A – Reconstruction of the tectonic paleogeography of continental blocks at ca. 560 Ma (modified from Merdith et al., 2017). Note the central position of the São Francisco craton. B - Cratonic blocks of southwest Gondwana in South America and Africa continents (modified from Meira et al., 2015). Cratons abbreviations: Am-Amazonia; Aus-Australia; C-Congo; I-India; K-Kalahari; L-Laurentia; LA-Luis Alves; Pp-Paranapanema; RA-RioApa; RP-Rio de la Plata; SF-São Francisco; SM-Sahara Metacraton; WAC-West Africa. Records of Ediacaran extreme positive carbon isotope excursions: 1-Bambuí Basin; 2-Rio Pardo basin; 3-Una Group; 4-São Desidério Formation (Rio Preto Belt); 5-Barra Bonita Formation (Riacho do Pontal Belt); 6-Olhos D'água Formation (Sergipana Belt). Abbreviations in red colour mean B-Brasília Belt; A-Araçuaí Belt; Ri-Ribeira Belt. (For interpretation of the references to colour in this figure legend, the reader is referred to the web version of this article.)

Member (and in other upper Bambuí carbonates; Uhlein et al., 2017), suggest a temporary (and short-lived) local effect over the carbon cycle.

6. Conclusions

New stratigraphic and chemostratigraphic data acquired in the northern Minas Gerais state (the Januária paleo-high) and presented here provide new insights into the Ediacaran depositional evolution of the Bambuí Basin and its chemostratigraphic record.

Above a typical post-Marinoan cap carbonate succession (~10 m-thick) and a likely hiatus, the late Ediacaran, mixed carbonate-siliciclastic Bambuí Group makes up transgressive-regressive intervals that preserved many carbonate and siliciclastic shallow-water facies along its stratigraphy. Although carbonates tend to be of shallower water depths, sandstones and shales with mudcracks and salt casts from the middle Serra de Santa Helena Formation imply that sea-level changes are not determinant for clastic or carbonate sedimentation in the basin. Other factors, such as enhanced detrital input induced by tectonic events occurring in the surrounding high topographic areas or climate change must have been significant.

From a complete $\delta^{13}C$ section of the Bambuí Group, the Middle Bambuí Excursion (MIBE) extends for circa 350 m, starts in the upper Sete Lagoas Formation and fluctuates between +6 and +14‰ throughout most of the section and extending to the lower Serra da Saudade Formation. We suggest that short-lived changes in total carbon input to the basin and higher burial rates of authigenic carbonate during restricted (and probably anoxic) basin periods are relevant to highly positive $\delta^{13}C$ values of sedimentary carbonates during the MIBE. Carbonates of the Jaíba Member (upper Bambuí Basin) yield a different carbon isotopic data (+2 to +3‰) and are probably related to deposition in a distinct context, out of the singular biogeochemical condition that generated the MIBE.

The occurrence of identical positive carbon isotope excursions in other basins over the eastern São Francisco craton and along its current northern margin suggests a broader effect on the carbon cycle. The central position of the São Francisco craton in the mosaic of collisional blocks and the consequent enclosure of its intracratonic and marginal basins probably favored basin restriction periods, which, by a reservoir effect, enhanced the influence of local isotopic signals that affected the global $\delta^{13}C$ budget by an offset of at least +4‰. Nevertheless, the MIBE may be correlated to the late Ediacaran positive carbon isotope plateau (EPIP) recorded in other successions positioned after the Shuram excursion (and first *Cloudina* occurrences) and before the Ediacaran-Cambrian boundary. In the light of these findings, it appears that the Ediacaran paleoenvironmental conditions in the Bambuí Basin varied dramatically through a complex interplay of biogenic and abiogenic processes.

Supplementary data to this article can be found online at https://doi.org/10.1016/j.palaeo.2018.12.022.

Acknowledgments

Special thanks to C.J.S. Alvarenga and D.G.C. Fragoso for fruitful discussions over the Bambuí stratigraphy. The manuscript benefited from constructive reviews of H. Cui, A. Bekker and an anonymous reviewer. Brazilian funding agencies CNPq (grants 447449/2014-1 and 444070/2014-1) and FAPEMIG (grants APQ-01711-14, APQ-00914-14, PPM-00539-15) made possible the acquisition of the data presented here. FAC thanks CNPq for financial support through the project "Chemostratigraphy of Proterozoic sedimentary sequences of the Minas Gerais state, Brazil, and the fluctuations of atmospheric oxygenation in the Precambrian". JO thanks FAPESP for grant 2015/07391-0.

References

Allen, P.A., Allen, J.R., 2005. Basin analysis. In: Principles and Applications, 2nd edition. Blackwell Publishing, Maiden, USA (549 pp).

Alvarenga, C.J.S., Della Giustina, M.E.S., Silva, M.G.C., Santos, R.V., Gioia, S.M.C., Guimarães, E.M., Dardenne, M.A., Sial, A.N., Ferreira, V.P., 2007. Variações dos isótopos de C e Sr em carbonatos pré e pós-glaciação Jequitaí (Esturtiano) na região de Bezerra-Formosa, Goiás. Rev. Bras. Geosci. 37 (4), 147–155.

Alvarenga, C.J.S., Dardenne, M.A., Vieira, L.C., Martinho, C.T., Gumarães, E.M., Santos, R.V., Santana, R.O., 2012. Stratigraphy of western edge of the São Francisco basin. Boletim de Geociências da Petrobras 20, 145–164.

Alvarenga, C.J.S., Santos, R.V., Vieira, L.C., Lima, B.A.F., Mancini, L.H., 2014. Meso-Neoproterozoic isotope stratigraphy on carbonates platforms in the Brasília Belt of Brazil. Precambrian Res. 251, 164–180.

Amthor, J.E., Grotzinger, J.P., Schröder, S., Bowring, S.A., Ramezani, J., Martin, M.W., Matter, A., 2003. Extinction of *Cloudinae* and *Namacalathus* at the Precambrian-Cambrian boundary in Oman. Geology 31, 431–434.

Berner, R.A., Scott, M.R., Thomlinson, C., 1970. Carbonate alkalinity in the pore waters of anoxic marine sediments. Limnol. Oceanogr. 15, 544–549.

Bishop, J.W., Osleger, D.A., Montañez, I.P., Sumner, D.Y., 2014. Meteoric diagenesis and fluid-rock interaction in the Middle Permian Capitan backreef: Yates Formation, Slaughter Canyon, New Mexico. AAPG Bull. 98, 1495–1519.

Boggiani, P.C., Gaucher, C., Sial, A.N., Babinski, M., Simon, C.M., Riccomini, C., Ferreira, V.P., Fairchild, T.R., 2010. Chemostratigraphy of the Tamengo Formation (Corumbá Group, Brazil): a contribution to the calibration of the Ediacaran carbon-isotope curve. Precambrian Res. 182 (4), 382–401.

Brand, U., Veizer, J., 1980. Chemical diagenesis of a multicomponent carbonate system: 1. Trace elements. J. Sediment. Petrol. 50, 1219–1236.

Brandalise, L.A., 1980. Projeto Sondagens Bambuí em Minas Gerais: Relatório Final. Belo Horizonte, DNPM/CRRM. vol. 1.

Calver, C.R., 2000. Isotope stratigraphy of the Ediacarian (Neoproterozoic III) of the

Adelaide Rift complex, Australia, and the overprint of water column stratification. Precambrian Res. 100, 121–150.
Canfield, D.E., 1994. Factors influencing organic carbon preservation in marine sediments. Chem. Geol. 114, 315–329.
Caxito, F.A., Halverson, G.P., Uhlein, A., Stevenson, R., Dias, T.G., Uhlein, G.J., 2012a. Marinoan glaciation in east central Brazil. Precambrian Res. 200–203, 38–58.
Caxito, F.A., Uhlein, A., Sanglard, J.C.D., Gonçalves-Dias, T., Mendes, M.C.O., 2012b. Depositional systems and stratigraphic review proposal of the Rio Preto Fold Belt, northwestern Bahia/southern Piauí. Rev. Bras. Geosci. 42, 523–538.
Caxito, F.A., Araujo, R.G., Uhlein, A., Uhlein, G.J. 2014. Folha Mata do Jaíba SD-23-Z-C-III. Mapa geológico em escala 1:100.000. CODEMIG-UFMG.
Caxito, F.A., Uhlein, A., Dantas, E.L., Stevenson, R., Salgado, S.S., Dussin, I.A., Sial, A.N., 2016. A complete Wilson Cycle recorded within the Riacho do Pontal Orogen, NE Brazil: implications for the Neoproterozoic evolution of the Borborema Province at the heart of West Gondwana. Precambrian Res. 282, 97–120.
Caxito, F.A., Frei, R., Uhlein, G.J., Dias, T.G., Árting, T.B., Uhlein, A., 2018. Multiproxy geochemical and isotope stratigraphy records of a neoproterozoic oxygenation event in the Ediacaran Sete Lagoas cap carbonate, Bambuí Group, Brazil. Chem. Geol. 481, 119–132.
Cezario, W.S., 2011. Quimioestratigrafia isotópica (C, O e Sr) em duascapas carbonáticas Neoproterozoicas, Bacia do Rio Pardo e Cinturão Rio Preto, Bahia. Universidade Federal de Pernambuco, Recife, Nordeste do Brasil (Dissertação de Mestrado). (129 pp).
Chang, H.K., Miranda, F.P., Magalhães, L., Alkmim, F.F., 1988. Considerações sobre aevolução tectônica da bacia do São Francisco. In: Congresso Brasileiro de Geologia. Anais, 5, vol. 35. pp. 2076–2090.
Crockford, P.W., Hodgskiss, M.S.W., Uhlein, G.J., Caxito, F.A., Hayles, J.A., Halverson, G.P., 2017. Linking paleocontinents through triple oxygen isotope anomalies. Geology 46 (2), 179–182.
Cui, H., Kaufman, A.J., Xiao, S., Peek, S., Cao, H., Min, X., Cai, Y., Siegel, Z., Liu, X.M., Peng, Y., Schiffbauer, J.D., Martin, A.J., 2016. Environmental Context for the Terminal Ediacaran Biomineralization of Animals. vol. 14. pp. 344–363.
Dardenne, M.A., 1978. Síntese sobre a estratigrafia do Grupo Bambuí no Brasil Central. In: Congresso Brasileiro de Geologia. Recife. Anais, 2 30. pp. 597–610.
Derry, L.A., 2010. A burial diagenesis origin for the Ediacaran Shuram-Wonoka carbon isotope anomaly. Earth Planet. Sci. Lett. 294, 152–162.
Des Marais, D.J., 1997. Isotopic evolution of the biogeochemical carbon cycle during the Proterozoic eon. Org. Geochem. 27, 185–193.
Drummond, J.B.R., Pufahl, P.K., Porto, C.G., Carvalho, M., 2015. Neoproterozoic peritidal phosphorite from the Sete Lagoas Formation (Brazil) and the Precambrian phosphorus cycle. Sedimentology 62, 1978–2008.
Egydio-Silva, M., Karmann, I., Trompette, R., 1989. Litoestratigrafia doSupergrupo Espinhaço e Grupo Bambuí no noroeste do Estado da Bahia. Rev. Bras. Geosci. 19 (2), 141–152.
Fike, D.A., Grotzinger, J.P., Pratt, L.M., Summons, R.E., 2006. Oxidation of the Ediacaran Ocean. Nature 444, 744–747.
Gaucher, C., Boggiani, P.C., Sprechmann, P., Sial, A.N., Fairchild, T., 2003. Integrated correlation of the Vendian to Cambrian Arroyo del Soldado and Corumba' groups (Uruguay and Brazil): palaeogeographic, palaeoclimatic and palaeobiologicimplications. Precambrian Res. 120, 241–278.
Grotzinger, J.P., Bowring, S.A., Saylor, B.Z., Kaufman, A.J., 1995. Biostratigraphic and geochronologic constraints on early animal evolution. Science 270, 598–604.
Halverson, G.P., Hoffman, P.F., Schrag, D.P., Maloof, A.C., Rice, A.H.N., 2005. Toward a Neoproterozoic composite carbon-isotope record. GSA Bull. 117, 1181–1207.
Hayes, J.M., Strauss, H., Kaufman, A.J., 1999. The abundance of C in marine organic carbon and isotopic fractionation in the global biogeochemical cycle of carbon during the past 800 Ma. Chem. Geol. 161, 103–125.
Higgins, J.A., Fischer, W.W., Schrag, D.P., 2009. Oxygenation of the ocean and sediments: Consequences for the seafloor carbonate factory. Earth Planet. Sci. Lett. 284, 25–33.
Hippertt, J.P.T.M., 2018. The Fate of a Neoproterozoic Intracratonic Marine Basin: Trace Elements, TOC and Iron Speciation Geochemistry of the Bambuí Basin, Brazil. (MSc dissertation). Univ. Federal de Minas Gerais (74pp, unpublished).
Hoffman, P.F., 2011. Strange bedfellows: glacial diamictite and cap carbonate from the Marinoan (635 Ma) glaciation in Namibia. Sedimentology 58, 57–119.
Hoffman, P.F., Schrag, D.P., 2002. The snowball Earth hypothesis: testing the limits of global change. Terra Nova 14, 129–155.
Isotta, C.A.L., Rocha-Campos, A.C., Yoshida, R., 1969. Striated pavement of the Upper Precambrian glaciation in Brazil. Nature 222, 466–468.
Iyer, S.S., Babinski, M., Krouse, H.R., Chemale Jr., F., 1995. Highly ^{13}C-enriched carbonate and organic matter in the Neoproterozoic sediments of the Bambuí Group, Brasil. Precambrian Res. 73, 271–282.
Jacobsen, S.B., Kaufman, A.J., 1999. The Sr, C and O isotopic evolution of Neoproterozoic seawater. Chem. Geol. 161, 37–57.
Johnston, D.T., Macdonald, F.A., Gill, B.C., Hoffman, P.F., Schrag, D.P., 2012. Uncovering the Neoproterozoic carbon cycle. Nature 483, 320–323.
Kaufman, A.J., Xiao, S., 2003. High CO_2 levels in the Proterozoic atmosphere estimated from analyses of individual microfossils. Nature 425, 279–282.
Kaufman, A.J., Hayes, J.M., Knoll, A.H., Germs, G.J.B., 1991. Isotopic compositions of carbonates and organic carbon from upper Proterozoic successions in Namibia: stratigraphic variation and the effects of diagenesis and metamorphism. Precambrian Res. 49, 301–327.
Kaufman, A.J., Knoll, A.H., Narbonne, G.M., 1997. Isotopes, ice ages, and terminal Proterozoic earth history. Proc. Natl. Acad. Sci. U. S. A. 94, 6600–6605.
Kaufman, A.J., Sial, A.N., Frimmel, H.E., Misi, A., 2009. Neoproterozoic to Cambrian Palaeoclimatic events in Southwestern Gondwana. In: Gaucher, C., Sial, A.N., Halverson, G.P., Frimmel, H. (Eds.), Neoproterozoic-Cambrian Tectonics, Global Change and Evolution: a focus on southwestern Gondwana. Developments in Precambrian Geology. vol. 16. Elsevier, Amsterdam, pp. 369–388.
Krissansen-Totton, J., Buick, R., Catling, D.C., 2015. A statistical analysis of the carbon isotope record from the Archean to Phanerozoic and implications for the rise of oxygen. Am. J. Sci. 315, 275–316.
Kuchenbecker, M., Atman, D., Costa, R.D. 2013. Folha Barreiro da Jaíba SD.23-Z-C-VI. Mapa geológico em escala 1:100.000. CODEMIG-UFMG.
Kuchenbecker, M., Reis, H.L.S., Silva, L.C., Costa, R.D., Fragoso, D.G.C., Knauer, L.G., Dussin, I.A., Pedrosa-Soares, A.C., 2015. Age constraints for deposition and sedimentary provenance of EspinhaçoSupergroup and Bambuí Group in eastern São Francisco craton. Geonomos 23 (2), 14–28.
Kuchenbecker, M., Babinski, M., Pedrosa-Soares, A.C., Lopes-Silva, L., Pimenta, F., 2016a. Chemostratigraphy of the lower Bambuí Group, southwestern São Francisco craton, Brazil: insights on Gondwana paleoenvironments. Braz. J. Geol. 46 (1), 145–162.
Kuchenbecker, M., Atman, D., Costa, R.D., Pedrosa-Soares, A.C., Babinski, M., 2016b. A Formação Gorutuba: sedimentação litorâneaa continental na margem leste da Bacia Bambuí (MG). Série Científica 16, 2. Geologia USP, pp. 67–81.
Kump, L.R., Arthur, M.A., Patzkowsky, M.E., Gibbs, M.T., Pinkus, D.S., Sheehan, P.M., 1999. A weathering hypothesis for glaciation at high atmospheric pCO2 during the Late Ordovician. Palaeogeogr. Palaeoclimatol. Palaeoecol. 152, 173–187.
Li, C., Hardisty, D.S., Luo, G., Huang, J., Algeo, T.J., Cheng, M., Shi, W., An, Z., Tong, J., Xie, S., Jiao, N., Lyons, T.W., 2016. Uncovering the spatial heterogeneity of Ediacaran carbon cycling. Geobiology 15, 211–224.
Macdonald, F.A., Strauss, J.V., Sperling, E.A., Halverson, G.P., Narbonne, G.M., Johnston, D.T., Kunzmann, M., Schrag, D.P., Higgins, J.A., 2013. The stratigraphic relationship between the Shuram carbon isotope excursion, the oxygenation of Neoproterozoic oceans, and the first appearance of the Ediacara biota and bilaterian trace fossils in northwestern Canada. Chem. Geol. 362, 250–272.
Martins, M., Lemos, V.B., 2007. Análise estratigráfica das sequências neoproterozóicas da Bacia do São Francisco. Rev. Bras. Geosci. 37 (4), 156–167.
Martins-Neto, M.A., 2009. Sequence stratigraphic framework of Proterozoic successions in eastern Brazil. Mar. Pet. Geol. 26, 163–176.
McKirdy, D.M., Burgess, J.M., Lemon, N.M., Yu, X., Cooper, A.M., Gostin, V.A., Jenkins, R.J.F., Both, R.A., 2001. A chemostratigraphic overview of the late Cryogenian interglacial sequence in the Adelaide Fold-Thrust Belt, South Australia. Precambrian Res. 106, 149–186.
Meert, J.G., Lieberman, B.S., 2008. The Neoproterozoic assembly of Gondwana and its relationship to the Ediacaran–Cambrian radiation. Gondwana Res. 14, 5–21.
Meira, V.T., García-Casco, A., Juliani, C., Almeida, R.P., Schorscher, J.H.D., 2015. The role of intracontinental deformation in supercontinent assembly: insights from the Ribeira Belt, Southeastern Brazil (Neoproterozoic West Gondwana). Terra Nova 27 (3), 206–217.
Merdith, A.S., Collins, A.S., Williams, S.E., Pisarevsky, S., Fodenc, J.D., Archibald, D.B., Blades, M.L., Alessio, B.L., Armistead, S., Plavsa, D., Clark, C., Müller, R.D., 2017. A full-plate global reconstruction of the Neoproterozoic. Gondwana Res. 50, 84–134.
Misi, A., Kaufman, A.J., Veizer, J., Powis, K., Azmy, K., Boggiani, P.C., Gaucher, C., Teixeira, J.B., Sanches, A.L., Iyer, S.S., 2007. Chemostratigraphic correlation of Neoproterozoic successions in South America. Chem. Geol. 237, 143–167.
Misi, A., Kaufman, A.J., Azmy, K., Dardenne, M.A., Sial, A.N., Oliveira, T.F., 2011. Neoproterozoic successions of the São Francisco Craton, Brazil: The Bambuí, Una, Vazante and VazaBarris/Miaba groups and their glaciogenic deposits. In: Arnaud, E., Halverson, G.P., Shields-Zhou, G. (Eds.), The Geological Record of Neoproterozoic Glaciations. Memoir 36, Chapter 48 Geological Society of London, London, pp. 509–522.
Narbonne, G.M., 2005. The Ediacara Biota: neoproterozoic origin of animals and their ecosystems. Annu. Rev. Earth Planet. Sci. 33, 421–442.
Narbonne, G.M., Xiao, S., Shields, G.A., 2012. The Ediacaran Period. In: The Geologic Time Scale. Elsevier, pp. 413–435. https://doi.org/10.1016/B978-0-444-59425-9.00018-4.
Noffke, N., Gerdes, G., Klenke, T., Krumbein, W.E., 1996. Microbially induced sedimentary structures – examples from modern sediments of siliciclastic tidal flats. Zbl. Geol. Paläontol. 1, 307–316.
Nogueira, A.C.R., Riccomini, C., Sial, A.N., Moura, C.A.V., Trindade, R.I.F., Fairchild, T.R., 2007. C and Sr isotope fluctuations and paleoceanographic changes in the Late Neoproterozoic Araras carbonate platform, southern Amazon craton, Brazil. Chem. Geol. 237, 168–190.
Okubo, J., Muscente, A., Luvizotto, G.L., Uhlein, G.J., Warren, L., 2018. Phosphogenesis, aragonite fan formation and seafloor environments following the Marinoan glaciation. Precambrian Res. 311, 24–36.
Paula-Santos, G.M., Babinski, M., Kuchenbecker, M., Caetano-Filho, S., Trindade, R.I.F., Pedrosa-Soares, A.C., 2015. New evidence of an Ediacaran age for the Bambuí Group in southern São Francisco craton (eastern Brazil) from zircon U-Pb data and isotope chemostratigraphy. Gondwana Res. 18, 1–19.
Paula-Santos, G.M., Caetano-Filho, S., Babinski, M., Trindade, R.I., Guacaneme, C., 2017. Tracking connection and restriction of West Gondwana São Francisco Basin through isotope chemostratigraphy. Gondwana Res. 42, 280–305.
Paula-Santos, G.M., Caetano-Filho, S., Babinski, M., Enzweiler, J., 2018. Rare earth elements of carbonate rocks from the Bambuí Group, Southern São Francisco Basin, Brazil, and their significance as paleoenvironmental proxies. Precambrian Res. 305, 327–340.
Pedreira, A.J., 1999. Evolução sedimentar e tectônica da Bacia metassedimentar do Rio Pardo: uma síntese. Rev. Bras. Geosci. 29 (3), 339–344.
Penny, A.M., Wood, R., Curtis, A., Bowyer, F., Tostevin, R., Hoffman, K.H., 2014. Ediacaran metazoan reefs from the Nama Group, Namibia. Science 344, 1504–1506.
Perrella, P., Uhlein, A., Uhlein, G.J., Sial, A.N., Pedrosa-Soares, A.C., Lima, O.N.B., 2017. Facies analysis, sequence stratigraphy and chemostratigraphy of the Sete Lagoas

Formation (Bambui Group), northern Minas Gerais State, Brazil: evidence of a cap carbonate deposited on the Januária basement high. Braz. J. Geol. 47 (1), 59–77.

Petsch, S.T., Berner, R.A., Eglinton, T.I., 2000. A field study of the chemical weathering of ancient sedimentary organic matter. Org. Geochem. 31, 475–487.

Porada, H., Ghergut, J., Bouougri, E.H., 2008. Kinneyia-type wrinkle structures - critical review and model of formation. PALAIOS 23, 65–77.

Prokoph, A., Shields, G.A., Veizer, J., 2008. Compilation and time-series analysis of a marine carbonate $\delta^{18}O$, $\delta^{13}C$, $^{87}Sr/^{86}Sr$ and $\delta^{34}S$ database through Earth history. Earth Sci. Rev. 87, 113–133.

Raiswell, R., Berner, R.A., 1987. Organic carbon losses during burial and thermal maturation of normal marine shales. Geology 15, 853–856.

Reis, H.L.S., Suss, J.F., 2016. Mixed carbonate-siliciclastic sedimentation in forebulge grabens: an example from the Ediacaran Bambuí Group, São Francisco Basin, Brazil. Sediment. Geol. 15, 83–103.

Rodrigues, J.B., 2008. Proveniência de sedimentos dos grupos Canastra, Ibiá, Vazante e Bambuí e um estudo de zircões detríticos e Idades Modelo Sm-Nd (PhD Thesis). Univ. Brasília (141 pp., unpublished).

Romano, A.W., Knauer, L.G., Costa, R.D., Joncew, H.C., Vasconcelos, R.A.C. 2014. Folha São João da Ponte SE.23-Z-C-V. Mapa Geológico em escala 1.100.000. CODEMIG-UFMG.

Romano, A.W., Knauer, L.G., Costa, R.D., Nascimento, B.L., Figueiredo, L.N. 2015. Folha São Francisco SE.23-Z-C-IV. Mapa geológico em escala 1:100.000. CODEMIG-UFMG.

Sahoo, S.K., Planavsky, N.J., Jiang, G., Kendall, B., Owens, J.D., Wang, X., Shi, X., Anbar, A.D., Lyons, T.W., 2016. Oceanic oxygenation events in the anoxic Ediacaran Ocean. Geobiology 14 (5), 457–468.

Saltzmann, M.R., Ripperdan, R.L., Brasier, M.D., Lohmann, K.C., Robison, R.A., Chang, W.T., Peng, S., Ergaliev, E.K., Runnegar, B., 2000. A global carbon isotope excursion (SPICE) during the late Cambrian: relation to trilobite extinctions, organic-matter burial and sea level. Palaeogeogr. Palaeoclimatol. Palaeoecol. 162, 211–223.

Samuelsson, J., Strauss, H., 1999. Stable carbon and oxygen isotope geochemistry of the upper Visingso Group (early Neoproterozoic), southern Sweden. Geol. Mag. 136, 63–73.

Sansjofre, P., Ader, M., Trindade, R.I.F., Elie, M., Lyons, J., Cartigny, P., Nogueira, A.C.R., 2011. A carbon isotope challenge to the snowball Earth. Nature 478, 93–97.

Sansjofre, P., Trindade, R.I.F., Ader, M., Soares, J.L., Nogueira, A.C.R., Tribovillard, N., 2014. Paleoenvironmental reconstruction of the Ediacaran Araras platform (Western Brazil) from the sedimentary and trace metals record. Precambrian Res. 241.

Santos, R.V., Alvarenga, C.J.S., Dardenne, M.A., Sial, A.N., Ferreira, V.P., 2000. Carbon and oxygen isotope profiles across Meso-Neoproterozoic limestones from central Brazil: Bambuí and Paranoá groups. Precambrian Res. 104, 107–122.

Santos, R.V., Alvarenga, C.J.S., Babinski, M., Ramos, M.L., Cukrov, N., Fonseca, M.A., Sial, A.N., Dardenne, M.A., Noce, C.M., 2004. Carbon isotopes of Mesoproterozoic–Neoproterozoic sequences from Southern São Francisco craton and Araçuaí Belt, Brazil: Paleographic implications. J. S. Am. Earth Sci. 18, 27–39.

Schrag, D.P., Higgins, J.A., Macdonald, F.A., Johnston, D.T., 2013. Authigenic carbonate and the history of the global carbon cycle. Science 339, 540–543.

Shields, G.A., Stille, P., Brasier, M.D., Atudorei, N.-V., 1997. Stratified oceans and oxygenation of the late Precambrian environment: a post-glacial geochemical record from the Neoproterozoic of W. Mongolia. Terra Nova 9, 218–222.

Shields, G.A., Brasier, M.D., Stille, P., Dorjnamjaa, D., 2002. Factors contributing to high $\delta^{13}C$ values in Cryogenian limestones of western Mongolia. Earth Planet. Sci. Lett. 196, 99–111.

Sial, A.N., Dardenne, M.A., Misi, A., Pedreira, A.J., Gaucher, C., Ferreira, V.P., Silva Filho, M.A., Uhlein, A., Pedrosa-Soares, A.C., Santos, R.V., Egydio-Silva, M., Babinski, M., Alvarenga, C.J.S., Fairchild, T.R., Pimentel, M.M., 2009. The São Francisco Palaeocontinent. In: Gaucher, C., Sial, A.N., Halverson, G.P., Frimmel, H.E. (Eds.), Neoproterozoic-Cambrian Tectonics, Global Change and Evolution: a focus on southwestern Gondwana. Developments in Precambrian Geology. 16. Elsevier, pp. 31–69.

Sial, A.N., Gaucher, C., Misi, A., Boggiani, P.C., Alvarenga, C.J.S., Ferreira, V.P., Pimentel, M.M., Pedreira, J.A., Warren, L.V., Fernández-Ramírez, R., Geraldes, M., Pereira, N.S., Chiglino, L., Cezario, W.S., 2016. Correlations of some Neoproterozoic carbonate-dominated successions in South America based on high-resolution chemostratigraphy. Braz. J. Geol. 46, 439–488.

Sinclair, H.D., Allen, P.A., 1992. Vertical versus horizontal motions in the Alpine orogenic wedge: stratigraphic response in the foreland basin. Basin Res. 4, 215–232.

Sternbeck, J., Sohlenius, G., 1997. Authigenic sulfide and carbonate mineral formation in Holocene sediments of the Baltic Sea. Chem. Geol. 135, 55–73.

Tahata, M., et al., 2013. Carbon and oxygen isotope chemostratigraphies of the Yangtze platform, South China: decoding temperature and environmental changes through the Ediacaran. Gondwana Res. 23, 333–353.

Tohver, E., D'Agrella Filho, M., Trindade, R.I.F., 2006. Paleomagnetic record of Africa and South America for the 1200–500 Ma interval, and evaluation of Rodinia and Gondwana assemblies. Precambrian Res. 147, 193–222.

Tohver, E., Trindade, R.I.F., Solum, J.G., Hall, C.M., Riccomini, C., Nogueira, A.C., 2010. Closing the Clymene Ocean and bending a Brasiliano belt: evidence for the Cambrian Formation of Gondwana, southeast Amazon craton. Geology 38 (3), 267–270.

Uhlein, A., Alvarenga, C.J.S., Dardenne, M.A., Trompette, R.R., 2011a. The glaciogenic Jequitaí Formation, southeastern Brazil. In: Arnaud, E., Halverson, G.P., Shields-Zhou, G. (Eds.), The Geological Record of Neoproterozoic Glaciations. Memoirs 36. Geological Society, London, pp. 541–546.

Uhlein, A., Baptista, M.C., Seer, I.J., Caxito, F.A., Uhlein, G.J., Dardenne, M.A., 2011b. A Formação Lagoa Formosa, Grupo Bambuí: sistema deposicional de leque submarino em bacia de ante-país. Geonomos 19 (2), 163–172.

Uhlein, G.J., Carvalho, J.F.M.G., Uhlein, A., Caxito, F.A., Halverson, G.P., Sial, A.N., 2013. Estratigrafia e sedimentologia da Formação Carrancas, Grupo Bambuí, nas regiões de Belo Horizonte e Pitangui – MG. Geonomos 20 (2), 79–97.

Uhlein, A., Perrella, P., Uhlein, G.J., Caxito, F. A., Neiva, G. S., Souza, R.D., Mendes, T.A. A. 2014. Folha Januária SD-23-Z-C-II. Mapa geológico em escala 1:100.000. CODEMIG-UFMG.

Uhlein, G.J., Salgado, S.S., Uhlein, A. 2014. Folha Catolé SD-23-Z-C-I. Mapa geológico em escala 1:100.000. CODEMIG-UFMG.

Uhlein, G.J., Uhlein, A., Halverson, G.P., Stevenson, R., Caxito, F.A., Cox, G.M., Carvalho, J.F.M.G., 2016. The Carrancas Formation, Bambuí Group: a record of pre-Marinoan sedimentation on the southern São Francisco craton, Brazil. J. S. Am. Earth Sci. 71, 1–16.

Uhlein, G.J., Uhlein, A., Stevenson, R., Halverson, G.P., Caxito, F.A., Cox, G.M., 2017. Early to late Ediacaran conglomeratic wedges from a complete foreland basin cycle in the southwest São Francisco Craton, Bambuí Group, Brazil. Precambrian Res. 299, 101–116.

Vieira, L.C., Almeida, R.P., Trindade, R.I.F., Nogueira, A.C.R., Janikian, L., 2007a. A Formação Sete Lagoas em sua área-tipo: fácies, estratigrafia e sistemas deposicionais. Rev. Bras. Geosci. 37 (4), 1–14.

Vieira, L.C., Trindade, R.I.F., Nogueira, A.C.R., Ader, M., 2007b. Identification of a Sturtian cap carbonate in the Neoproterozoic Sete Lagoas carbonate platform, Bambuí Group, Brazil. Compt. Rendus Geosci. 339, 240–258.

Vieira, L.C., Nédélec, A., Fabre, S., Trindade, R.I.F., Almeida, R.P., 2015. Aragonite crystal fans in Neoproterozoic cap carbonates: a case study from Brazil and implications for the post-snowball earth coastal environment. J. Sediment. Res. 85 (285), 300.

Warren, L.W., Fairchild, T.R., Gaucher, C., Boggiani, P.C., Poiré, D.G., Anelli, L.E., Inchausti, J.C.G., 2011. *Corumbella* and in situ *Cloudina* in association with thrombolites in the Ediacaran Itapucumi Group, Paraguay. Terra Nova 23, 382–389.

Warren, L.W., Pacheco, M.L.A.F., Fairchild, T.R., Simões, M.G., Riccomini, C., Boggiani, P.C., Cáceres, A.A., 2012. The dawn of animal skeletogenesis: ultrastructural analysis of the Ediacaran metazoan *Corumbellawerneri*. Geology 40, 691–694.

Warren, L.V., Quaglio, F., Riccomini, C., Simoes, M.G., Poire, D.G., Strikis, N.M., Anelli, L.E., Strikis, P.C., 2014. The puzzle assembled: Ediacaran guide fossil Cloudina reveals an old proto-Gondwana seaway. Geology 42, 391–394.

Xiao, S., Narbonne, G.M., Zhou, C., Laflamme, M., Grazhdankin, D.V., Moczydlowska-Vidal, M., Cui, H., 2016. Towards an ediacaran time scale: problems, protocols, and prospects. Episodes 39 (4), 540–555.

Zhu, M., Babcock, L.E., Peng, S., 2005. Advances in Cambrian stratigraphy and paleontology: integrating correlation techniques, paleobiology, taphonomy and paleoenvironmental reconstruction. Palaeoworld 15, 217–222.

Zhu, M., Zhuravlev, A.Y., Wood, R.A., Zhao, F., Sukhov, S.S., 2017. A deep root for the Cambrian explosion: Implications of new bio and chemostratigraphy from the Siberian Platform. Geology 45, 459–462.